PRODUCTION AND PERFORMANCE EVALUATION OF ZIF-8 BASED BINARY AND TERNARY MIXED MATRIX GAS SEPARATION MEMBRANES

A THESIS SUBMITTED TO
THE GRADUATE SCHOOL OF NATURAL AND APPLIED SCIENCES
OF
MIDDLE EAST TECHNICAL UNIVERSITY

BY

NİLAY KESER

IN PARTIAL FULFILLMENT OF THE REQUIREMENTS
FOR
THE DEGREE OF MASTER OF SCIENCE
IN
CHEMICAL ENGINEERING

August 2012

Approval of the thesis:

PRODUCTION AND PERFORMANCE EVALUATION OF ZIF-8 BASED BINARY AND TERNARY MIXED MATRIX GAS SEPARATION MEMBRANES

submitted by **NİLAY KESER** in partial fulfillment of the requirements for the degree of **Master of Science in Chemical Engineering Department, Middle East Technical University,** by

Prof. Dr. Canan Özgen
Dean, Graduate School of **Natural and Applied Sciences** _____

Prof. Dr. Deniz Üner
Head of Department, **Chemical Engineering** _____

Prof. Dr. Levent Yılmaz
Supervisor, **Chemical Engineering Dept., METU** _____

Assoc. Prof. Dr. Halil Kalıpçılar
Co-supervisor, **Chemical Engineering Dept., METU** _____

Examining Committee Members:

Prof. Dr. Nihal Aydoğan
Chemical Engineering Dept., H.Ü. _____

Prof. Dr. Levent Yılmaz
Chemical Engineering Dept., METU _____

Assoc. Prof.Dr. Halil Kalıpçılar
Chemical Engineering Dept., METU _____

Assist. Prof. Dr. Çerağ Dilek
Chemical Engineering Dept., METU _____

Assist. Prof. Dr. P.Zeynep Çulfaz Emecen
Chemical Engineering Dept., METU _____

16.08.2012

I hereby declare that all information in this document has been obtained and presented in accordance with academic rules and ethical conduct. I also declare that, as required by these rules and conduct, I have fully cited and referenced all material and results that are not original to this work.

Name, Last name: Nilay Keser

Signature:

ABSTRACT

PRODUCTION AND PERFORMANCE EVALUATION OF ZIF-8 BASED BINARY AND TERNARY MIXED MATRIX GAS SEPARATION MEMBRANES

Keser, Nilay
M.Sc., Department of Chemical Engineering
Supervisor : Prof. Dr. Levent YILMAZ
Co-supervisor : Assoc. Prof. Dr. Halil KALIPÇILAR

August 2012, 181 pages

Mixed matrix membranes (MMMs) have gained importance because they combine the desirable properties of the polymers and the organic/inorganic filler materials and they may have a very big potential. In this study polyethersulfone (PES) was used as polymeric material, and Zeolitic Imidazolate Framework-8 (ZIF-8) was used as porous filler material, and 2-hydroxy 5-methyl aniline(HMA), was used as a third component in membrane formulation.

In this study, ZIF-8 crystals were synthesized with varying particle sizes, and a novel recycling methodology was developed to improve the efficiency of ZIF-8 production. ZIF-8 nano-crystals were synthesized by a 1-hour stirring method at room temperature and characterized by X-ray diffractometer, scanning electron microscopy (SEM), transmission electron microscopy (TEM), dynamic light scattering (DLS) and thermal gravimetric analysis (TGA). In order to investigate the effect of ZIF-8 loading on the membrane performance, different types of membranes were prepared with varying amounts of ZIF-8 between 10-60% (w/w). Moreover, ternary mixed matrix membranes were synthesized consisting of different amounts of ZIF-8 between 10-30% (w/w) and HMA 1-10% (w/w). Gas transport properties of the membranes were investigated by single gas permeation experiments of H_2, CO_2 and CH_4 at 3 bar feed pressure. In order to investigate the effect of feed pressure on the gas transport properties of the membranes, single gas experiments were conducted on 3, 6, 8, 10 and 12 bar feed pressures. Moreover, binary gas permeation experiments of CO_2/CH_4 pair were conducted through selected membranes at 3 bar and 12 bar feed pressures. In addition to gas

permeation experiments, the morphology and thermal characteristics of the membranes were characterized by SEM, TGA and differential scanning calorimetry (DSC) analysis.

The incorporation of ZIF-8 crystals into continuous PES matrix resulted in high performance gas separation membranes. The permeabilities of all studied gases increased with ZIF-8 loading while the ideal selectivities showed a slight decrease compared to neat PES membrane. Highly reproducible and repeatable results were obtained up to 30 % w/w ZIF-8 loading, while membrane formulation reproducibility was decreased for higher ZIF-8 contents (>30 w/w %). Addition of HMA improved the gas separation performances of the binary membranes significantly by decreasing permeabilities and increasing ideal selectivities. PES/ZIF-8(%20)/HMA(%7) membrane has the best separation performance for all gases among the ternary membranes. When 7 w/w % HMA was added to PES/ZIF-8(%20) membrane, H_2 permeability decreased from 26.3 to 13.7 barrer, while H_2/CH_4 ideal selectivity increased from 61.8 to 103.7.

Increasing feed pressures appreciably increased the separation performances of all membranes. While the H_2 permeability is pressure independent, the CO_2 and CH_4 permeabilities were reduced with increasing feed pressures and the highest selectivity improvement was observed in H_2/CH_4 pair for all membrane compositions. For instance, when the feed pressure was increased from 3 bar to 12 bar, the percentage improvements in ideal selectivities through PES/ZIF-8(%10)/HMA(%4) membrane were calculated as 26, 69, 113 % for the H_2/CO_2, CO_2/CH_4 and H_2/CH_4 gas pairs; respectively. This results show that working at higher feed pressures will be more advantageous for separation of the studied gas pairs. The ideal selectivities and the separation factors were equal to each other for all membrane compositions both for 3 and 12 bar operating pressures.

Keywords: Gas separation, Mixed matrix membranes, Zeolitic Imidazolate Framework-8(ZIF-8), Low molecular weight additive

ÖZ

ZIF-8 KATKILI İKİLİ VE ÜÇLÜ KARIŞIK MATRİSLİ GAZ AYRIM MEMBRANLARININ ÜRETİMİ VE PERFORMANSLARININ DEĞERLENDİRİLMESİ

Keser, Nilay
Yüksek Lisans, Kimya Mühendisliği Bölümü
Tez Yöneticisi : Prof. Dr. Levent Yılmaz
Ortak Tez Yöneticisi : Doç. Dr. Halil Kalıpçılar

Ağustos 2009, 181 sayfa

Karışık matrisli membranlar yüksek potansiyelleri ve polimerlerle inorganik materyallerin avantajlarını birleştirip sinerji yaratmaları nedeniyle son yıllarda büyük önem kazanmıştır. Bu çalışmada polimer olarak polietersülfon(PES), gözenekli katı olarak Zeolitik Imidazolat Kafes-8 (ZIF-8), uyumlaştırıcı olarak düşük molekül ağırlıklı 2-hidroksi 5-metilanilin(HMA) kullanılmıştır.

Bu çalışmada farklı boyutlarda ZIF-8 kristalleri sentezlenmiş ve sentez yönteminin verimliliği arttırabilmek için yeni bir geri dönüşüm yöntemi geliştirilmiştir. ZIF-8 kristalleri oda sıcaklığında 1 saatlik karıştırma yöntemi ile sentezlenmiştir ve sentezlenen kristaller X-ray ışını kırınımı (XRD), taramalı electron mikroskobu (SEM), geçirimli electron mikroskobu(TEM), diferansiyel taramalı kalorimetre(DSC) ve termogravimetrik analiz(TGA) ile karakterize edilmiştir. Membran formulasyonundaki ZIF-8 miktarının gaz ayrım performansına olan etkisini incelemek için ZIF-8'in ağırlıkça miktarı %10 ile %60 arasında değiştirilerek farklı membranlar hazırlanmıştır. Ayrıca, ağırlıkça %10,20 ve 30 ZIF-8 içeren membranlara ağırlıkça %1 ile %10 arasında değişen miktarlarda HMA eklenerek üçlü membranlar sentezlenmiştir. Membranları gaz ayrım performansları 3 bar besleme basıncında yapılan tekli H_2, CO_2 ve CH_4 gaz geçirgenlik deneyleri ile incelenmiştir. Tekli gaz geçirgenlik deneyleri 3, 6, 8, 10 ve 12 bar basınçlarında tekrarlanarak, besleme basıncının performansa olan etkisi araştırılmıştır. Ayni zamanda seçilen membranlarda 3 ve 12 bar besleme basıncında CO_2/CH_4 gaz çifti için ikili gaz deneyleri yapılmıştır. Gaz aktarım deneylerinin yanı sıra membranlar SEM, TGA ve DSC yöntemleri ile karakterize edilmiştir.

Sürekli PES fazın içine ZIF-8 kristallerinin eklenmesiyle yüksek performanslı gaz ayrım membranları elde edilmiştir. Membran içerisindeki ZIF-8 konsantrasyonunun arttırılmasıyla kullanılan tüm gazlar için geçirgenlik değerleri artarken, ideal seçicilik değerlerinde küçük düşüşler gözlenmiştir. Ağırlıkça %30'un altında ZIF-8 içeren membranlarda yüksek oranda tekrarlanılabilir gaz aktarım sonuçları elde edilirken, yüksek konsantrasyonda (>% 30) ZIF-8 içeren membranlarda membran formulasyon tekrarlanılabilirliği düşmüştür. HMA'nın formulasyona eklenmesiyle geçirgenliklerde düşüş gözlenirken, ideal seçicilik değerleri artmıştır ve ikili membranların gaz ayrım performansları önemli ölçüde artmıştır. Hazırlanan üçlü membranlar arasında en yüksek performansa sahip membran PES/ZIF-8(%20)/HMA(%7)'dır. PES/ZIF-8(%20) membranına ağırlıkça %7 oranında eklenen HMA' nın etkisiyle, H_2 geçirgenliği 26.3'ten 13.7 barrer'e düşerken, H_2/CH_4 ideal seçiciliği 61.8'den 103.7'ye kadar yükselmiştir.

Besleme basıncının arttırılması tüm membranların ayrım performanslarını önemli oranda arttırmıştır. CO_2 and CH_4 geçirgenlikleri artan besleme basıncı etkisiyle düşerken, H_2 geçirgenliği basınçtan bağımsızdır ve tüm membran kompozisyonları için en yüksek ideal seçicilik artışı H_2/CH_4 gaz çiftinde görülmüştür. Örneğin, PES/ZIF-8(%10)/HMA(%4) membranında besleme basıncı 3 bardan 12 bara yükseltildiğinde H_2/CO_2, CO_2/CH_4 ve H_2/CH_4 gaz çiftleri için ideal seçiciliklerde gözlenen artışlar sırasıyla % 26, % 69 ve %113 olarak hesaplanmıştır. Bu sonuçlar kullanılan gazların ayrımı için yüksek basınçlarda çalışmanın daha avantajlı olacağını göstermektedir. Tüm membran kompozisyonları için 3 ve 12 bar besleme basınçlarında birbirine çok yakın ideal seçicilik ve karışım seçicilik değerleri elde edilmiştir.

Anahtar Kelimeler: Gaz ayrımı, Karışık matrisli membran, Zeolitik Imidazolat Kafes-8 (ZIF-8), Küçük moleküler ağırlıklı uyumlaştırıcı,

To my family

ACKNOWLEDGEMENTS

I wish to express my deepest gratitude to my supervisor Prof. Dr. Levent Yılmaz for his invaluable guidance, support and interest throughout all stages of my study. I would also like to thank my co-supervisor Assoc. Prof. Dr. Halil Kalıpçılar for his suggestions, criticisim and exceptional supervision. It was a great honour for me to study under their supervision. I would like to express my special thanks to Dr. Berna Topuz for her support, kind friendship and precious encouragement.

I would like to thank the financial supports from The Scientific and Technological Research Council of Turkey (TUBITAK) through the grant number 111M400. I also thank to the technicians of Chemical Engineering Department of Middle East Technical University.

I would like to thank my colleagues Aylin Önder, Nihan Uzunoğlu, Merve Başdemir, Gökhan Sarıalp for their helps, suggestions, solutions to my problems, and conveying their invaluable laboratory experiences to me. Thanks also to all my lab mates for their helpful and enjoyable friendships throughout this study. Foremost, I owe special thanks to my family for their unconditional love and unlimited patience from the very beginning. Finally but not the least, I would like to special thanks to my husband İshak Demir, not only his unconditional and endless support but also his very special intimacy.

TABLE OF CONTENTS

LIST OF TABLES

TABLES

LIST OF FIGURES

FIGURES

LIST OF SYMBOLS AND ABBREVATIONS

A : Effective membrane area (cm^2)

dn/dt : Molar flow rate (mol/s)

dp/dt : Pressure increase

J : Flux (cm3/cm2.s)

K : adjustable parameter

M : Molecular weight of the gas

P : Permeability (Barrer)

P_f : Feed side pressure (cmHg)

P_p : Permeate side pressure (cmHg)

R : Ideal gas constant

T : Temperature (°C)

Tg : Glass transition temperature (°C)

Vd : Dead volume (cm^3)

Greek Letters

α : Selectivity

ρ : Density of the gas

ν : Volumetric flow rate (cm^3/s)

Δp : Transmembrane pressure difference (cmHg)

CHAPTER 1

INTRODUCTION

Membrane based gas separation is a superior alternative to other competing technologies such as pressure swing adsorption and cryogenic adsorption due to its technical and economical advantages [1]. The advantages can be asserted as low capital investment, simplicity and ease of installation and operation, low maintenance requirements, low weight and space requirements and high processability [1]. Since the potential usage areas (given in Table 1.1) of membrane separation are very wide, the industrial market could grow with the developments in membrane efficiency [2]. A membrane is a semi-permeable barrier between two phases which allows the passage of some molecules and reject the others. The efficiency of a gas separation membrane could be determined by two characteristics of it, which are permeability and selectivity. If a membrane is described as a selective barrier between two phases, only certain molecules could be transported under the influence of a gradient in pressure through this membrane [1]. The permeability of a membrane is defined as ;

$$P = \frac{J*l}{P_f - P_p} \tag{1.1}$$

where J is flux of gas through the membrane, P_f and P_p are the partial pressures of the gas on the feed and permeate side, respectively; and l is the thickness of the membrane. The unit of permeability is usually given in Barrer, defined as;

$$Barrer = 1 * 10^{-10} \frac{cm^3(STP).cm}{cm^2.s.cmHg} \tag{1.2}$$

The other efficiency index, ideal selectivity is the ratio of the permeabilities of the single gases, defined as;

$$a_{AB} = \frac{P_A}{P_B} \tag{1.3}$$

Conventionally, ideal selectivity is equal to or greater than one since the permeability of the slower gas is used as denominator, which gives a basis to compare the different materials. The permeability and the selectivity are the intrinsic properties of the homogenous materials and they are functions of temperature and pressure [3]. For a binary gas mixture composed of A and B, a new separation definition is used as separation selectivity. The separation factor can be stated as the ratio of mole fractions of gases while A is faster permeating gas;

$$a_{A/B} = \frac{(y_A/y_B)_p}{(x_A/x_B)_f} \tag{1.4}$$

where y_A and $y_B$are the permeate side mole fractions of component A and B, x_A and x_B are the feed side mole fractions of them. The ideal selectivity is equal to the separation selectivity when the conditions is the case; i) the components of the gas mixtures do not interact to each other, ii) they do not affect the each other's interaction with the membrane material, iii) the permeate pressure is zero[4].

Table 1.1 Potential applications of gas separation membranes, adopted list from[5](HC=Hydrocarbon)

Category	**Gas Pair**	**Application**
Hydrogen	H_2/N_2	Ammonia Purge Gas
	H_2/CH_4	Refinery Hydrogen Recovery
	H_2/O_2	Fuel Cells
Air	O_2/N_2	O_2-enriched Air Combustion
Acid Gases	CO_2/CH_4	Landfill and Natural Gas Sweeting
	CO_2/N_2	Digester Gas Treatment
Drying	H_2O/HC	Hydrocarbon Drying
	H_2O/Air	Air Drying
Hydrocarbons	HC/Air	Pollution Control; Stack Gas or Solvent Recovery
	HC/N_2	Upgrading Low-BTU Gas
Helium	He/HC	Helium Recovery from Gas Wells
	He/N_2	Helium Recovery from Diving Air

Polymers are most commonly used materials in gas separation membranes. They provide a range of desirable properties that are important for gas separation processes including, good mechanical stability, and high permeability, low cost and easy processability[4].

Although, there are numerous studies in literature which attempt to improve the separation properties of polymers, current polymeric membrane materials have a limit in the tradeoff between permeability and selectivity. Permeability-selectivity trade off plot for the H_2/CO_2 gas pair is shown in Figure 1.1, which was reported (revisited at 1998) by Robeson[6]. The high performance membranes would be in the upper right-hand corner of this figure, with both high permeability and selectivity. Freeman stated that the upper bound line cannot be exceeded by changing the chemical structure of classical polymers [7].

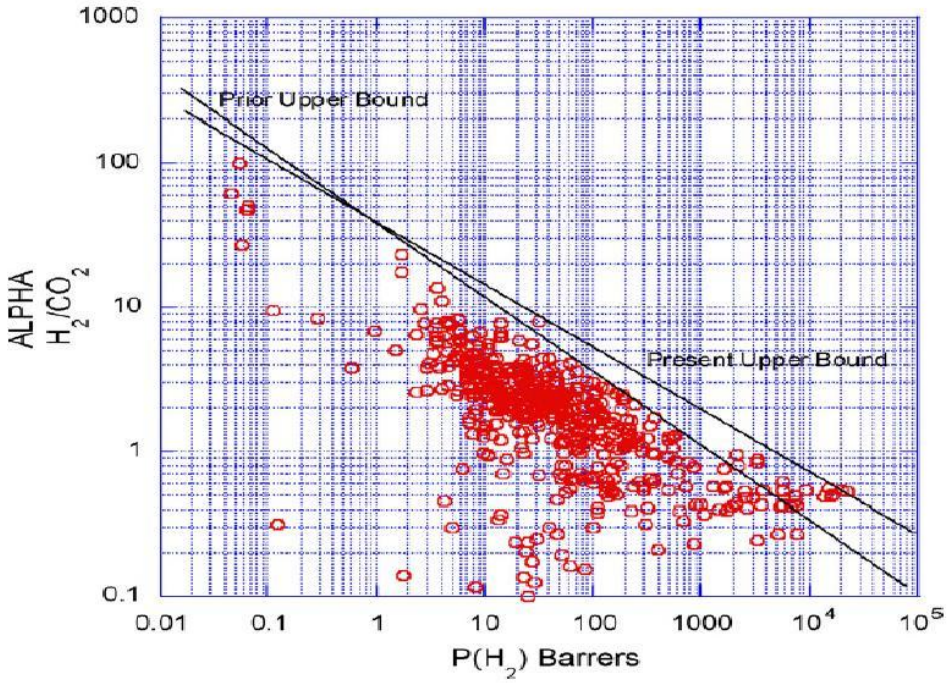

Figure 1.1 Revisited upper bound trade of curve for H_2/CO_2 pair [6]

Inorganic membranes are alternative materials for gas separation because of their high permeability and selectivity. However, they need a complex manufacturing procedure with high cost and low reproducibility; also they can be mechanically weak [5].

Since both the polymeric and inorganic membranes are inefficient when they are used separately, a new type of hybrid membrane material has been developed by incorporating the inorganic materials into the polymeric matrices named as mixed matrix membranes (MMM) [8]. There are different types of filler materials that can be used for MMM fabrication such as carbon molecular sieves (CMS),

microporous molecular sieves (zeolites), mesoporous molecular sieves, silicas and metal organic frameworks [9-14]. Mixed matrix membranes are the challenging materials for gas separation. Because, they combine the shape selectivity and specific sorption characteristics of filler materials and, economical processing of polymeric material[1]. Both the permeability and the selectivity will be improved and high performance mixed matrix membranes can be developed with the ideal combination of these two phases; however, different types of interface defects may be arisen due to weak polymer-filler compatibility. There are different methods in literature to overcome this problem such as annealing membranes above T_g of polymer [15,16], adding a plasticizer into membrane [17], modifying external surface of zeolites with silane coupling agents [18], using low molecular weight additives (LMWA) with multifunctional groups [19-21].

Zeolitic Imidazolate Frameworks (ZIFs) are promising crystalline materials for many technological applications [22] especially in gas storage [23], gas separation [24], and catalysis [25] and sensing [26]. They exhibit zeolite like structures and combine the appealing features of both metal organic frameworks and zeolites such as tunable framework and pore structures, high microporosity, and large surface areas, chemical and thermal stability. ZIF-8 has sodalite (SOD) topology with a pore size of 0.34 nm. It exhibits thermal stability up 400^{o}C and has a BET surface area of 1300–1600m^2/g [27]. The surface area of filler material in mixed matrix membranes is an important issue, because the higher the adsorption capacity of filler material, the better the gas permeation performance of membranes [28, 29]. ZIF-8 has a high selective adsorption capacity to CO_2 which is a desirable property for development of selective membrane materials [30].

The objective of this study is to synthesize ZIF-8 crystals with varying particle sizes and to improve the synthesis efficiency by developing a novel recycling methodology for ZIF-8 production. Then these ZIF-8 crystals were used to develop ZIF-8 incorporated binary and ternary mixed matrix membranes with high separating performance. ZIF-8 nano-crystals were synthesized by a 1-hour stirring method at room temperature and characterized by X-ray diffractometer, scanning electron microscopy (SEM), transmission electron microscopy (TEM), dynamic light scattering (DLS) and thermal gravimetric analysis (TGA). MMMs were prepared using polyethersulfone (PES) as the polymer matrix with ZIF-8 as the dispersed phase. The third component used in the ternary membranes is 2-hydroxy 5-methyl aniline (HMA). In order to investigate the effect of ZIF-8 loading on the membrane performance, different types of membranes were prepared with varying amounts of ZIF-8 between 10-60% (w/w). Moreover, ternary mixed matrix membranes were synthesized consisting of different amounts of ZIF-8 between 10-30% (w/w) and HMA 1-10% (w/w). Gas transport properties of the membranes were investigated by single gas permeation experiments of H_2, CO_2 and CH_4 at 3 bar feed pressure. Also in order to investigate the effect of feed pressure on the gas transport properties of the membranes, single gas experiments were conducted on 3, 6, 8, 10 and 12

bar feed pressures. Binary gas permeation experiments of CO_2/CH_4 pair were conducted at 3 bar and 12 bar feed pressures. In addition to gas permeation experiments, the morphology and thermal characteristics of the membranes were characterized by SEM, TGA and differential scanning calorimetry (DSC) analysis.

CHAPTER 2

LITERATURE SURVEY

2.1 Polymeric Gas Separation Membranes

Polymers are the most frequently preferred materials as membrane material in gas separation applications due to their low capital cost, stability at high pressures, easy scalability and easy fabrication into commercially viable hollow fibers and flat sheets [1]. The polymers have a glass transition temperature (Tg) at which the polymer traverses from glassy to rubbery state and the chain characteristics of the material changes. The most important two characteristics, chain mobility and the free volume, of the polymers are affected by this transition significantly and they are important factors in controlling the gas permeation properties.

Since the chain mobility is restricted in glassy state, free volumes occur in non-equilibrium state having entangled chains with immobile molecular backbones in frozen conformation [9]. Diffusion coefficients in glassy polymers are dependent on the molecular size and the shape due to the restricted chain mobility, and thus glassy polymers are more favorable than the rubbery polymers for the membrane applications with better selectivities. Polycarbonates, polyimides, polysulfones, polyphenylene oxides and cellulose derivatives are the most common polymers that are used for this application [1].

The gas separation mechanism through the dense polymeric membranes is explained by combination of two mechanisms, namely solution-diffusion model. According to the solution-diffusion model, the permeating molecule is sorped by the membrane at one interface, transferred to the other interface by diffusion through the voids between polymer chains and desorbed at the other interface. Hence, the permeation of molecules through membranes equals to the product of the solubility coefficient S, and diffusion coefficient, D, in a given membrane [1]:

$$P = S * D \tag{2.1}$$

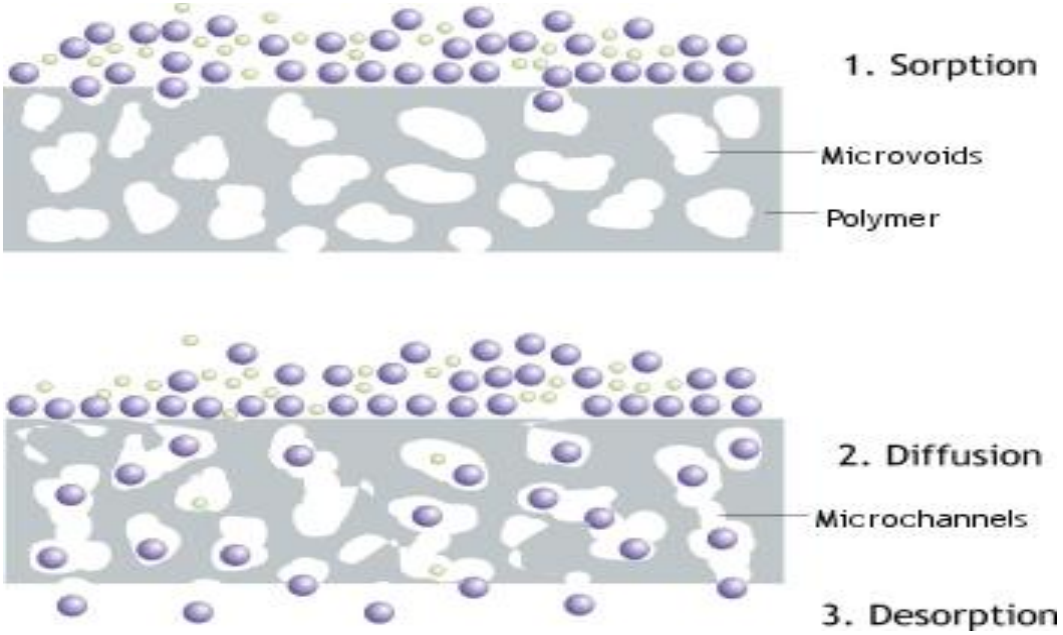

Figure 2.1 Solution-Diffusion Mechanism

Diffusion coefficient D, is defined as the rate of transport of a penetrating gas through the membrane which is kinetic parameter. Solubility coefficient S, is a measure of the amount of penetrant gases adsorbed by the membrane under equilibrium conditions which is a thermodynamic parameter. Both of which depend on temperature, pressure and pressure gradient of penetrants [31]. The gas transport mechanism through porous membranes is explained by the molecular sieving mechanism which separates the gas molecules based on size discrimination [32].

2.2 Mixed Matrix Membranes

Mixed matrix membranes are the challenging candidates for membrane applications due to the combination of desired properties of the polymer matrices such as economical, easy scability, and fabrication and high selectivity of organic-inorganic filler phase [33]. Several studies were conducted by using different types of filler materials as CMS, silicas, mesoporous molecular sieves and zeolites[9-15,34,35]. In most of the MMM applications different types of zeolites have been used as filler phase and the detailed information about them can be found in these review articles [36-39] and these thesis studies [5,40-43]. In recent years metal organic frameworks (MOF) have been emerged as a new class of microporous crystalline material with desirable properties (easy, quick and cheap synthesis [44], highly tailorable size, shape and organic functionality [45], high surface area, etc.) for using in gas separation applications [44].

Vu et.al [9] prepared MMMs by incorporating carbon molecular sieves(CMS) into Matrimid 5218 and Ultem® 1000 polymers and they reported enhancements in both permeability and selectivity. While the improvements were calculated as 40% in CO_2/CH_4 selectivity and 8% in O_2/N_2 selectivity for Ultem® CMS membrane, they were calculated as 45% in CO_2/CH_4 selectivity and 20 % in O_2/N_2 for Matrimid–CMS membranes.

Mesoporous materials have also been used as fillers in MMM preparation to provide better wetting and dispersion. Since the polymer could penetrate into the large mesopores, the interfacial contact is enhanced and the permeabilities are increased. However, the large size of mesopore causes a loss of selectivity. This concept was demonstrated by MCM-41/polysulfone MMMs, wherein gas permeabilities increased but selectivities remain unchanged [35].

Dual pore systems were constructed by incorporating both micropores which provide size and shape selectivity and mesopores which enhance the interfacial contact into polymer matrix [34]. For instance, carbon aerogel having both micropores and mesopores were incorporated in Matrimid® matrix and higher ideal selectivities for H_2/N_2, O_2/N_2, and CO_2/CH_4 gas pairs relative to pure Matrimid® were obtained. Moreover, carbon aerogel-ZSM-5/Matrimid® MMMs were fabricated by the addition of nano-sized ZSM-5 crystals and higher selectivity for CO_2/CH_4 separation was observed [34].

In mixed matrix membranes, different properties of two phases, strong aggregation tendency between fillers and weak polymer-filler compatibility cause different types of interface defects on the membrane morphology. This defects, that can strongly affect the overall membrane properties, can be classified into three categories; 1) rigidified polymer layer around the particles, 2) interface voids or sieve-in-a-cage, 3) particle pore blockage[33,46].

In the first case, due to good adhesion between polymer-filler phases, the free volume occurs near the fillers is reduced and thus the polymer chain mobility is reduced in this places. Lower permeabilities and higher ideal selectivities are expected in the presence of rigidified polymer by improved diffusive selectivity in this region [47, 48]. In one of the studies representing the matrix rigidification defect, Li et.al [49] prepared zeolite 4A filled polyethersulfone mixed matrix membranes. They reported that, the permeabilities for the gases of H_2, O_2 and N_2 were decreased with the addition of zeolite into PES matrix, and they explained this decrease with the matrix rigidification.

The story in the second case is completely reverse of the first case, in which the adhesion between the polymer and filler is insufficient, and that causes non-selective interfacial voids to form. The penetrating gas molecules prefer to pass through less resistant interfacial voids instead of particle pores.

Therefore, selectivity of the membrane is reduced while the permeability is increasing [36]. Hybrid membranes were reported which consist of organosilicate domains covalently bonded to a 6FDA–6FpDA–DABA polyimide using partially hydrolyzed tetramethoxysilane (TMOS), methyltrimethoxysilane (MTMOS) or phenyltrimethoxysilane (PTMOS). They were tested for permeabilities of the He, O_2, N_2, CH_4, CO_2 gases before and after an anneallig period. While the permeabilities incresed 200-500 % after annealing period, the selectivities decreased 0-50 % [50].

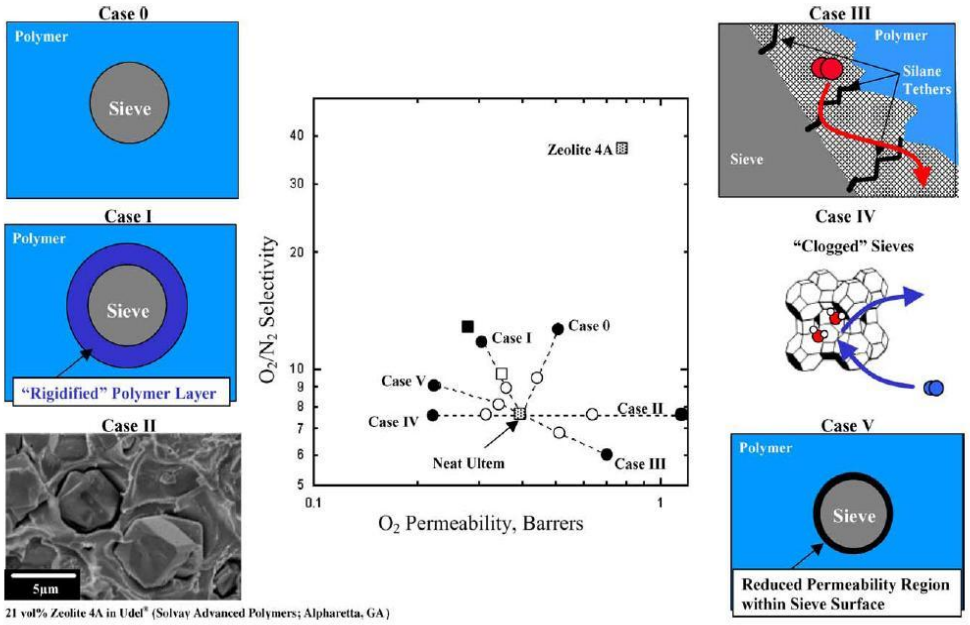

Figure 2.2 Summary of the relationship between mixed matrix membrane morphologies and transport properties [33]

In the pore blockage case, which is observed only in the mixed matrix membranes comprising of porous fillers, pores of the particles are congested with a sorbent, solvent, contaminant or polymer chains. When the pores are blocked partially, the selectivity may be increased while the permeability decreases which observed in the case of larger pore dimensions than molecular gas diameters,. When the pores are clogged totally which is the result of kinetic diameter of tested gases and the pore dimensions in the same range, both permeabilities and selectivities decrease [36,46].

The strong dependency of the transport properties of the membranes on the morphology were explained by Moore and Koros [33] in five cases in detail, Figure 2.2 shows the summary of these five cases together. Case 0, increase in both permeability and the selectivity, represents the ideal morphology which is difficult to obtain. Case I caused by a rigidified polymer layer surrounding the

zeolite that is slow down the gas transport. Case II and III are explained by the same theory, interfacial voids between the polymer chains and zeolites increase the permeabilities when the selectivities stay constant or decreased. Case IV and V are the results of the sorption of a strongly held gas molecule on the zeolite pores.

Improving the overall morphology is a requirement to enhance the gas separation performances of mixed matrix membranes with additional methodologies suggested in literature [51-59], some of which are creating special zeolite surfaces having whiskers or asperities by using modification agents[60], using coupling agents which can react both with the polymer and zeolite surface[61] and decreasing the Tg of polymer matrix by adding plasticizers into membrane formulation[17].

There are several studies that suggest the fabrication of MMM above Tg of the polymeric material [15-17], in order to reduce the stress induced during the solvent evaporation period, thereby to prevent interface voids between polymer chains and filler particles. In the study of Li et.al[49] membranes were annealed at 30^{o}C above the glass transition temperature in order to eliminate the interaction problems, but two different cooling procedures, which are natural cooling and quenching, were applied to the membranes after same annealing periods. Higher quality membranes were obtained by natural cooling than quenching. Because, some voids were formed during rapid cooling due to the difference in thermal expansions of two phases.

As a strategy for improving the membrane performance, Zhang et.al [62] proposed to use mesoporous ZSM-5 nanoparticles into Matrimid phase. The ideal selectivities of Matrmid/ZSM-5 membranes for the gas pairs of O_2/N_2 and CO_2/CH_4 showed 56 % and 90 % increase relative to the pure Matrimid membrane, respectively. Since the polymer chains can penetrate into the mesopores, the adhesion between the polymer and zeolite were improved.

Another alternative method proposed in literature is zeolite surface modification by silane –coupling agent. Mahajan et.al [17] prepared Matrimid/zeolite 4A membranes with modified and unmodified zeolites and they were tested by O_2 and N_2 permeation experiments. While the O_2 permeability showed a slight increase from 1.32 to 1.40, O_2/N_2 selectivity was not changed with the addition of modified zeolite 4A compared to neat Matrimid membrane. However, both the permeability and ideal selectivity were increased in the case of unmodified zeolite 4A incorporation. The bond formation between the polymer and sieves was assumed to improve the gas permeation properties of the membrane. However, the silylation method did not effectively decrease the non-selective voids in the membrane; hence the membrane performance was not improved.

Instead of using bond formation between polymer and sieve, and modification of the sieve surface, the space between two phases were proposed to be filled with a third component which can contact to both polymer and sieve and the voids between them would be decreased by this component[51-59] The first example of ternary mixed matrix membranes were prepared by using a low molecular weight additive, 2,4,6-triaminopyrimidine (TAP) which enhanced the adhesion between the polymer (Matrimid (PI)) and zeolite (13X and 4A) crystals by forming hydrogen bonding in between. Since the percentage weight of TAP in the membrane was very high (up to 40 % wt.), it acted as a main component in the membrane formulation other than an additive. Different behaviors were reported for interfacial void-free PI / zeolite 13X / TAP and PI / zeolite 4A / TAP membranes compared to the PI/TAP membrane, which were increasing permeabilities with a slight decrease in ideal selectivities and decreasing permeabilities with increasing selectivities, respectively. These adverse results were related to the pore sizes of zeolites. The gas permeation performance of the PI/zeolite membranes was improved for two cases with the addition of additive. In the case of PI / zeolite 4A / TAP membranes, the ideal selectivity for the gas pair of CO_2/CH_4 was increased from 1.22 to 84 by TAP addition to neat PI membrane, and increased from 84 to 617 with the incorporation of zeolite 4A into PI/TAP membrane [51].

In a study [63] of our research group paranitroaniline (pNA) was proposed as low molecular weight additive. Binary and ternary MMMs were prepared using constant PC concentration (20% w/v) and changing pNA and zeolite 4A concentrations between 1-5% (w/w) and 5-30% (w/w), respectively. The gas permeation performance of the PC/zeolite 4A (20% w/w) membrane was improved significantly with the addition of only 1% w/w pNA, of which H_2/CH_4 and CO_2/CH_4 selectivities are three times higher than those of pure PC membrane. DSC analysis was also used to investigate the effect of pNA on the PC-zeolite 4A interaction. It was reported that zeolite addition into PC/pNA increased the Tg of the material, whereas the addition of zeolite into pure PC had no effect. It was concluded as pNA was a necessary agent for interaction between zeolite 4A and PC matrix.

In another study[19] of our research group, HMA was used as a third component in order to investigate the effect of low molecular weight additive loading on the gas permeation properties of the pure PES membranes and PES/SAPO-34 membranes with constant SAPO-34 loading(20 % w/w). Incorporation of only SAPO-34 particles into polymeric phase made the membranes more permeable but less selective than neat PES membrane for H_2, CO_2, CH_4 gases. This behavior was related to the formation of voids around the zeolite crystals due to incompatibility between polymer and zeolite. With the addition of HMA (10% w/w) into PES/SAPO-34 membrane, while permeabilities decreased, the ideal selectivities showed 93%, 27%, 146% percent increase for H_2/CO_2, CO_2/CH_4 and H_2/CH_4 gas pairs, respectively. In addition to the enhanced membrane performance, Tg values changed with addition of HMA and remained constant with addition of SAPO-34, showing that third component

have a significant effect on the membrane morphology and transport properties. It was suggested that the Robeson trade-off curve would be overcome using suitable polymer-zeolite-additive and membrane formulation protocol.

These studies show that the poor interaction between polymers and zeolite particles which is one of the main problems in fabrication of high quality membranes can be reduced by low molecular weight additives into the formulation of MMMs. This information in zeolite literature lead to treatment of MOF incorporated mixed matrix membranes with low molecular weight additives in this study.

2.3 Metal Organic Frameworks (MOF)

Metal Organic Frameworks (MOFs) are new class of crystalline porous materials which are formed from metal containing nodes and organic bridges. Since they have geometrically and crystallographically well defined structures, diffraction methods can be used to characterize them easily. As being different from traditional porous materials, the structures and the properties of MOFs can be designed and tuned systematically. By the easy optimization in pore sizes and structures and also with their high surface areas, they have high potential to be used in specific applications. For instance they could be very suitable as adsorbent or membrane material for gas separation and storage applications [44], and there are some studies in literature using the MOF materials as membrane material.

Li et.al.[64] prepared ZIF-7 membranes on asymmetric alumina discs using first a seeding step and then the microwave assisted secondary growth step. The membranes were characterized by single and mixed gas permeation experiments of H_2, CO_2, CH_4, N_2 gases at elevated temperatures. In addition to intrinsic high H_2/CO_2 selectivity, they showed good thermal and hydrothermal stabilities. They concluded that MOF materials are very promising candidates for gas separation applications.

MOF-5 is one of the widely used metal organic framework due to its high surface area, large pore size and thermal stability [65,66]. For example, continuous and well-intergrown MOF-5 membrane was prepared by solvothermal synthesis on porous α-alumina supports. Liu et.al [66] claimed that since the adhesion between the MOF-5 crystals and support are strong enough to conduct the gas permeation experiments, there is no need to additional surface treatment in order to synthesize MOF-5 membranes. The permeation results for H_2, CH_4, N_2, CO_2 and SF_6 gases through MOF-5 membrane indicated that the diffusion of the gases follows the Knudsen diffusion behavior. In another study, secondary growth synthesis method was used after a seeding period for fabricating MOF-5 membranes. The quality of the membrane was investigated by using a molecule probing method in which many organic compounds with different sizes passed through the membranes, and the

pervaporation fluxes were measured. The fluxes indicated that the size of the largest void in the membrane is equal to the size of crystalline pores of MOF-5, which implies that MOF-5 membranes were fabricated as continuous and crack-free membranes [65].

2.3.1 Zeolitic Imidazolate Framework-8 (ZIF-8)

Zeolitic Imidazolate Frameworks (ZIFs) are new type of crystalline porous materials which is a subclass of MOFs [22]. They have a zeolite topology and combine the valuable properties of both zeolites and MOFs such as diversity of framework structure and pore systems, modifiable organic, bridging ligand, high surface area, high chemical and thermal stability [22]. Therefore, they have a great potential for usage in different application areas [23]; namely, gas storage and separation, catalysis, chemical sensing, construction of advanced nanotechnology devices [24]. Generally, divalent metal cations such as Zn and Co and N atoms of bridging imidazolate anions are bonded for ZIF production and M-Im-M (M=Co and Zn) bridges are constructed with a bond angle of 145^{o}.[25] This imidazolate linkers in ZIF framework increase the hydrophobicity of the material and provide a better interfacial property between the sieve and polymer matrix than aluminosilicate zeolites.[67]

ZIF-8 is a special type of ZIF compound with sodalite(SOD) topology. It has large pores of 11.6 A which is two times larger than SOD zeolites. The pores are accessible through small channels (3.4A) [25]. The structure of ZIF-8 can be seen in Figure 2.3 calculated using Materials Studio® software [68]. Another feature of ZIF-8 is its apparent thermal stability up to nearly 400 $^{\circ}$C. Also it has a high surface area of 1300–1600m^2/g [26] Especially, the ZIF-8 crystals in the range of nanometers have been used in -thin films with dual micro- and mesoporosity for selective adsorption and sensing of vapors, supported membranes with random and preferred crystal orientation for gas separation, capillary coatings for the chromatographic separation of alkanes, fabricating porous composite nanofibers by electrospinning [69]. It is expected that ZIF-8 nanoparticles yield better contact with polymer matrix and reduction in interfacial voids due to their large surface area [26].

A number of studies have been published reporting the synthesis of ZIF-8 crystals using different solvents (i.e. methanol, dimethyl formamide (DMF) [70], diethylformamide (DEF) [71], water [71, 72]) by solvothermal and rapid mixing methods. Synthesis temperatures have changed between room temperature and 140^{0}C, and the synthesis time was between 5 minutes [71] and 1 month [72].

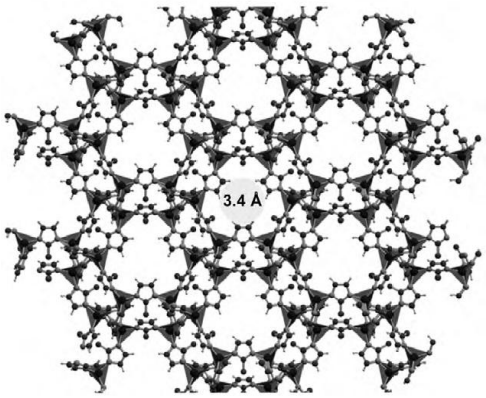

Figure 2.3 The calculated structure of ZIF-8 by Materials Studio® software [69]

Due to its wide range of potential applications, some studies aimed for production of nanometer sized ZIF-8 crystals and some investigations tried to control the crystal size. For example; Balkus *et al* synthesized ZIF-8 crystals using a solvothermal method at 140^0C for 6-8 hours by using DMF as the solvent [70]. They obtained 50 to 150 nanometer-sized crytals with a BET surface area of 1300 m^2/g so as to use in fabrication of mixed matrix membranes. They achieved the nanosized crystal synthesis by adding a base into the synthesis solution. Cravillon *et al* reported that the ZIF-8 crystals have been synthesized in 1 h in methanol at room temperature with 50 nm crystal size [69]. They controlled the ZIF-8 nano- and microcrystal formation by employing an excess of the bridging bidentate ligand and various simple auxiliary monodentate ligands with different chemical functionalities (carboxylate, N-heterocycle, alkylamine). Both the nanoscale and macroscale crystals exhibit good thermal stability in air and high surface areas. [65]. Venna *et al*.[27] reported synthesis of ZIF-8 in the presence of excess solvent (i.e.methanol) at room temperature. Structural evaluation of ZIF-8 was studied as a function of time and evaluation of the crystal size and extent of crystallinity were analyzed. After 1 hour synthesis period, 230 nm homogeneous ZIF-8 crystals were obtained with a BET surface area of 744m^2/g.

Another method in literature used for controlling the size of the crystals is changing the concentration of synthesis solution [73-76]. The main idea in this method is controlling the balance of kinetics of nucleation and growth [73, 74, 77]. For the zeolite synthesis, the rate of nucleation is higher than the growth rate in highly concentrated solutions and thereby, high concentrated solution medium results in smaller particle size and vice versa [74]. In one of the studies, zeolite A was synthesized with different water contents and very prominent changes were observed between the final particle size distributions, of which reason may be explained as when the water content is increased, the particle size is increased [78].

However for the MOF type materials, the trend is opposite to the zeolites, in which the more diluted systems cause higher nucleation rates, and thus crystals with smaller particle size are obtained. [76, 79, 80] Fernandez et.al reported the effect of the concentrations of the reactants on the particle size of MIL-101(Cr) crystals, and the lowest particle size was obtained from the most diluted system. In a study[76], three different water contents were used in the synthesis of chromium-benzenedicarboxylate, MIL-101, as 250, 400, 550 moles when all contents of other reactants and the reaction conditions were same, and the particle size for these contents were reported as 800, 400 and 200 nm respectively. Moreover, Gascon et.al [79] reported that, when coating the copper benzene tricarboxylate ,$Cu_3(BTC)_2$, on α-alumina supports, using a solvent as diluted as possible is important in order to have small crystals and controlled layer growth. The increasing amount of solvent in the system makes a more reducing effect on the crystal growth rates when compared with the nucleation rates. [76] In another study, Pan et.al [71] reported that varying such as the molar ratio of 2-methyl imidazole to zinc nitrate can reduce the particle size, but has little effect on the morphology. Highly crystalline ZIF-8 crystals were synthesized in a purely aqueous system at room temperature for only 5 minutes with a 85 nm crystal size. The crystal size reduced from 85 nm to 50 nm, when the 2-methyl imidazole/zinc nitrate ratio was increased from 70 to 200.

The adjustable pore sizes and group functionalities, low densities and unusually high surface areas of the MOFs make them attractive materials for many applications especially for CO_2 separation and storage [81]. In gas permeation mechanism (solution-diffusion) of dense membranes, adsorption, diffusion and desorption are three important steps [1]. In mixed matrix membrane applications, the adsorption capacities and the contents of the filler materials are important parameters for the permeation performances of the membranes [28, 29]. Recently, there are numerous studies in literature investigating the CO_2 adsorption characteristics of MOFs experimentally and theoretically. They reported much higher adsorption capacities of CO_2 on different types of MOFs than those of the conventional adsorbents such as activated carbons and zeolites [82], which are tabulated in Table 2.1.

Table 2.1 CO_2 Adsorption Capacities of Different types of MOFs [82]

MOF Type	**Adsorption Capacity**	**Operation Pressure**	**Operation Temperature**
MOF-5	92.4 mgCO_2/g	1.0 bar	296 K
Cu-BTC	616 mgCO_2/g	NA?	NA
MOF-177	1496 mgCO_2/g	43 bar	NA
MIL-101	1760mgCO_2/g	50 bar	303K

As it is mentioned above those ZIFs have a related topology to zeolites with an exceptional thermal and chemical stability [22]. The M-Im-M bond in the structure of ZIFs is analogous to Si-O-Si units

in zeolites, but it is longer. Hence the pore volume is also larger [81]. Larger pore volume and pore size in the nanometer range result in a likely high adsorption capacity [72, 83, 84]. Pérez-Pellitero et.al [81] reported the N_2, CH_4 and CO_2 adsorption characteristics determined by both experimentally measurements and molecular simulations for two zeolitic imidazolate frameworks, ZIF-8 and ZIF-76. It is clearly seen from Figure 2.4 that the experimental results for N_2, CH_4 and CO_2 adsorptions on ZIF-8 were coinciding with the simulation results. While the highest adsorption capacity of ZIF-8 belonged to CO_2, the adsorbed amounts for all three gases were sharply increasing with increasing pressures, (i.e. when the pressure was raised to 10 bar from 1 bar, the adsorbed CO_2 amount was increased nine fold).

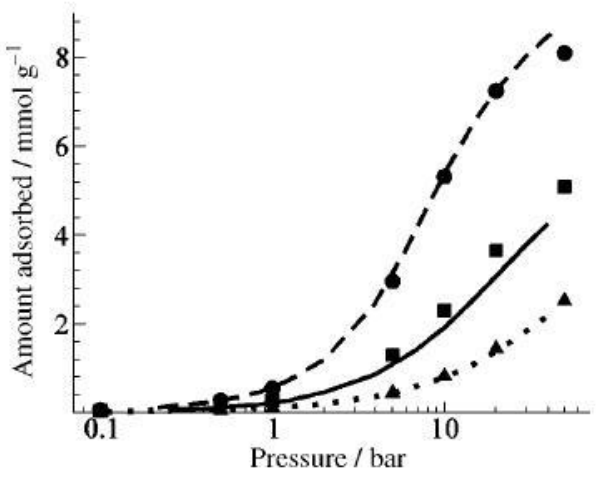

Figure 2.4 Comparison of experimental N_2, CH_4 and CO_2 isotherms in ZIF-8 at 303 K with the simulation results obtained with the optimized force field. The experiments are denoted by lines (·····N_2, ——CH_4, – – – CO_2) and the simulations by symbols (▲ N_2, ■ CH_4, and ● CO_2) [Ref 81].

In another literature study, Zhou et.al [83] studied on three types of adsorption isotherms (absolute, excess, effective) of H_2 and CH_4 in ZIF-8 over a large temperature (30-300 K) and pressure (up to 65 bar) range. Amount of adsorbed H_2 and CH_4 in ZIF-8 was directly proportional to the pressure at each operational temperature, while there was an inverse proportion between adsorption and temperature (Figure 2.5). Moreover, it was reported that the adsorption and desorption process for ZIF-8 was completely reversible with no hysteresis, indicating a fast adsorption/desorption process. This is a very useful characteristic for a material in practical gas storage applications which observed in porous materials with large surface area.

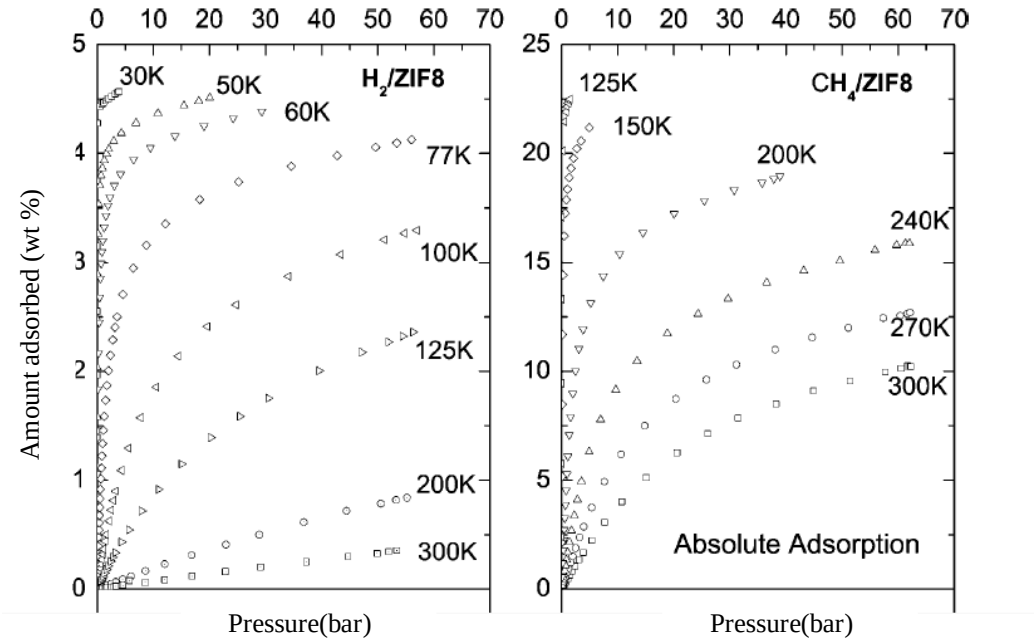

Figure 2.5 Absolute adsorption isotherms of H_2(left) and CH_4(right) in ZIF-8 over a broad pressure and temperature range[83].

In literature, the number of ZIF-8 membranes used in gas separation applications has been increased rapidly due to their promising molecular sieve performances. For instance, Venna et.al [30] prepared tubular alumina supported ZIF-8 membranes and reported the gas separation performance of the membranes for CO_2/CH_4 gas pair. The CO_2 permeances of the membranes were evaluated as unprecedented with a maximum value of ~2.4×10^{-5} mol/m^2 · s · Pa and the selectivities were reported between 4 and 7, which is comparable with the literature.

McCarty et.al.[86] reported a method for ZIF film and membrane fabrication based on surface modification of porous supports with organic ligands. This method promotes the heterogenous nucleation and film growth owing to resultant strong covalent bonds between the supports and imidazolate ligands. The fabricated ZIF-8 membranes using this method indicated a molecular sieving behavior with an ideal selectivity for H_2/CH_4 of 13.

In another study [87], ZIF-8 membranes were used to separate the ethene/ethane mixtures with equimolar ratio, at room temperature, and for feed pressures of 1 and 6 bar where the selectivities were obtained as 2.8 and 2.4, respectively. Sorption uptake studies for ethene/ethane mixture were conducted on a large ZIF-8 crystal in order to explain the reason of ethene selectivity, and the results indicated that the preferential ethane adsorption selectivity competes with the preferential ethene

diffusion selectivity in ZIF-8 crystals. In other words, while the ethane adsorps stronger than ethene, ethene diffuses faster and compensates the adsorption of ethane.

Moreover, ZIF-8 membranes prepared by hydrothermal seeded growth method were reported to have excellent performances for separation of propylene/propane binary mixtures with varying feed compositions. The propylene/propane separation performance of the membrane surpassed the upper-bound trade-off line with a propylene permeability of 200 Barrer and propylene/propane separation factor of 50. Furthermore the ZIF-8 membranes were reported to have long-term and thermal stability. The membrane fabrication procedure was evaluated as highly reproducible and economical compared to conventional cryogenic distillation [88].

2.4 MOF Based Mixed Matrix Membranes

Metal-organic frameworks (MOFs) are another class of porous materials that has been employed in MMMs. It is expected to have an improved interaction between the MOF particles and polymer due to the functional groups of the organic ligands and the metal ions in MOF structures. Moreover the percentage loading of MOF particles in polymer matrix can be increased easily due to the better polymer/particle interfacial contact.[70] There are limited number of examples for MOF incorporated mixed matrix membrane applications in literature as a new developing filler type[11-14] of which performance results are tabulated in Table 2.2.

Adams et.al [44] suggested that MOFs are attractive alternatives to the zeolites to be used in MMM applications due to their infinite number of possible structures. They were synthesized copper and terephthalic acid (CuTPA) incorporated poly(vinyl acetate)(PVAc) mixed matrix membranes, and characterized its gas transport properties. The CuTPA loading was kept constant at 15% (w/w) and the permeation experiments were performed for the pure gases of He, N_2, O_2, CO_2, CH_4. Both the permeabilities of all gases and ideal selectivities of all gas pairs showed an improvement when compared to the pure PVAc membranes. Moreover, they reported that the CuTPA incorporated MMM were free of interfacial voids.

Perez et.al [11] used metal organic framework-5(MOF-5) with 100 nm in size and high surface area(3000m^2/g) as filler material in fabrication of Matrimid/MOF-5 mixed matrix membranes. For 30% MOF-5 loaded MMM, the permeabilities of the gases increased 120%, while the selectivities remained constant compared to pure Matrimid despite the high surface area of MOF-5 crystals. Constant selectivities were explained by the lack of non-selective voids due to high affinity between the polymer matrix and MOF-5 nano-particles. This high affinity increased the plastic deformation of the polymer and polymer veins were formed. Moreover, MOF-5 crystals cannot be dispersed in the

polymer completely due to the stronger interaction between the nanoparticles than with the polymer which inclines the formation of cavities in the polymer matrix upon freeze fracture.

The particle size of filler material is also an important factor in determining the gas transport properties of the mixed matrix membrane. Bae et.al [12] used three different types of polymers and ZIF-90 crystals with two different sizes for fabricating MMMs. The synthesis of submicrometer sized ZIF-90 crystals was introduced by nonsolvent-induced crystallization method. Then, using Ultem, Matrimid and 6FDA-DAM as polymer matrices, nanocomposite membranes were prepared with a 15% of ZIF-90 loading. While the CO_2 permeabilities of the Ultem and Matrimid membranes enhanced very significantly, the CO_2/CH_4 selectivities remained nearly constant. The observed constant selectivity was explained by the mismatch between the permeabilities of filler material and polymer matrices by the Maxwell model predictions. While the estimated CO_2 permeability of ZIF-90 is about several thousand Barrer, the ones of Matrimid and Ultem 10 and 1 Barrer, respectively. However for the third polymer matrice (6FDA-DAM) with higher CO_2 permeability (390 Barrer), the performance of the membrane were enhanced substantially with ZIF-90 addition. With a 1.8 times enhancement in CO_2 permeability, the CO_2/CH_4 mixed-gas (with a 1:1 pressure ratio) selectivity was increased from 24 to 37 and the membrane exceeded the upper bound trade-off curve. That was assessed as the consequence of well match in terms of permeabilities between the polymer and MOF and also defect-free membrane morphology. Moreover, so as to investigate the effect of filler size on the performance of membrane, two different sized ZIF-90 crystals were used, and better results were reported for membranes containing smaller particle.

As well as the intrinsic properties of polymer and the filler, the interaction between these two phases, also the percentage of filler loading in the membrane has an important effect on the permeability of a gas through MMM [89]. Figure 2.6 indicates the effect of MOF loading on the permeability and selectivity of MMMs. The transport properties of the polymeric membranes are not affected in an important way for the loadings lower than a certain value. The optimum MMM performance can be obtained with a good dispersion of filler in the polymer matrix without any interfacial defects. The filler particles cannot be surrounded by the polymer chains completely at higher loadings and some undesirable voids can be formed. Moreover, high amounts of filler particles may disrupt the polymer chain packing, thereby increase the free volume of the polymer [84]. There are some examples in literature examining the effect of MOF loading on MMM performance, which were aimed to utilize the separation advantages of the filler material more efficiently. For instance; MOF-5 crystals were incorporated into Matrimid matrix with different amount varying between 10-30wt. % and they showed that the 30wt. % MOF-5 loaded membrane has the best MMM performance [11].

Table 2.2 Ideal selectivities of MOF incorporated mixed matrix membranes in literature [11, 12, 13, 44, 70, 92]

REF.	Membrane Materials			Ideal Selectivities		
	Polymer	MOF	Loading (% w/w)	H_2/CO_2	CO_2/CH_4	H_2/CH_4
Perez et.al (2009) [11]	Matrimid	MOF-5	0	2.71	41.7	113.0
			10	2.69	51.0	137.4
			20	2.78	40.5	112.0
			30	2.66	44.7	120.0
Bae et.al (2009) [12]	Matrimid	ZIF-90	0	-	35	-
			15	-	35	-
	Ultem		0	-	38	-
			15	-	39	-
	6FDA-DAM		0	-	17	-
			15	-	27	-
Ordonez et. al (2010) [70]	Matrimid	ZIF-8	0	3.03	39.84	120.80
			20	3.46	51.06	176.68
			30	3.33	38.22	128.10
			40	2.96	27.84	80.77
			50	3.82	124.89	471.88
			60	4.43	80.77	356.93
Adams et.al (2010) [44]	PVAc	CuTPA	0	-	34.9	-
			15	-	40.4	-
Yang et.al (2011) [13]	PBI	ZIF-7	0	8.7	-	-
			10	12.9	-	-
			25	11.9	-	-
			50	14.9	-	-
Diaz et.al (2011) [92]	PPEES	ZIF-8	0	1.4	22.9	31.6
			10	2.2	29.5	64.8
			20	1.8	24.1	43.5
			30	1.9	20.8	38.5

Moreover, Zornoza et.al [85] prepared PSF (polysulfone)/NH_2-MIL-53 membranes with changing NH_2-MIL-53 concentrations as 8, 16, 25, 40wt. % and they reported the optimum filler loading for best performance as 25wt. %. Cu-BPY-HFS (Cu-4,4' bipyridine-hexafluorosilicate) was used as filler material in fabrication of Matrimid/ Cu-BPY-HFS MMMs which were characterized by H_2, CO_2, CH_4, O_2, N_2 single gas permeation experiments. The filler loading in the membrane was changed between 10 and 40 wt. % and 20 wt. % is reported as the optimum filler loading for this MMM materials [91].

Yang et.al [13] reported the gas separation performances of mixed matrix membranes fabricated using zeolitic imidazolate framework-7 (ZIF-7) nanocrystals and polybenzimidazole(PBI) with three different compositions. The gas permeability of H_2 showed a significant improvement with the addition of increasing amount of ZIF-7. Comparing to the pure PBI membrane, while H_2 permeability increased from 3.7 to 26.2 Barrer for a composition of 50/50 (w/w) ZIF-7/PBI, the H_2/CO_2 ideal selectivity was almost doubled. That superior performance was evaluated as the result of strong chemical interaction between ZIF-7 surface and PBI, minimal non-selective voids and rigidified PBI chains on ZIF-7 nanocrytals. Moreover, they investigated the temperature effect on the membrane performance with binary gas experiments between room temperature and 180°C. With the effect of increasing temperature, H_2 permeabilities showed a raise without any improvement in H_2/CO_2 separation factors. The ideal selectivity results for all reference studies can be seen in Table 2.3.

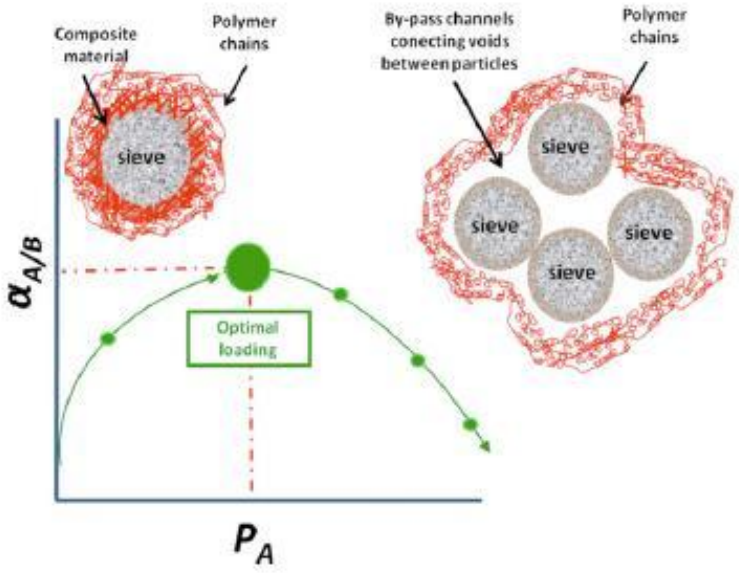

Figure 2.6 Selectivity versus permeability of a MMM at increasing filler loading [90]

Since most of the MOFs have flexible structures, the operation pressure may have an important influence on the adsorption characteristics of them. The effect of transmembrane pressure on CO_2/CH_4 separation performance of MOF based MMMs was investigated by changing the pressure between 2 bar and 13 bar. Amino functionalized MIL-53(Al) (NH2-MIL-53) was incorporated as filler material in PSF Udel_ P-3500 polymer up to a loading of 40 % w/w. Figure 2.7 shows the separation performances of different PSF/NH_2-MIL-53 membranes with that of PSF membrane for 1:1 CO_2/CH_4 mixture as a function of pressure. The separation factors were increasing while the CO_2 permeabilities were decreasing as a function of transmembrane pressure. They reported that the selectivity improvement is a consequence of intrinsic flexibility of MOF filler. In other words, the adsorption capacity of MOF becomes more prominent with the effect of pressure [85].

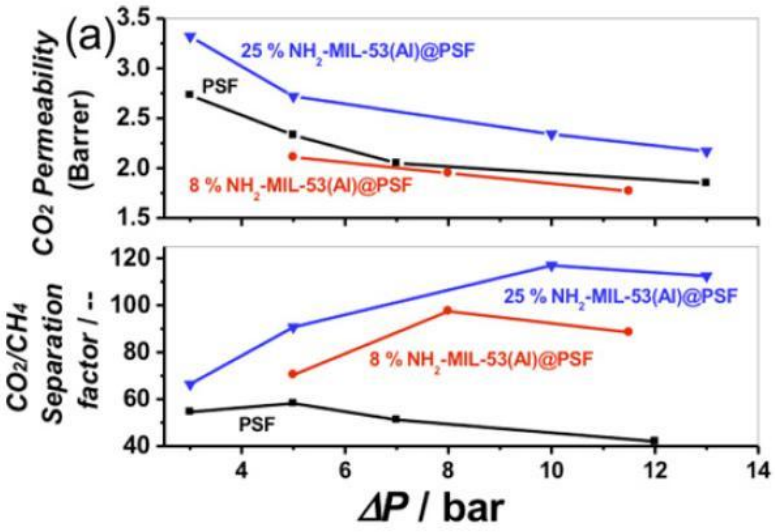

Figure 2.7 Separation performance of PSF/NH_2-MIL-53 membranes for 1:1 CO_2/CH_4 mixture a a function of pressure @ -10^oC [85]

2.4.1 ZIF-8 Based Mixed Matrix Membranes

There are few studies in literature investigating the gas transport properties of ZIF-8 filled MMMs [14, 70, 93, 94]. In the study of Basu et.al [14] three different types of MOFs ([Cu_3(BTC)$_2$], ZIF-8 and MIL-53(Al)) were used to prepare dense and asymmetric Matrimid membranes for separating binary gas mixtures. While the filler particles dispersed in the polymer matrix successfully in dense membranes, sealing method was used with PDMS coating in asymmetric membrane preparation so as to prevent the formation of non-selective voids. The permeability and selectivity of gas pairs CO_2/CH_4 and CO_2/N_2 showed an improvement with increasing filler loadings for dense membranes.

Also the mechanical properties of the dense membranes filled with [$Cu_3(BTC)_2$], ZIF-8 and MIL-53(Al) were improved with increasing loading. However in the asymmetric membranes, the improvements were changing from gas to gas and MOF to MOF according to the interactions between the gas molecules and the MOF particles.

Ordonez et.al [70] used ZIF-8 crystals with a particle size of 50- 150nm in order to fabricate Matrimid/ZIF-8 mixed matrix membranes with different ZIF-8 loadings up to 80 % (w/w). The permeability values for the pure gases of H_2, CO_2, O_2, N_2, CH_4, C_3H_8 and the gas mixtures of H_2/CO_2 and CO_2/CH_4 were increased to 40%(w/w), but they decreased for the 50%(w/w) and 60%(w/w) loadings. The ideal selectivities for the gas pairs containing small gases showed a substantial increase for the high ZIF-8 loaded membranes (50%(w/w) and 60%(w/w)) that was accepted as the indicator of a transition from a polymer-driven to ZIF-8 controlled gas transport process. The 80% (w/w) ZIF-8 loaded mixed matrix membrane could not be tested for permeability due to the loss in mechnical strength and flexibility.

Moreover, Diaz et.al [93] used PPEES (poly(1,4-phenylen ether-ether-sulfone)) as polymer material and prepared hybrid membranes with 10, 20 and 30 % w/w of ZIF-8 crystals with a particle size of 4.9 μm. The incorporation of 10 % w/w ZIF-8 crystals into the polymer increased both the permeabilities and ideal selectivities for H_2, CO_2 and CH_4 gases at 30^{o}C and ideal selectivities for H_2/CO_2, CO_2/CH_4 and H_2/CH_4 gas pairs. However, when the amount of crystals in the membrane raised to 20 and 30 % w/w, the ideal selectivities started to decrease for all gas pairs (given in Table 2.3). While the performance of a membrane is defined as the closeness of its selectivity to the Robeson's upper bound, the increasing ZIF-8 content improved the gas separation performances of the MMMs.

An important step in MMM fabrication procedures is the dispersion of filler particles in polymer solution especially for high filler loadings to get non-defected membrane morphologies. In order to prevent the particle aggregation in polymer matrix, some additional techniques may be required such as using surfactants or salts, and the most widely used one, ultrasonication. Thompson et.al [94] suggested to use two different ultrasonication method during Matrimid/ZIF-8 membrane fabrication; direct and indirect sonication for dispersing the ZIF-8 nanocrytals in polymer matrix. They reported that the direct sonication with high intensity ultrasonication prevented the aggregation of the ZIF-8 nanocrystal during membrane synthesis. Moreover the gas permeation data and Maxwell predictions indicated that these membranes have a defect-free microstructure. The use of indirect sonication caused the formation of voids in the regions of ZIF-8 aggregates, and while the permeabilities were increased, the selectivities decreased.

Moreover, Shi et.al [95] prepared ZIF-8 filled PBI MMMs containing different ZIF-8 contents to be used in pervaporation dehydration of ethanol, isopropanol (IPA) and butanol. The results showed that with the incorporation of 33.7 wt% ZIF-8 in PBI membrane, water permeability increased four times without a significant loss in water selectivity. While the percent weight of ZIF-8 in the membrane was increased to 58.7 wt% , very high water permeability was observed with a relatively low selectivity.

In addition to the studies reporting dense MMM membranes containing ZIF-8 crystals, Dai et.al [96] prepared mixed matrix asymmetric hollow fiber membranes by using ZIF-8 as filler phase. Ultem 1000 was used as polymer matrix and membranes were prepared by the dry jet-wet quench method as a dual layer composite. These membranes of which outer layers contain 13 wt. % ZIF-8 were tested at different operation temperatures and pressures for a variety of gas pairs and successful permeation results were reported for especially CO_2/CH_4 mixture. The CO_2/CH_4 selectivity was increased from 30 to 36 with the 13 wt% ZIF-8 addition to the pure Ultem hollow fiber membrane.

The literature studies stated up to now imply that ZIF-8 is a challenging filler material to be used in MMM applications due to its desirable properties and high adsorption capacity especially at high pressures. Matrimid is the mostly used polymer in dense MMM studies and generally the permeation experiments were conducted at low feed pressures. Moreover, there is not any example for ZIF-8 filled ternary MMM applications in literature. These information lead to preparation of ZIF-8 filled ternary MMMs using PES as polymer matrix and HMA as LMWA and conducting the permeation experiments at high transmembrane pressures to investigate the characteristics of membranes.

2.5 Separation of Binary Gas Mixtures

Single gas permeation experiments are performed usually so as to characterize the membranes. It is beneficial to get a general idea about the performance of the membranes, but it is not sufficient to predict the detailed permeation behavior of a mixture through the membrane. Because, the permeation property of one component in gas mixture can be affected by any other component or by any interaction between one component and polymer matrix [97-99]. Especially for industrial applications it is a must to investigate the permeation characteristics of the membrane materials for binary or multicomponent gas mixtures [97, 98].

The CO_2/CH_4 binary gas mixture is a critical pair due to natural gas purification applications [100]. There are several polymeric membrane studies in literature comparing the binary and single gas separation performances [100-104]. For instance, while the CO_2/CH_4 binary selectivity of pure PI-TPI membrane at 50/50 % v/v feed composition reported as higher than ideal selectivity [100], in the case of pure PC membrane the relationship is completely reverse [102]. These variations are attributed to

the plasticization phenomena, the competition between the penetrants, concentration polarization, and non-ideal gas behavior [105, 106]. Moreover for PES membrane no difference is observed between the ideal selectivity and mixed gas selectivity for CO_2/CH_4 gas pair which is explained by the non-interactive permeation of gases through the membrane [101]. As an example for binary gas separation through polymeric membrane, Tin et.al [106] explored the performance of Matrimid membranes for a feed gas mixture contains 40% of CO_2 in CH_4. The obtained mixed gas selectivities are lower than the ideal selectivities which is explained by the reduced CO_2 solubility coefficient and thereby permeability in the presence of CH_4 due to the competition in occupying the unrelaxed volume. The solubility coefficient of CH_4 is also reduced owing to same reason, however the CO_2 in the medium increases the CH_4 diffusivity and CH_4 transport is facilitated.

The complex structure and the sorption properties of filler materials may lead to different effects on the mixture permeation characteristics of MMMs [21]. There are fewer studies investigating the mixture permeation properties of MMMs in literature [40, 42, 101]. Çakal et.al [21] investigated the effect of feed composition on the separation performances of binary and ternary membranes prepared using the PES/SAPO-34/HMA materials for CO_2/CH_4 gas mixtures with a CO_2 composition varying between 0 and 100 %. They reported that the separation performances of all types of membranes are independent of feed composition which is accepted as an advantage in practical applications. Moreover they found that the separation factors are lower than the ideal selectivities of neat PES and PES/ZIF-8(%20) membranes for a 50/50 % (v/v) CO_2/CH_4 mixture.

Şen et.al [42] prepared binary and ternary MMMs using the PC/zeolite 4A/pNA materials with different compositions, and investigated the binary permeation properties of the membranes for CO_2/CH_4 gas mixture. Also the effect of CO_2 composition in the mixture was analyzed. They reported that the separation factors were around the ideal selectivities for pure PC and PC/pNA membranes regardless of the feed gas composition, suggesting that the presence of a second gas did not affect the permeation properties of these dense homogenous membranes. PC/zeolite 4A and PC/zeolite 4A/pNA membranes behaved in a different way with respect to CO_2 composition in feed mixture, in which the separation factors were decreased with increasing CO_2 concentration in feed mixture owing to its high sorption property in membrane matrices and all the separation factors were lower than the ideal selectivities. They reported that, the reduction observed in ternary membranes was sharper than the binary membranes because the pNA changed the MMM morphology and the interaction between gases and the matrix. Also, Battal et.al [101] investigated the separation properties of PES/zeolite 4A MMMs for H_2/CH_4 gas pair and they concluded that, the separation selectivies were decreaased with increasing CH_4 composition in feed mixture.

There are also some studies which investigate the separation performances of MOF-based MMMs for CO_2/CH_4 gas mixtures. Nik et.al [107] prepared MMMs using 5 different types of MOFs with a 25 % w/w loading and investigated the separation characteristics of the membranes for CO_2/CH_4 mixture with a 1:1 molar ratio. The ideal selectivities and the separation factors obtained for different membrane compositions were tabulated in Table 2.3. They reported that the ideal selectivities are higher than the separation factors for all types of MOF-based MMMs which was evaluated as an expected behavior. In the presence of a second gas, the gases may interact to each other or to membrane material which resulted in the variations in the permeability and the selectivity values. In an abovementioned study [12], 6FDA-DAM/ZIF-90 (15 wt%) mixed matrix membranes were characterized for separation of both single gases and binary gas mixtures. The separation selectivity of CO_2/CH_4 measured by a gas mixture with a 1:1 molar ratio was higher than the ideal selectivity of which reason was explained by the selective sorption and diffusion of CO_2 in the ZIF-90 crystals.

Table 2.3 Ideal selectivities and the separation factors for CO_2/CH_4 gas system [107]

Polymer	MOF (loading% 25wt.)	CO_2/CH_4 Ideal sel.	CO_2/CH_4 Sep.factor
6FDA-ODA	-	44.1	41.7
	UiO-66	46.1	42.3
	NH_2-UiO-66	51.6	44.7
	MOF-199	51.2	50.7
	NH_2-MOF-199	59.6	52.4
	UiO-67	15	15

Balkus et.al [70] reported binary gas separation data for H_2/CO_2 (50:50 mol%) and CO_2/CH_4 (10:90 mol%) of Matrimid/ZIF-8 membranes with loadings of 50% and 60% ZIF-8. The observed variations between the ideal selectivities and the separation selectivities were presumed to be results of penetrant competition, plasticization of the polymer, and gas polarization. Since both small gas molecules can diffuse through the aperture of ZIF-8, there is no competitive adsorption for H_2/CO_2 gas pair, hence ideal and separation selectivity are closed to each other. On the other hand, an increase in separation selectivity was expected for CO_2/CH_4 gas pair due to faster diffusion of smaller molecule, but the ideal selectivities were higher than separation ones. This behaving was elucidated with the pore aperture blockage of ZIF-8 crystals by CH_4 molecule which is larger in size and higher in concentration than CO_2.

In another mentioned literature study [11], Matrimid/MOF-5 membranes were characterized for separation of binary mixtures; CH_4/N_2 (94:6, 50:50 mol %), H_2/CO_2 (75:25, 50:50, and 25:75 mol %) and CO_2/CH_4 (50:50 and 10:90 mol %) at 35˚C with a feed pressure of 2.7 bar to investigate the effect of feed composition. While the separation selectivity of H_2/CO_2 did not change with CO_2 feed ratio, CO_2/CH_4 separation selectivity decreased with increasing CO_2 feed concentration from 10 to 50%. These phenomena were explained by the competition between the gases for the fixed free volume of the polymer and the high solubility of CO_2 in the membrane. Since the solubility of CH_4 in membrane was reduced with the effect of high CO_2 solubility, it was transported through the membrane by mostly diffusion, which enhanced by the porosity of MOF-5 crystals. Moreover, addition of MOF-5 crystals reduced the sorption sites in polymer which decreased the CO_2 permeability.

The literature studies show that membrane systems behave differently in mixture separation applications. The mixture separation performances of the membranes may depend on different parameters as material combinations in membrane composition, filler loading, operation temperature and pressure, etc. In this study, the binary gas separation performances of selected membranes were investigated for CO_2/CH_4 mixture at two different feed pressures.

CHAPTER 3

EXPERIMENTAL AND COMPUTATIONAL METHODOLOGY

3.1 ZIF-8 Preparation

3.1.1 Materials for ZIF-8 Preparation

Zinc nitrate tetrahydrate [$Zn(NO_3)_2 \cdot 6H_2O$, 98% purity] and 2- methylimidazole [Hmim, 99% purity] were purchased from Acros and Sigma–Aldrich, respectively, and used as purchased. Methanol [MeOH, 98% purity] was purchased from Sigma-Aldrich and used as received.

3.1.2 ZIF-8 Preparation Methodology

In typical synthesis, 2.4 g of zinc nitrate hexahydrate was dissolved in 90.4 g methanol. Another solution was prepared with 5.28 g of 2-methyl imidazole and 90.4 g of MeOH. These two solutions were then mixed rapidly and synthesis was completed stirring for 1 hour at room temperature to give a mixture with molar composition of Zn^{+2}: 7.9Hmim: 695.1 MeOH[27].

Table 3.1 Synthesis parameters employed for the preparation of ZIF-8 crystals.

Sample Codes	Zn^{2+}	Hmim	MeOH
ZIF-8.1	1	7.9	1043
ZIF-8.2	1	7.9	695
ZIF-8.3	1	7.9	528
ZIF-8.4	1	7.9	348
ZIF-8.5	1	7.9	174
ZIF-8.6	1	7.9	867

In order to investigate the effect of methanol amount on particle size MeOH/Zn^{2+} was varied in the 87-1043 range (Table 3.1). The product was collected by centrifugation at 6000 rpm and washed with MeOH for two times. The ZIF-8 powder was dried at 80^{o}C overnight.

3.1.3 Recycle of MeOH

The mother liquor was reused for the subsequent ZIF-8 synthesis upon the crystalline product was collected by centrifugation from the synthesis solution. ZIF-8 synthesis through the recycling process was conducted based on the several assumptions relating the reaction kinetics;

1. High amount of initial Hmim remains unused in the solution based on the overall reactions for the formation of ZIF-8 with a molecular formula of $Zn_6N_{24}C_{48}H_{60}$ [108]
2. $Zn(NO_3)_2$ was assumed as a limiting reactant and both consumed amount and the initial amount of $Zn(NO_3)_2$ was added to the mother liquor for subsequent synthesis in different routes. (For Route C)
3. It is assumed that the ZIF-8 formation may be precluded by the disruption of ionic balance of reaction medium in the presence of formed H^+ and NO_3^- ions [22] as well as the unreacted species. Therefore the ion concentrations should be preserved by additional treatment.

Three different procedures were carried out for recycling of the mother liquor which was detailed in Figure 3.1. In procedure A, one-day aged mother liquor was reutilized to synthesize ZIF-8 crystals by adding only the initial amount of Zn^{+2}. However, in procedure B, firstly the pH of the mother liquor was increased approximately from 7.0 to 9.0 by adding NaOH, after 1 h stirring ZIF-8 powders were recovered upon centrifugation. Then, consumed amount of Zn^{+2} was added into the second mother liquor and ZIF-8 crystals were extracted by centrifugation from the solution after 1h synthesis. In procedure C, the same steps with procedure B were followed, but initial amount of Zn^{+2} was added. The third mother liquor was aged for 1 day and all same procedures were applied for further synthesis. The addition of different amount of Zn^{+2} for procedure B and C caused the change in synthesis solution composition significantly. The powder codes and compositions are given in Table 3.1.

3.1.4 Characterization of ZIF-8

Phase identification of the solid products was made by Philips model PW1840 (1729) X-ray diffractometer using Ni filtered Cu-Kα radiation at a scan rate of 0.05 ^{o}/sec. The voltage and current were 30 kV and 24 mA, respectively. The area under the curve of the highest peaks corresponding to

the planes (011), (112) and (222) were used to determine the relative crystallinities of powders while ZIF-8.6 was assigned the reference with 100%. The percent yield of ZIF-8 was calculated based on maximum amount of ZIF-8 that can be handled in the situation that all the Zn^{+2} source is consumed in the synthesis solution. The N_2 adsorption-desorption isotherms were obtained using Quantochrome Corporation Autosorb-1-C/MS equipment at 77 K at using liquid nitrogen. Before these measurements, the ZIF-8 samples were degassed at 135°C for 24h under the vacuum. The surface area was calculated using the Brunauer–Emmett–Teller (BET) equation. Morphology and crystal size were determined by using a QUANTA 400F Field Emission series scanning electron microscopy (SEM). The crystal shape and the sizes were also determined by using a FEI 120kV HCTEM series transmission electron microscopy (TEM). TGA (DTG-60H, Shimadzu) was used to determine the thermal behavior of the ZIF-8 crystals where the samples were heated at a rate of 10°C/min up to 600°C in air. Dynamic light scattering (DLS) was used to determine the particle size distribution of the ZIF-8 crystals (Mastersizer 2000, Malvern). The samples were dispersed and diluted with methanol before the DLS experiments.

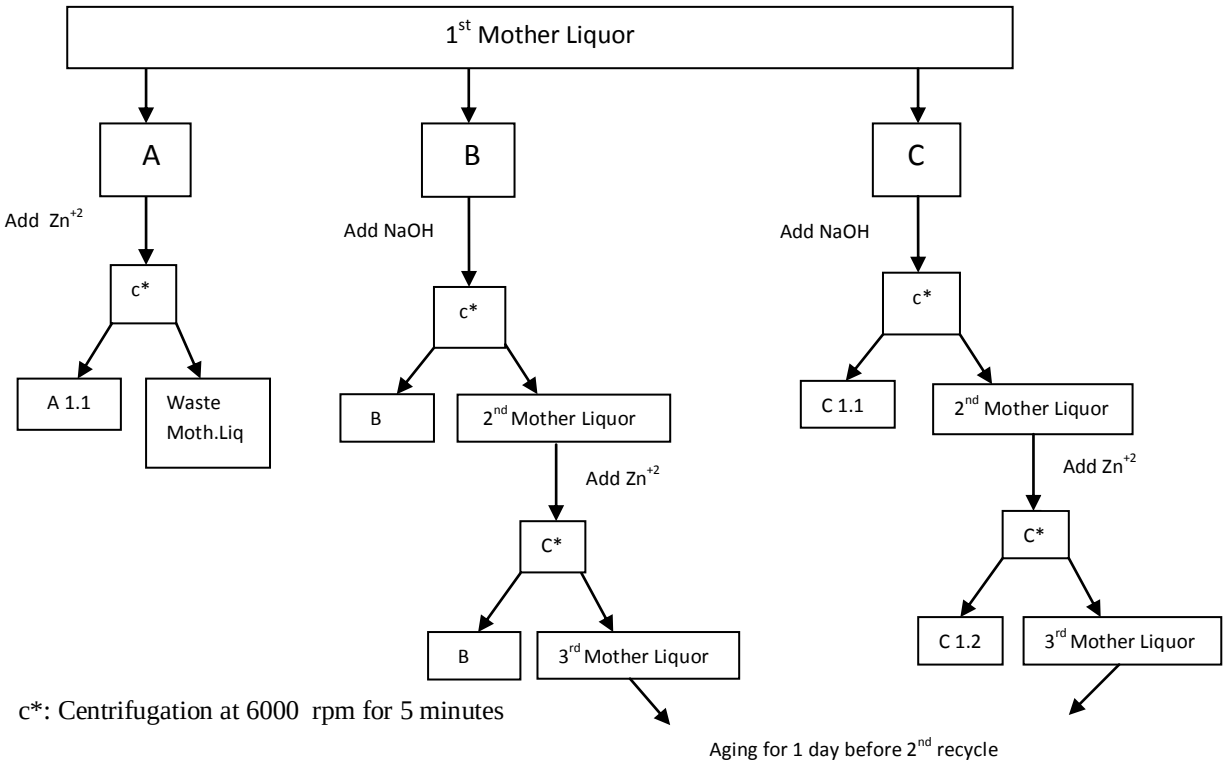

Figure 3.1. Schematic representation of recycle of mother liquor

Turbidity measurements were performed in-situ during the synthesis of ZIF-8 nanocrystals (JENWAY 6035) to determine the formation rates as a novel and reliable technique for ZIF-8 crystallization. Turbidimeter was calibrated by using ZIF-8 solutions with various concentrations in MeOH before the measurements, the concentration that coincided with turbidimeter maximum value was assigned to 100 NTU even the reactions are not terminated. Although this limitation prevented to detect further increase in turbidity during the progress of reactions but gave an insight for the determination of the formation rates. All experiments were repeated two times and almost same turbidity values were obtained. Induction time was estimated from the turbidity vs. time graph by taking time to corresponding to intersection of the two tangential lines.

3.2 Membrane Preparation

3.2.1Materials for Membrane Preparation

The morphology and the transport properties of mixed matrix membranes are strongly related to the types of polymer, solvent, filler material and the additives used in fabrication. Polyethersulfone (PES) was used for membrane preparation which is a commercial Radel A-100 grade provided by Solvay. It is commercially attractive due to its high chemical resistance, stability to oxygen and thermal degradation [5]. The glass transition temperature (Tg) and weight average molecular weight of the polymer (PES) are 220^0C and 53,000, respectively. The repeating unit of polyethersulfone is shown in Figure 3.2 (a). Its gas transport properties lie near the upper bound line on the middle region of Robeson's plot for attractive gas pairs like CO_2/CH_4, H_2/CH_4. The numbers for these gases were reported as 5.85 and 2.61 Barrer for H_2 and CO_2 permeabilities, respectively, and 53.66 and 23.95 for H_2/CH_4 and CO_2/CH_4 selectivities[101].

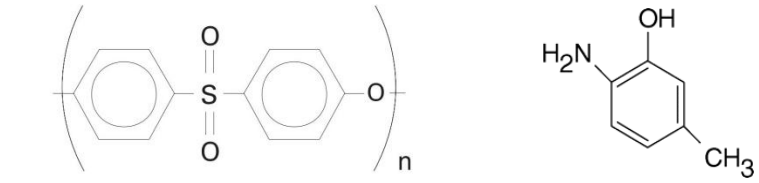

(a) (b)

Figure 3.2 (a) Repeating unit of PES, (b) the chemical structure of HMA

Dimethylformamide (DMF), obtained from Lab-Scan Analytical Sciences, was used as solvent due to its strong dissolving power for many components. It has the chemical formula of C_3H_3ON, and boiling point of 153^0C. The filler ZIF-8 was synthesized in this research. 2-hydroxy 5-methyl aniline, HMA, was used as low molecular weight additive in membrane preparation. It was purchased from Aldrich

and it did not require any treatment before using in membranes. Figure 3.2 (b) shows the chemical structure of 2-hydroxy 5-methyl aniline which has the chemical formula of C_7H_9NO and melting point of 140^0C.

In order to focus on the effect of ZIF-8 on the membrane performance, PES, DMF, HMA are considered to be used in membrane preparation which were selected and used in previous studies of our research group [40, 43] owing to their desirable properties.

3.2.2 Membrane Preparation Methodology

Solvent-evaporation method was used for preparation of the membranes throughout the study. PES and ZIF-8 were dried at 80^0C and 180^0C overnight before using in the membrane synthesis. Three different types membranes were prepared in this study, pure PES, PES/ZIF-8 and PES/ZIF-8/HMA membranes with different ZIF-8 and HMA contents. PES concentration in DMF, 20 w/v %, was kept constant for all membranes. Only the solution preparation steps are different for these three types of membranes. The amounts of materials used in membrane preparation for all compositions are tabulated in Appendix A.

3.2.2.1 Pure PES Membrane Solution Preparation

Overnight dried PES was added into the solvent DMF step by step in order to prevent a sudden increase in the viscosity of solution and thereby to ease the stirring. Then, the solution was stirred for overnight by a magnetic stirrer.

3.2.2.2 PES/ZIF-8 Membrane Solution Preparation

Overnight dried ZIF-8 was dispersed in the solvent DMF in three or four steps according to the amount of ZIF-8. Between each two steps, the solution was ultrasonicated for 30 min in order to ease the dispersion and minimize the agglomeration of ZIF-8 particles in the solution. After completing the ZIF-8 addition, PES was primed by adding 15 w % of the total amount so as to increase the compatibilization between ZIF-8 and PES and the solution was stirred for overnight by a magnetic stirrer. Then, remaining amount of PES was added to the solution in three or four steps with 30 min ultrasonications in between the steps and again the solution was stirred for overnight. While the PES concentration was kept constant, the ZIF-8 contents in the membranes were varied between 10- 60 w/w % and the compositions of prepared membranes are shown in Table 3.2.

Table 3.2 Various membrane compositions used in this study

Sample	Composition(weight ratio with respect to PES content)		
	PES	ZIF-8	HMA
PES	1.0	0.0	0.0
PES-ZIF8-10	1.0	0.1	0.0
PES-ZIF8-20	1.0	0.2	0.0
PES-ZIF8-30	1.0	0.3	0.0
PES-ZIF8-40	1.0	0.4	0.0
PES-ZIF8-50	1.0	0.5	0.0
PES-ZIF8-60	1.0	0.6	0.0
PES-ZIF8-10-HMA-4	1.0	0.1	0.04
PES-ZIF8-20-HMA-4	1.0	0.2	0.04
PES-ZIF8-20-HMA-7	1.0	0.2	0.07
PES-ZIF8-30-HMA-1	1.0	0.3	0.01
PES-ZIF8-30-HMA-2	1.0	0.3	0.02
PES-ZIF8-30-HMA-4	1.0	0.3	0.04
PES-ZIF8-30-HMA-10	1.0	0.3	0.1

3.2.2.3 PES/ZIF-8/HMA Membrane Solution Preparation

Same steps with PES/ZIF-8 membrane solution preparation were applied up to completion of the ZIF-8 addition. After completing the ZIF-8 addition, HMA was added, and the solution was stirred for overnight by a magnetic stirrer. Next, it was ultrasonicated for 30 min and PES primed by adding 15 w % of the total amount and the solution was stirred overnight. After that, remaining amount of PES was added to the solution in three or four steps with 30 min ultrasonications in between the steps, and again the solution was stirred for overnight. The ZIF-8 and HMA contents were changed throughout the study and used membrane compositions are shown in Table 3.2. The solutions for all types of membranes were blade cast on a glass plate using a stainless steel film applicator (Automatic Film Applicator, Sheen 1133) and a casting knife of 500 μm. Casting was performed at room temperature in air, and it was placed in an oven preheated to 60^{o}C. Then, the temperature was increased to 80^{o}C, and the solvent in the solution was evaporated at 0.2 bar for 8h in $N_{2.}$

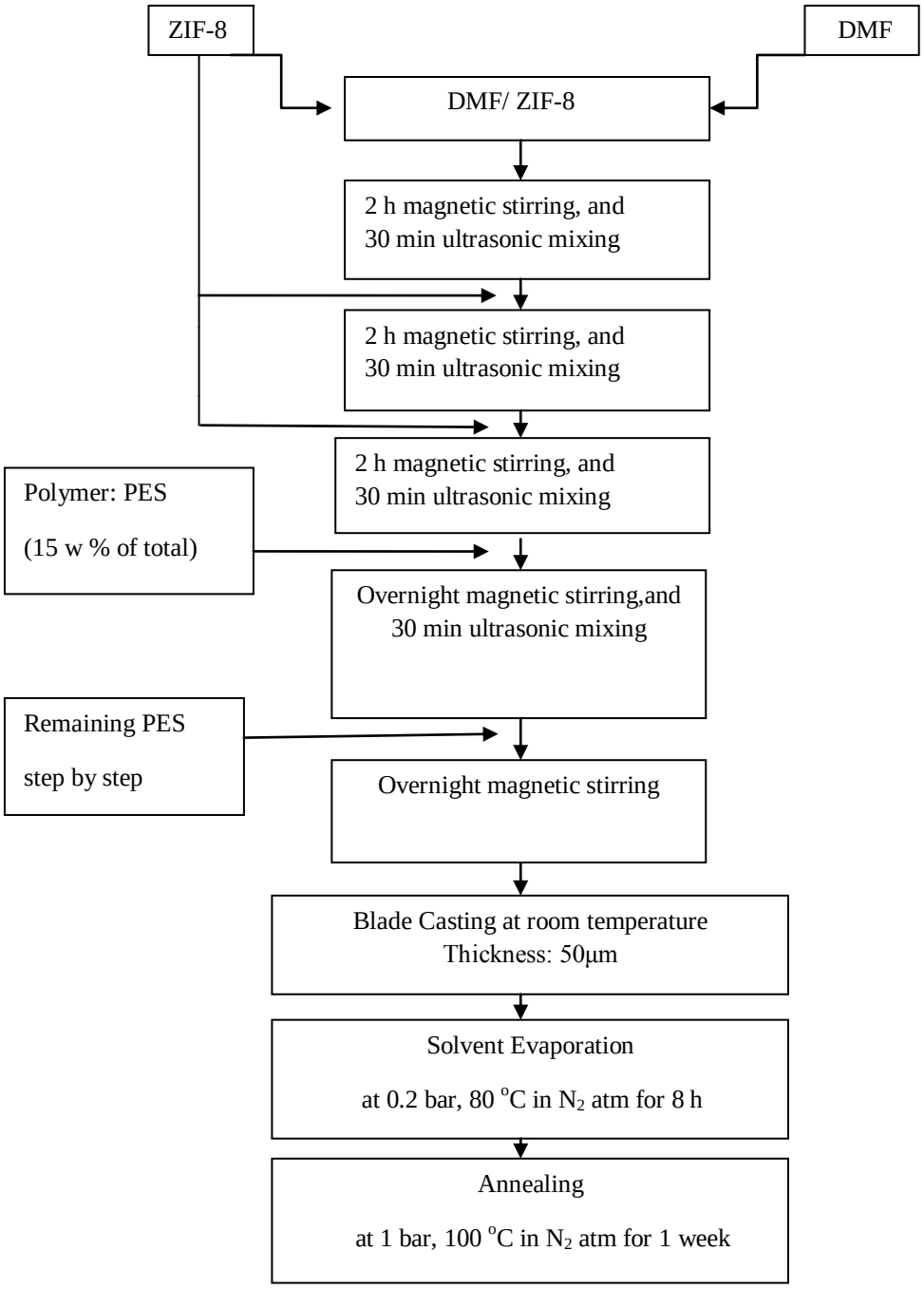

Figure 3.3 Flowchart for the preparation of PES/ZIF-8 mixed matrix membranes

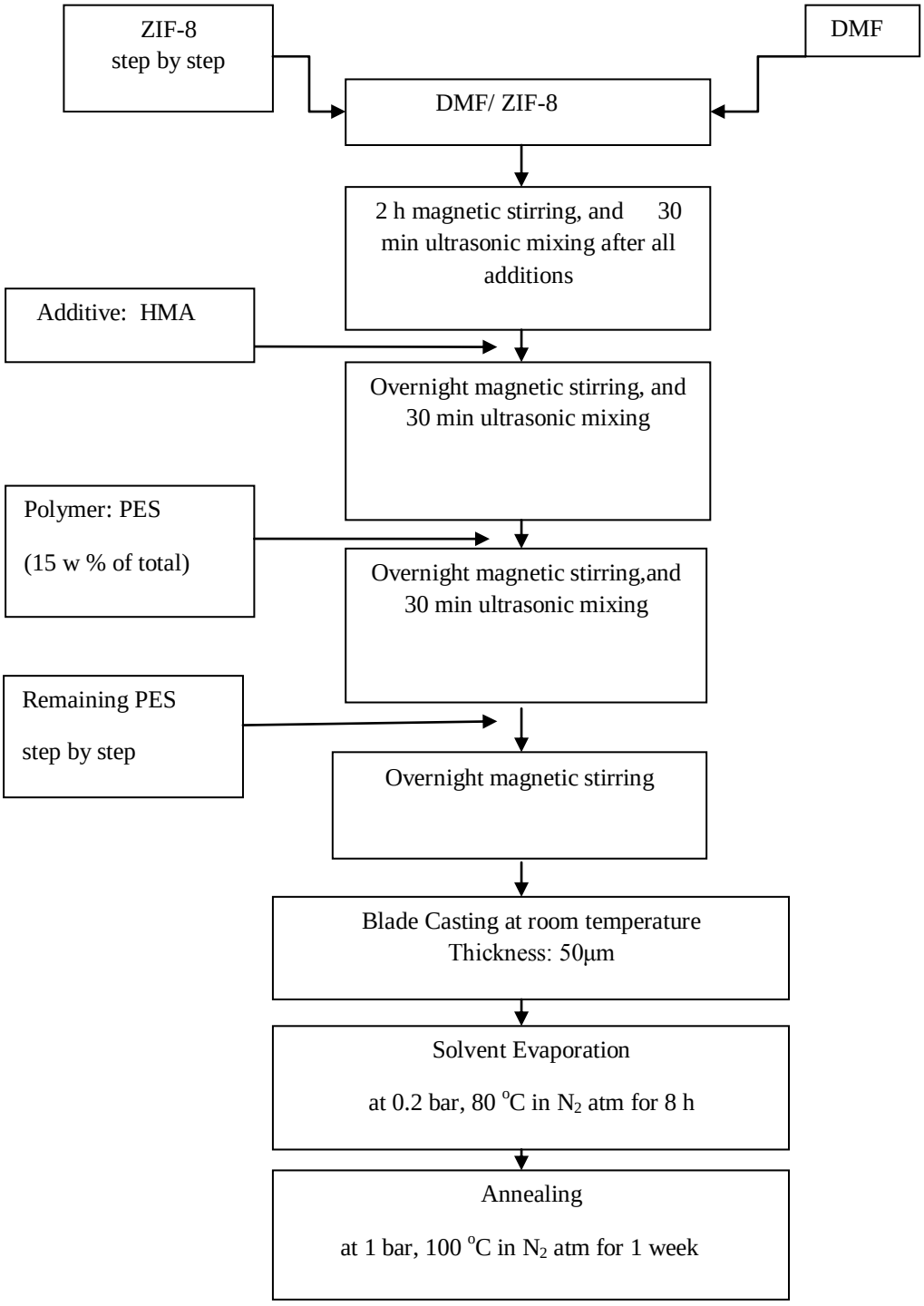

Figure 3.4 Flowchart for the preparation of PES/ZIF-8/HMA mixed matrix membranes

After that, the film was carefully detached from the plate and was annealed at 100°C in N_2 at 1 bar for 1 week to remove the residual solvent. All the membranes were kept in vacuum desiccators before and after gas permeation experiments. The flow charts for the solution preparation procedures of PES/ZIF-8 and PES/ZIF-8/HMA mixed matrix membranes are given in Figure 3.3 and Figure 3.4.

3.2.3 Characterization of Membranes

Membranes were characterized by two different types of thermal analysis. The first thermal analysis is differential scanning calorimetry (Perkin Elmer Diamond DSC), which was used in order to determine the glass transition temperatures (Tg) of the membranes with different compositions. Before performing the analysis, small parts of membrane film were cut, weighed, and placed in aluminum DSC pans. Sample was heated from 30°C to 250°C, and then was cooled down to 30^{0}C, and again was heated to 250^{0}C. The aim of the first scan was to remove the thermal history of the material and in the second scan, the glass transition temperature of the membranes were determined. The analysis was performed in N_2 atmosphere with a heating rate of 10°C/min. The second thermal analysis is thermal gravimetric analysis (Shimadzu DTG-60H), which was performed so as to determine the amount of residual solvent in the membrane. The samples were heated at a rate of 10^{0}C/min up to 250°C in N_2 atmosphere with nitrogen flow rate of 75 ml/min. The TGA analyses were performed also up to 650 °C in N_2 atmosphere to determine the decomposition temperature of the membranes and up to 800 °C at air atmosphere to calculate the ZIF-8 contents of the MMMs.

In addition to thermal characterizations, scanning electron microscopy (FEI Quanta-400 F) was used to determine the morphology of the membranes. The membranes were fractured in liquid N_2 and the films were mounted vertically a circular aluminum sample holder with carbon tape. After that the samples were coated with gold/palladium in order to have an electrically conductive layer and various magnifications were used between 1000x-50000x during the analysis.

3.3 Gas Permeability Measurements

3.3.1 Single Gas Permeability Set-Up and Procedure

The gas permeation experiments were conducted in a constant volume variable pressure system which was previously designed [102-103] by our research group and modified in this study to be used only for single gas experiments. The schematic drawing of the experimental set-up is shown in Figure 3.5. It consists of a membrane cell, a pressure transducer, a gas tank, a vacuum pump, a temperature controller. A heating tape (Cole Parmer, Barnstead/Thermolyne) was used to wrap the system which equipped with J-type thermocouple and PID controller. The membrane cell was a stainless steel

Millipore filter holder (Millipore, part no.XX45047 00) with double-Viton O-ring seals. The pressure transducer (MKS Baratron, 0-100 Torr) which was used to record the downstream pressure increase has a sensitivity of 0.01 Torr. The dead volume of the set-up was measured as 22cm^3 which is the volume from permeate side of the membrane cell to the pressure transducer [42]. The gases used in the permeation experiments, H_2, CO_2 were purchased from Oksan, and CH_4 was purchased from Linde with purity higher than 99%.

For each experiment, 9.6 cm^2 membranes were inserted into stainless steel cell and both sides of the membrane and the feed tank were evacuated (<3x10^{-4} bar) for many hours. Then the feed tank was filled with the penetrant gas up to a pressure of 3.0 bar and the permeability experiments were conducted at 35^{o}C. The downstream pressure rise against time was recorded to calculate permeability. The recording time interval is changing from gas to gas according to the duration of permeation tests, for instance it 5 s for H_2, 10 s for CO_2 and 30s for CH_4. At least two membranes were cast for each different membrane formulation and two parts of all membranes were characterized by permeation experiments. Moreover, the permeability of each gas through a membrane was measured at least twice.

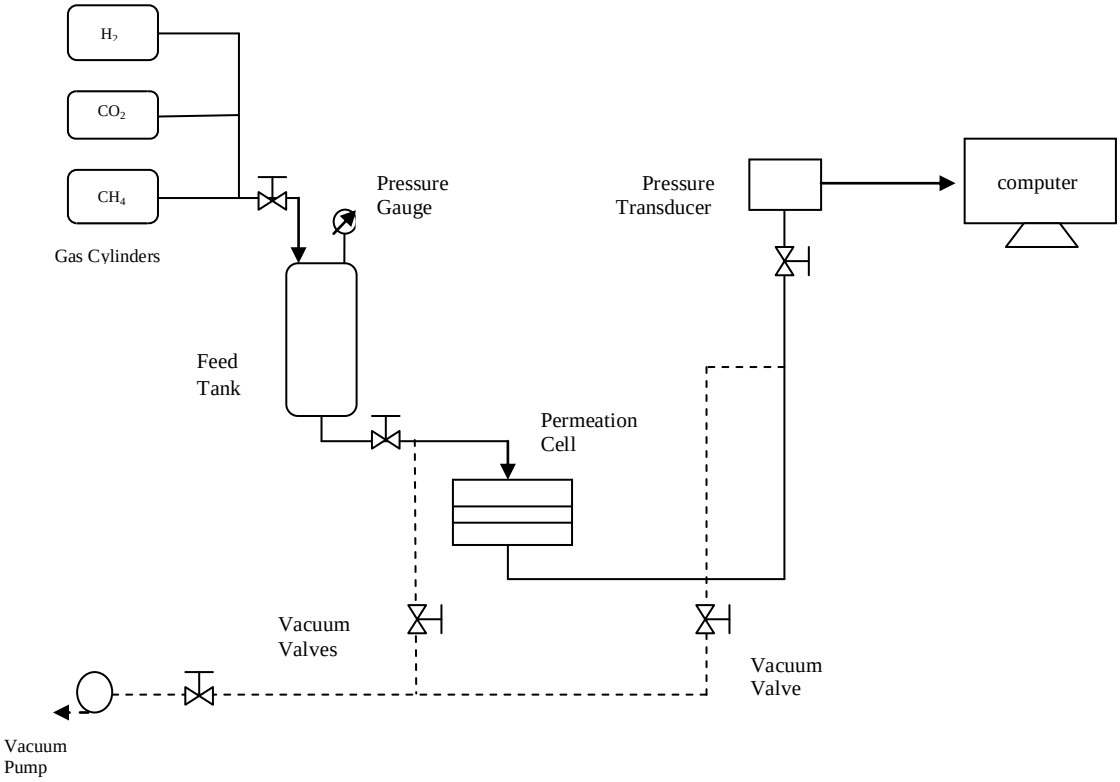

Figure 3.5 Schematic representation of single gas permeation experimental set-up

3.3.2 High Pressure Single Gas Permeability and Binary Gas Permeability Set-Up and Procedure

The selected membranes were evaluated by their separation performances of CO_2/CH_4 binary gas mixtures by a system equipped with an on-line Gas Chromotograph (Varian CP-3800) of which schematic representation is shown in Figure 3.6. Measurements were performed by constant volume-variable pressure technique as in the single gas experiments; only distinction is the dead volume of the set-up. In order to determine the dead volume of this set-up, firstly the volume of all parts, i.e. tubings, valves, were measured and calculated. Since the dead volume cannot calculated by this method accurately, due to the volume in membrane cell, single permeability experiments were conducted with standard membranes of known permeabilities and ideal selectivities from single gas permeation set-up. Pure PES and PES/ZIF-8(%20) membrane were used as standard test membranes and the volume was determined as 18 cm^3. Two different feed pressures (3 and 12 bars) were used while the permeate side was initially at vacuum ($<7x10^{-4}$ bar). Before gas permeation experiments, firstly a binary gas mixture was prepared in the feed tank by keeping the pressure at 3 bar and 12 bar for different pressure measurements. One of the gases is fed to the tank up to half of the desired pressure and then the other is allowed to the tank to final pressure. This mixture was fed to the membrane cell and the pressure rise at the permeate side was recorded. Then the composition of gas collected at the permeate side was analyzed by GC. Moreover the feed gas composition was analyzed. All the analyses were performed for at least three times in order to be sure the repeatability of the GC analysis. The compositions of the feed and permeate streams were used to calculate the selectivity factor of the membrane.

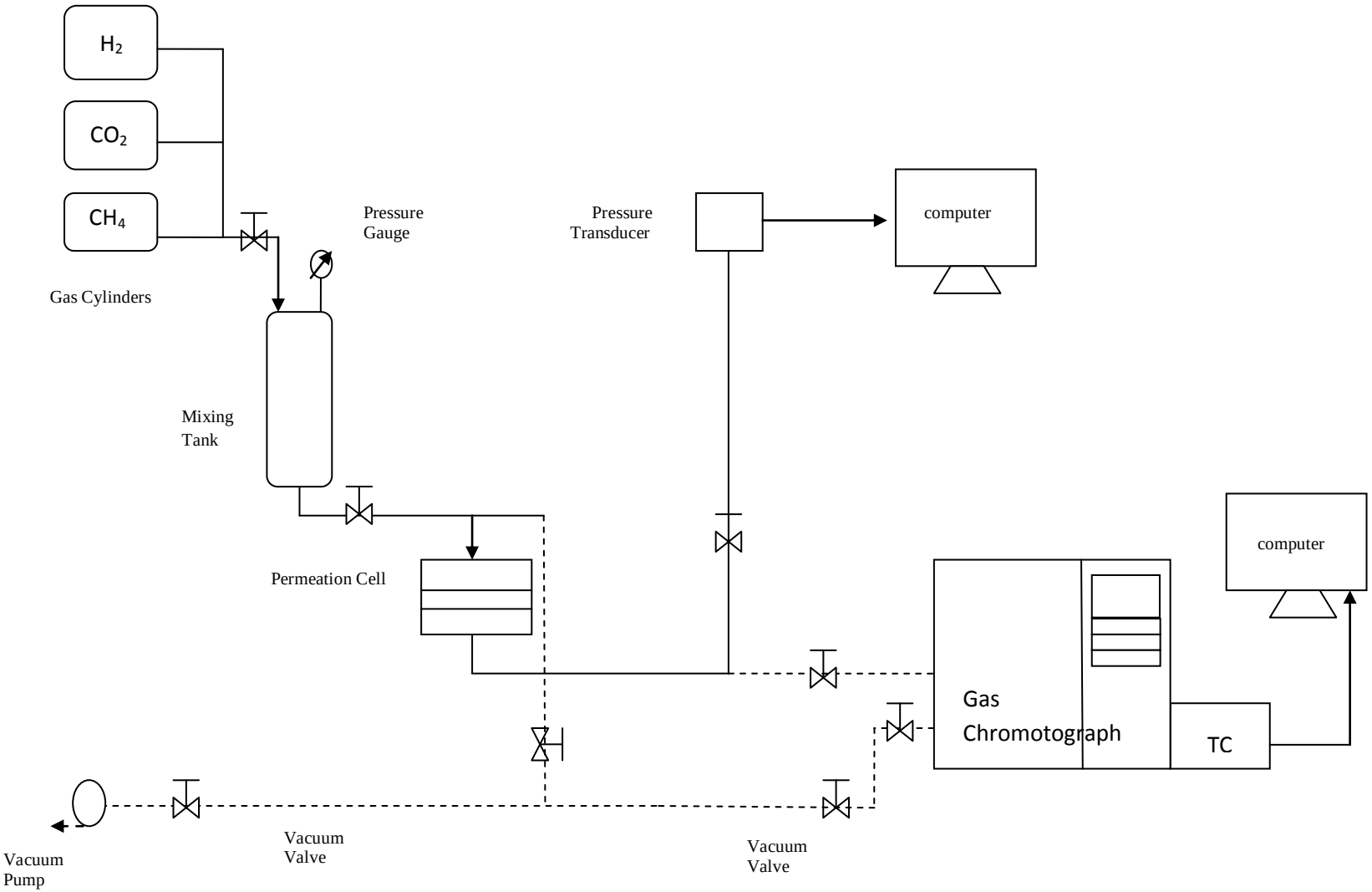

Figure 3.6 Schematic representation of high pressure binary gas permeation experimental set-up

3.3.2.1 Analysis with GC

A gas chromotography (GC) was used to analyze the relative amounts of the components in the gas mixtures by using their different chemical and physical properties. There is a cyclic procedure in GC which operated by a 6-port valve shown in Figure 3.7. To start the cyclic procedure firstly the GC inlet valve, V1, was opened for 3 s to introduce a sample of gas mixture into the sample loop, while the GC outlet valve, V2 was closed and the sample loop was degassed.

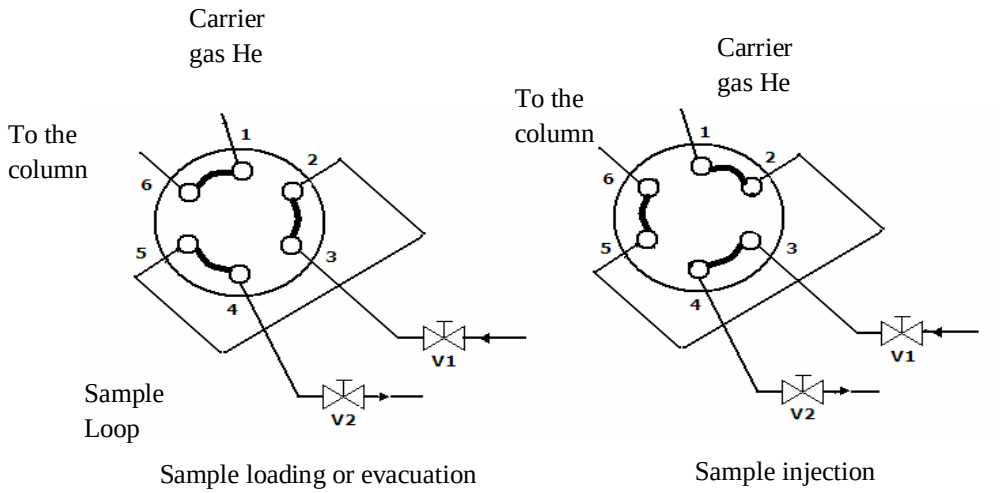

Figure 3.7 Gas injection procedures into the GC using the six-port injection valve.

Then the V1 was closed and therefore the gas sample was directly sent to the GC column. When the injection sequence was completed, V2 was again opened to degas the sample loop.

Before the analysis, the GC was calibrated for CO_2 and CH_4 gases to obtain their amounts in the gas mixtures. The calibration curves were drawn as the pressure versus the corresponding area under the peak. These pure gas calibration curves were used so as to calculate the partial pressures of each component in binary gas mixtures. The details of GC calibration were shown in Appendix C. The operating conditions of GC were given in Table 3.3.

Table 3.3 Operating conditions of gas chromatograph.

Column	Chromosorp 102, 80-100 mesh
Detector	Thermal Conductivity Dedector(TCD)
Detector temperature	100 °C
Column temperature	80 °C
Valve temperature	80 °C
Column pressure	50 psi
Sample flow rate	50 ml/min
Reference gas and flow rate	He, 30 ml/min

3.3.3 Single and Binary Gas Permeability Calculations

The detailed calculations for the single gas permeation experiments were reported in previous stuides of our research group [5], therefore a summary of the calculation procedure can be seen in Appendix B. Moreover, the permeability of gas mixture through a membrane can be calculated by the similar procedure given in Appendix X. In order to determine the permeabilities of each components in gas mixture, the following equation was utilized in which the feed and permeate gas stream concentrations were used;

$$P_i = \frac{v.y_i.l}{(P_{feed}.x_i - P_{permeate}.y_i).A} \quad (3.1)$$

where,

P_i= the permeability of component i in gas mixture (Barrer),
P_{feed} and $P_{permeate}$= the pressures of the feed and permeate sides, (cmHg),
x_i ve y_i= mole fraction of component i in the feed and permeate sides, respectively,
l= membrane thickness (μm),
v= volumetric flow rate (cm^3/s),
A= effective membrane area (cm^2).

The separation selectivity for a binary gas mixture was described as the ratio of permeate side and feed side components mole fractions as follows,

$$\alpha_{ij} = \frac{(y_i/y_j)_{permeate}}{(x_i/x_j)_{feed}} \quad (3.2)$$

The detailed sample calculations for binary gas permeability and separation selectivity were given in Appendix D.

3.4 Theoritical Models Used for MMM Performance Prediction

The performance of mixed matrix membrane materials can be predicted quantitatively by using various theoretical expressions; for instance, Landuer model, effective medium theory, the Higuchi model and Maxwell model. Mahajan et.al [109] used various theoritical expressions (i.e., Arithmetic Mean, Maxwell, Higuchi, Bruggeman, Bottcher) to predict the O_2/N_2 selectivity for Matrimid/Zeolite 4A composite membrane with increasing volume fractions of zeolite 4A. It was reported that all the models gave very similar predictions at low zeolite concentrations. For high zeolite loadings Maxwell model gave the closest values to the experimental results while the predictions of arithmetic mean lower and the predictions of the Bottcher higher than the experimental results. The Maxwell model was reported as the most appropriate method to use in MMM predictions owing to its successful predictions and simple expression.

The Maxwell model is a simple quantitative method to predict the transport properties of MMMs when the transport properties of constituent phases are known. It represents the ideal membrane morphology, with no defects and no interaction between two phases of the membranes. The effective permeability (P_{eff}) of composite materials is given by the following expression;

$$P_{eff} = P_c\left[\frac{P_D+2*P_C-2*\phi_D(P_C-P_D)}{P_D+2*P_C+\phi_D(P_C-P_D)}\right] \quad (3.3)$$

where P_D is the permeability of dispersed phase, P_C is the permeability of continuous phase, ϕ_D is the volume fraction of dispersed phase[109]. The volume fraction of the ZIF-8 is expressed as;

$$\frac{weight\ of\ ZIF{-}8/\rho_{ZIF-8}}{weight\ of\ ZIF{-}8/\rho_{ZIF-8}+weight\ of\ PES/\rho_{PES}} \quad (3.4)$$

in which ρ is the density. A density of 1.37 g/cm^3[110] was taken for PES and 0.95 g/cm^3[111] for ZIF-8.

The Maxwell model accounts the flux through the filler and the polymer phase in parallel and series pathways, as in electrical circuits. Since, the interfacial morphologies occur around the filler phase is not considered, it is more applicable for low filler loadings [90].

There are some studies in literature that try to predict the permeation characteristics of MOF-based MMMs using different theoritical models [112-115]. For instance, Keskin et.al [112] combined the detailed atomic simulations with the Maxwell model to predict the permeation performance of IRMOF-1/Matrimid MMMs for CO_2/CH_4 gas pair which is the first quantitative information for predictions of MOF based MMM performances. Moreover, Atçı et.al [113] used Maxwell model for permeation characteristic predictions in Matrimid/ZIF-90 and Ultem/ZIF-90 membranes, and they reported very reproducible results with the experimental data. In another study, different theoritical models as Maxwell, modified Maxwell, Lewis-Nielson, Pal, etc. were tested by comparing the experimental data in literature for Matrimid/IRMOF-1 and Matrimid/CuBTC MMMs for CO_2/CH_4 separations [114].

Maxwell model was used in this study for predicting the performances of the binary membranes with increasing ZIF-8 contents, and also the performances of the binary and ternary membranes with respect to varying feed pressure.

CHAPTER 4

RESULTS AND DISCUSSION

4.1 ZIF-8 Preparation

4.1.1 Synthesis and Characterization of ZIF-8 with Different MeOH/Zn^{+2} Ratios

ZIF-8 crystals were synthesized at room temperature for 60 min using synthesis mixtures with MeOH/Zn^{+2} molar ratios between 87 and 1043. Figure 4.1 shows the XRD patterns of powders of which compositions are given in Table 3.1. The patterns compares well with the simulated pattern of ZIF-8 [68] and the patterns of ZIF-8 synthesized at room temperature [27, 71, 72] and 140°C [70], indicating that the synthesized powder is only ZIF-8 without any other crystalline phase.

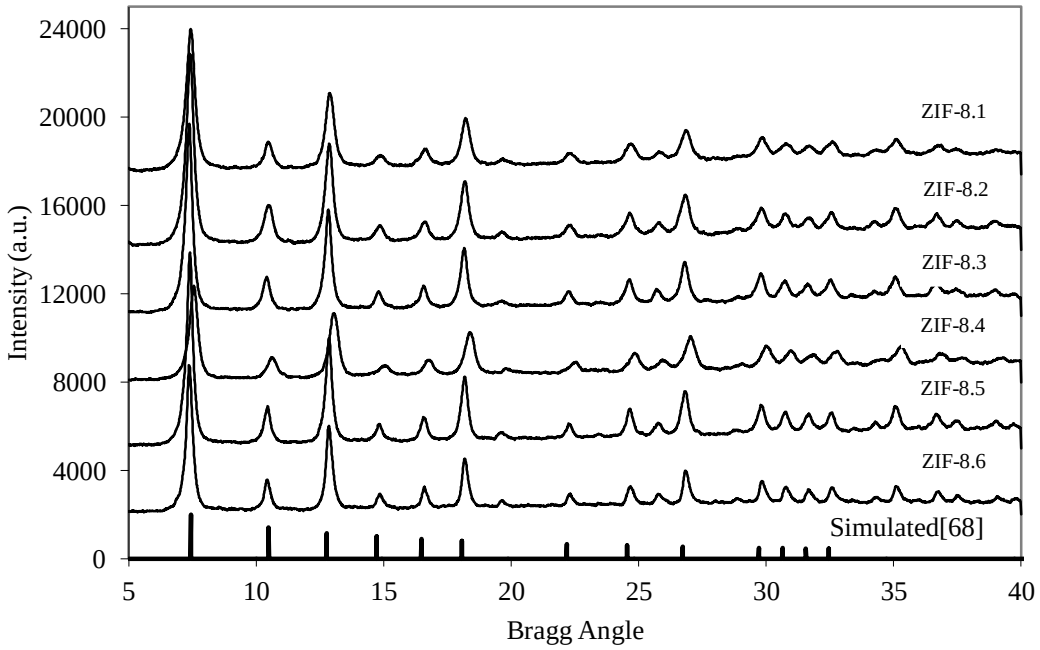

Figure 4.1 XRD patterns of ZIF-8 nanocrystals with different MeOH/Zn^{2+} molar ratio

In order to show the reproducibility of the synthesis with various amounts of MeOH, all the synthesis was performed for two times, and the XRD patterns of second trial are shown in Appendix E. The relative crystallinity and yield as a function of MeOH/Zn^{2+} molar ratio are shown in Figure 4.2. In all synthesis mixtures the Hmim was in excess amount and the Hmim/Zn^{+2} molar ratio was 7.9. The relative crystallinities are above 90% regardless of MeOH/Zn^{+2} ratio of synthesis mixture, implying that all samples are pure ZIF-8. All conversion values were below 40% after a crystallization period of 60 min. Apparently the mother liquor remained at the end of crystallization contains substantial amount of unreacted $Zn(NO_3)_2$ and Hmim. The percent conversion increased with MeOH/Zn^{2+} molar ratio, showing that dilute synthesis mixtures favor the formation of ZIF-8. Unlike the classical nucleation theory the increase in MIL-101 yield with water content has also been reported by Khan et al [76]. Three different samples were synthesized from each composition; the error bars on the figure also show that the synthesis recipe is highly reproducible.

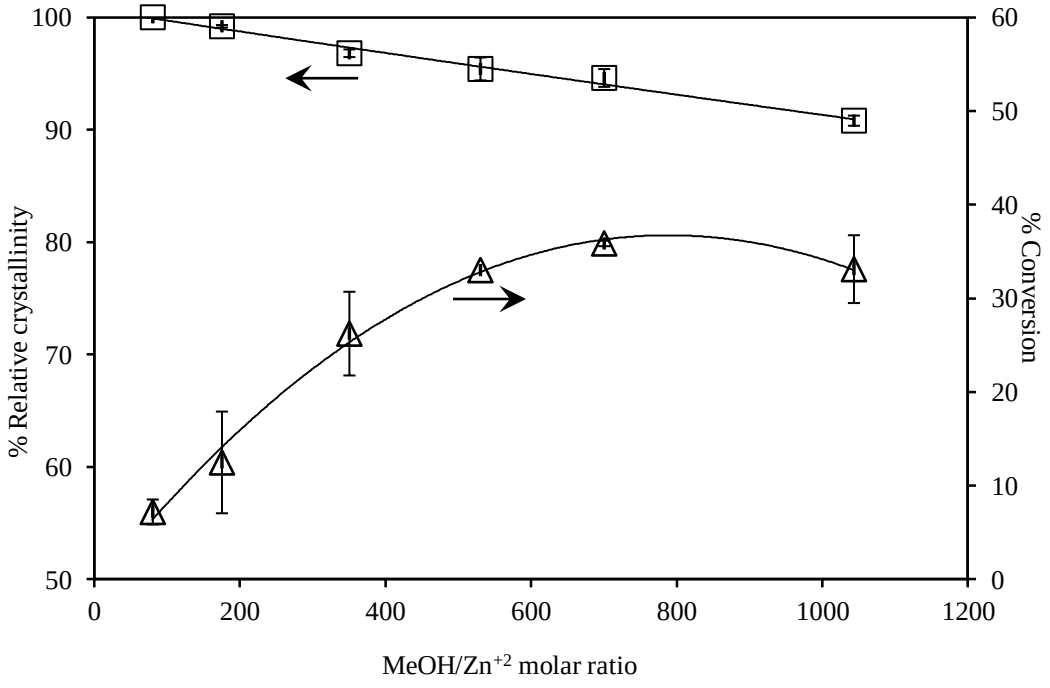

Figure 4.2 The change in relative crystallinity/conversion % as a function of MeOH/Zn^{2+} mole ratio

Figure 4.3 shows the particle size distribution of ZIF-8 samples determined by DLS. ZIF-8 obtained from all mixtures had monomodal and narrow particle size distribution. The crystals in the size range of 60 to several hundred nanometers (~600 nm) were produced from synthesis mixtures with different MeOH/Zn^{+2} ratios. Producing ZIF-8 crystals in such a wide range of particle size by this easy way makes this ZIF-8 synthesis method very attractive. Morphology and crystal size was also examined by SEM images (Figure 4.4). The shape of crystals from all mixtures was rhombic dodecahedral without

an intergrowth [87]. ZIF-8 crystals of uniform size were observed from the SEM images, confirming the results obtained by DLS. The mean particle size was estimated as 60 nm for the MeOH/Zn^{+2} ratio of 1043 and 600 nm for the ratio of 87 revealed by SEM images. The particle sizes by DLS seemed slightly larger than the size of particles observed in SEM micrographs, which was possibly due to the presence of agglomerates in MeOH during the DLS measurement.

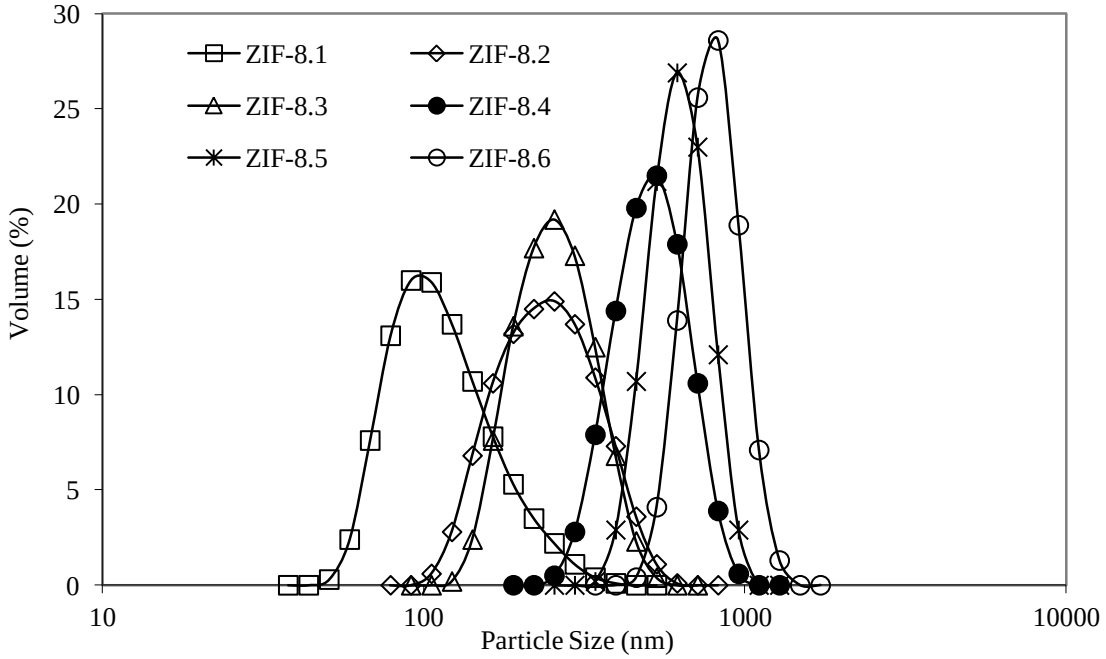

Figure 4.3 Effect of methanol amount on the particle size distributions of ZIF-8 crystals.

Table 4.1 shows the average particle sizes of ZIF-8 samples based on DLS measurements. The average particle size increased from 138 to 890 by decreasing the MeOH/Zn^{+2} ratios from 1043 to 87. A similar effect of MeOH amount of the synthesis mixture was reported earlier for ZIF-8 synthesis [22, 71]. Low MeOH/Zn^{+2} ratios which denotes high Zn^{+2} and Hmim concentration, may reduce the number of nuclei formed and stimulates the crystal growth leading to the formation of larger crystals. [76, 79, 80] The low conversion values at low MeOH/Zn^{+2} ratios may also support that the number of nuclei formed is low. The number of particles, which was calculated from the average particle size and yield using the skeleton density of ZIF-8 as 1.4 g/cm^3 [23] and assuming spherical particles, was $3.19x10^{11}$/100 g synthesis mixture with MeOH/Zn^{+2} ratio of 87. The number of particles is likely to be equal or less than the number of nuclei [116, 117]. High MeOH/Zn^{+2} ratio denoting lower Zn^{+2} and Hmim concentrations favor nucleation to crystal growth, resulting in smaller crystals. [76, 79, 80] The high conversion values at high MeOH/Zn^{+2} ratios may also support that the number of nuclei

formed is high. The number of particles was found to be $1.93x10^{14}$/100 g synthesis mixture with MeOH/Zn^{+2} ratio of 1043.

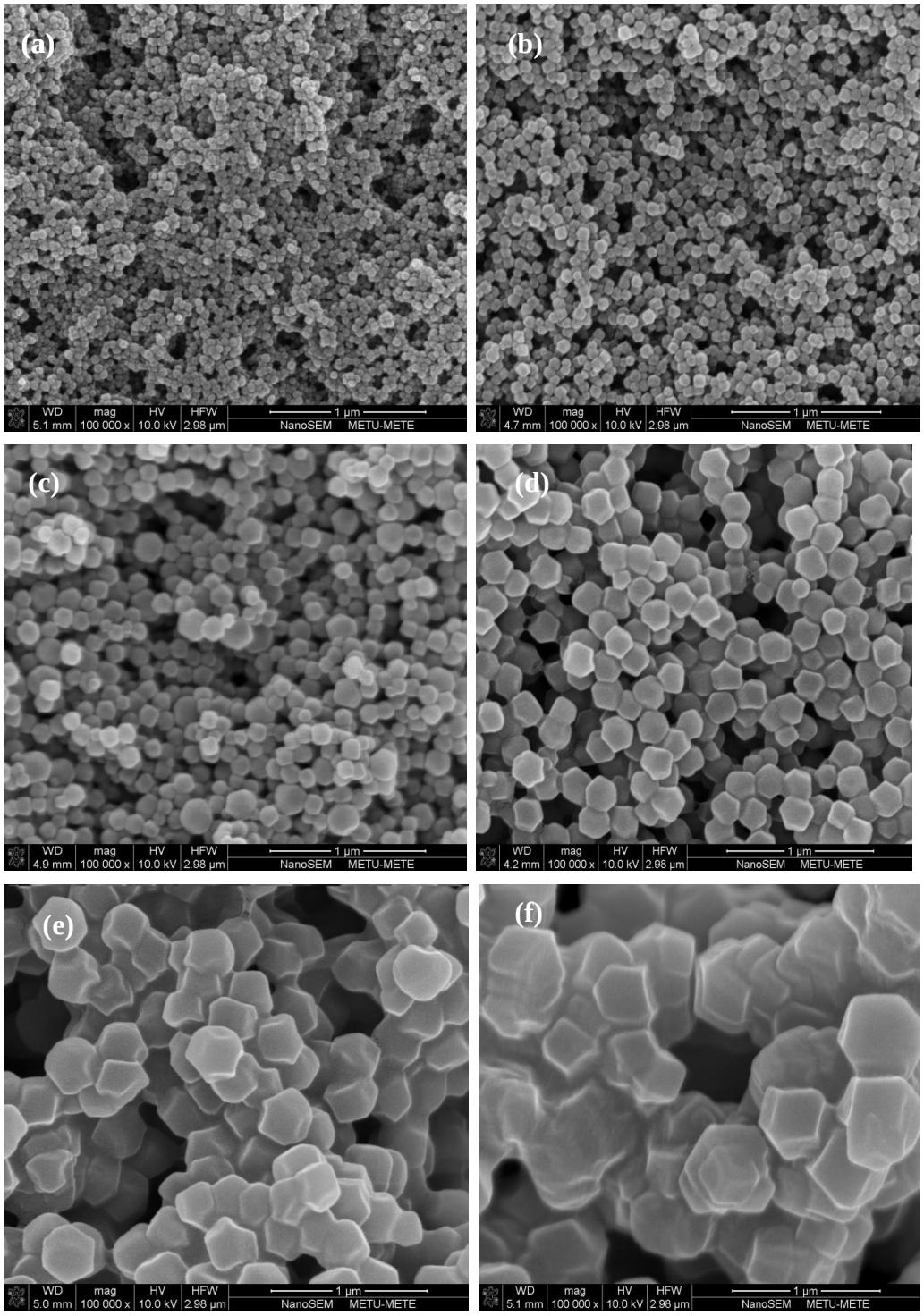

Figure 4.4 SEM micrographs of ZIF-8 as a function of MeOH amount: (a)ZIF-8.1; (b) ZIF-8.2; (c) ZIF-8.3; (d) ZIF-8.4; (e) ZIF-8.5; (f) ZIF-8.6.

The conversion to ZIF-8 could be increased by extending the crystallization period, in which all the limiting reactant (Zn^{+2}) in the mixture is likely to be exhausted or most probably an equilibrium conversion is attained. However, crystal size may increase by increasing the crystallization time due to Ostwald ripening, in which small crystals disappear at the expense of the formation of larger crystals [27, 118]. These results suggest that the crystallization period be short to produce nanosized ZIF-8 crystals in the expense of low conversion. The efficiency of nanosize ZIF-8 production can be increased by recycling the mother liquor, which is still rich with the reactants.

The nanosize ZIF-8 samples were further characterized by N_2 adsorption and desorption at 77 K (Figure 4.5). The isotherms that has a plateau preceeding a rapid increase at low relative pressures demonstrated Type-I behavior, which is characteristic to microporous materials. Although this behavior of ZIF-8 was often observed [22, 119], more sensitive measurements at relative pressures less than 0.1 bar revealed that N_2 adsorption on ZIF-8 is a two-step process [68, 69, 72,].

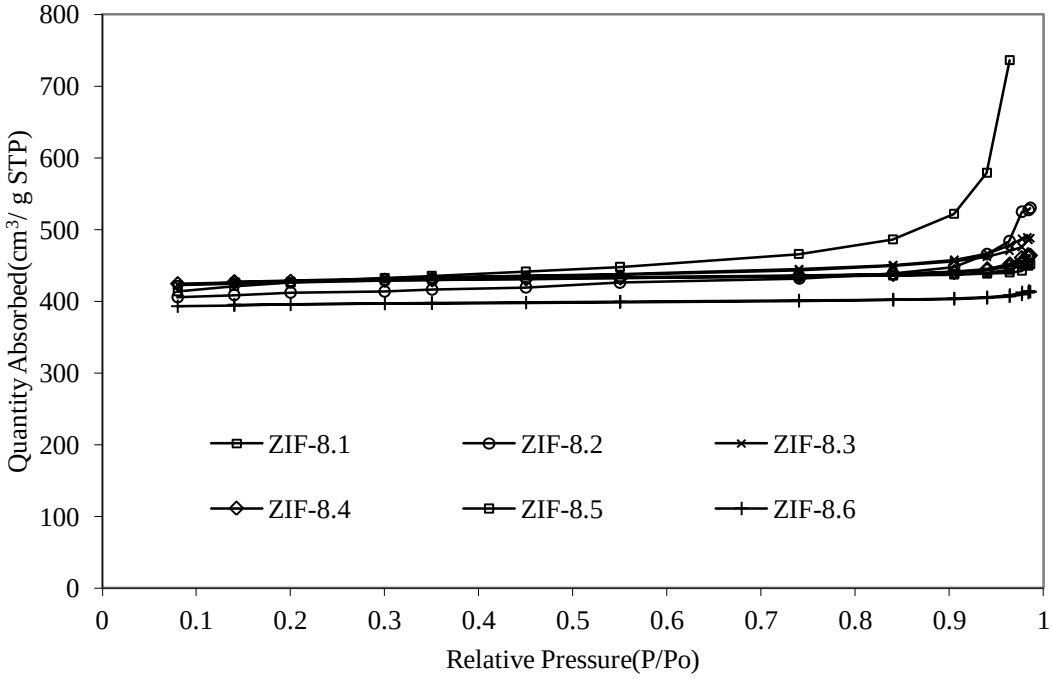

Figure 4.5 N_2 adsorption /desorption isotherms of ZIF-8s

Table 4.1 shows the microstructural characteristics of ZIF-8 samples. The pore volume and BET surface area increased from 413 to 581 cm^3 (STP)/g and from 1143 to 1309 m^2/g with MeOH/Zn^{+2} molar ratio from 87 to 1043, respectively. The BET surface areas are comparable with those reported in many studies.

Venna et.al synthesized ZIF-8 crystals with a surface area of 744 m^2/g from the same synthesis conditions applied in our study [27]. Surface area of ZIF-8 crystals was also reported as 962 m^2/g [22], 1030 m^2/g [72]. ZIF-8 synthesized by Park et.al [68] has a BET surface area of 1630 m^2/g, which is the highest surface area reported in the literature. Zhu et.al [118] attributed this difference to residual Hmim that could not be desorbed from ZIF-8 pores during the activation before the sorption measurements. The high BET surface area of our ZIF-8 samples shows that the crystals have fully developed microstructure with high crystallinity. The external surface area increased with MeOH/Zn^{+2} molar ratios, which is compatible with the decrease in particle size (Table 4.1). The ZIF-8 sample with 138 nm average particle size had an external surface area of 213m^2/g, whereas ZIF-8 sample with 890 nm average particle size exhibited a low external surface area of 46 m^2/g. The high external surface area values suggest limited intergrowth among crystals.

Table 4.1 Effect of methanol amount on particle size and surface area of crystals

Sample Name	Amount of MeOH	Average Particle Size (nm)	BET Surface Area (m^2/g)	External Surface Area (m^2/g)	Volume Adsorbed (cm^3/g STP)
ZIF-8.1	1042.7	138	1309	213	581
ZIF-8.2	695.1	238	1192	130	529
ZIF-8.3	527.8	246	1245	100	489
ZIF-8.4	347.5	462	1238	60	465
ZIF-8.5	173.8	588	1238	76	453
ZIF-8.6	86.9	890	1143	46	413

The crystallization of ZIF-8 at room temperature is a fast process and crystallization is likely to continue during the recovery of solid product from sample mixture either by filtration or centrifugation. The characteristics of the solid recovered after centrifugation could, therefore, be different from those of solid present in the liquid at the sampling time. In-situ methods have been adopted to monitor the crystallization of ZIF-8 [120], MOF's [121] and different zeolites [122, 123] continuously in the reaction medium, which may overcome the difficulties regarding sampling. One of the methods often applied for in-situ monitoring of crystallization is to measure the turbidity of synthesis mixture with time [124]. Turbidity, which relies on the scattering of light by growing

crystals, increases when the particle size and the number of particles are sufficiently large to scatter adequate light to be sensed by the turbidimeter.

The crystallization of ZIF-8 was monitored by a turbidimeter in the present study since the homogenized solution of $Zn(NO_3)_2$ and Hmim in methanol that was clear to naked eye initially was turned to a white suspension as the crystallization proceeded. Figure 4.6 shows the change of turbidity of the synthesis mixture with time for mixtures with different $MeOH/Zn^{+2}$ ratios.

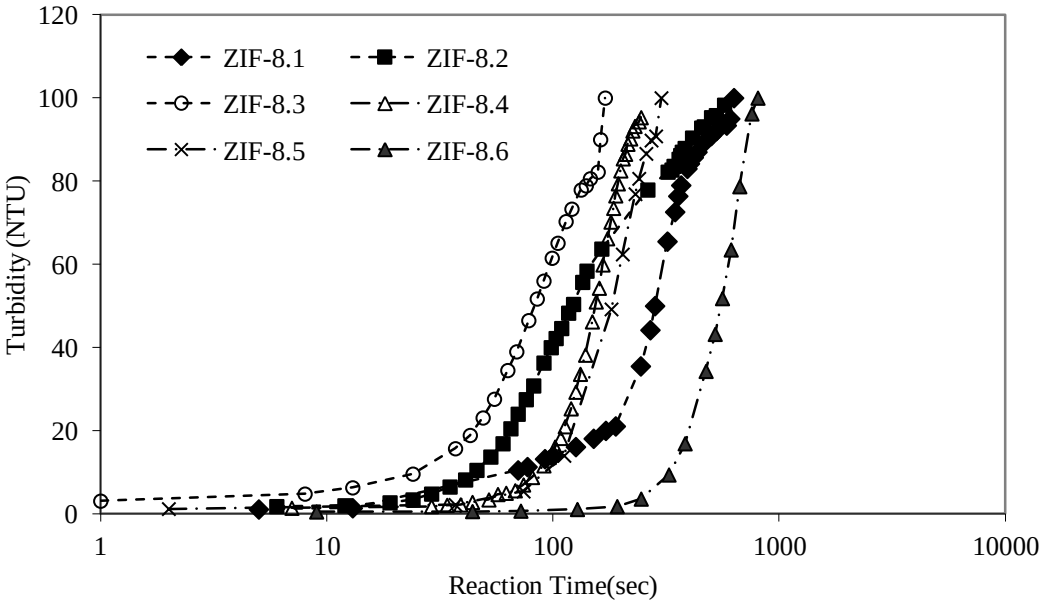

Figure 4.6 Turbidity vs reaction times for ZIF-8 nanocrystals

The turbidity curves comprise of two regions: an induction time with a slight increase in turbidity preceding a sharp rise in turbidity. This behavior is often attributed to the nucleation period and crystal growth. The turbidimeter that was used in this study can sense the particles larger than 30 nm, which is greater than one-twentieth of the wavelength of incident light [124], so the nuclei formed in the synthesis mixture cannot be detected. The induction time, therefore, includes the nucleation period as well as the time for crystal growth up to a size that could be detected. The induction time, which was arbitrarily defined as the time needed for 15 NTU increase of turbidity, was 51 and 43 sec for mixtures with $MeOH/Zn^{+2}$ ratio of 695 and 528, respectively. Those short induction periods, which comprise the nucleation, suggest that nucleation is a very fast process in the synthesis of ZIF-8 as also inferred by Cravillon et al [22].

Following the induction, the increase in turbidity essentially shows the increase of number of particles greater than 30 nm, which corresponds to the yield. The rate of crystallization can therefore be regarded as directly proportional to the slope of the turbidity curve after induction time. The induction time and the rate of turbidity change as a function of MeOH/Zn^{+2} ratios of synthesis mixtures were shown in Table 4.2. The induction period passed through a minimum, yet the rate of turbidity increase exhibited a maximum with increasing MeOH/Zn^{+2} molar ratios.

Table 4.2 Growth Rates and Induction Times

Sample Name	Growth Rate (NTU/sec)	Induction Time (sec)
ZIF-8.1	0.3±0.02	210±10
ZIF-8.2	0.52±0.09	51±1
ZIF-8.3	0.85±0.05	43±2
ZIF-8.4	0.82±0.02	93±5
ZIF-8.5	0.48±0.04	150±60
ZIF-8.6	0.19±0.02	430±20

The turbidity curves for all mixtures were terminated when the turbidity values exceed 100 NTU. This maximum turbidity does not indicate the end of crystallization, but stands for the point at which the synthesis mixture does not transmit the light. The crystallization process may continue after the turbidity values are out-of-scale. Turbidimeter is an inexpensive, simple and fast responding device to investigate the effect of different parameters on the crystallization of ZIF-8, though the data should be interpreted carefully because of constraints related to the particle size and opaqueness of synthesis mixture. The turbidity measurements should be complemented by other techniques which are not limited with particle size and opaqueness.

4.1.2 Recycling of Mother Liquor

ZIF-8 was synthesized from the precursor solution with a molar composition of Zn^{+2}:7.9Hmim:695CH_3OH at room temperature. The solid product was recovered and the residual mother liquor was recycled for the synthesis of new generations of ZIF-8 at room temperature. Three different recycling routes were followed. The powder XRD analysis results of selected samples

obtained from different recycling routes are shown in Figure 4.7. The XRD patterns were matched with the simulated powder pattern of ZIF-8 [68], indicating that the products were single-phase ZIF-8. NaOH was added to the recycled synthesis mixture in routes B and C, though no Na^+ and NO_3^- containing crystalline compounds were detected in the solid products by XRD analysis.

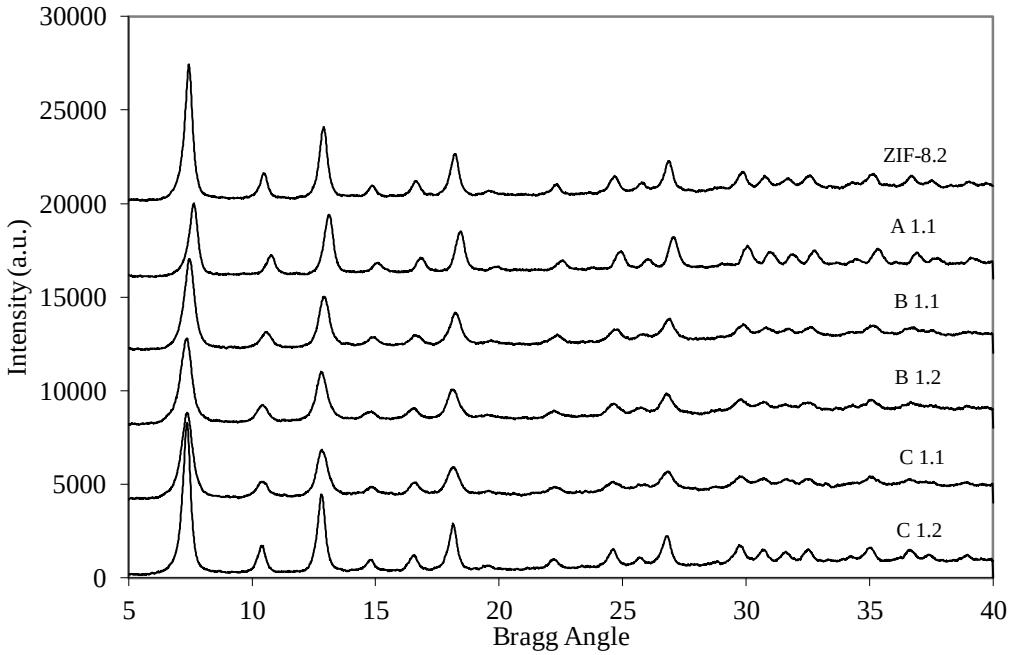

Figure 4.7 XRD patterns of recycled products

The mother liquor was then recycled several more times. The solid products obtained from higher order recycling steps were also pure ZIF-8. All recycling routes were repeated at least three times to ascertain the reproducibility of the procedures. The results showed that recycling process is robust in yielding pure ZIF-8 crystals at room temperature. The XRD patterns of all the samples obtained by recycling procedures B and C can be found in Appendix E.

The relative crystallinities and yields with corresponding molar synthesis solution compositions were shown in Table 4.3. The sample calculations of yield and synthesis compositions for both B and C procedures are given in Appendix F. Highly crystalline ZIF-8s were obtained from routes B and C, but route A yielded ZIF-8 with the lowest crystallinity. The route B could be repeated for two times and totally 4 different ZIF-8 powders were obtained, though by route C, the recycling process was repeated for four times to obtain 7 different ZIF-8 powders. The ZIF-8 yield is calculated based on the maximum ZIF-8 amount that could be obtained from the synthesis solution. Since no Zn^{+2} source is

added to the mother liquor in the first steps of the recycle procedures, the remained amount of $Zn(NO_3)_2.6H_2O$ and maximum ZIF-8 amount were calculated considering the ZIF-8 yield in the orginal synthesis. The lowest ZIF-8 yield (~8%) belongs to the A route product which is non-NaOH treated procedure. Considering the routes B and C, the yields in the first steps are higher than the ones in the second steps.

Table 4.3 Characterization Results of Recycled ZIF-8s

Sample Name	Gel Composition (Zn^{2+}: Hmim: MeOH)	Crystallinity (%)	Yield (%)	BET Surface Area(m^2/g)	External Surface Area (m^2/g)
A.1.1	1/4.35/427	65.6	7.8	1198	32
B 1.1	1/11.8/1186	80.9	90.9	1261	382
B 1.2	1/7.9/910	82.3	32.4	1086	174
B 2.1	1/10.7/1374	73.9	70.3	1193	418
B 2.2	1/7.9/1126	67.6	27.3	686	103
B 3.1	1/9.66/1459	No ZIF-8			
C.1.1	1/ 11.66/ 1123.5	82.9	76.7	1049	155
C.1.2	1/ 5.5/ 618.6	99.8	31.7	1250	110
C.2.1	1/ 7.2/ 903.9	84.4	73.8	1179	235
C.2.2	1/ 3.68/ 583.8	95.3	26.7	1216	166
C.3.1	1/ 4.28/ 801.9	79.2	67.6	1216	230
C.3.2	1/ 2.01/ 549.5	49.5	5.6	943	102
C.4.1	1/ 2.01/ 589.1	96.3	63.2	1208	140
C.4.2	1/ 0.63/ 505	No ZIF-8			

The first steps and the second steps should be evaluated between each other and classified as separate synthesis. The B and C routes percent yield decreased with increasing order of recycling from 90.9 to 70.3, and from 76.7 to 63.2 for the first steps and from 32.4 to 27.3 and from 31.7 to 5.6 for the second steps, respectively due to the reduce in Hmim amount.

ZIF-8 comprises Zn atoms connected by 2-methylimidazole ligands [27]. The synthesis mixtures with Zn^{+2}/Hmim molar ratio of 0.5 resulted in micron-size crystals [72]. Cravillon et al [22], who showed excess amount of Hmim with reference to the amount of Zn^{+2} in the synthesis mixture is essential to produce nanosize ZIF-8, obtained ZIF-8 crystals as small as 50 nm from a synthesis mixture with a molar composition of approximately 1 Zn^{+2}:8 Hmim:700 CH_3OH. In the current study, ZIF-8 synthesis initiated from a solution with a Zn^{+2}/Hmim molar ratio of 0.127. The second

and higher generations of ZIF-8 were then synthesized from the recycled mother liquors that were enriched with Zn^{+2} by adding $Zn(NO_3)_2$ to the medium while no additional Hmim was introduced during the recycling steps. High Zn^{+2}/Hmim ratios favored the formation of ZIF-8 and resulted in higher yields. As the Hmim content of the mother liquor decreased with increasing recycling steps, the conversion to ZIF-8 became more limited and the yield decreased without a substantial change in the crystallinity. At the end of 4 recycling steps, Zn^{+2}/Hmim molar ratio increased to 1.59 and the recycling process was ceased probably because the concentrations of Hmim and Zn^{+2} attained an equilibrium level. The remaining Hmim in solution was insufficient to fulfill the requirements of crystallization, thus no crystals could be recovered at higher Zn^{+}/Hmim ratios.

Our results reported in Section 4.1.1 showed that high MeOH/Zn^{+2} ratios promoted the formation of ZIF-8, thus yield increased with MeOH/Zn^{+2} ratios. During the synthesis by recycled mother liquid, although the MeOH/Zn^{+2} ratio of synthesis mixture increased with increasing order of recycling, yield decreased. The descending concentrations of Hmim probably surpassed the effect of methanol.

In route B, so as to prevent the Zn^{+2} accumulation in the mother liquor the Zn^{+2}/Hmim ratio in the second steps is kept constant. (It is calculated considering the yield of previous step.) However the dilution is increased by the cycles due to decreasing Zn^{+2} and Hmim amounts in the liquid. Moreover, Zn^{+2}/Hmim ratio is decreased to 0.1 and thereby no ZIF-8 yields in B 3.1.

In route C, since the initial amount of Zn^{+2} source is added to the mother liquor, as the number of cycles are increased, the Zn^{+2}/Hmim ratio is increased. This raise asserts the accumulation of Zn^{+2} in the medium. Since no Zn^{+2} is added to the mother liquor in the first steps of the cycles, most of it is consumed and this amount of accumulation does not pose an obstacle for the formation of ZIF-8 crystals. Quite to contrary, in this route numbers of cycles are twice of the number of cycles in route B. When the ratio became 1.59 in the 4th cycles, the amount of Hmim was insufficient for the synthesis and the production was stopped. If required amount of Hmim is added to the mother liquor at that stage, and Zn^{+2}/Hmim ratio is made suitable for the ZIF-8 formation, this recycle procedure may be repeated for more times.

Figure 4.8 shows the change of turbidity by time during the synthesis from fresh mixture and the first recycled mother liquors. The behavior of fresh and recycled mother liquors was very similar. There was an induction time before the onset of a sharp increase in turbidity. The shortest induction time was 30 sec obtained from route C, which was comparable with the induction time obtained from the fresh synthesis mixture. The longest induction time was 12500 sec that was obtained from route A. The major difference of route A from the others was that NaOH was added to the recycled mother liquid in routes B and C.

NaOH possibly diminished the effects of H^+ and NO_3^- ions in the mother liquor and changed the electrolyte balance of the mixture. Cravillon et.al [22] stated that Hmim has a dual function in the synthesis mixture: as a linker in its deprotonated form and as a stabilizer in its neutral form. Venna et al. showed that the concentration of the deprotonated Hmim and pH decreases as the crystallization of ZIF-8 proceeds. Low pH leads to stabilization of the neutral Hmim, which then limits the rate of phase transformation [27]. The protonated and neutral forms of the imidazole linker coexist in solution at equilibrium. The NaOH added to the mother liquor increases the pH of medium, which may then induce deprotonation of the excess neutral Hmim that was already in equilibrium with the protonated Hmim. NaOH facilitated the initiation of nucleation and stimulated crystal growth. The solution pH decrease with ZIF-8 crystal formation was thus compensated with the addition of NaOH into the recycled mother liquor in order to provide the reaction medium with initial pH value of approximately 9. The amount of NaOH was determined by controlling the pH of the mother liquor which is defined as the amount that increase the pH from 7 to 9.

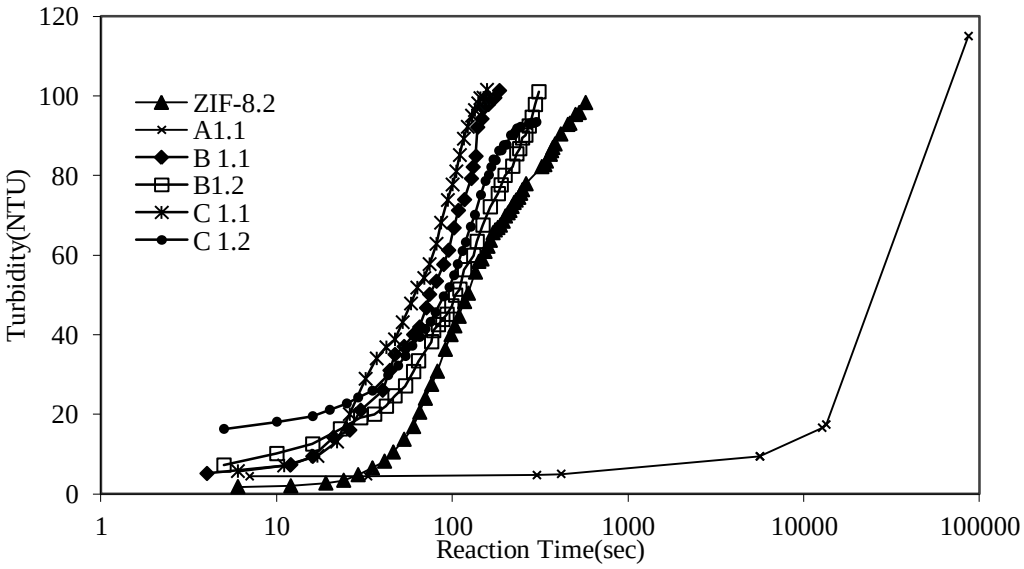

Figure 4.8 Turbidity vs. Reaction Times for Recycled Products

4.1.3 Characterization of Recycled ZIF-8

The SEM micrographs of the ZIF-8 powders obtained from three recycle procedures (A, B and C) are shown in Figure 4.9 and Figure 4.10. As shown in Figure 4.9(a) nanocrystalline powder with ill-defined gel-like morphology was obtained from procedure A in which no NaOH treatment was performed. Although we can not identify the particle shapes of the each separate crystal in this micrograph, the average sizes are bigger than the all other ZIF-8s which may be caused by long

synthesis period. Both the mean particle sizes and the shapes of crystals derived from procedures B and C are much closer to those of the original ZIF-8.

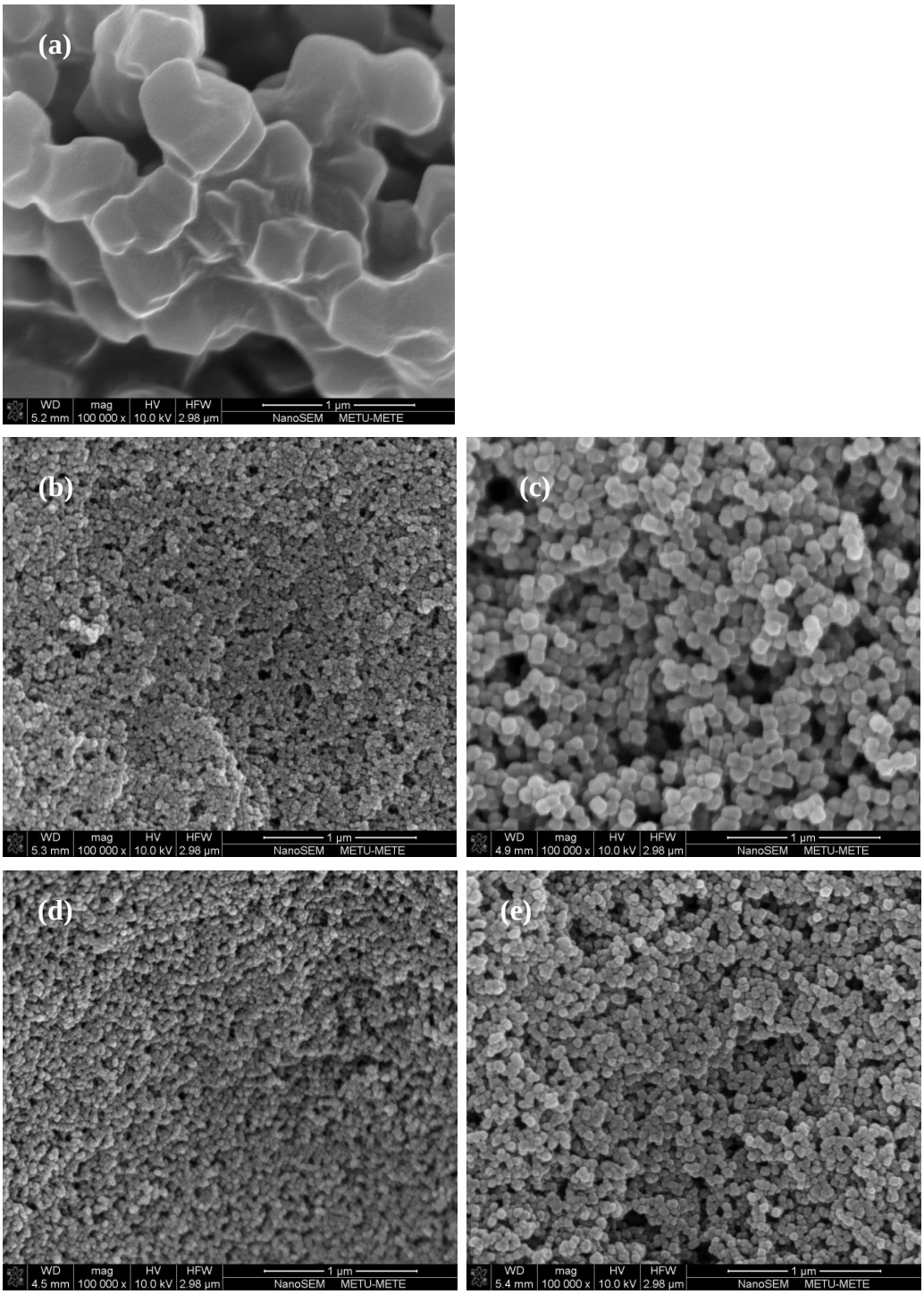

Figure 4.9 SEM micrographs of the recycled ZIF-8s. (a) A1.1; (b) B1.1; (c) B1.2; (d) B2.1; (e) B2.2 at magnification of 100.000x

Considering the recovery products of procedure B in detail (Figure 4.9), all the images have well-defined structures with varying particle sizes. Especially B 2.1 has approximately same structure and particle size with the original ZIF-8 sample. While the average particle sizes of the ZIF-8 nanoparticles of the first steps are increasing from 30 nm to 40 nm, the ones of the second step products are decreasing from 100 nm to 80 nm.

The SEM images of procedure C products are seen in Figure 4.10. The first step product of the first cycle has particles with well defined structure and about 30 nm size. When the Zn^{+2} was added to the second mother liquor, the particle size was increased to 100 nm which is a consequence of the changes in chemical composition of the mother liquor given in Table 4.3. The high dilution and high Hmim/Zn^{+2} ratio may cause smaller particles in the first steps of the route B and C and with the decrease in Hmim/Zn^{+2} and MeOH/Zn^{+2} ratios, the crystals are enlarged in the second steps [22]. While the mean particle sizes of the crystals handled from the first steps of the each cycle are increasing with increasing order of recycle (from 30 to 80 nm), the particle sizes of the crystals obtained from the second steps of each cycle are decreasing (100 to 20 nm).

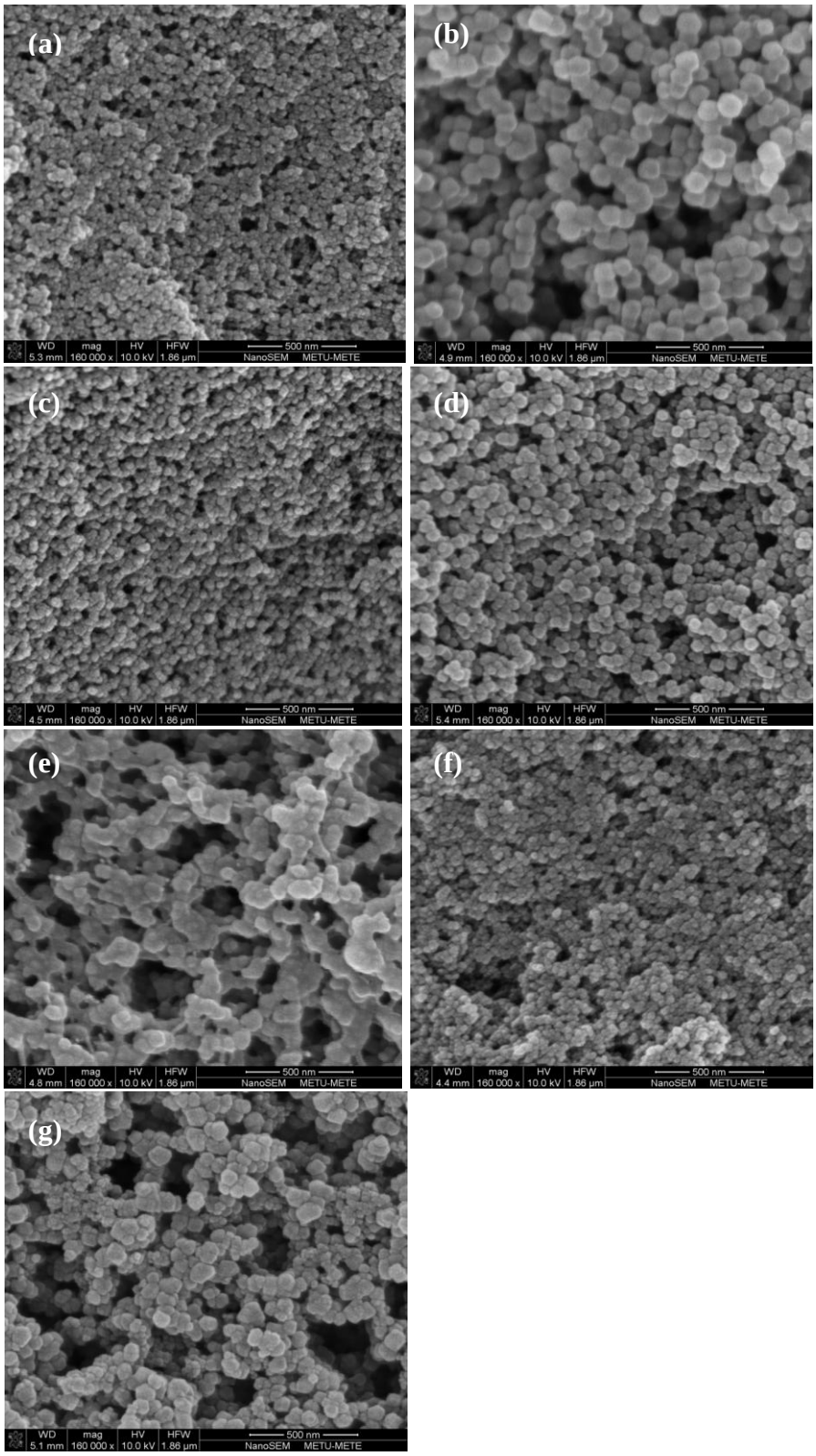

Figure 4.10 SEM micrographs of the recycled ZIF-8s. (a) C1.1; (b) C1.2; (c) C2.1; (d) C2.2; (e) C3.1; (f) C3.2; (g) C4.1 at 160.000x magnification

In order to see the shapes of the ZIF-8 crystals in detail, TEM analysis was used and the images are given in Figure 4.11. The addition of NaOH strongly influenced the morphology of the resulting ZIF-8 crystals and provided highly small spherical nanoparticles (~30-50 nm in size). However, in the second step of the recycle procedure ZIF-8 crystals were obtained with well-defined hexagonal shape and ~70 nm particle size which is very close to the particle size of ZIF-8.2.

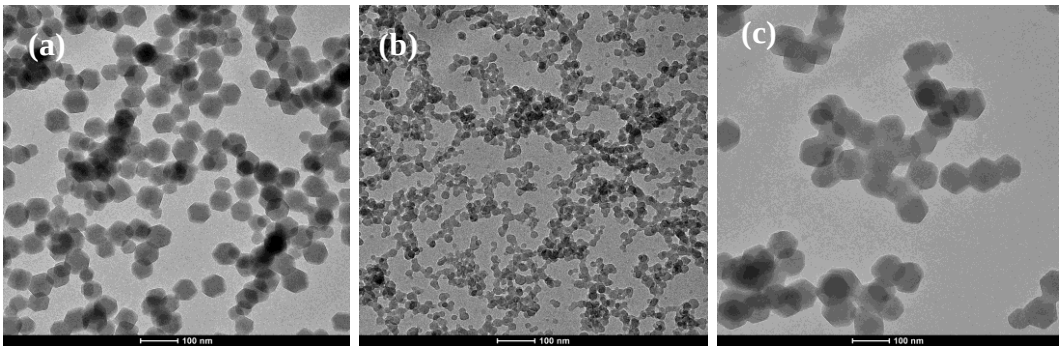

Figure 4.11 TEM images of the original and recycled ZIF-8s. (a) ZIF-8.2; (b) C1.1; (c) C1.2

The BET surface areas and external areas of the recycled samples are given in Table 4.3. The BET surface areas for all crystals obtained from three recycle routes are very similar to each other (changing between 1000 and 1200m^2/g) and also to the original ZIF-8. The change in the external surface areas is again compatible with the change in the particle sizes of the crystals. The lowest external surface (32 m^2/g) belongs to the product of A route which has the largest particle size (~800nm). For both the routes B and C, the external surface areas of the first step products are greater than the ones of first steps.

Thermal behaviour of recycled ZIF-8 crystals is given in Figure 4.12. The thermal stability was not affected by the recycling process and, the framework was preserved up to 450^{o}C for all crystals. They all exhibited a slight weight loss up to approximately 450^{o}C in air, that corresponds to the removal of guest molecules (MeOH) indicating the stability of framework up to this temperature. The highest weight lost up to 450^{o}C belongs to C 1.1 which was treated by NaOH, of which reason may be the impurities. The sharp weight loss in the temperature interval of 450-600 ^{o}C is due to the decomposition of organic groups leading to the collapse of the structure. The total weight loss was about 66% upon heat treatment up to 600^{o}C and the remaining part of the material which corresponds to about %35 of the sample is same with the calculated ZnO percent composition of this material. All ZIF-8 crystals synthesized with different MeOH compositions decomposed after 450 ^{o}C. The slight difference in weight loss in the temperature interval of 500-600 ^{o}C may be caused by the removal of unreacted species/MeOH from cavities for the crystals with a smaller particle sizes.

While high stability (up to 400^{o}C) has been reported for the ZIF-8 crystals with particle size in the microscale [68, 72]. Nune et.al [126] also reported the framework stability up to 400^{o}C for the nano sized hexagonally shaped ZIF-8 crystals derived in the presence of high molecular weight poly (diallyldimethylammoniumchloride) solution and methanol. Although Cravillon et.al [69] reported that ZIF-8 nanocrystals are stable up to 250 ^{0}C in the case of the smaller 18 nm-sized nanocrystals, and up to 300 ^{0}C in the case of larger nanocrystals and microcrystals, our results indicated that in the case of 60-400 nm-sized ZIF-8 crystals are thermally stable up to 450 ^{0}C.

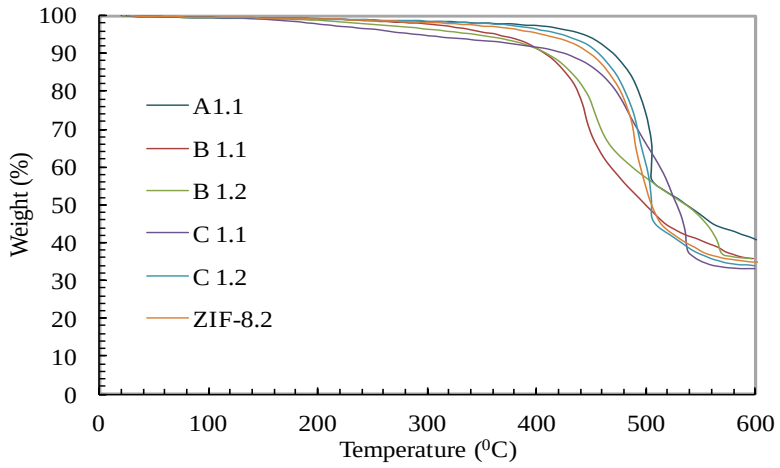

Figure 4.12 TGA curves of recycled ZIF-8 crystals

4.1.4 Evaluation of Recycling Process

Numerous studies and methods have been reported for the synthesis of nano-size ZIF-8 crystals due to the desirable properties of it in the application areas of gas storage, separation, sensing, catalysis [118] due to high surface to volume ratio and development of nanotechnology devices [22]. In the synthesis of MOF type materials, more diluted systems cause higher nucleation rates and thus crystals with smaller particle size are obtained [76, 79, 80]. Moreover, using excess amount of Hmim in the synthesis solutions makes the particle size smaller [22]. Thus, so as to synthesize nanosize ZIF-8 crystals, the system should be as diluted as possible with a high Hmim/Zn^{+2} ratio despite of low conversion. Mother liquor recovered after the original synthesis, contains substantial amount of unused Zn^{+2}, Hmim and methanol due to the low conversion. The efficiency of nanosize ZIF-8 production can be increased by recycling the mother liquor, which is still rich in the reactants.

Two-steps recycling procedure which has been developed based on using the mother liquor of the original synthesis solution results in many advantages for nano-sized ZIF-8 production in the aspects of production efficiency, economics, environment without any lost in the desirable properties of the

crystals. It is seen form the XRD patterns that no amorphous or any other phases are obtained for the crystals derived from recycling processes and also the relative crystallinities of the samples are comparable to the original one. The SEM images show well defined crystal structure, and the BET surface areas and thermal stabilities of the all recycle products are very similar to ones of the original synthesis product.

Table 4.4 Overall Yields and Production Costs

Samples	**Yield Based on Max. ZIF-8**	**Cost of Production($/gr)**
Original Synthesis	38	14
Route B	82	2
Route C	82	3

Another important point is the crystallization periods, which is same for all samples except the product of route A. Addition of NaOH remarkably accelerates the ZIF-8 production. Use of the starting solvent and unreacted species in this solvent enables a substantial increase in the crystalline yield of nanosized ZIF-8 crystals. After consuming the remaining $Zn(NO_3)_2.6H_2O$ in the mother liquor by changing the ion balance with NaOH addition in the first step, only Zn^{+2} source was added to the mother liquor in the second step and again ZIF-8 crystals were recovered by one-hour synthesis. By the effect of NaOH, almost all the Zn^{+2} source was consumed in the first step and this might be the main reason of the increase in crystalline yield. While the ZIF-8 yield is about 38 % in original synthesis, it is raised to about 80 % with this recycling procedure.

The production cost of ZIF-8 crytals in the original batch is calculated as 14 dollars/gram for only the expenses of chemicals used in the synthesis. However the cost of the production is reduced to 3 and 2 dollars/gram when the recycling approaches B and C were applied, respectively. This significant cost reduction arises from mostly re-using the residual Hmim in the mother liquor. Naturally, re-using the starting solvent and the unused reactant Hmim for 3 or 4 times decreased the amount of waste produced and thereby reduced the harmful environmental effects of the chemicals.

4.2 Membrane Characterization

4.2.1 SEM Results

The membrane morphologies and the polymer-filler interfaces of all membranes were investigated by scanning electron microscopy (SEM). Figure 4.13 depicts the SEM images of cross section views of PES/ZIF-8 MMMs having varying amounts of ZIF-8 particles between 10-60 % w/w.

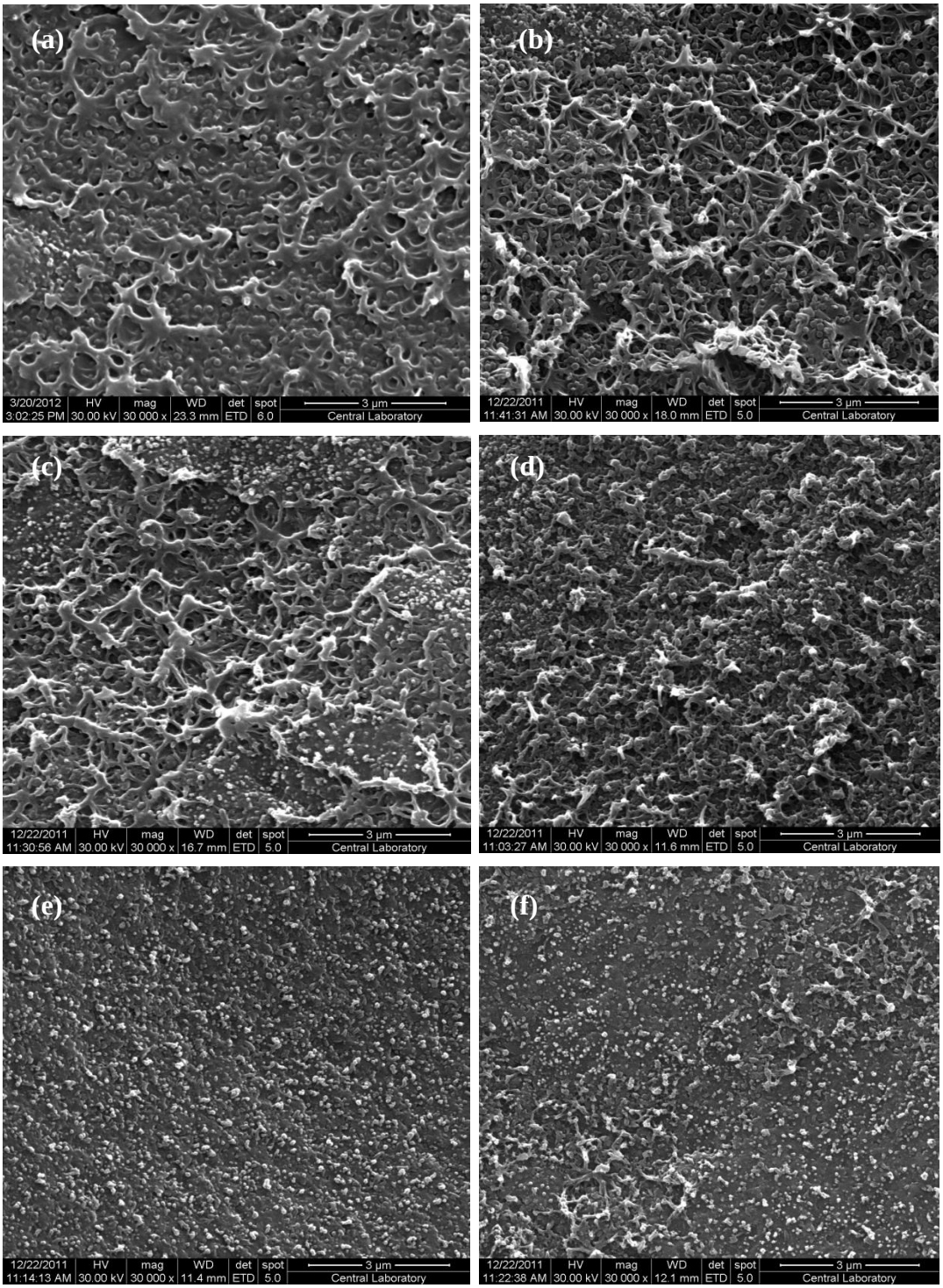

Figure 4.13 Cross-sectional SEM images of PES/ZIF-8 mixed matrix membranes with various ZIF-8 loadings; (a) PES/ZIF-8(%10), (b) PES/ZIF-8(%20), (c) PES/ZIF-8(%30), (d) PES/ZIF-8(%40), (e) PES/ZIF-8(%50), (f) PES/ZIF-8(%60)

Binary mixed matrix membranes have heterogenous structures for all ZIF-8 contents, where hexagonal uniform particles are ZIF-8 and the continuous phase is PES. ZIF-8 nano particles are homogenously dispersed in the polymer matrices.

SEM images of PES/ZIF-8(%20) membrane at higher magnifications were shown in Figure 4.14 in order to analyze the interfacial regions around the ZIF-8 crystals in detail. It is observed that voids were formed at the interfacial region around ZIF-8 crystals. The higher weight percent of ZIF-8 particles was added to the membrane, the more interfacial contacts between ZIF-8 and PES were formed. Therefore the amount of voids in the membrane was increased with increasing ZIF-8 loading. This morphology was observed especially in the PES/ZIF-8 membranes with ZIF-8 contents 20, 30 and 40% w/w which is named as sieve-in-a-cage [33]. The reason underlying the interfacial void formation was explained by poor compatibility between filler particles and polymer matrix in literature [10, 33, 49, 51]. Moreover, freeze fracturing of the membranes during sample preparation could have resulted in the cavity formation between ZIF-8 crystals and polymer matrix [70].

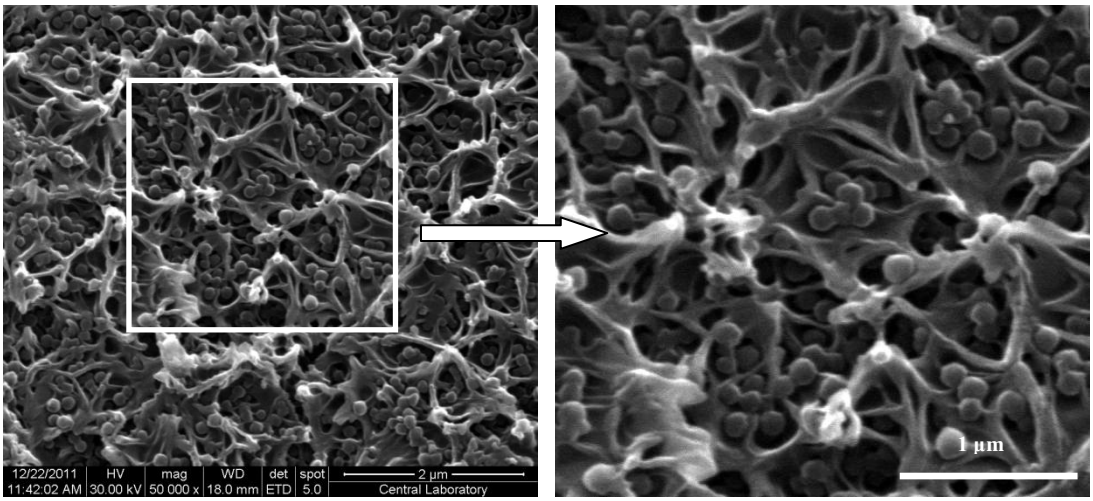

Figure 4.14 Cross-sectional SEM images of PES/ZIF-8(%20) membrane

For higher ZIF-8 loadings (>40%w/w), the membrane morphology is completely different from the others. The voids around the crystals become less evident, continuous ZIF-8 crystals are more prominent and polymer act as binder between the crystals at high loadings. Similar morphology was seen in Matrimid/ZIF-8 mixed matrix membranes with a 80%(w/w) of ZIF-8 loading [70]. Moreover, the mechanical properties of the membranes are changing with increasing ZIF-8 loadings; for instance, the mixed matrix membranes containing ZIF-8 crystals above 40 w/w % are brittle and difficult to handle. At least half of the membranes prepared with high ZIF-8 loadings were cracked during the vacuuming of permeation chamber during gas permeation experiments.

This may be attributed to the reduction of percent amount of polymer in the membrane formulation. The SEM images of ternary membranes with 10 and 20 w/w % ZIF-8 loading are given in Figure 4.15 to perceive the impact of third component on the membrane morphologies. The cross-sectional images of PES/HMA membranes reported to have a single phase, dense homogenous structure similar to the images of pure PES membrane [21, 43].

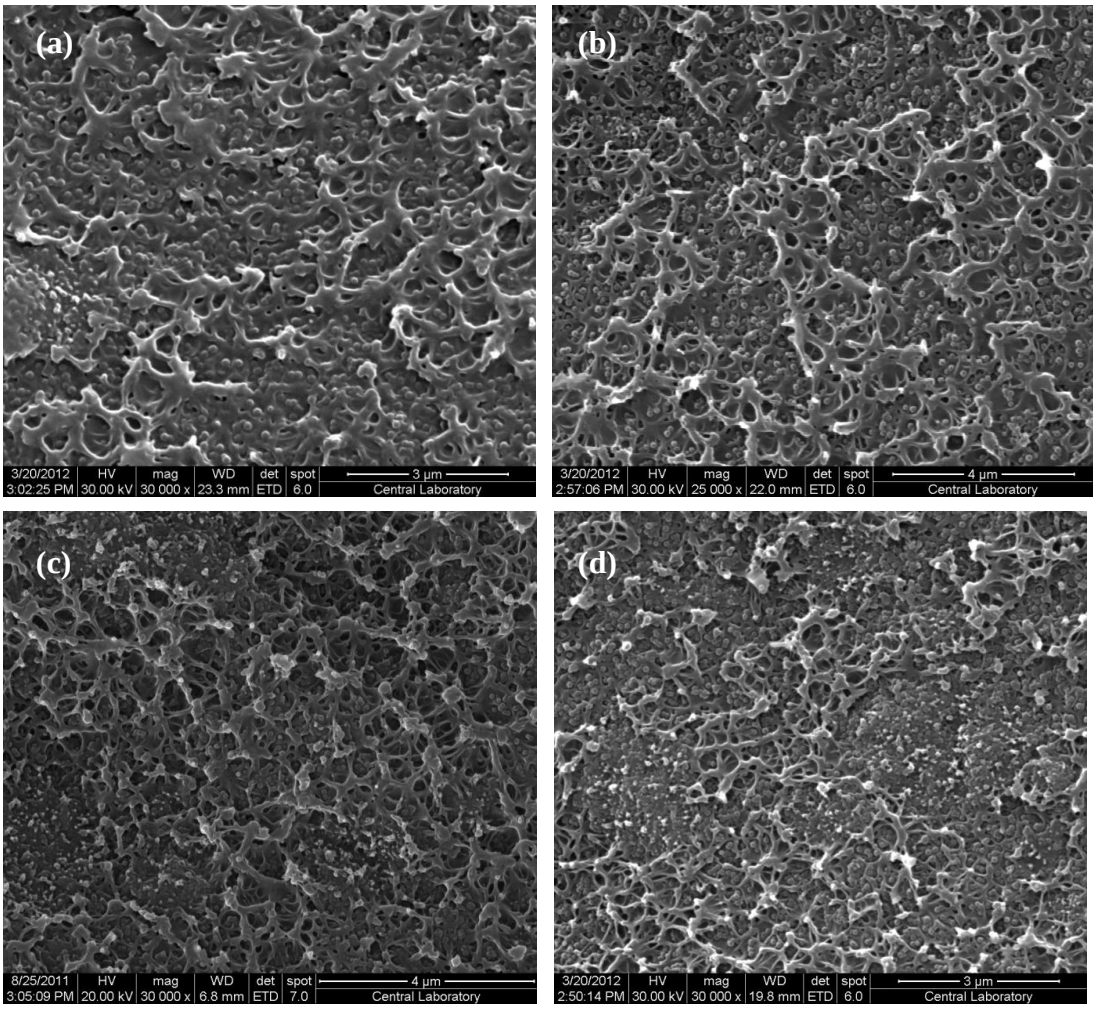

Figure 4.15 Cross-sectional SEM images of binary and ternary MMMs; (a) PES/ZIF-8(%10), (b)PES/ZIF-8(%10)/HMA(%4); (c)PES/ZIF-8(%20)/HMA(%4); (d)PES/ZIF-8(%20)/HMA(%7)

Incorporation of ZIF-8 crystals into PES/HMA formulation induced a heterogenous structure as in the binary membranes and the micrographs of PES/ZIF-8(%10) membrane and its ternary pair PES/ZIF-8(%10)/HMA(%4) show very similar morphologies in macroscale. Moreover, ternary membranes which contain 20 w/w % ZIF-8 and 4, 7 w/w % HMA have still interfacial voids around the filler

particles, but the extent of voids is likely to be reduced when compared to PES/ZIF8(%20) membrane.

Figure 4.16 displays the cross sectional SEM images of 30 w/w % ZIF-8 loaded ternary mixed matrix membranes with various HMA loadings. The effect of HMA loading on the membrane structure can not be observed in SEM images; all the membranes have very similar morphologies regardless of HMA content. The ZIF-8 crystals are dispersed homogenously in the polymer matrix and there are still some interfacial voids around the crystals.

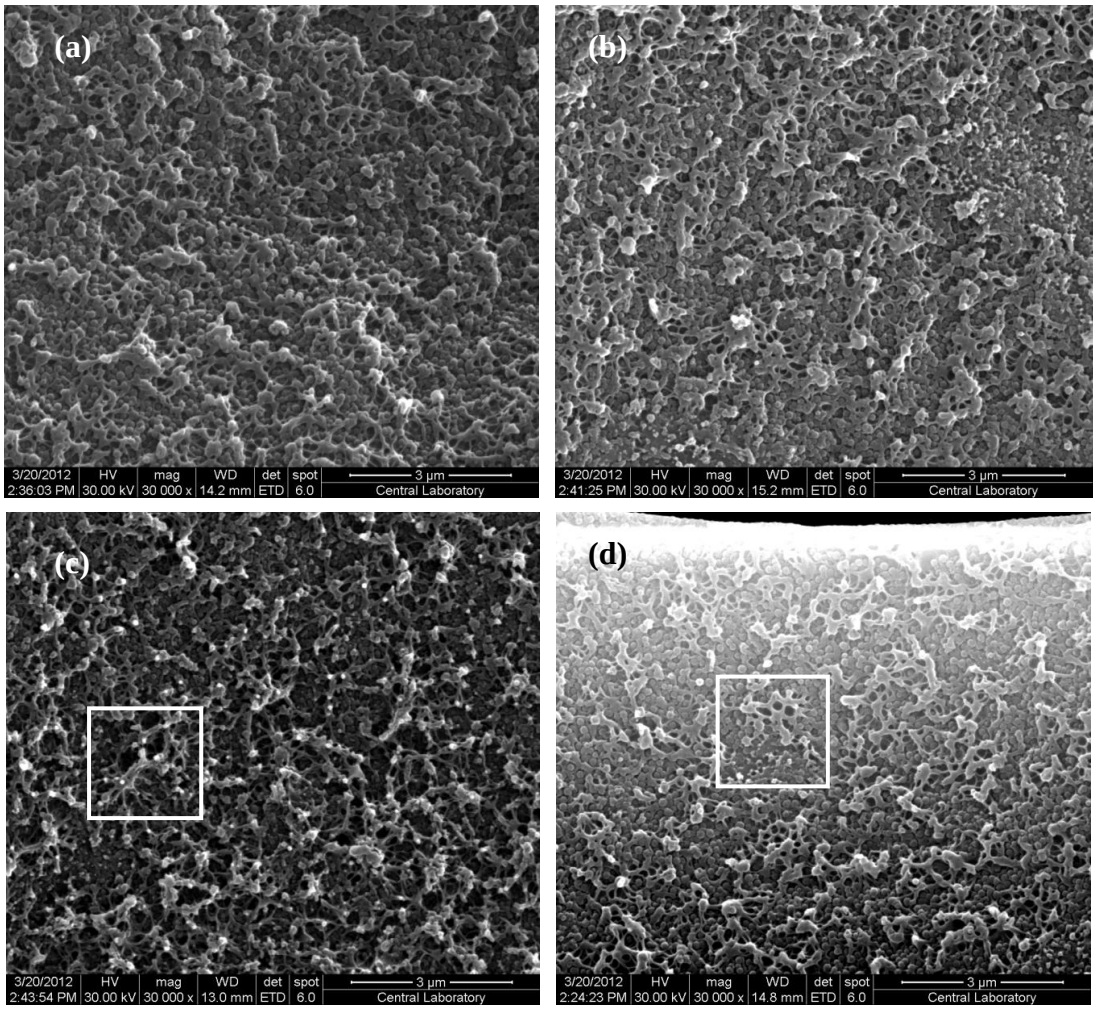

Figure 4.16 Cross-sectional SEM images of ternary MMMs containing 30 w/w % of ZIF-8; (a) PES/ZIF-8(%30)/HMA(%1), (b)PES/ZIF-8(%30)/HMA(%2), (c)PES/ZIF8(%30)/HMA(%4), (d) PES/ZIF-8(%30)/HMA(%10)

4.2.2 DSC Results

Differential scanning calorimetry was used in order to analyze the glass transition temperatures (Tg) of the membranes which give a significant information about the chain stiffness and chain flexibility of the polymer [43]. DSC analyses were done for binary and ternary membranes with different compositions and the second scan thermograms are given in Appendix J.

The glass transition temperatures of binary and ternary membranes are shown in Table 4.5. Table 4.5 shows the effect of ZIF-8 content on the Tg of binary membranes. The glass transition temperature of the pure PES membrane did not change with the ZIF-8 incorporation. There are some studies in literature reporting constant glass transition temperatures in spite of incorporation of filler materials into polymer matrix which may be attributed to lack of interaction between polymer and filler at the molecular level [42, 63]. Moreover, the same trend was reported in a previous study of our research group in which the filler material is SAPO-34[19].

Table 4.5 also indicates the Tg values for HMA included binary and ternary membranes. Incorporation of 4 % w/w of HMA reduced the glass transition temperature compared to the neat PES membrane. Generally, the addition of low molecular weight additives is reported to decrease the Tg of polymeric materials owing to dilution effect even at very low concentrations [20, 127]. Moreover, the rates of segmental motion in polymer chain are decreased with LMWA addition in glassy polymers and the free volume of polymer decreases and it stiffens owing to the antiplasticization effect [41]. The relatively low reduction observed in Tg of PES/HMA membrane may be explained by the antiplasticization effect of HMA. On the other hand, the Tg of the resultant ternary membranes increased nearly $4^{O}C$ independently of filler loadings when compared to PES/HMA (4%). This increase may be explained by the chain rigidification occured around the ZIF-8 crystals implying a stronger interaction between the PES/HMA blend and ZIF-8 crystals. The Tg of polymer increased with the addition of ZIF-8 crystals only in the presence of HMA, in which case HMA may facilitate the interaction between filler and polymer phases [19]. Similar behaviour was reported in our previous study for PES/SAPO-34/HMA system [19].

Table 4.5 Glass transition temperatures of the membranes

Membrane	PES/ZIF-8(%y)/HMA(%x)		Tg (^{O}C)
	x	y	
PES/ZIF-8	0	0	217
		10	215
		20	218
		30	217
		40	219
		50	219
		60	218
PES/ZIF-8/HMA	4	0	212
		10	217
		20	216
		30	216

.

4.2.3 TGA Results

Thermal gravimetric analysis (TGA) is used so as to analyze the amount of remaining solvent in the membranes. The analysis was performed with a heating rate of 10°C/min in the temperature range from 30 to 300°C in N_2 atmosphere. All the binary and ternary mixed matrix membranes were tested and the results given are given in Table 4.6 and 4.7. Moreover, the TGA thermograms for all membranes are given in Appendix G.

Table 4.6 Weight losses of the binary MMM with different ZIF-8 loadings

Membrane Type	Weight Loss Up to 105 ^{0}C (%)	Weight Loss Between 105-200 ^{0}C (%)	Weight Loss Between 200-300 ^{0}C (%)	Total Weight Loss(%)
Pure PES	1.14	0.72	3.04	4.90
PES/ZIF-8(%10)	1.06	0.92	3.11	5.09
PES/ZIF-8(%20)	1.03	0.27	2.65	3.95
PES/ZIF-8(%30)	0.37	0.46	3.52	4.35
PES/ZIF-8(%40)	0.46	0.61	3.61	4.68
PES/ZIF-8(%50)	0.57	0.39	3.48	4.43
PES/ZIF-8(%60)	0.52	0.48	5.36	6.36

The total weight loss up to 105 ^{o}C and between the temperatures of 105 and 200^{0}C of both binary and ternary membranes is around 1 % or below independently from ZIF-8 and HMA loading which can be attributed to the release of moisture sorped by the membrane. Since the boiling boint of the used solvent (DMF) is 153^{0}C, the analysis should be done up to higher temperatures to provide the complete removal of the residual solvent. There is a sharp decrease in TGA isotherms for all membrane compositions at about 210 ^{O}C and most of the weight loss was observed after that point. Since the chains of polymer become more flexible above its glass transition temperature, the residual solvent may be removed easily at higher temperatures and these sharp decreases may be attributed as the cursor of the sudden relaxation at Tg. The total amount corresponds to the remaining solvent gained by ZIF-8 crystals and polymer/ZIF-8 interfaces [43]. When Table 4.6 and 4.7 were compared it is observed that the total amounts of weight loss for ternary membranes are about 2 % higher than the loss for binary membranes which may be related to some loss of low molecular weight additive.

Moreover, in order to estimate the decomposition temperature of the polymer, this analysis was performed between 30 and 650°C for neat PES membrane under same operation conditions. The TGA thermogram shown in Figure 4.17 indicates a total 58.83 % weight loss up to 650 ^{o}C. The most substantial weight loss was being taken place after about 430^{o}C which may be attributed as the temperature that the polymer decomposition starts.

Table 4.7 Weight losses of the ternary MMM with different ZIF-8 and HMA loadings

PES/ZIF-8(%x)/HMA(%y)					
x	y	Weight Loss Up to 105 ^{0}C (%)	Weight Loss Between 105-200 ^{0}C (%)	Weight Loss Between 200-300 ^{0}C (%)	Total Weight Loss(%)
10	4	1.16	0.75	3.02	4.93
20	4	0.56	0.32	5.07	5.94
20	7	0.63	0.54	5.10	6.27
30	1	0.82	0.23	3.60	4.65
30	2	1.00	0.97	6.43	8.40
30	4	0.73	0.40	5.47	6.59
30	10	0.89	0.54	5.44	6.87

It can be concluded that the weight loss seen up to 300 ^{o}C corresponds to only moisture and residual solvent in the membrane material not decomposition. This analysis was performed for the membranes with different compositions so as to indicate the relationship between membrane composition and the decompositon temperature of the material and Table 4.8 shows the weight losses up to various temperatures. The thermograms can be found in Appendix H. While the total weight losses are around 60 % up to 650 ^{o}C, the 85 % of total is being lost between 430 and 650 ^{o}C for all membrane compositions.

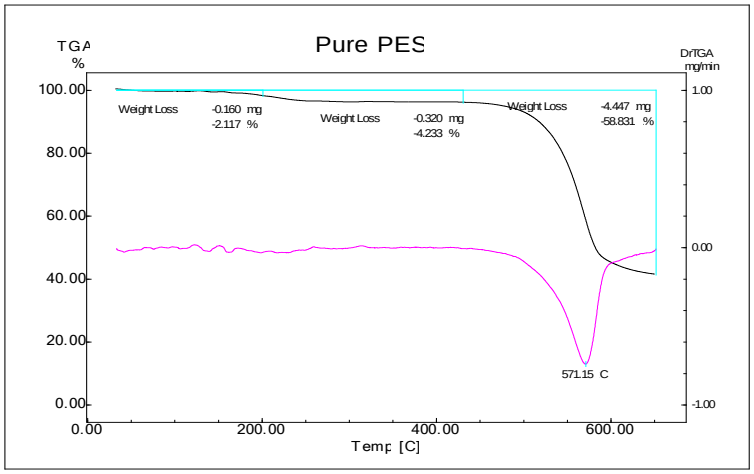

Figure 4.17 TGA thermogram of pure PES membrane up to 650 ^{O}C

Table 4.8 Weight losses of the membranes with different ZIF-8 and HMA loadings up to 650 ^{O}C

PES/ZIF-8(%x)/HMA(%y)		Weight Loss Up to 105 ^{0}C(%)	Weight Loss Between 105-300 ^{0}C (%)	Weight Loss Between 300-430 ^{0}C (%)	Weight Loss Between 430-650 ^{0}C (%)	Total Weight Loss(%)
x	y					
0	0	0.54	3.59	0.11	54.60	58.83
10	0	0.98	4.21	0.61	55.07	60.87
30	0	0.57	4.67	1.29	52.42	58.94
60	0	0.36	4.25	1.96	43.99	50.57
10	4	0.67	5.42	1.51	55.28	62.88
30	1	0.64	4.75	1.51	52.40	59.30
30	10	0.73	8.63	2.54	53.76	65.67

Thermogravimetric analysis was also used to check the ZIF-8 content of some of the MMMs. A small sample of membrane films with was heated from room temperature to 800^{O}C with a 10^{O}C/min rate in air atmosphere to decompose polymer and ZIF-8 as well as to oxidize all the elements. Zhang et.al [67] showed that the only solid oxide remaining in the final residues of ZIF-8 crystals is zinc oxide which analyzed by EDX. The mass percentage of ZIF-8 in the membranes can be calculated using the mass of zinc oxide left after analysis. The ZnO mass percentage of pure ZIF-8 crystals was 34.7 % which was also determined by TGA analysis between room temperature and 800^{O}C. The theoretical ZnO mass percentage of ZIF-8 calculated by formula weight is 28.5 % [67]. The detailed calculation procedure and TGA determined ZnO amounts and the back calculated ZIF-8 amounts for all types of membrane compositions can be found in Appendix I.

Table 4.9 indicates the back calculated ZIF-8 loadings for all binary and some of the ternary membranes. The calculated ZIF-8 amounts are lower than the expected values for most of the membrane compositions. Especially for both binary and ternary membranes incorporating 10 w/w % of ZIF-8, the back calculated values are lower than half of the expected values. The reason of these low values may be attributed to the possible agglomeration of ZIF-8 crystals in some parts of the membranes. Moreover, since there are very small amounts of ZIF-8 in these membranes, the weighing errors done during the analysis can affect the margin of error easily.

Table 4.9 Back calculated ZIF-8 loadings of binary and ternary membranes

Membrane Code	MembraneComposition	ZIF-8 (w/w %)
NK-77	PES/ZIF-8(%10)	3.9
NK-72	PES/ZIF-8(%10)/HMA(%4)	4.4
NK-102	PES/ZIF-8(%20)	17.0
NK-49	PES/ZIF-8(%20)/HMA(%7)	14.0
NK-87	PES/ZIF-8(%30)	27.0
NK-74	PES/ZIF-8(%30)/HMA(%1)	27.4
NK-84	PES/ZIF-8(%40)	32.9
NK-91	PES/ZIF-8(%50)	44.2
NK-93	PES/ZIF-8(%60)	55.8

Considering the PES/ZIF-8(%40) membrane, while the ZIF-8 percent in NK-54 is calculated as 42.7 %, NK-84 includes 32.9 % of ZIF-8 according to the TGA results. Since a very small part of membrane was used in TGA analysis, the overall composition of a membrane sheet can not be estimated form one point data and it is not enough to evaluate the membranes as reproducible or unreproducible, but it may give a general idea about the homogenity. For instance, the percent amount of ZIF-8 in the NK-54 implies that the filler content in some other parts of the sheet should be lower than 40%.

4.3 Permeation Results for PES/ZIF-8 and PES/ZIF-8/HMA MMMs

4.3.1 Reproducibility and Repeatability of the Results

Table 4.10 and 4.11 show the average permeability values of binary and ternary mixed matrix membranes. Moreover, the standard deviations were calculated for H_2, CO_2, CH_4 permeabilities through all types of membranes in order to examine the reproducibility. The maximum relative standard deviation[(standard deviation/average)×100] was found about 6% for H_2 for low ZIF-8 loaded binary and ternary membranes (< 30 w/w %) which is similar to the standard deviations

reported in the literature [5, 61], and confirm the reproducibility of the membrane preparation and testing methods.

Table 4.10 The permeabilities of the binary membranes with standard deviations

Membrane	Permeabilities(Barrer)		
	H_2	CO_2	CH_4
Pure Pes	9.5±0.2	4.5±0.1	0.13±0.00
PES/ZIF8(%10)	15.4±0.9	7.2±0.3	0.24±0.01
PES/ZIF8(%20)	26.3±0.4	12.4±0.5	0.43±0.01
PES/ZIF8(%30)	50.4±27.0	27.0±4.2	1.34±0.59
PES/ZIF8(%40)	50.5±15.8	30.0±6.2	1.61±0.54
PES/ZIF8(%50)	74.6±27.7	41.6±16.5	2.19±1.29
PES/ZIF8(%60)	106.6±48.2	79.2±34.4	5.43±3.83

However for high ZIF-8 loaded binary and ternary membranes (≥ 30 w/w %) the relative standard deviations are changing between 15% and 70% which are very high values for reproducibility confirmation. Three different reproducibility types were investigated for high ZIF-8 loaded membranes; measurement reproducibility (repeatability), preparation reproducibility and formulation reproducibility. Firstly, all the permeability measurements were performed twice (except CH_4 owing to its long permeation time) so as to indicate the repeatability of measurements. The table (given in Appendix K) indicated that the permeabilities for same membrane part obtained by two successive experiments are completely repeatable for high ZIF-8 loaded binary and ternary membranes. Two different parts from all membrane sheets were characterized by permeation experiments so as to analyze for preparation reproducibility, and very similar results were obtained except the small deviations observed in CH_4 permeabilities through these membranes. Finally, three different membranes were prepared for each composition in order to examine the formulation reproducibility and the results show that high ZIF-8 loaded binary and ternary MMMs have not formulation reproducibility.

Table 4.11 The permeabilities of the ternary membranes with standard deviations

Membrane	Permeabilities(Barrer)		
	H_2	CO_2	CH_4
PES/ZIF8(%10)/HMA(%4)	8.8±0.2	3.2±0.2	0.11±0.02
PES/ZIF8(%20)/HMA(%4)	15.5±0.4	5.9±0.3	0.22±0.02
PES/ZIF8(%20)/HMA(%7)	13.7±0.8	4.7±0.8	0.13±0.02
PES/ZIF8(%30)/HMA(%1)	23.7±3.3	11.0±0.8	0.39±0.09
PES/ZIF8(%30)/HMA(%2)	26.9±1.9	11.0±0.7	0.43±0.02
PES/ZIF8(%30)/HMA(%4)	20.6±3.0	9.7±2.9	0.38±0.18
PES/ZIF8(%30)/HMA(%10)	13.7±0.4	4.9±0.3	0.17±0.04

To sum up, the repeatability and reproducibility experiments suggest that the optimum ZIF-8 contents for this membrane materials 20 % w/w. The standard deviations show that very reproducible ternary membranes obtained with the addition of HMA into the 10 and 20 w/w % ZIF-8 loaded membranes. However, the maximum relative standard deviations for 30 % w/w loaded membranes are calculated as 15%, 30%, 47% for H_2, CO_2 and CH_4 gases, respectively.

Reproducibility in membrane preparation is a significant issue since it shows the reliability and robustness of the membranes [41, 42]. The high loadings of nanosized ZIF-8 particles may be one possible disadvantage in this study while the reproducibility problem is considered. Especially, in the case of small sized filler materials, crystal particles in the membranes will attain very large numbers as the loading is increased. As the particle size is decreased, the number of the zeolite particles increase by factor $(R_1/R_2)^3$, where R_1 and R_2 denote the relatively larger and smaller particle size, respectively [89]. As the number of particles is increased in the polymer matrices, the extent of polymer-filler interface is increased, and thus the probability for interfacial defect formation is raised. Moreover, the different membrane structure for high ZIF-8 loadings observed from SEM micrographs may be the reason for reproducibility problem. The reduction in the percent amount of polymer in the formulation may change the structural properties.

On the other hand, the optimum filler content for high performance membrane preparation may change according to the characteristics of MOF and polymer type and the interaction between these two phases. For instance, while the optimum HKUST-1 content was reported as 30 w/w % for efficient CO_2/N_2 separation [14], the composition of ZIF-8 was reported as 50 w/w % for a high separation performance for various gas pairs in Matrimid matrix [70]. Moreover, the optimum ZIF-8 contents were reported as 30 [92], 15 [93], 48 [67] w/w % in PPEES, PMPS and 6FDA-DAM polymer matrices; respectively, so as to obtain high performance separation membranes for either single or binary gas separation experiments. The optimum filler content for the materials used in this study may be 20 w/w % for reproducible binary membrane fabrication.

4.3.2 Single Gas Permeation Results of PES/ZIF-8 MMMs

The single gas permeabilities of manifactured pure PES and PES/ZIF-8 binary MMM are presented together in Figure 4.18. CH_4 permeabilities were reported by multiplying 10. Figure 4.18 shows that, the single gas permeabilities of the PES/ZIF-8 MMMs are increasing with increasing ZIF-8 loadings. Especially, with the addition of 30 w/w % and higher ZIF-8 nano-crystals, the raise in the permeabilities were very strong and the highest increase was in the permeability of CH_4. In literature, there are similar increasing permeability trends with increasing loadings of nano-size filler materials. Balkus et.al [70] prepared Matrimid/ZIF-8 MMM which contains varying amounts of ZIF-8 nano-crystals(50-150nm in size) between 10 w/w % and 80w/w % and reported that the single gas permeabilities for all gases were increasing up to 40 w/w % due to the increasing free volume. However, for the higher percentage of ZIF-8 nanocrystals, the gas permeabilities were reduced. This trend was claimed as the result of reduction in the amount of polymer for gas transport, increase in the diffusion path length for the gas penetrants, and reducing free volume in the membrane due to increasing density.

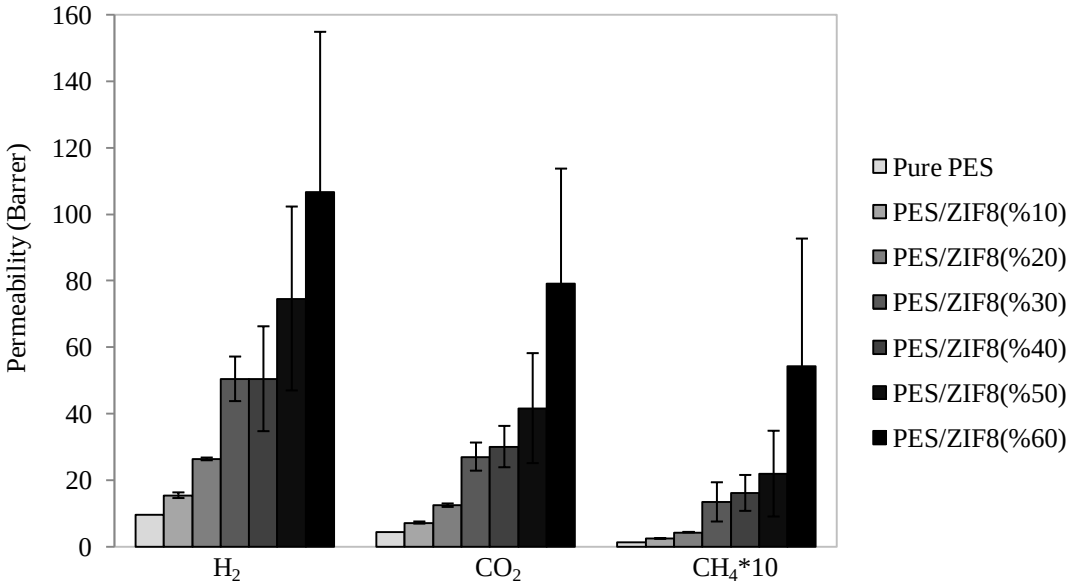

Figure 4.18 Effect of ZIF-8 loading on single gas permeabilities of PES/ZIF-8 MMM

Moreover, Perez et.al [11] used different amounts of MOF-5 nanocrystals in MMMs (10, 20 and 30 w/w %) and investigate the permeation characteristics of those for the gases H_2, CO_2, CH_4, N_2, O_2. They reported that, while the permeability of all gases increased with MOF-5 loading, the ideal selectivities stayed nearly constant. When 30 w/w % of MOF-5 incorporated into Matrimid, the permeabilities increased 120% with respect to pure polymeric membrane suggesting that MOF-5 crystals were facilitating the gas transport. The increase observed in the permeability values with increasing ZIF-8 loading may be due to the enhanced free volume and number of resistless ZIF-8–polymer interfaces that the gas molecules can cross through the membrane.

The ideal selectivities of the PES/ZIF-8 MMM for H_2/CO_2, CO_2/CH_4, and H_2/CH_4 gas pairs are represented in Table 4.12. The incorporation of ZIF-8 at low loadings (< 30 w/w %) improved the performances of the membranes. While the addition of 10 w/w % ZIF-8 into polymer increased the permeabilities ~2 times for all gases, the ideal selectivities for CO_2/CH_4, and H_2/CH_4 gas pairs showed a slight loss (~14%), with a constant H_2/CO_2 selectivity. When the weight percent of ZIF-8 was increased to 20, the ideal selectivities for all gases are about the same with the results of PES/ZIF-8(%10), and still lower than the pure PES selectivities. The increase in the permeabilities is about 3 times while the loss in selectivities for CO_2/CH_4, and H_2/CH_4 gas pairs was about 16 % compared to results of pure PES membrane.

For the higher ZIF-8 loadings (≥ 30 w/w %), while the permeabilities are increasing, the ideal selectivities started to reduce very rapidly. Since the most sensible increase in permeabilities was observed in CH_4, the ideal selectivities decreased in the order of $H_2/CH_4 > CO_2/CH_4 > H_2/CO_2$ for all membranes. In general the ideal selectivities are improved with the addition of filler into glassy polymers up to 20% and 30% loadings [70].

Table 4.12 Effect of ZIF-8 loading on ideal selectivities of PES/ZIF-8 MMM

Membrane Composition	Ideal Selectivities		
	H_2/CO_2	CO_2/CH_4	H_2/CH_4
Pure Pes	2.1	34.5	72.9
PES/ZIF8(%10)	2.1	29.8	64.0
PES/ZIF8(%20)	2.1	29.1	61.8
PES/ZIF8(%30)	1.9	22.3	42.9
PES/ZIF8(%40)	1.6	19.9	33.2
PES/ZIF8(%50)	1.6	20.3	32.1
PES/ZIF8(%60)	1.3	16.9	22.1

There are also other studies that show decreasing selectivities with increasing zeolite loadings after a certain point, and that was related to the voids between the polymer chains and the fillers which are the new directions for the gas molecules to pass through instead of the open pores of zeolites[12]. Balkus et.al [70] reported that with the addition of 20 w/w % ZIF-8, the ideal selectivities were increased from 3.03 to 3.46, from 39.84 to 51.06 and from 120.8 to 176.68 for the gas pairs of H_2/CO_2, CO_2/CH_4, and H_2/CH_4, respectively. However, for higher loadings the ideal selectivities for all gas pairs are decreased.

Figures 4.19, 4.20 and 4.21 depict the permeation results of binary membranes on the Robeson's upper bound curves for H_2/CO_2, H_2/CH_4 and CO_2/CH_4 gas pairs, respectively. For H_2/CO_2 gas pair, it is obviously seen that the membranes are moving on a nearly constant selectivity value with increasing permeabilities and this behaviour of the membrane can be explained by Case II, sieve-in-a cage morphology, which is the confirmation of poor interaction and non-selective voids between PES

and ZIF-8 nano-crystals. Since these voids are less-resistant directions, the gas molecules prefer to pass through them instead of pores of the particles, and thereby selectivities are not increased.

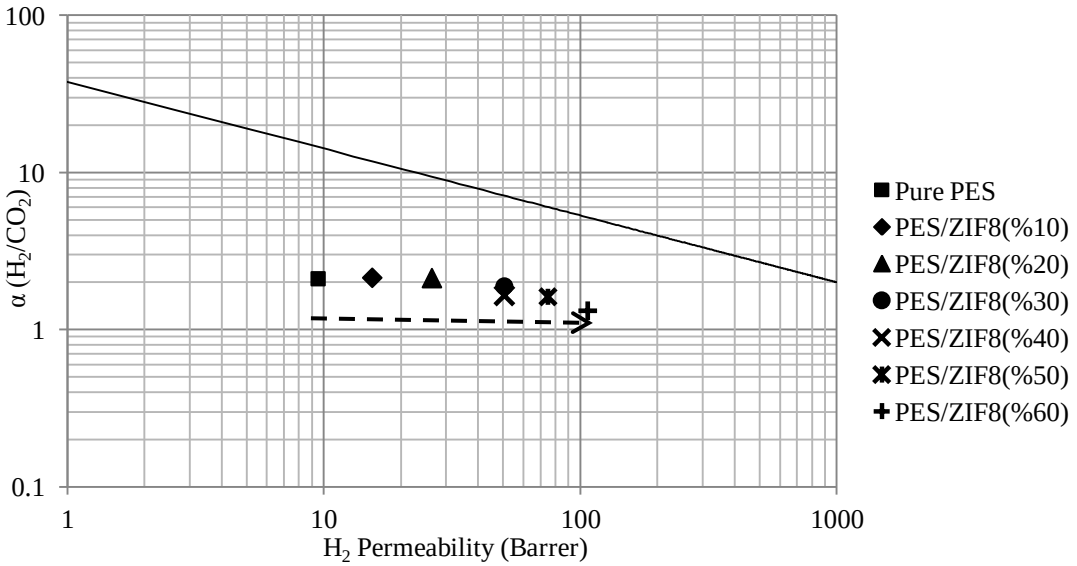

Figure 4.19 Single gas permeabilities of membranes with reference to upper bound line for H_2/CO_2

In the case of H_2/CH_4 and CO_2/CH_4 gas pairs, the trend for the membranes having increasing ZIF-8 contents can be explained by Case II and III together. Up to 30 w/w % ZIF-8 loading, there was a slight difference between the selectivities of the membranes, however for the higher loadings of ZIF-8, the selectivities were reduced with increasing ZIF-8 loading. In other words, as the number of crystals in the polymer matrice was increased, the number of voids that occurs around the ZIF-8 crystals were raised and thereby, the voids contact to each other more easily and larger voids were constructed. The sharp decrease in the selectivities for high ZIF-8 loadings(≥30 w/w %) might be the consequence of the more prominent interfacial voids. Nevertheless, all the membranes are permeselective for all gas pairs with very high permeabilities.

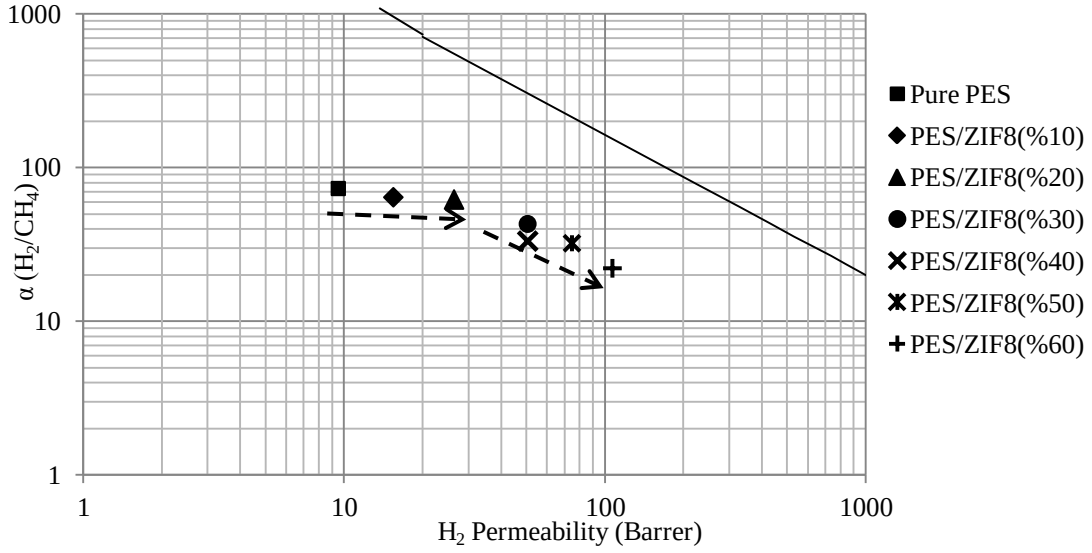

Figure 4.20 Single gas permeabilities of membranes with reference to upper bound line for H_2/CH_4 pair

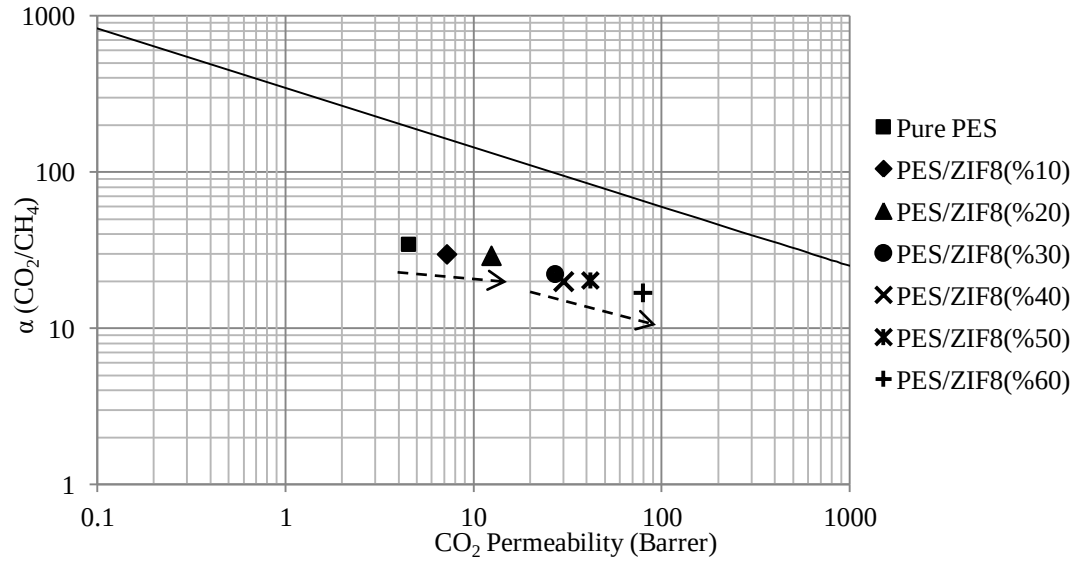

Figure 4.21 Single gas permeabilities of membranes with reference to upper bound line for CO_2/CH_4 pair

These results suggest that the incorporation of ZIF-8 nano-crystals into the polymer changes the structure of the membranes and increase the membrane performance significantly for both low and high ZIF-8 loadings.

ZIF-8 crystals might cause formation of microcavities in the structure due to the partial incompatibility between the polymer and the filler particles and the reason of increase in the permeabilities might be explained by the interfacial voids around the ZIF-8 particles. Since the alternative ways for gas transport are less resistant paths, this may lead to decrease in selectivities. Nevertheless, all the membranes are permselective for all gas pairs with very high permeabilities even at high loadings. However for high ZIF-8 loaded membranes, the structure of the membranes is completely different from the others. The continuous phase is changing from polymer matrix to the ZIF-8 crystals and polymer act as a binder between them. The reproducibility problem in these membranes could be the outcome of this different structure. This inference suggested the modification of the PES/ZIF-8 membranes with 10, 20 and 30 w/w % of ZIF-8 by addition of low molecular weight additive as a third component to the membrane formulation so as to have better membranes.

Figure 4.22, 4.23 and 4.24 show the Maxwell model predictions of all ZIF-8 contents and experimental results of some membranes for H_2/CO_2, H_2/CH_4 and CO_2/CH_4 gas pairs, respectively. While the experimental positions are nearly coincidenced with the theoritical positions for PES/ZIF-8(%10) membrane which has minimum ZIF-8 content, the highest distance between the experimental results and theoretical predictions belongs to PES/ZIF-8(%60) membrane for all gas pairs. The expanding variations between the experimental results and theoritical predictions with increasing ZIF-8 content may be evaluated as another precursor of the non-selective interfacial voids between polymer and ZIF-8 crystals. Moreover, there is a formulation reproducibility problem in high ZIF-8 loaded (>30 %w/w) membranes.

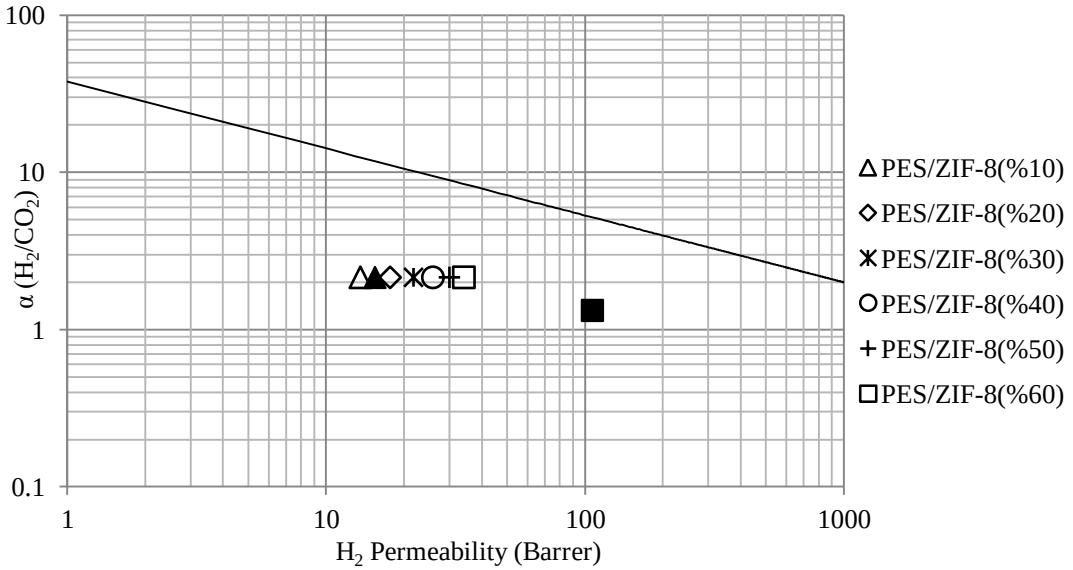

Figure 4.22 Single gas permeabilities of membranes with reference to upper bound line for H_2/CO_2 pair (The filled symbols indicate the experimental results)

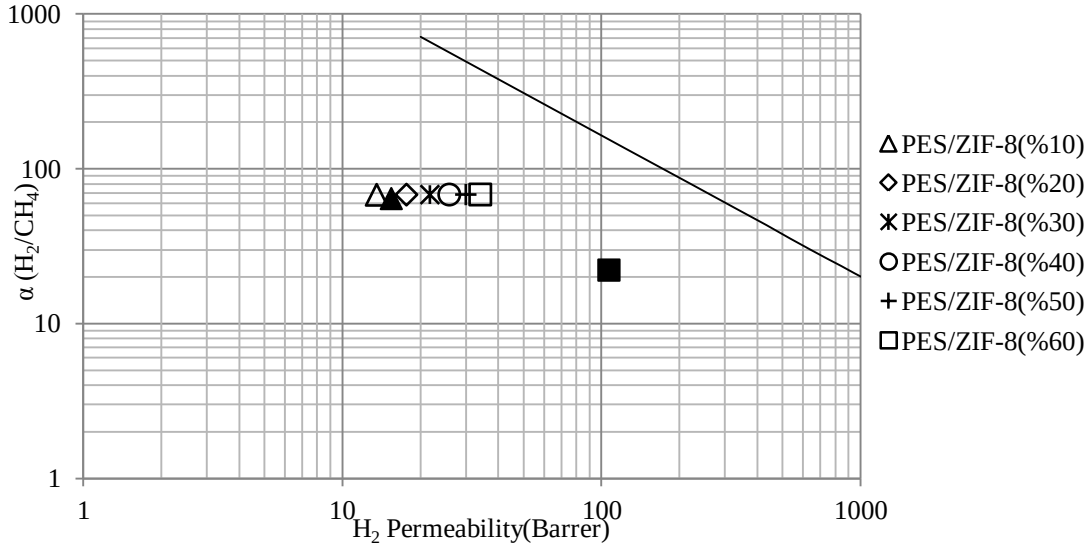

Figure 4.23 Single gas permeabilities of membranes with reference to upper bound line for H_2/CH_4 pair (The filled symbols indicate the experimental results)

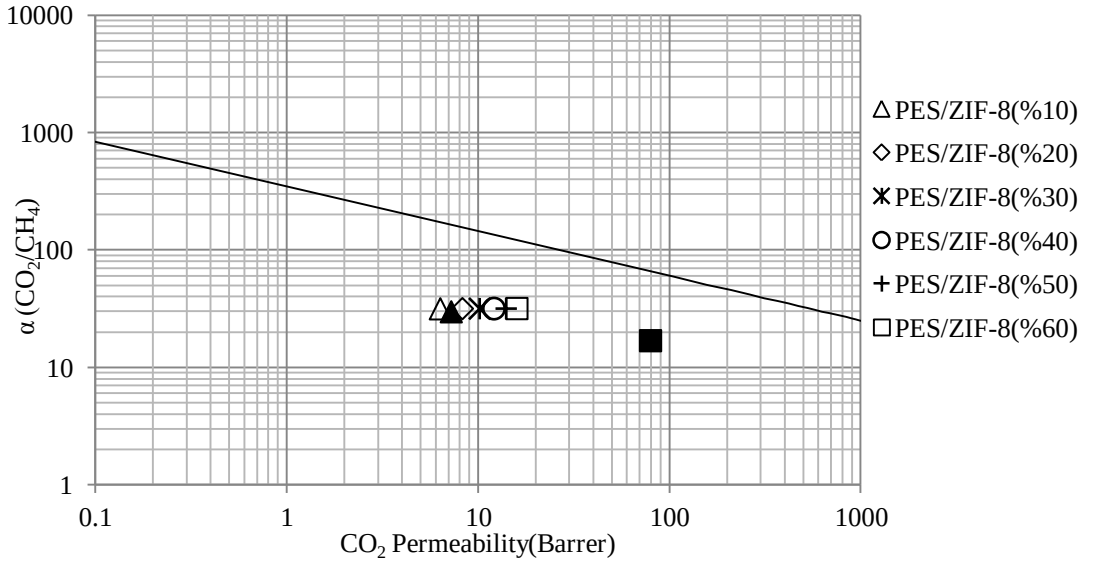

Figure 4.24 Single gas permeabilities of membranes with reference to upper bound line for CO_2/CH_4 pair (The filled symbols indicate the experimental results)

4.3.3 Single Gas Permeation Results of PES/ZIF-8/HMA MMMs

The single gas permeabilities of H_2, CO_2, and CH_4 through PES/ZIF-8/HMA mixed matrix membranes and ideal selectivities for each gas pairs are tabulated in Table 4.13. PES/HMA(%4) membrane has lower permeabilities and higher ideal selectivities than neat PES membrane. Very similar results were obtained in the previous studies of our research group, in which studies this behavior was explained by the antiplasticization effect of HMA. Because, HMA reduces the free volume of the polymer and the membrane stiffens [40, 41, 42].

For the 10 w/w % ZIF-8 loaded mixed matrix membranes, HMA addition reduced the permeabilities for H_2, CO_2, and CH_4 gases when compared with both pure PES and PES/ZIF-8(%10) membranes. The H_2 permeability of 10 w/w % ZIF-8 loaded binary membranes decreased from 15.4 to 8.8 barrer, by 4% w/w HMA addition. Similarly CO_2 permeability decreased from 7.2 to 3.2 and CH_4 permeability decreased from 0.24 to 0.11. While the percent decrease observed in CO_2 and CH_4 permeabilities were about 55 %, H_2 permeability showed the smallest decrease (~45%). Ideal selectivities for all gas pairs were calculated using single permeabilities. The ideal selectivity for H_2/CO_2 increased from 2.1 to 2.8 with the addition of 4 % w/w HMA. While the CO_2/CH_4 selectivity stayed nearly constant and H_2/CH_4 selectivity increased from 63.9 to 83.3. The percent increases of the selectivities with the addition of %4 w/w HMA to the PES/ZIF-8(%10) membrane were calculated as about 30 % for both gas pairs H_2/CH_4 and H_2/CO_2.

The incorporation of low molecular weight additives into neat polymeric membrane materials is generally resulted in decreasing permeabilities with increasing selectivities.[19, 20, 21] Karatay et.al [19] reported increasing selectivities with decreasing permeabilities for H_2, CO_2 and CH_4 gases in PES/SAPO-34/HMA membrane system. The reason underlying the decreasing permeabilities of PES/ZIF-8/HMA ternary MMMs may be explained by the antiplasticization effect of HMA. Due to this effect of HMA, the free volume of the membrane material were reduced and the membrane stiffens [20, 41].

Table 4.13 Gas permeation performances of binary and ternary MMMs

PES/ZIF8(%x)/HMA(%y)		Permeabilities(Barrer)			Ideal Selectivities		
x	y	H_2	CO_2	CH_4	H_2/CO_2	CO_2/CH_4	H_2/CH_4
0	0	9.5±0.2	4.5±0.1	0.13±0.00	2.1	34.5	72.9
	4	5.9±0.1	1.9±0.1	0.06±0.00	3.1	31.4	97.4
10	0	15.4±0.9	7.2±0.3	0.24±0.01	2.1	29.8	63.9
	4	8.8±0.2	3.2±0.2	0.11 ±0.02	2.8	29.9	83.3
20	0	26.3±0.4	12.4±0.5	0.43±0.01	2.1	29.1	61.8
	4	15.6±0.5	5.9±0.3	0.22±0.02	2.7	26.8	70.5
	7	13.7±0.8	4.7±0.8	0.13±0.02	2.9	35.3	103.7
30	0	50.4±27.0	27.0±4.2	1.34±0.59	1.9	22.3	42.9
	1	23.7±3.3	11.0±0.8	0.39±0.09	2.2	28.9	62.5
	2	26.9±1.9	11.1±0.7	0.43±0.02	2.4	25.6	62.0
	4	20.6±3.0	9.7±2.9	0.38±0.18	2.2	27.3	62.9
	10	13.7±0.4	4.9±0.3	0.17±0.04	2.8	29.3	83.1

Figure 4.25 indicates the permeabilities and ideal selectivities with respect to increasing HMA concentration of PES/ZIF-8(%20) membranes. Considering the 20 w/w % ZIF-8 loaded mixed matrix membranes, increasing concentrations of HMA resulted in decreasing permeabilities for all gases, when all are above those of the pure PES membrane. The percent reduction in single permeabilities for the gases H_2, CO_2, and CH_4 were calculated as 48 %, 62 % and 70%, respectively comparing with PES/ZIF-8(%20) membrane. The change in gas permeabilities of the membrane was related to the kinetic diameters of the gases (Table 4.14) in which relationship HMA additon mostly affected the largest gas molecule.

Table 4.14 Kinetic diameters of studied gases[1]

GAS	H_2	CO_2	CH_4
Kinetic Dimater(nm)	0.289	0.33	0.38

The ideal selectivities were calculated for all gas pairs and it was observed that a considerable improvement was achieved with increasing concentration of HMA in the polymer formulation. The ideal selectivities for all gas pairs were shown an increasing trend when compared with the PES/ZIF-8(%20) binary mixed matrix membrane and the ideal selectivities for H_2/CO_2 and H_2/CH_4 gas pairs are higher than those of the pure PES membrane. Especially for H_2/CH_4 gas pair, the selectivity was increased from 61.8 to 103.7 with the addition of 7 w/w% HMA which corresponds to about 70 % improvement which is clearly seen from Figure 4.25.

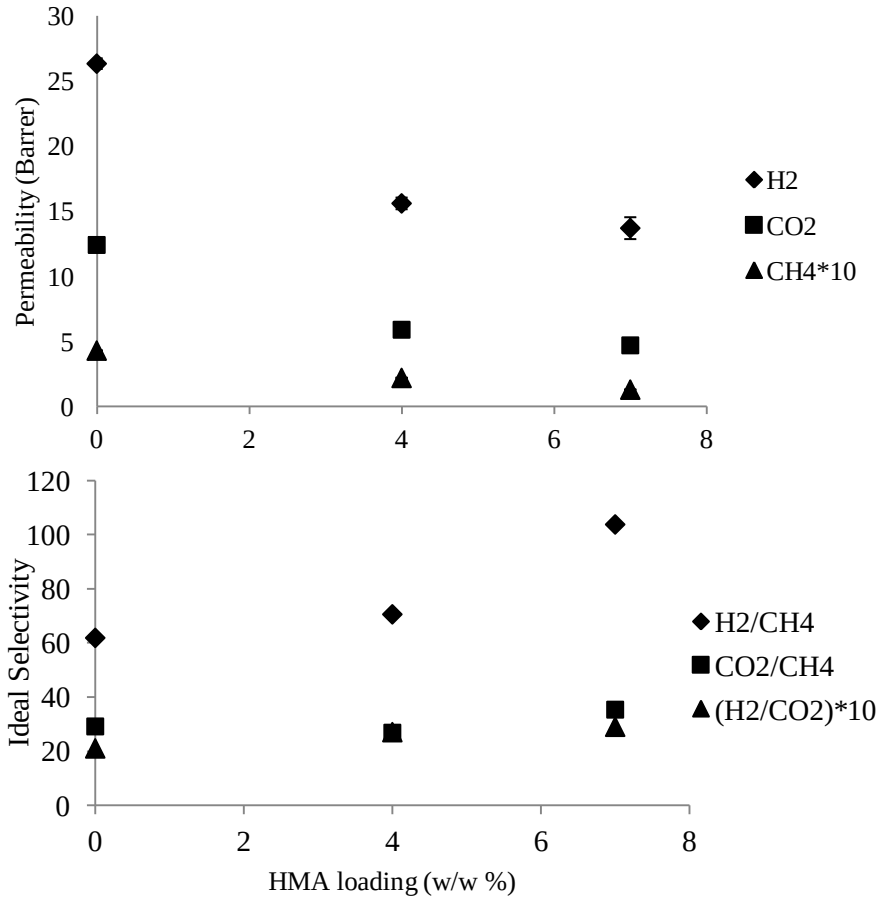

Figure 4.25 Effect of HMA loading on the permeabilities and the selectivities of the PES/ZIF-8(%20)/HMA(%x) MMMs

The highest selectivity increment was observed for the H_2/CH_4 gas pair in which the smallest molecule permeated fast and the largest molecule permeated slowly. The ideal selectivity for CO_2/CH_4 gas pair was less affected pair with a 21 % increase from the addition of 7 w/w% HMA. In a previous study of our research group, paranitroaniline and 4-amino 3 nitro-phenol were used as low molecular weight additives into polycarbonate membranes and nearly same results were observed for CO_2/CH_4 gas pair [63]. Karatay et.al [19] also reported that the highest selectivity increment was observed in H_2/CH_4 gas pair by HMA addition for PES/SAPO-34/HMA membrane system of which reason was explained as HMA addition improve the size selectivity of the ternary membranes[19,20].

While the permeation results of the 20 w/w % loaded ternary MMMs with different HMA contents are plotted on the Robeson plot for H_2/CH_4 gas pair, the performance improvement with increasing HMA content is seen obviously with reference to the neat PES membrane (Figure 4.26). It is seen that with the addition of HMA into neat PES membrane, the position on the Robeson plot is changing in the direction of Case I in which the polymer is rigidified and chain mobility is reduced. In the presence of rigidified polymer, lower permeability and higher selectivity is expected by improved diffusive selectivity in this region [47, 48].

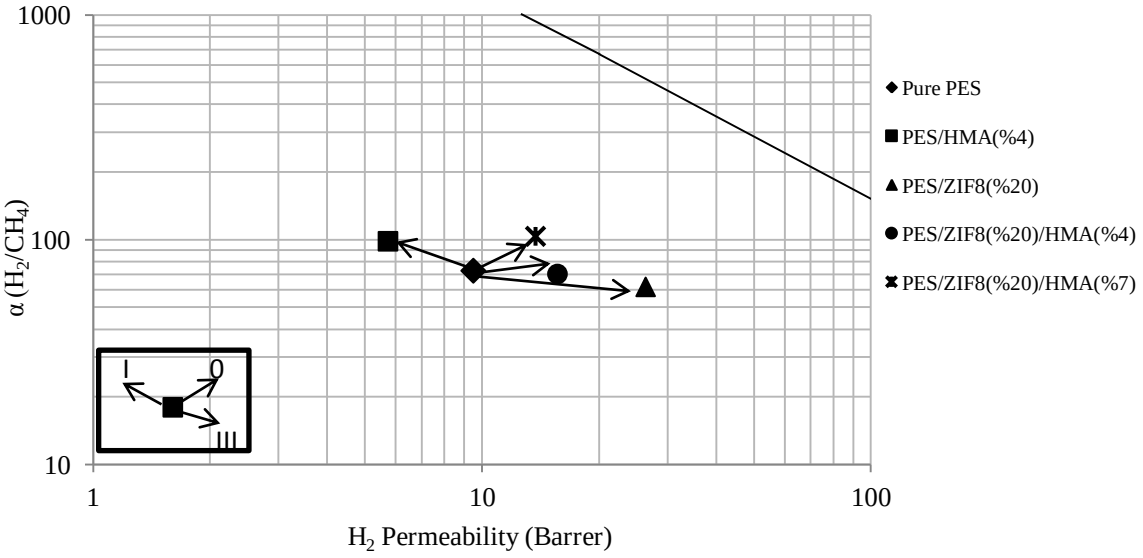

Figure 4.26 Single gas permeabilities of binary and ternary membranes with reference to upper bound line for H_2/CH_4 pair

By incorporation of ZIF-8 nanoparticles into polymer matrix, while the H_2 permeability was increased, H_2/CH_4 ideal selectivity was decreased. That behavior, which named as Case III, caused by the unselective voids at the polymer/particle interfaces.

With the addition of third component into binary MMMs, both the permeabilities and selectivities were increased compared to the neat PES membrane. This behaviour corresponds to the Case 0 which is the ideal case with non-defect membrane morphology in reference to neat PES membrane. If the direction of motion PES/ZIF-8(%20)/HMA(%7) is evaluated with respect to PES/ZIF-8(%20) membrane, the antiplasticization effect of HMA becomes prominent.

Figure 4.27 presents both the permeability and selectivity changes of 30 % w/w ZIF-8 loaded ternary MMMs with respect to HMA composition in the membrane formulation. The same behaviour was observed with the membranes including 20 %w/w of ZIF-8, reducing permeabilities and increasing ideal selectivities for incremental HMA contents. The permeation results of PES/ZIF-8(%30)/HMA(%2) membrane are not complied with overall behaviour. The highest increment was again seen in H_2/CH_4 gas pair which was almost doubled with the addition of 10 % w/w HMA into PES/ZIF-8(%30) membrane, while the percent increases in CO_2/CH_4 and H_2/CH_4 gas pairs were calculated as 30 %.

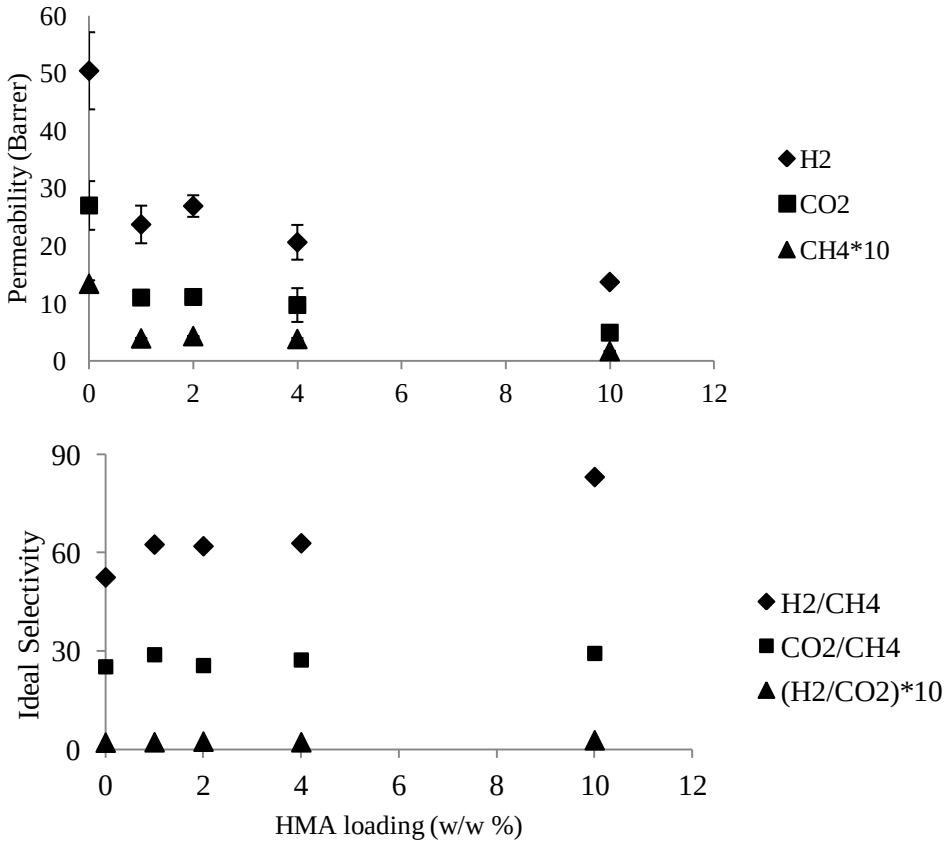

Figure 4.27 Effect of HMA loading on the permeabilities and the selectivities of the PES/ZIF-8(%30)/HMA(%x) MMMs

Figure 4.28 depicts the gas separation performances of 30 w/w % ZIF-8 loaded ternary membranes for H_2/CH_4 gas pair. The performances of Pure PES and PES/ZIF-8(%30) membranes were also presented on the Robeson curve so as to analyze the improvements and/or declinations in the gas transport performances. When the performances of the ternary membranes were evaluated in reference to PES/ZIF-8(%30) membrane, the direction of motion corresponds to Case I for all HMA contents as a result of polymer rigidification around the ZIF-8 crystals. PES/ZIF-8(%30)/HMA(%10) membrane showed an ideal case movement with respect to the position of neat PES membrane, in which case both the permeability and ideal selectivity were increased.

Incorporation of third component to the MMM formulation for all ZIF-8 contents, resulted in same effects on the gas permeation performances, in which the permeabilities decreased, while the ideal selectivities increased. The experimental results obtained up to now indicated that HMA addition improved the gas separaton performances of the membranes, significantly. Especially, PES/ZIF-8(%20)/HMA(%7) membranes have very high permselectivities with their reproducible membrane composition.

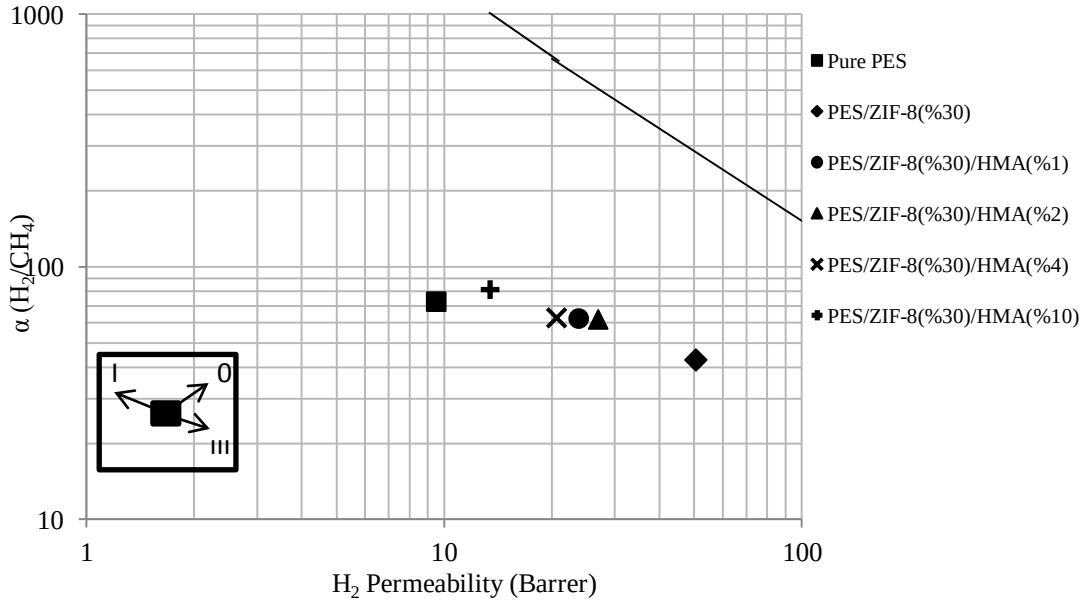

Figure 4.28 Single gas permeabilities of binary and ternary membranes with reference to upper bound line for H_2/CH_4 pair

4.3.4 Effect of Feed Pressure on the Performance of Binary and Ternary MMMs

Most of the permeation and separation measurements of various gas separation membranes were carried out at constant low pressures in literature. However the processes in industrial applications as H_2 separation from gas mixtures, removal of CO_2 from high-pressure natural gas and H_2/CO_2 separation occur at high feed pressure ranges. Therefore, to assess the gas separation performance of the membranes entirely, low pressure experiments may not be enough. The pressure dependent gas separation characteristics and performances of the membranes should be known so as to develop high performance membranes for gas separation processes. There are limited numbers of studies investigating the effect of feed pressure on the performance of mixed matrix membranes. Since the adsorption characteristics of the filler materials and the chain structure of the polymer matrix may be affected by the pressure significantly [129, 130], it is very meaningful to analyze the effect of pressure on MMMs. In this study, five different membranes were chosen of which separation performances to be investigated at 5 different feed pressures. All the experiments were conducted at least for three different parts of membranes and the standard deviations were calculated. The results and the experimental conditions of the permeability and selectivity tests of all types of membranes are given in Appendix K. Figures 4.29 shows the permeabilities for H_2, CO_2 and CH_4 in pure PES and binary membranes as a function of the upstream driving pressure. There are error bars showing the standard deviations in the results for all gases and membranes.

The experimental results indicated that the permeability of CO_2 and CH_4 gases was reduced for pure PES membrane with increasing pressure whereas the permeability of H_2 do not depend on pressure. Decreasing permeabilities with increasing pressure was reported as an expected response of glassy polymers in literature [129]. The PES molecules pack more effectively with the effect of increasing pressure, so the free volume and transport mobility are decreased [130]. Since the H_2 is the smallest gas, it is least affected.

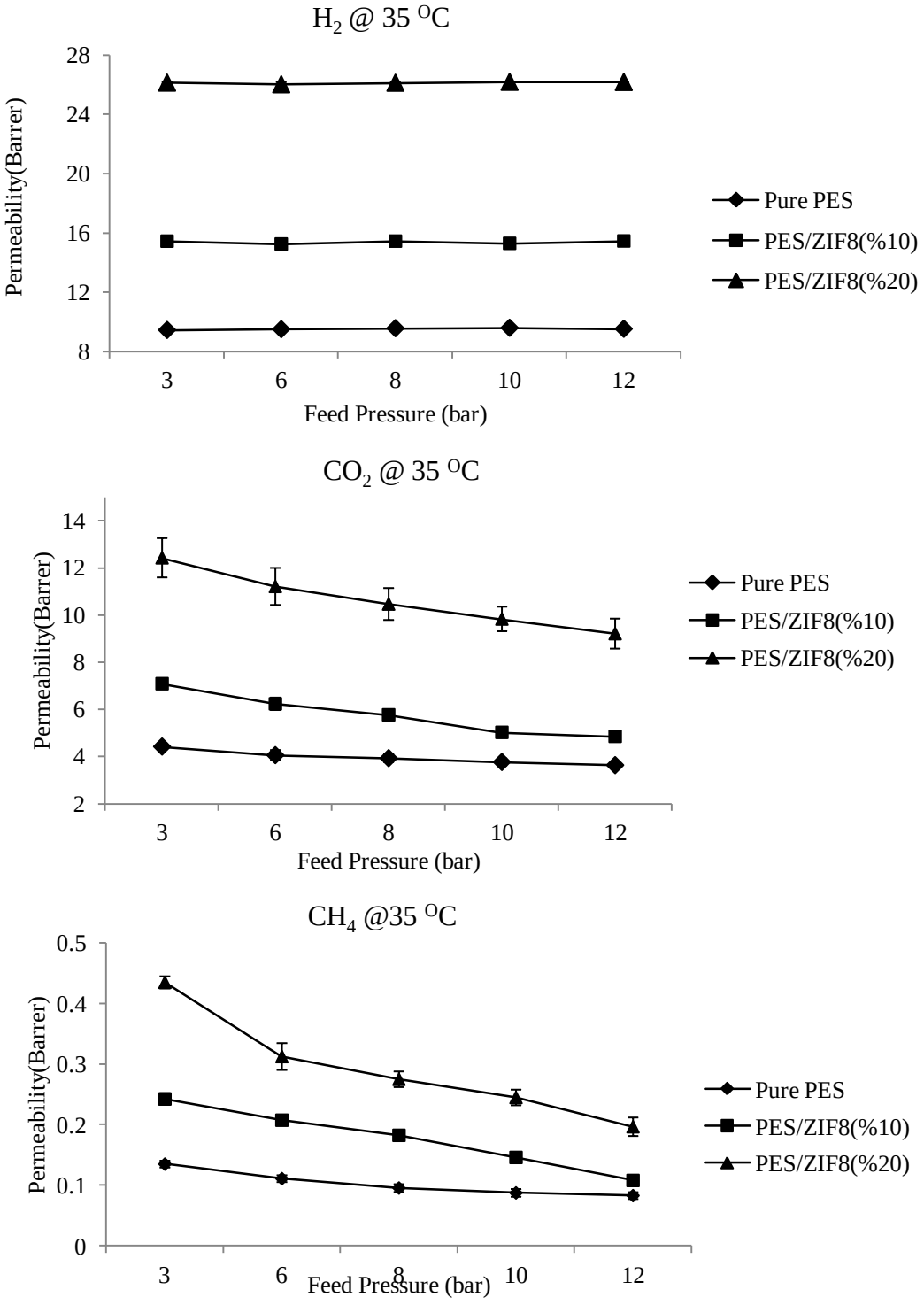

Figure 4.29 The permeabilities for H_2, CO_2 and CH_4 in pure PES and binary membranes as a function of the upstream driving pressure.

The percent decreases observed in the CO_2 and CH_4 permeabilities of pure PES membrane are calculated as 18% and 41%; respectively, when the feed pressure were increased from 3 bar to 12 bar. The change amounts in single permeabilities are very similar to the reported results in literature [129].

Figure 4.29 also shows the gas permeation characteristics of binary membranes with respect to increasing feed pressure. The general behaviour reported for pure PES membrane is also observed for both PES/ZIF-8(%10) and PES/ZIF-8(%20) membranes, but the percent decreases in the permeabilities of binary MMMs are higher than the ones of pure PES membrane. While the percent decrease in CH_4 permeabilities is about 55% for both 10 and 20 w/w % ZIF-8 loaded membranes, the reduction in CO_2 permeability changing with ZIF-8 amount; 31% for PES/ZIF-8(%10) and 26% for PES/ZIF-8(%20) membrane.

The reason of higher permeability reductions may be explained by the heterogenous micro structure of binary membranes. In PES/ZIF-8 membranes, as well as the chain structure of the polymer phase, the adsorption characteristics of ZIF-8 nanocrystals and the interphase morphologies between polymer and particles determine the gas separation performance of the membrane material. Incorporation of ZIF-8 crystals into PES resulted in interfacial void formation and the voids in the membrane expand when the ZIF-8 content is increased, as a result the permeabilities were increased with ZIF-8 content. Since the packing effect of pressure may eliminate some of these voids, the gas molecules may be started to pass through the pores of crystals. For PES/ZIF-8(%10) membrane the permeabilities at 12 bar are very closed to the permeabilities of pure PES membrane at 3 bar which is free of voids.

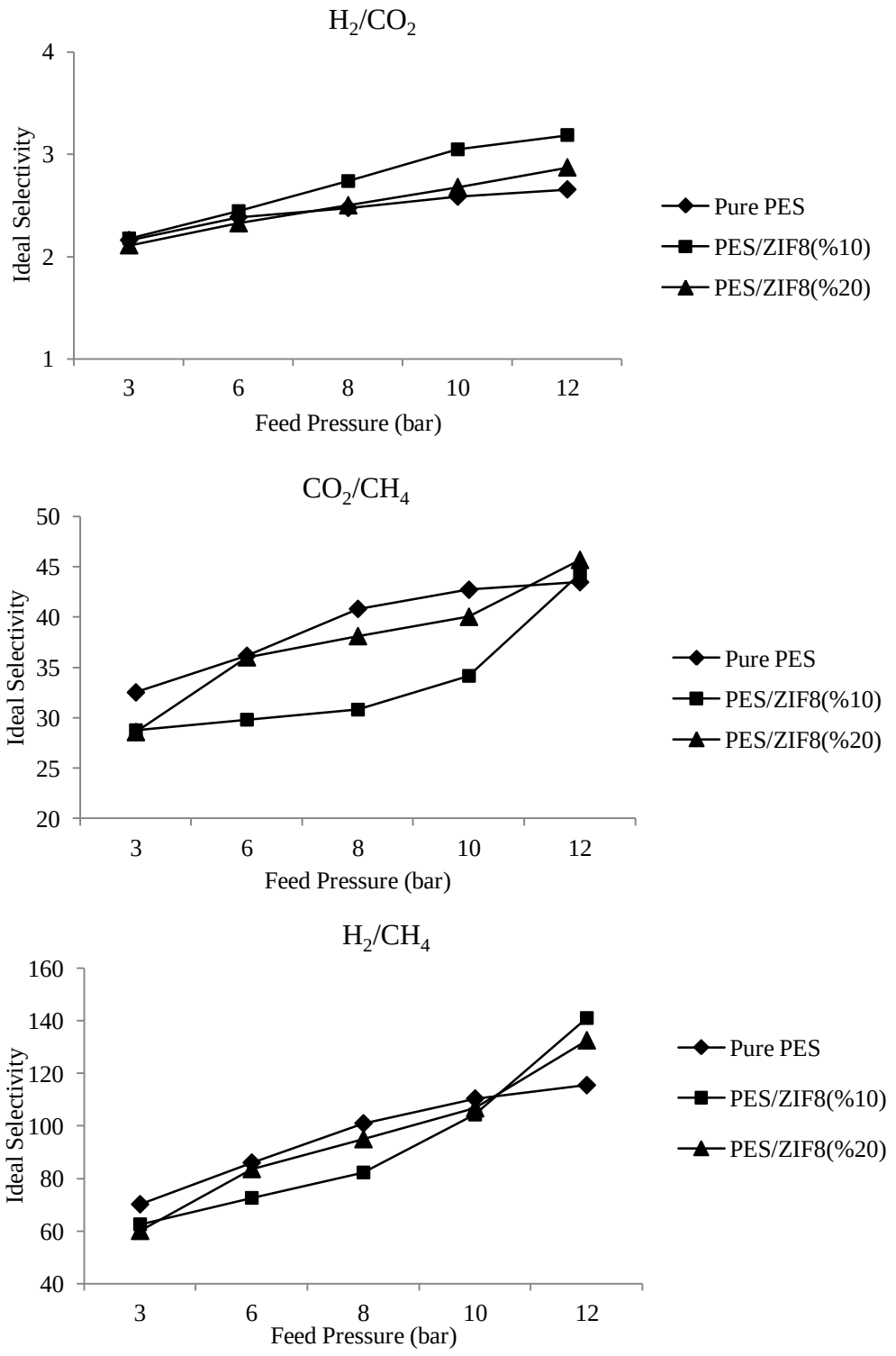

Figure 4.30 The ideal selectivities for H_2/CO_2, CO_2/CH_4 and H_2/CH_4 gas pairs in pure PES and binary membranes.

Figure 4.30 indicates the change in the ideal selectivities for all gas pairs with respect to increasing feed pressure. The ideal selectivities for all gas pairs were improved with the effect of pressure in all types of binary membranes, but the amount of increase in ideal selectivities is changing from membrane to membrane as shown in Table 4.15. Minimum improvement belongs to pure PES membrane with a dense homogenous structure and with the incorporation of 10 w/w % ZIF-8 into PES matrix, the improvement with pressure nearly doubled. The comparison of the improvements in pure PES and PES/ZIF-8(%10) membranes suggests that in addition to elimination of the voids by packing effect of the pressure, the adsorption capacity of the crystals may become more prominent on the gas transport mechanism at higher pressures. The slight reduction observed in the improvements for H_2/CO_2 and H_2/CH_4 gas pairs with 20 w/w % ZIF-8 addition compared to PES/ZIF-8(%10) membrane may be result of larger unselective channels. However, the CO_2/CH_4 selectivity is still increased which may be explained by the CO_2 selective adsorption capacity of ZIF-8.

Table 4.15 Percentage increases calculated in ideal selectivities of binary membranes when the pressure increased from 3 to 12 bars.

Membrane	H_2/CO_2	CO_2/CH_4	H_2/CH_4
Pure PES	23 %	34 %	65 %
PES/ZIF8(%10)	46 %	54 %	125 %
PES/ZIF8(%20)	36 %	60 %	121 %

The gas transport performances of ternary membranes were also investigated at various feed pressures between 3 and 12 bar. Figure 4.31 indicates the change in the H_2, CO_2 and CH_4 permeabilities of ternary membranes with respect to feed pressure. While the experimental results of binary membranes were reported in reference to neat PES membrane, the performances of ternary membranes were compared with the PES/HMA(%4) results. Since the addition of LMWAs results in substantial changes in polymer matrices, PES/HMA(%4) membrane could be treated as a new polymer phase with a dense homogenous structure[21]. The behaviour of the PES/HMA(%4) and ternary membranes against the increasing feed pressure is very similar to the pure PES and binary membranes. While the H_2 permeability did not depend on pressure, CO_2 and CH_4 permeabilities decreased for all membrane compositions. The least reduction in CO_2 and CH_4 permeabilities was observed for PES/HMA(%4) membrane with dense morphology without any voids as in the pure PES. The decrease in permeabilities for both gases was increased with the addition of ZIF-8.

Figure 4.32 shows the ideal selectivity changes of the ternary membranes. The ideal selectivities for all gas pairs were improved and the calculated percent improvements are shown in Table 4.16. PES/HMA(%4) membrane shows the minimum improvement with the effect of pressure and ZIF-8 addition increase the improvements as in the case of binary membranes.

Table 4.16 Percentage increases calculated in ideal selectivities of ternary membranes when the pressure increased from 3 to 12 bars.

Membran	H_2/CO_2	CO_2/CH_4	H_2/CH_4
PES/HMA(%4)	20 %	58 %	90 %
PES/ZIF8(%10)/HMA(%4)	26 %	69 %	113 %
PES/ZIF8(%20)/HMA(%4)	33 %	45 %	93 %

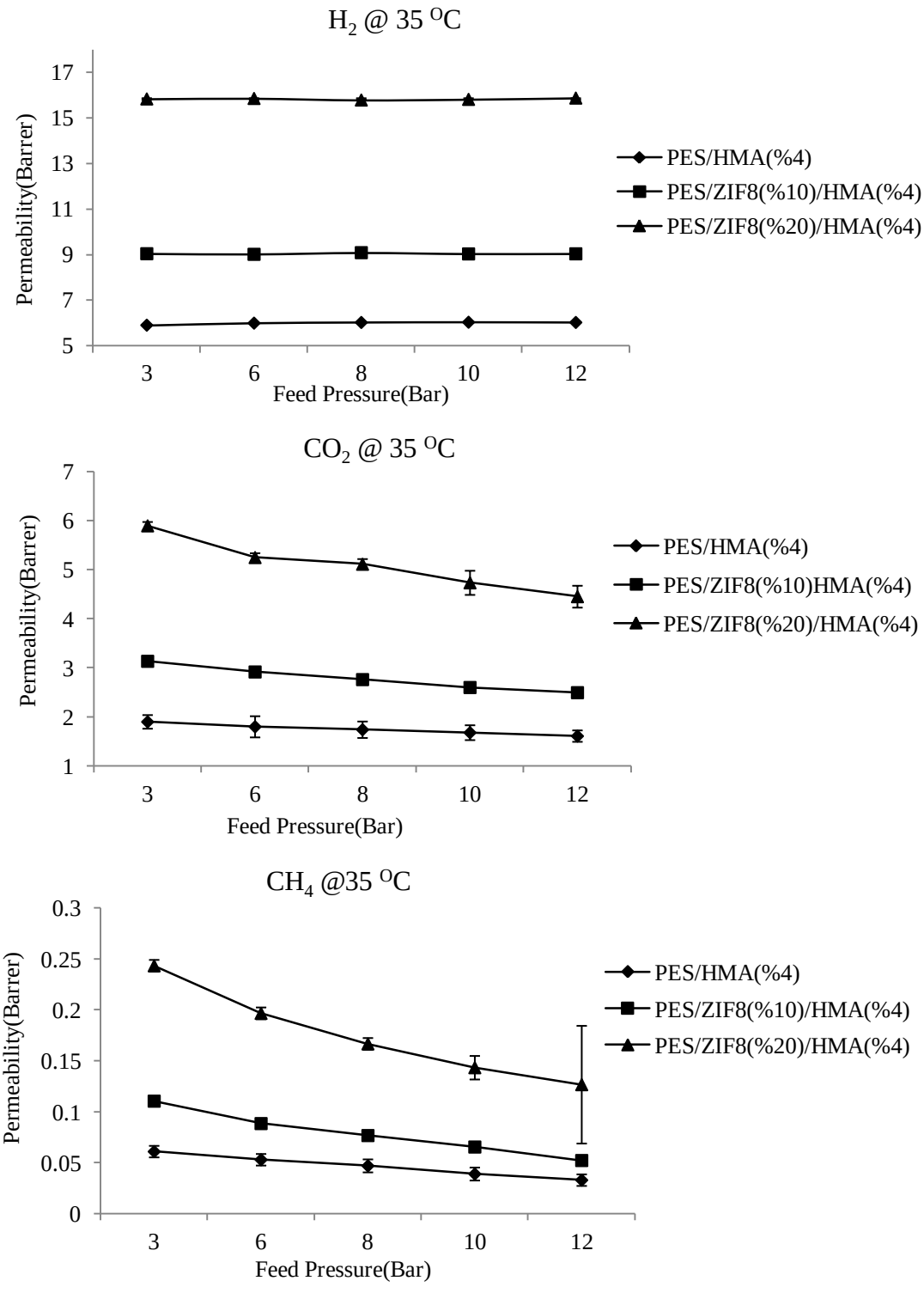

Figure 4.31 The permeabilities for H_2, CO_2 and CH_4 in PES/HMA(%4) and ternary membranes as a function of the upstream driving pressure.

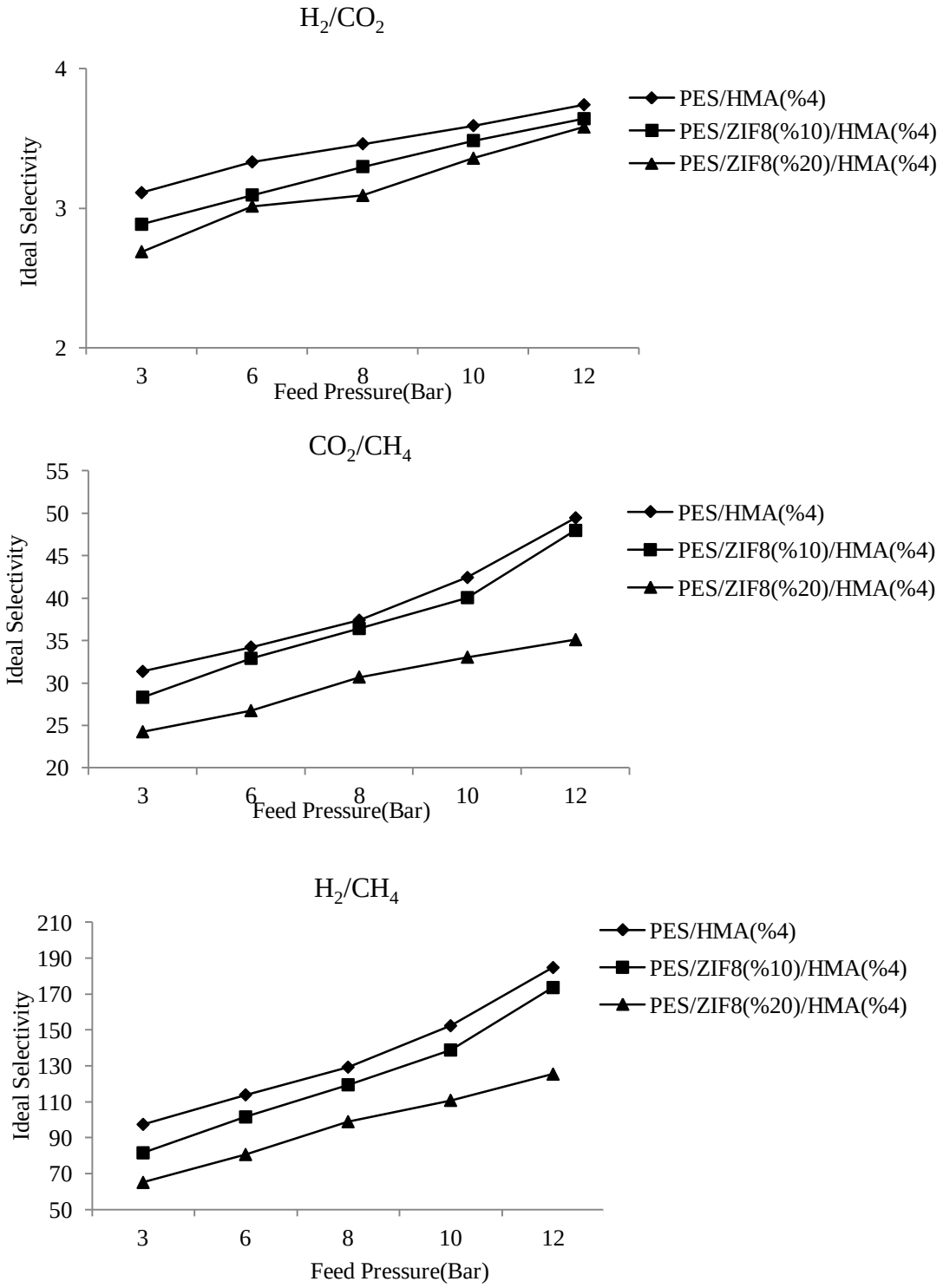

Figure 4.32 The ideal selectivities for H_2/CO_2, CO_2/CH_4 and H_2/CH_4 gas pairs in PES/HMA(%4) and ternary membranes.

Reduction was observed in the improvements for CO_2/CH_4 and H_2/CH_4 gas pairs with 20 w/w % ZIF-8 addition compared to PES/ZIF-8(%10) membrane being different from the binary membranes which may attributed to the complex micro structure of ternary membranes.

The trade-off graphs for H_2/CO_2 gas pair are presented in Figure 4.33 and 4.34 and the graphs for H_2/CH_4 gas pair are presented in Figure 4.35 and 4.36 for binary and ternary membranes, respectively. The membrane with the highest permeability and the highest selectivity (i.e, high permselectivity) stands at the lowest distance to the trade-off limit which can be evaluated as a high quality membrane [131]. The positions of the membranes moves on a constant permeability and increasing selectivity line for both H_2/CO_2 and H_2/CH_4 gas pairs and all of them come close to trade-off line with the effect of increasing pressure. The data illustrated in Figure 4.33 and 4.35 clearly show that the highest permselectivity belonged to the PES/ZIF-8(%20) membrane at 12 bar feed pressure when compared to other membranes. Moreover PES/ZIF-8(%20)/HMA(%4) membrane has the highest permselectivity among the membranes presented in Figure 4.34 and 4.36.

For preferable permeating gas, H_2, the permeabilities were almost constant while the ideal selectivities for H_2/CO_2 and H_2/CH_4 gas pairs increased in the case of increasing feed pressures. Despite of decreasing CO_2 and CH_4 permeabilities, CO_2/CH_4 selectivities through all membranes were also increased with the effect of pressure. Both binary and ternary MMMs showed very successful gas separation performances at high pressure.

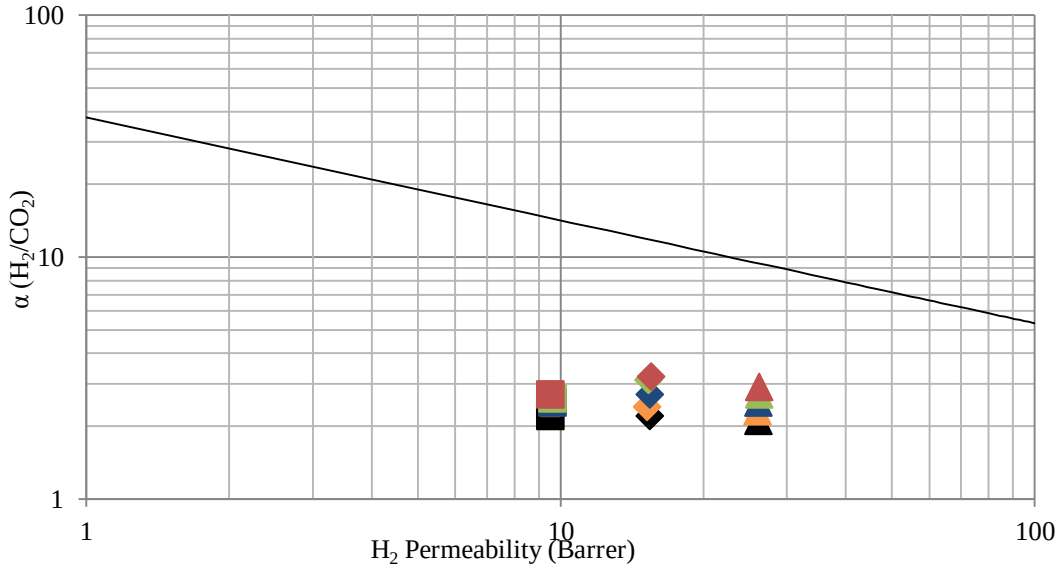

Figure 4.33 The effect of feed pressure on the binary membrane performances in reference to Robeson upper bound for H_2/CO_2 gas pair; □ indicates the Pure PES membrane, ◇_PES/ZIF-8(%10) membrane, △__PES/ZIF-8(%20) membranes (black=3bar, yellow=6bar, blue= 8bar, green= 10bar, red= 12bar)

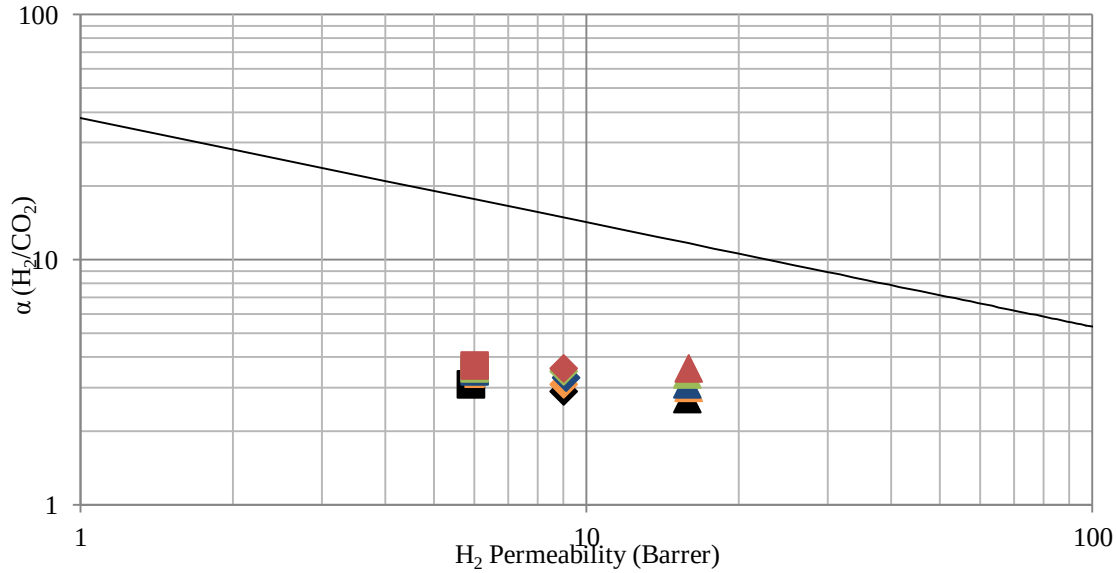

Figure 4.34 The effect of feed pressure on the ternary membrane performances in reference to Robeson upper bound for H_2/CO_2 gas pair; □indicates the PES/HMA(%4), ◇ __PES/ZIF-8(%10)/HMA(%4) membrane,△ _PES/ZIF-8(%20)/HMA(%4) membranes. (black=3bar, yellow=6 bar, blue= 8bar, green= 10bar, red= 12bar)

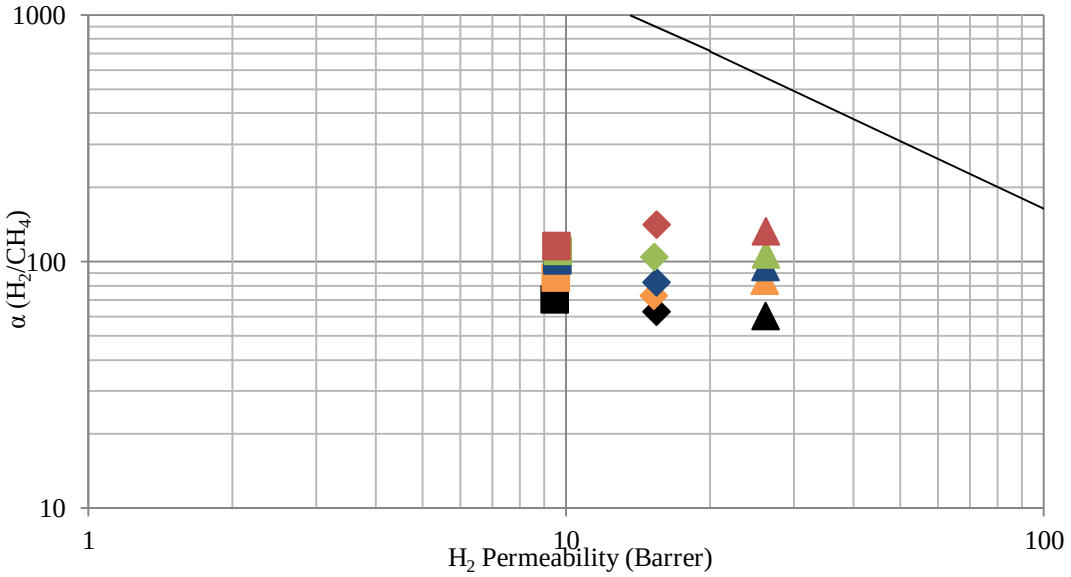

Figure 4.35 The effect of feed pressure on the binary membrane performances in reference to Robeson upper bound for H_2/CH_4 gas pair; □ indicates the Pure PES membrane, ◇_PES/ZIF-8(%10) membrane, △ __PES/ZIF-8(%20) membranes (black=3bar, yellow=6bar, blue= 8bar, green= 10bar, red= 12bar)

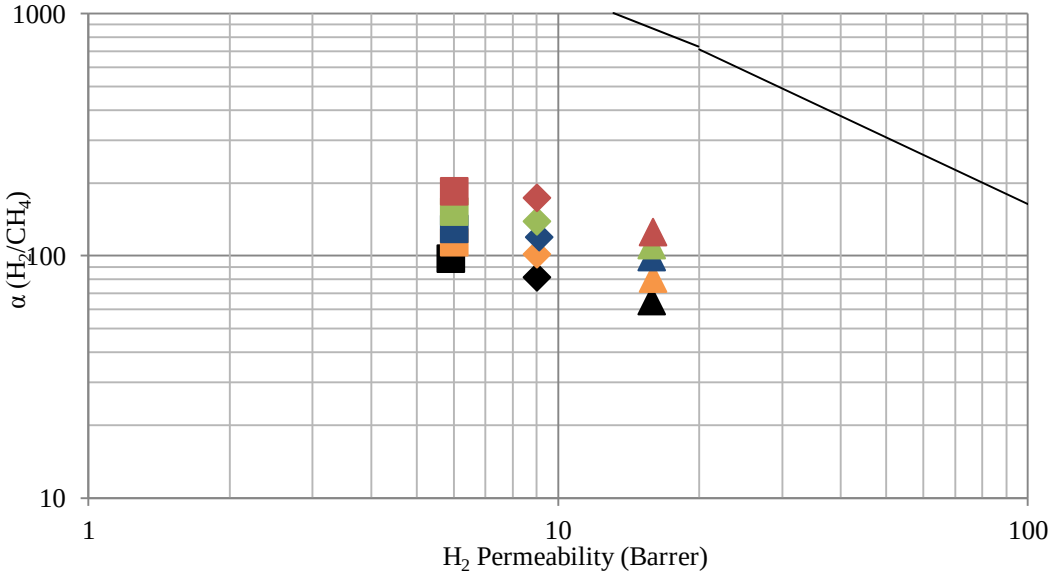

Figure 4.36 The effect of feed pressure on the ternary membrane performances in reference to Robeson upper bound for H_2/CH_4 gas pair; □ indicates the PES/HMA(%4), ◇ PES/ZIF-8(%10)/HMA(%4) membrane, △ PES/ZIF-8(%20)/HMA(%4) membranes. (black=3bar, yellow=6 bar, blue=8bar, green= 10bar, red= 12bar)

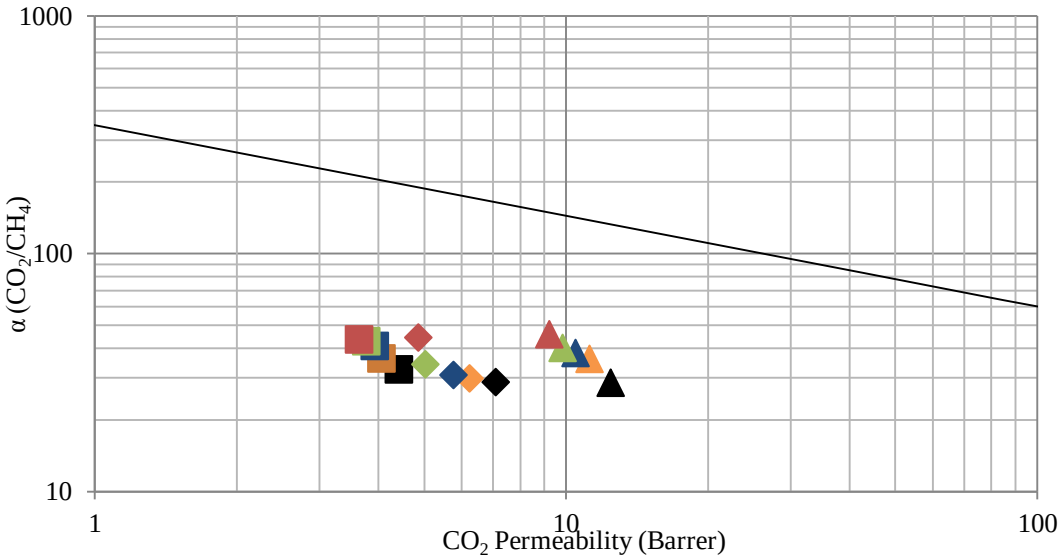

Figure 4.37 The effect of feed pressure on the binary membrane performances in reference to Robeson upper bound for CO_2/CH_4 gas pair; □ indicates the Pure PES membrane, ◇_PES/ZIF-8(%10) membrane, △ __PES/ZIF-8(%20) membranes (black=3bar, yellow=6bar, blue= 8bar, green= 10bar, red= 12bar)

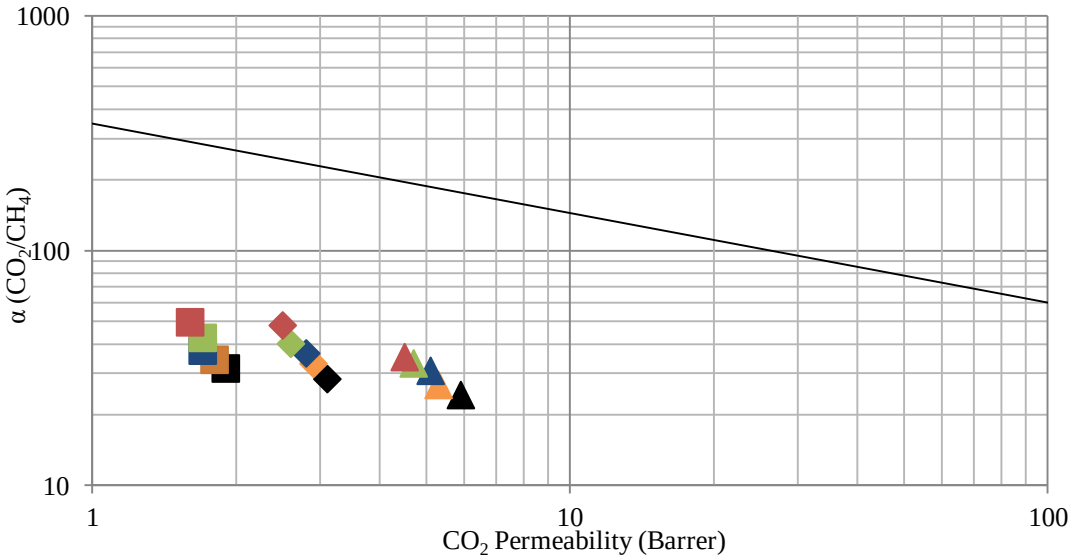

Figure 4.38 The effect of feed pressure on the ternary membrane performances in reference to Robeson upper bound for CO_2/CH_4 gas pair; □ indicates the PES/HMA(%4), ◇ PES/ZIF-8(%10)/HMA(%4) membrane, △ PES/ZIF-8(%20)/HMA(%4) membranes. (black=3bar, yellow=6 bar, blue= 8bar, green= 10bar, red= 12bar)

Maxwell model was used to predict the gas transport properties of the binary and ternary MMMs with respect to increasing feed pressures. Our experimental results were used for permeability data of pure PES membranes at different feed pressures for binary MMM predictions. Moreover, the PES/HMA blend was assumed to be a new material with its transport properties and its experimental data at different feed pressures were utilized as the permeability of continuous phase in ternary MMM performance predictions. The theoretical permeability values were used as 54000 for H_2, 27000 for CO_2 and 2250 for CH_4 through the ZIF-8 membranes, at constant 10 bar pressure [132], because the permeability through microporous materials does not depend on pressure [133]. On the other hand, the frameworks of many MOFs are reported to be flexible which resulted in breathing effect during the adsorption processes [90].

The predicted permeability results for binary and ternary MMMs with respect to feed pressure were given with the experimental results through Figures 4.39 and 4.42. The general behaviour of the membranes predicted under various feed pressures is completely agreed with the experimental results. While H_2 permeability is pressure independent, CO_2 and CH_4 permeabilities are decreasing with increasing feed pressure. However, the experimentally observed permeabilities are much higher than those of predicted by the Maxwell model for all gases and membranes. While the experimental CO_2 and CH_4 permeabilities through PES/ZIF-8(%10) and PES/ZIF-8(%10)/HMA(%4) membranes nearly coincided with the predicted values, the percent variation between the results is increasing with increasing ZIF-8 loading for both binary and ternary membranes. The discrepancies between the experimental and predicted results may be attributed to formation of voids around the ZIF-8 crystals. Since the higher crystal loading yields an increased interface between the polymer and ZIF-8 particles, the chance for void formation in the membrane structure is increased [131]. Moreover, the permeabilities of pure ZIF-8 membranes which assumed to be constant regardless of pressure during the calculations may be resulted in some deviations due to the breathing characteristics of MOF type materials [90]. Another observation is the decrease in the variations at high pressures especially for CO_2 and CH_4 gases. Since the chains of the polymer are packed more efficiently, the role of the voids on gas transport may be suppressed at high pressures and the experimental results come close to Maxwell predictions. It can be concluded that the Maxwell model gives some useful information about the transport properties of the MMMs, especially for low volume fractions of dispersed phases [134].

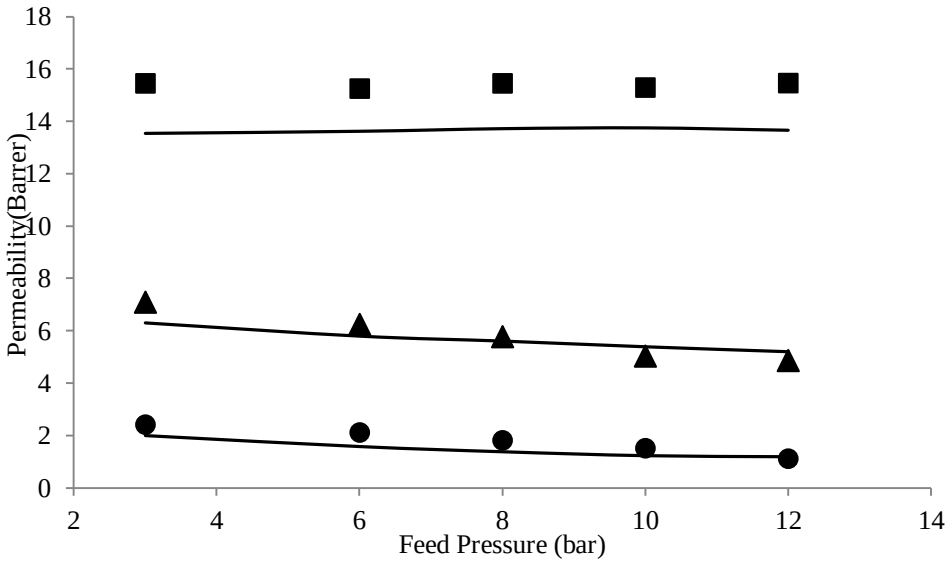

Figure 4.39 The permeation results for PES/ZIF-8(%10) membrane as a function of feed pressure. The experiments are denoted by filled symbols (■_ H_2, ▲_CO_2, ● _ CH_4) and the Maxwell-model predictions by lines.

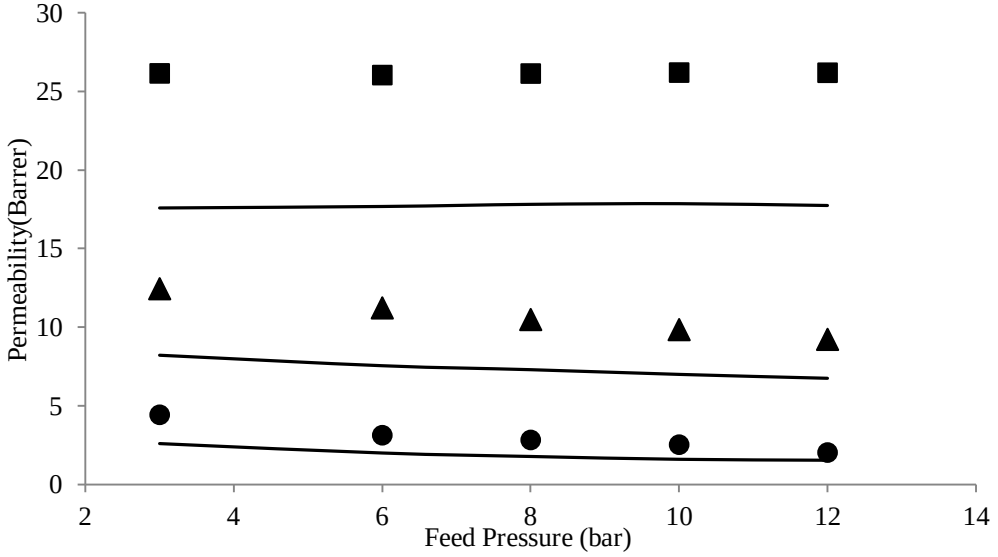

Figure 4.40 The permeation results for PES/ZIF-8(%20) membrane as a function of feed pressure. The experiments are denoted by filled symbols (■_ H_2, ▲_CO_2, ●_ CH_4) and the Maxwell-model predictions by lines.

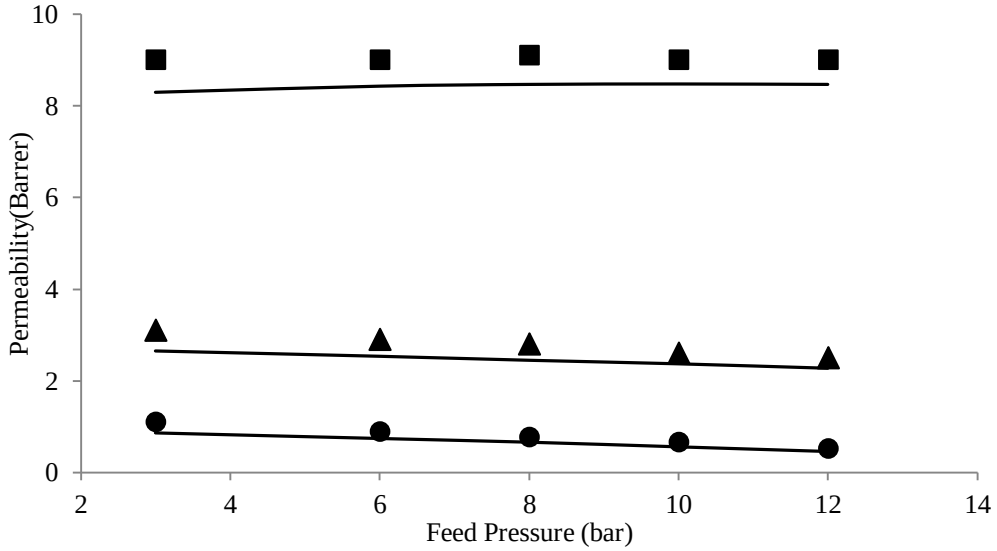

Figure 4.41 The permeation results for PES/ZIF-8(%10)/HMA(%4) membrane as a function of feed pressure. The experiments are denoted by filled symbols (■ _ H_2, ▲_CO_2,●_CH_4) and the Maxwell-model predictions by lines.

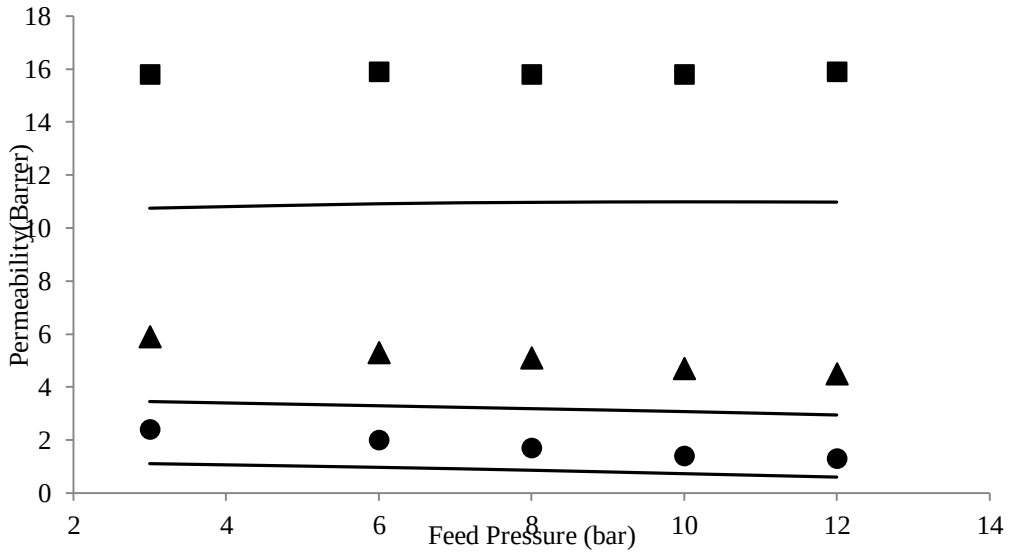

Figure 4.42 The permeation results for PES/ZIF-8(%20)/HMA(%4) membrane as a function of feed pressure. The experiments are denoted by filled symbols (■ _ H_2, ▲ _CO_2, ●_ CH_4) and the Maxwell-model predictions by lines.

4.3.5 Binary Gas Permeation Results of Binary and Ternary MMMs

The performances of pure PES, PES/ZIF-8(%10) and PES/ZIF-8(%10)/HMA(%4) membranes on the separation of binary gas mixtures were investigated for 50/50 % v/v CO_2/CH_4 gas mixture. Moreover, the effect of feed pressure on binary gas separation performances of these membranes was studied at two different feed pressures, 3 bar and 12 bar. Prior to the binary permeation experiments, the feed gas stream and after conducting the experiments, the permeated gas mixture was analyzed by GC. At least three runs were performed for the feed side and permeate side composition analysis, to have reliable results, and the reported values are the averages of these three runs.

Table 4.17 shows the average binary gas permeabilities of the performed membranes with calculated standard deviations comparing with the single results. The relative standard deviations for mixture and CO_2 permeabilities are around 6 % which is consistent with literatural data. The maximum deviation was observed in CH_4 permeabilities which were around 15 %. The mixture permeabilities were between the pure CO_2 and CH_4 permeabilities for pure PES membrane at both feed pressures. The same result was reported by our research group in a previous study for PES/SAPO-34/HMA membrane system at constant pressure [21]. The binary permeabilities of CO_2 and CH_4 in mixture were calculated separately by the algorithm given in Appendix D and very close numbers to single results were reported in Table 4.17 for both CO_2 and CH_4 gases at 3 and 12 bar feed pressures.

Table 4.17 Binary permeabilities for CO_2/CH_4 mixture

Membran	P	P_{mix}	P_{CO2} Single	P_{CO2} Binary	P_{CH4} Single	P_{CH4} Binary
Pure PES	3	2.1±0.1	4.4	4.4±0.2	0.14	0.13±0.02
	12	1.8±0.1	3.6	3.9±0.2	0.08	0.10±0.00
PES/ZIF-8(%10)	3	2.5±0.0	7.1	6.7±0.6	0.25	0.20±0.01
	12	2.3±0.1	4.9	4.8±0.3	0.11	0.15±0.00
PES/ZIF8(%10)/HMA(%4)	3	1.5±0.1	3.1	3.2±0.1	0.11	0.09±0.00
	12	1.4±0.0	2.5	2.7±0.1	0.05	0.07±0.00

Considering the PES/ZIF-8(%10) membrane, the mixture permeabilities were again between the pure CO_2 and CH_4 permeabilities, however the binary permeabilities are slightly different from the single ones. Especially for 3 bar experiments both the CO_2 and CH_4 permeabilities were lower than the single results. Since the presence of a second gas may affect the interactions between gas-gas molecules and gas-polymer matrix, the changes observed in permeability and selectivity are inevitable [135]. Finally the binary permeability results of PES/ZIF-8(%10)/HMA(%4) membrane were very consistent with the results of single experiments as in the case of pure PES membrane.

The separation selectivities of the membranes for CO_2/CH_4 gas pair were calculated using the calculation method in Appendix D and the results were shown in Table 4.18. Since the membranes have high CO_2/CH_4 selectivities, the CH_4 content of permeate gas is very low. Therefore, very small fluctuations observed in permeate gas mixture compositions strongly affect the ideal selectivities. All the membranes behaved similar at 3 bar at which the ideal selectivities are equal to the separation factors. In a previous study of our research group, the binary gas separation performances of the membranes prepared using the PES/SAPO-34/HMA materials were investigated [63]. The ideal selectivities were found to be equal to the separation factors for CO_2/CH_4 mixture through ternary membranes. While both types of selectivity factor are equal to each other for ternary membrane,

Table 4.18 Separation factors for CO_2/CH_4 gas mixture

Membrane	P	Feed Composition		Permeate Composition		CO_2/CH_4 (Ideal)	CO_2/CH_4 (Separation)
		X_{CO2}	X_{CO2}	X_{CO2}	X_{CH4}		
Pure PES	3	0.52	0.48	0.973	0.027	32.5	33.4
	12	0.52	0.48	0.976	0.024	43.5	38.4
PES/ZIF-8(%10)	3	0.50	0.50	0.970	0.030	28.8	32.9
	12	0.52	0.48	0.972	0.028	44.3	32.4
PES/ZIF8(%10)/HMA(%4)	3	0.51	0.49	0.974	0.026	28.3	35.3
	12	0.53	0.47	0.975	0.025	48.0	36.7

However, in the case of high feed pressure, the separation factors are slightly lower than the ideal selectivities. Usually, lower separation factors than ideal selectivities were reported for binary gas mixtures in literature owing to some morphological reasons as concentration polarization, competition between the penetrants, plasticization phenomena [21]. The reason underlying the variation between the ideal selectivities and the separation factors may be the measurement difficulties in GC due to very low CH_4 concentrations.

4.4 Summary of the Results

In this study, ZIF-8 was synthesized in order to use in binary and ternary mixed matrix membranes. The effect of ZIF-8 loading on the performance of binary MMMs was investigated, and the ternary MMMs were prepared by incorporating HMA at different concentrations into the membrane formulation. The gas permeation properties and morphologies of prepared pure PES, PES/ZIF-8 and PES/ZIF-8/HMA membranes were characterized.

Pure, homogenous, 100 nm ZIF-8 crystals with well defined shapes were synthesized by a 1-hour stirring method at room temperature with a synthesis solution composition of Zn^{+2}: Hmim:MeOH=1:7.9:695.1. The effect of MeOH amount on the particle size of the ZIF-8 crystals was investigated by changing the MeOH/Zn+2 ratios between 86.9 and 1042.7 and pure, homogenous, highly crystalline ZIF-8s were obtained with a very wide range of particle size between 60 and 600 nm. Two steps recycling synthesis approach based on the using the unreacted mother liquor of ZIF-8 synthesis solution has been developed to synthesize nanosized ZIF-8 crystals. This recycle procedure repeated for at least three times and all the products have the same crystalline framework and thermal stability, and have particle sizes in the 20-100 nm range.

PES/ZIF-8 binary membranes were prepared with ZIF-8 loadings changing between 10 and 60 % w/w and characterized by single gas permeation experiments. Very reproducible and repeatible permeation results were obtained up to 30 % w/w ZIF-8 loading, after that point membrane formulation reproducibility was decreased. While the permeabilities were increased with ZIF-8 loading, the ideal selectivities showed a slight decreased compared to neat PES membrane, they all are permselective membranes with very high permeabilities. The optimum ZIF-8 loading for the binary membrane fabrication may be chosen as 20 %w/w. The SEM micrographs showed homogenous dispersion of the ZIF-8 crystals without any agglomeration or sedimentation in polymer matrix. Moreover, they indicated some interfacial voids between the crystals and polymer chains up to 30 % w/w ZIF-8 loading, for higher ZIF-8 loadings of 40-60 % w/w, a completely different structure was observed in which the ZIF-8 crystals were more prominent and PES acted as a binder between these crystals. The results of DSC analysis implied that the addition of ZIF-8 crystals to neat PES membrane did not affect the glass transition temperature of the polymer suggesting the weak interaction between two phases.

HMA was incorporated into the pure PES, PES/ZIF-8(%10), PES/ZIF-8(%20) and PES/ZIF-8(%30) membranes (with high reproducibility) in the range of 1-10 % w/w. HMA changed the structures and the performances of all the membranes with its antiplasticization effect, by decreasing permeabilities with increasing ideal selectivities. Addition of HMA to the binary membranes effectively improved

the permselectivity of the membranes for all ZIF-8 and HMA compositions. Especially, PES/ZIF-8(%20)/HMA(%7) showed the highest separation performance with its high reproducible results among all membranes. The SEM images indicated that, the voids seemed to be eliminated partly with addition of HMA, but the structure of the membranes did not changed very significantly in macro scale. The incorporation of HMA reduced the Tg of the membrane. Moreover, addition of ZIF-8 to PES/HMA membrane caused increase in the Tg of the resultant ternary membranes independently of filler loadings due to chain rigidification.

The effect of feed pressure on the separation performances of Pure PES, PES/ZIF-8(%10), PES/ZIF-8(%20), PES/HMA(%4), PES/ZIF-8(%10)/HMA(%4), PES/ZIF-8(%20)/HMA(%4) membranes were investigated at 3, 6, 8, 10 and 12 bar. While the H_2 permeability is pressure independent, the CO_2 and CH_4 permeabilities through all membrane composition were reduced with increasing feed pressure. The highest selectivity improvement was observed in H_2/CH_4 pair for all membrane compositions. The highest ideal selectivity values belonged to the PES/HMA(%4) membrane for all gas pairs at 12 bar with the lowest permeabilities. Considering both the permeabilities and the selectivities PES/ZIF-8(%10)/HMA(%4) has the highest separation performance.

The separation performances of Pure PES, PES/ZIF-8(%10), PES/ZIF-8(%10)/HMA(%4) membranes were investigated for CO_2/CH_4 gas mixture with 1:1 molar ratio at 3 bar and 12 bar. The feed pressure does not have a significant effect on the separation factors for all membranes. While the ideal selectivities and the separation factors obtained at 3 bar were equal to each other, the ideal selectivities were slightly higher than the separation factors at 12 bar.

CHAPTER 5

CONCLUSION

The following conclusions were obtained;

1- In this study, pure, homogenous, highly crystalline ZIF-8 crystals with a very wide particle size range (20-600 nm) were synthesized. Moreover, the developed recycling process enables a substantial rise in the crystalline yield of nanosized particles and it is preferable from environmental and economical point of view, because recycling the starting solvent reduces the amount of waste produced.

2- The incorporation of ZIF-8 crystals into PES matrix resulted in high performance gas separation membranes with very high permeabilities and considerable ideal selectivities. 20 w/w % ZIF-8 is selected as optimum filler loading for binary membrane formulation considering both the permeation performances and reproducibility phenomena.

3- Addition of HMA into the formulation as a third component significantly improved the gas separation performances of the membranes. PES/ZIF-8(%20)/HMA(%7) membrane has the highest permselectivity for all gases among the ternary membranes.

4- For all types of membranes used, the feed pressure appreciably affected the separation performances for all gas pairs, in which the CO_2 and CH_4 permeabilities showed a slight decrease, while very significant improvement was observed in ideal selectivities. Both binary and ternary MMMs showed higher permselectivities at high feed pressures and working at higher feed pressures will be more advantageous for the separation of studied gases.

5- The ideal selectivities and the separation factors were equal to each other for all membrane compositions, both for 3 and 12 bar operating pressures.

REFERENCES

[1] Mulder, M., "Basic Principles of Membrane Technology", Kluwer Academic Publishers, Second edition, 1997, Dordrecht.

[2] Das, M., Perry, J. D., Koros, W. J.,"Gas-Transport-Property Performance of Hybrid Carbon Molecular Sieve-Polymer Materials" , Ind. Eng. Chem. Res,49, 2010, p. 9310–9321.

[3] Moore, T.T., "Effects of Materials, Processing, And Operating Conditions On The Morphology And Gas Transport Properties of Mixed Matrix Membranes", PhD Thesis, The University of Texas at Austin, December 2004.

[4] Damle, S., "Membrane Based Separations of Carbon Dioxide and Phenol under Supercritical Conditions", PhD Thesis, The University of Texas at Austin, May 2004.

[5] Karatay, E., "Effect of Preparation and Operation Parameters on Performance of Polyethersulfone Based Mixed Matrix Gas Separation Membranes", Master Thesis, Middle East Technical University, August 2009.

[6] Robeson, L.M., "The upper bound revisited", Journal of Membrane Science, 320, 2008, p. 390–400.

[7] Freeman, B.D., "Basis of permeability/selectivity tradeoff relations in polymeric gas separation membranes", Macromolecules, 32, 1999, p. 375-380.

[8] Liu, C., Kulprathipanja, S., Hillock, A.M.W., Husain, S., Koros, W.J., "Chapter 30, Recent progress in Mixed Matrix Membranes", Advanced Membrane Technology and Applications, John Wiley & Sons, Inc 2008.

[9] Vu, D.Q., "Formation and Characterization of Asymmetric Carbon Molecular Sieve and Mixed Matrix Membranes for Natural Gas Purification", PhD Thesis, University of Texas at Austin, December 2001.

[10] Huang, Z., Li, Y., Wen, R., Teoh, M.M., Kulprathipanja, S., "Enhanced gas separation properties by using nanostructured PES-zeolite 4A mixed matrix membranes", Journal of Applied Polymer Science, 101, 2006, p. 3800-3805.

[11] Perez, E.V., Balkus,K.J., Ferraris,J.P., Musselman,I.H., "Mixed-matrix membranes containing MOF-5 for gas separations", Journal of Membrane Science 328, 2009, p. 165–173.

[12] Bae, T.H., Lee, J.S., Qiu, W., Koros, W.J., Jones, C.W., Nair, S., "A High-Performance Gas-Separation Membrane Containing Submicrometer-Sized Metal–Organic Framework Crystals", Angew. Chem. Int. Ed. 49, 2010, p. 9863 –9866.

[13] Yang, T., Xiao, Y., Chung, T.S., "Poly-/metal-benzimidazole nano-composite membranes for hydrogen purification", Energy Environ. Sci., 4, 2011, p. 4171.

[14] Basu, S., Odena, A.C., Vankelecom, I.F.J., "MOF-containing mixed-matrix membranes for CO_2/CH_4 and CO_2/N_2 binary gas mixture separations", Separation and Purification Technology, 362, 2010, p.478.

[15] Duval, J. M., "Adsorbent filled polymeric membranes", Ph.D thesis, The University of Twente, 1995.

[16] Boom, J. P., "Transport through zeolite filled polymeric membranes", Ph.D. Thesis, The University of Twente, 1994.

[17]Mahajan, R., "Formation, characterization and modeling of mixed matrix membrane materials", PhD thesis, The University of Texas at Austin, 2000

[18] Mahajan, R., Burns, R., Schaeffer, M., Koros, W. J., "Challenges in forming successful mixed matrix membranes with rigid polymeric materials", Journal of Applied Polymer Science, 86, 2002, 881–890.

[19] Karatay, E., Kalıpcılar, H., Yılmaz, L., "Preparation and performance assessment of binary and ternary PES-SAPO 34-HMA based gas separation membranes", Journal of Membrane Science, 364, 2010, p. 75–81.

[20] Şen, D., Kalıpcılar, H., Yılmaz, L., "Gas Separation performance of polycarbonate membranes modified with multifunctional low-molecular weight additives", Separation Science and Technology, 41, 2006, p. 1813–1828.

[21] Cakal, U., Yilmaz, L., Kalipcilar, H., "Effect of feed gas compositionon theseparation of CO_2/CH_4 mixtures by PES-SAPO34-HMA mixed matrix membranes", Journal of Membrane Science, Article in Press.

[22] Cravillon, J., Munzer, S., Lohmeier, S.J., Feldhoff, A., Huber, K., Wiebcke, M., "Rapid Room-Temperature Synthesis and Characterization of Nanocrystals of a Prototypical Zeolitic Imidazolate Framework", Chem. Mater. 21, 2009, p. 1410–1412.

[23] Zhou, W., Wu, H., Hartman, M. R., Yildirim, T., Hydrogen and Methane Adsorption in Metal-Organic Frameworks: A High-Pressure Volumetric Study, J. Phys. Chem., 2007, 111, p. 16131 16137

[24] Venna, S. R., Carreon, M. A., Highly Permeable Zeolite Imidazolate Framework-8 Membranes for CO_2/CH_4 Separation, J. Am.Chem.Soc., 2010, 132, p. 76-78.

[25] Jiang, H. L., Liu, B., Akita, T., Haruta, M., Sakurai, H., Xu, Q., J. Am.Chem.Soc. 2009,131,p. 11302.

[26] Lu, G., Hupp, J. T., J. Am.Chem.Soc. 2010, 132, 7832.

[27] Venna, S.R., Jasinski, J.B., Carreon, M.A., "Structural Evolution of Zeolitic Imidazolate Framework-8", J. Am. Chem. Soc., 132, 2010, p. 18030–18033.

[28] Lin, L., Wang, A., Dong,M., Zhang,Y., Hea,B., Li,H., "Sulfur removal from fuel using zeolites/polyimide mixed matrix membrane adsorbents", Journal of Hazardous Materials, 203– 204, 2012, p.204– 212.

[29] Hu, J., Cai, H., Ren,H., Wei, Y., Xu, Z., Liu,H., Hu,Y., "Mixed-Matrix Membrane Hollow Fibers of Cu3(BTC)2 MOF and Polyimide for Gas Separation and Adsorption", Ind. Eng. Chem. Res.,49, 2010, p.12605–12612.

[30] Venna, S. R., Carreon, M. A., "Highly Permeable Zeolite Imidazolate Framework-8 Membranes for CO_2/CH_4 Separation", J. Am. Chem. Soc., 132, 2010, p.76–78.

[31] Staudt-Bickel, C., Koros, W.J., "Improvement of CO_2/CH_4 separation characteristics of polyimides by chemical crosslinking", Journal of Membrane Science, 155, 1999, p.145-154.

[32] Yi, L., "Development of Mixed Matrix Membranes for Gas Separation Application", PhD Thesis, Chemical and Biomolecular Engineering Department, National University of Singapore, 2006, China.

[33] Moore, T.T., Koros, W.J., "Non-ideal effects in organic–inorganic materials for gas separation membranes", Journal of Molecular Structure, 739, 2005, p. 87–98.

[34] Zhang, Y., Musselman, I.H., Ferraris, J.P., Balkus Jr., K.J., "Gas permeability properties of mixed-matrix Matrimid membranes containig a carbon aerogel: a material with both micropores and mesopores", Ind. Eng. Chem. Res., 47, 2008, p.2794–2802.

[35] Reid, B.D., Ruiz-Trevi˜no, F.A., Musselman, I.H., Balkus Jr., K.J., Ferraris, J.P., "Gas permeability properties of polysulfone membranes containing mesoporous molecular sieve MCM-41", Chem. Mater., 13, 2001, p.2366–2373.

[36] Aroon, M.A., Ismail, A.F., Matsuura, T., Montazer-Rahmati, M.M., "Performance studies of mixed matrix membranes for gas separation: A review", Separation and Purification Technology, 75, 2010, p.229–242.

[37] Chung, T. S., Jiang, L. Y., Li, Y., Kulprathipanja, S., "Mixed matrix membranes (MMMs) comprising organic polymers with dispersed inorganic fillers for gas separation", Progress in Polymer Science, 32, 2007, p.483-507.

[38] Noble, R. D., "Perspectives on mixed matrix membranes", Journal of Membrane Science, 378, 2011, p.393-397.

[39] Goh, P.S., Ismail, A.F., Sanip, S.M., Ng, B.C., Aziz, M., "Recent advances of inorganic fillers in mixed matrix membrane for gas separation", Separation and Purification Technology , 81, 2011, p.243-264.

[40] Çakal, Ü., "Natural Gas Purification by Zeolite Filled Polyethersulfone Based Mixed Matrix Membranes", Ms Thesis, Middle East Technical University, October, 2009.

[41] Şen, D., "Effect of Compatibilizers on the Gas Separation Performance of Polycarbonatebased Membranes", Ms thesis, Middle East Technical University, 2003.

[42] Şen, D., "Polycarbonate Based Zeolite 4A Filled Mixed Matrix Membranes: Preparation, Characterization, and Gas Separation Performances", PhD Thesis, Middle East Technical University, February 2008.

[43] Oral, E., "EFFECT OF OPERATING PARAMETERS ON PERFORMANCE OF ADDITIVE/ZEOLITE/ POLYMER MIXED MATRIX MEMBRANES", M.Sc Thesis, Middle East Technical University, February 2011

[44] Adams, R., Carson, C., Ward, J., Tannenbaum, R., Koros, W., "Metal organic framework mixed matrix membranes for gas separations", Microporous and Mesoporous Materials, 131, 2010, p. 13–20.

[45] Li, J.R., Mab,Y., McCarthy, M.C., Sculley, J., Yu, J., Jeong, H.K., Balbuena, P.B., Zhou, H.C., "Carbon dioxide capture-related gas adsorption and separation in metal-organic frameworks", Coordination Chemistry Reviews, 255, 2011, p. 1791–1823.

[46] Süer, M.G., Baç, N., Yilmaz, L., "Gas permeation characteristics of polymer-zeolite mixed matrix membranes", 91, 1994, p.77-86.

[47] Moore, T.T., Mahajan, R., Vu, D.Q., Koros, W.J., "Hybrid membrane materials comprising organic polymers with rigid dispersed phases", AIChE J. 50, 2004, p. 311–321.

[48] Hillock, A.M.W., Miller, S.J., Koros, W.J., "Cross-linked mixed matrix membranes for the purification of natural gas: effects of sieve surface modification", J.Membr. Sci., 314, 2008, p. 193–199.

[49] Li, Y., Chung, T., Cao, C., Kulprathipanja, S., "The effects of polymer chain rigidification,zeolite pore size and pore blockage on polyethersulfone (PES)-zeolite 4A mixed matrix membranes", Journal of Membrane Science, 260, 2005, p. 45-55.

[50] Hibshman, C., Cornelius, C.J., Marand, E., "The gas separation effects of annealing polyimide-organosilicate hybrid membranes", J. Membr. Science, 211, 2003, p.25–40.

[51] Yong, H.H., Park, N.C., Kang, Y.S., Won, J., Kim, W.N., "Zeolite filled polyimide membrane containing 2,4,6-triaminopyrimidine", Journal of Membrane Science, 188, 2001, p. 151–163.

[52] Robeson, L.M., "The effect of antiplasticization on secondary loss transitions and permeability of polymers", Polymer Engineering and Science, 9, 1969, p. 277-281.

[53] Maeda, Y., Paul, D.R., "Effect of antiplasticization on gas sorption and transport. I.Polysulfone", Journal of Polymer Science: Part B: Polymer Physics, 25, 1987, p. 957-980.

[54] Maeda, Y., Paul, D.R., "Effect of antiplasticization on gas sorption and transport. II.Poly(phenylene Oxide)", Journal of Polymer Science: Part B: Polymer Physics, 25, 1987, p.981-1003.

[55] Ruiz-Treviño, F.A., Paul, D.R., "Modification of polysulfone gas separation membranes by additives", Journal of Applied Polymer Science, 66, 1997, p. 1925-1941.

[56] Van Krevelen, D. W., "Properties of Polymers—Correlation with Chemical Structure",1990, Elsevier.

[57] Pechar, T. W., Kim, S., Vaughan, B., Marand, E., Baranauskas, V., Riffle, J., "Preparation and characterization of a Poly(imide siloxane) and zeolite L mixed matrix membrane", Journal of Membrane Science, 277, 2006, p. 210–218.

[58] Mahajan, R., Burns, R., Schaeffer, M., Koros, W. J., "Challenges in forming successful mixed matrix membranes with rigid polymeric materials", Journal of Applied Polymer Science, 86, 2002, p. 881–890.

[59] Hudiono, Y.C., Carlisle, T.K., Baraa, J.E., Zhanga, Y., Gina, D.L., Noble, R.D., "A three-component mixed-matrix membrane with enhanced CO_2 separation properties based on zeolites and ionic liquid materials", Journal of Membrane Science, 350, 2010, p. 117–123.

[60] Shu, S., Husain, S., Koros, W. J., "Formation of nano scale morphology on zeolite surface for enhanced interfacial interaction in mixed matrix membranes", North American Membrane Society, Chicago IL, 2006.

[61] Guiver, M. D., Robertson, G. P., Dai, Y., Bilodeau, F., Kang, Y. S., Lee, K. J., "Structural characterization and gas-transport properties of brominated matrimid polyimide", Journal of Polymer Science: Polymer Chemistry, 40, 2003, p. 4193–4204.

[62] Zhang, Y., Balkus, K. J., Musselman, I. H., Ferraris, J. P., "Mixed-matrix membranes composed of matrimid and mesoporous ZSM-5 nanoparticles", Journal of Membrane Science, 325, 2008, p. 28–39.

[63] Şen, D., Yilmaz, L., Kalipcilar, H., "Development of polycarbonate based zeolite 4A filled mixed matrix gas separation membranes", Journal of Membrane Science, 303, 2007, p. 194- 203.

[64] Yanshuo Li, Y., Lianga, F., Bux, H., Yang,W., Caro,J., "Zeolitic imidazolate framework ZIF-7 based molecular sieve membrane for hydrogen separation", Journal of Membrane Science, 354 ,2010, p.48–54.

[65] Zhao,Z., Ma,X., Li,Z., Lin, Y.S., "Synthesis, characterization and gas transport properties of MOF-5 membranes", Journal of Membrane Science, 382,2011, p. 82–90.

[66] Liu, Y., Ng, Z., Khan, E. A., Jeong,H., Ching, C., Lai,Z., "Synthesis of continuous MOF-5 membranes on porous α-alumina substrates", Microporous and Mesoporous Materials, 118, 2009, p.296–301.

[67] Zhang, C., Dai, Y., Johnson, J. R., Karvan, O., Koros, W. J., "High performance ZIF-8/6FDA-DAM mixed matrix membrane for propylene/propane separations", Journal of Membrane Science, 389, 2012, p.34–42.

[68] Park, K.S., Ni, Z., Cote, A.P., Choi, J.Y., Huang, R., Uribe-Romo, F.J., Chae, H.K., O'Keeffe, M., Yaghi, O.M., "Exceptional chemical and thermal stability of zeoliticimidazolate frameworks", Proc. Natl. Acad. Sci. U.S.A., 103, 2006, p.10186–10191.

[69] Cravillon, J., Nayuk, R., Springer, S., Feldhoff, A., Huber, K., Wiebcke, M., "Zeolitic Imidazolate Framework Nano- and Microcrystal Formation: Insight into Crystal Growth by Time Resolved In Situ Static Light Scattering", Chem. Mater., 23, 2011, p. 2130–2141.

[70] Ordo˜nez, M.J.C., Balkus, K.J., Ferraris, J.P., Musselman, I.H., "Molecular sieving realized with ZIF-8/Matrimid® mixed-matrix membranes", Journal of Membrane Science, 361, 2010, p. 28–37.

[71] Pan,Y., Liu, Y., Zeng, G., Zhao, L., Lai, Z., "Rapid Synthesis of Zeolitic Imidazolate Framework-8 (ZIF-8) Nanocrystals in an Aqeous System", Chem.Commun., 47, 2011, p. 2071-2073.

[72] Huang, X.C., Lin, Y.Y., Zhang, J.P., Chen, X.M., "Ligand-directed strategy for zeolite-type metal-organic frameworks: Zinc(II) imidazolates with unusual zeolitic topologies", Angew. Chem., Int. Ed., 45, 2006, p. 1557-1559.

[72] Renzo, F.D., "Zeolites as tailor-made catalysts: Control of the crystal size", Catal. Today, 41, 1998, p. 37.

[74] Lethbridge, Z.A.D., Williams, J.J., Walton, R.I., Evans, K.E., Smith, C.W., "Methods for the synthesis of large crystals of silicate zeolites", Micropor. Mesoporous Materials, 79, 2005, p. 339.

[75] Drews, T.O., Tsapatsis, M., "Progress in manipulating zeolite morphology and related applications", Curr. Opinion Colloid Interf. Sci., 10, 2005, p. 233.

[76] Khan, N.A., Kang, I.J., Seok, H.Y., Jhung, S.H., "Facile synthesis of nano-sized metal-organic frameworks, chromium-benzenedicarboxylate, MIL-101", Chem.Eng.Journal, 166, 2011, p. 1152-1157.

[77] Jhung, S.H., Lee, J.H., Chang, J.-S., "Crystal size control of transition metal ion-incorporated aluminophosphate molecular sieves: Effect of ramping rate in the syntheses", Microporous and Mesoporous Materials, 112, 2008, p. 178–186.

[78] Brar, T., France, P., Smirniotis, P.G., "Control of Crystal Size and Distribution of Zeolite A", Ind. Eng. Chem. Res., 40, 2001, p. 1133–1139.

[79] Gascon, J., Aguado, S., Kapteijn, F., "Manufacture of dense coatings of $Cu_3(BTC)_2$ (HKUST-1) on a-alumina", Microporous and Mesoporous Materials, 113, 2008, p. 132–138.

[80] Ramos-Fernandez, E.V., Garcia-Domingos, M., Juan-Alcãniz, J., Gascon, J., Kapteijn, F., "MOFs meet monoliths: Hierarchical structuring metal organic framework catalysts", Appl. Catal. A: Gen., 391, 2011, p. 261–267.

[81] Pellitero, J.P., Amrouche, H., Siperstein, F.R., Pirngruber, G., Draghi, C.N., Chaplais, G., Masseron, A.S., Bachi, D.B., Peralta, D., Bats, N., "Adsorption of CO_2, CH_4, and N_2 on zeolitic imidazolate frameworks: experiments and simulations", Chem. Eur. J., 16, 2010, p.1560–1571.

[82] Zhang, Z., Xian, S., Xi, H., Wang, H., Li, Z., "Improvement of CO_2 adsorption on ZIF-8 crystals modified by enhancing basicity of surface", Chemical Engineering Science, 66, 2011, p.4878–4888.

[83] Zhou, W., Wu, H., Hartman, M. R., Yildirim, T., "Hydrogen and Methane Adsorption in Metal−Organic Frameworks: A High-Pressure Volumetric Study", J. Phys. Chem. C, 111, 2007, p.16131 –16137.

[84] Banerjee, R., Phan, A., Wang, B., Knobler,C., Furukawa, H., Keeffe, M.O., Yaghi,O.M., "High-Throughput Synthesis of Zeolitic Imidazolate Frameworks and Application to CO_2 Capture", Science, 2008, 319, p. 939 –943.

[85] Zornoza, B., Martinez-Joaristi, A., Serra-Crespo, P., Tellez, C., Coronas, J., Gascon, J., Kapteijn, F., "Functionalized flexible MOFs as fillers in mixed matrix membranes for highly selective separation of CO_2 from CH_4 at elevated pressures", Chemical Communications, 47, 2011, p.9522-9524.

[86] McCarthy, M.C., Varela-Guerrero,V., Barnett, G. V., Jeong, H.K., "Synthesis of Zeolitic Imidazolate Framework Films and Membranes with Controlled Microstructures", Langmuir, 26,2010, p.14636–14641.

[87] Bux, H., Chmelik, C., Krishna,R., Caro,J., "Ethene/ethane separation by the MOF membrane ZIF-8: Molecular correlation of permeation, adsorption, diffusion", Journal of Membrane Science, 369, 2011, p.284-289.

[88] Pan, Y., Li, T., Lestari, G., Lai, Z., "Effective separation of propylene/propane binary mixtures by ZIF-8 membranes", Journal of Membrane Science, 390– 391, 2012, p. 93– 98.

[89] Tantekin-Ersolmaz, S. B., Atalay-Oral, Ç. , Tatlıer M., Erdem-Şenatalar,A., Schoemanb, B., Sterte,J., "Effect of zeolite particle size on the performance of polymer–zeolite mixed matrix membranes", Journal of Membrane Science, 175, 2000, p.285–288.

[90] Zornoza ,B., Tellez, C., Coronas ,J., Gascon ,J., Kapteijn,F., "Metal organic framework based mixed matrix membranes: An increasingly important field of research with a large application potential", Microporous and Mesoporous Materials, 2012, Article in Press.

[91] Zhang, Y., Musselman, I.H., Ferraris, J. P., Balkus Jr, K.J., "Gas permeability properties of Matrimid® membranes containing the metal-organic framework Cu–BPY–HFS", Journal of Membrane Science, 313, 2008, p.170–181.

[92] K. Diaz, M. Lopez-Gonzalez, L.F. del Castillo, E. Riande, Journal of Membrane Science 383 (2011) 206.

[93] X.L. Liu, Y.S. Li, G.Q. Zhu, Y.J. Ban, L.Y. Xu, W.S. Yang, Angewandte Chemie – International Edition 50 (2011) 10636.

[94] Thompson, J.A., Chapman, K.W., Koros, W.J., Jones, C.W., Nair, S., "Sonication-induced Ostwald ripening of ZIF-8 nanoparticles and formation of ZIF-8/polymer composite membranes", Microporous and Mesoporous Materials, 158, 2012, p.292–299.

[95] Shi, G.M., Yang, T., Chung, T.S., "Polybenzimidazole (PBI)/zeolitic imidazolate frameworks (ZIF-8) mixed matrix membranes for pervaporation dehydration of alcohols", Journal of Membrane Science, 2012, Article in Press.

[96]Y.Dai, J.R. Johnson, O. Karvan, D.S. Sholl, W.J. Koros, "Ultem®/ZIF-8 mixed matrix hollow fiber membranes for CO2/N2 separations", Journal of Membrane Science, 401– 402, 2012, p.76– 82.

[97] Dhingra, S.S., "Mixed gas transport study through polymeric membranes: A novel technique", PhD Thesis, Virginia Polytechnic Institute and State University, June 1997.

[98] Wu, F., Li, L., Xu, Z., Tan, S., Zhang, Z., "Transport study of pure and mixed gases through PDMS membrane", Chemical Engineering Journal, 117, 2006, p. 51-59.

[99] Ettouney, H., Majeed, U., "Permeability functions for pure and mixture gases in silicone rubber and polysulfone membranes: Dependence on pressure and composition", Journal of Membrane Science, 135, 1997, p. 251-261.

[100] Dhingra, S.S., Marand, E., "Mixed gas transport through polymeric membranes", Journal of Membrane Science, 141, 1998, p. 45-63.

[101] Battal, T., Baç, N., Yilmaz, L., "Effect of feed composition on the performance of polymer-zeolite mixed matrix gas separation membranes", Separation Science and Technology, 30, 1995, p. 2365- 2384.

[102] Jordan, S.M., Koros, W.J., Fleming, G.K., "The effects of CO_2 exposure on pure and mixed gas permeation behavior: comparison of glassy polycarbonate and silicone rubber", Journal of Membrane Science, 30, 1987, p. 191-212.

[103] Bos, A., Pünt, I.G.M., Wessling, M., Strathmann, H., "Plasticization resistant glassy polyimide membranes for CO_2/CH_4 separations", Separation and Purification Technology, 14, 1998, p. 27-39.

[104] Staudt-Bickel, C., Koros, W.J., "Improvement of CO_2/CH_4 separation characteristics of polyimides by chemical crosslinking", Journal of Membrane Science, 155, 1999, p. 145-154.

[105] Chern, R.T., Koros, W.J., Yui, B., Hoppenberg, H.B., Stannet, V.T., "Selective permeation of CO_2 and CH_4 through Kapton Polyimide: Effects of penetrant competition and gas phase non-ideality", Journal of Polymer Science: Polymer Physics Edition, 22, 1984, p. 1061-1084.

[106] Tin, P.S., Chung, T.S., Liu, Y., Wang, R., Liu, S.L., Pramoda, K.P. "Effects of crosslinking modification on gas separation performance of Matrimid membranes", Journal of Membrane Science, 225, 2003, p. 77-90.

[107] Nik, O.G., Chen, X.Y., Kaliaguine, S., "Functionalized metal organic framework-polyimide mixed matrix membranes for CO2/CH4 separation", Journal of Membrane Science, 2012, Article in Press.

[108] Wu, H., Zhou, W. , Yildirim, T., "Hydrogen Storage in a Prototypical Zeolitic Imidazolate Framework-8", J. Am. Chem. Soc.,129, 2007, p. 5314-5315.

[109] Mahajan,R., Koros, W. J., "Mixed Matrix Membrane Materials With Glassy Polymers. Part 1", Polymer Engineering and Science, 42, 2002, p.1420-1431.

[110] Sun,H., Sur,G.S., Mark,J.E., "Microcellular foams from polyethersulfone and polyphenylsulfone: Preparation and mechanical properties", European Polymer Journal, 38, 2002, p.2373-2381.

[111] Qi Shi, Zhaofeng Chen, Zhengwei Song, Jinping Li, and Jinxiang Dong, "Synthesis of ZIF-8 and ZIF-67 by Steam-Assisted Conversion and an Investigation of Their Tribological Behaviors", Angew. Chem. 2010, 122, p. 1 – 5.

[112] Keskin, S., Sholl, D.S., "Selecting metal organic frameworks as enabling materials in mixed matrix membranes for high efficiency natural gas purification", Energy Environ. Sci., 3, 2010, p.343–351.

[113] Atci, E., Keskin, S., "Atomically detailed models for transport of gas mixtures in ZIF membranes and ZIF/polymer composite membranes", Ind. Eng. Chem. Res., 2012, Article in Press.

[114] Erucar, I., Keskin, S., "Screening metal organic framework-based mixed matrix membranes for CO_2/CH_4 separations", Ind. Eng. Chem. Res., 50, 2011, p.12606–12616.

[115] Erucar, I., Keskin, S., "Computational screening of metal organic frameworks for mixed matrix membrane applications", Journal of Membrane Science, 407– 408, 2012, p.221– 230.

[116] Schoeman, B.J., Sterte, J., Otterstedt, J.E., "Analysis of the crystal growth mechanism of TPA-silicalite-1", Zeolite, 14, 1994, p.568-575.

[117] Aerts, A., Follens, L. R. A., Biermans, E., Bals, S., Van Tendeloo, G., Loppinet, B., Kirschhock, C. E. A. , Martens, J. A., "Modelling of synchrotron SAXS patterns of silicalite-1 zeolite during crystallization", Phys. Chem. Chem. Phys., 13, 2011, p.4318–4325.

[118] Zhu, M., Venna, S.R., Jasinski, J.B., Carreon, M.A., "Room-Temperature Synthesis of ZIF-8: The Coexistence of ZnO Nanoneedles", Chem. Mater., 23, 2011, p.3590–3592.

[119] Fairen-Jimenez, D., Moggach, S. A., Wharmby, M. T., Wright, P. A., Parsons, S., Duren, T., "Opening the Gate: Framework Flexibility in ZIF-8 Explored by Experiments and Simulations", J. Am. Chem. Soc., 133, 2011, p.8900–8902.

[120] Cravillon, J., Schröder, C.A., Nayuk, R., Gummel, J., Huber, K., Wiebcke, M., "Fast Nucleation and Growth of ZIF-8 Nanocrystals Monitored by Time-Resolved In Situ Small-Angle and Wide-Angle X-Ray Scattering", Angew. Chem. Int. Ed., 50, 2011, p.8067 –8071.

[121] Millange, F., Medina M.I., Guillou N., Ferey G., Golden K.M., Walton R.I., "Time-Resolved In Situ Diffraction Study of the Solvothermal Crystallization of Some Prototypical Metal–Organic Frameworks", Angew. Chem. Int. Ed., 49, 2010, p. 763 –766.

[122] Kirschhock, C. E. A., Ravishankar, R., Van Looveren, L., Jacobs, P. A., and Martens, J. A., "Mechanism of Transformation of Precursors into Nanoslabs in the Early Stages of MFI and MEL Zeolite Formation from TPAOH-TEOS-H_2O and TBAOH-TEOS-H_2O Mixtures," J. Phys. Chem., 103, 1999, p. 4972-4978.

[123] Walton, R.I., Millange, F., O'Hare, D., "An in Situ Energy-Dispersive X-ray Diffraction Study of the Hydrothermal Crystallization of Zeolite A. 1. Influence of Reaction Conditions and Transformation into Sodalite", Phys. Chem., 105, 2001.

[124] Jean, J.H., Ring, T.A., "Nucleation and Growth of Monosized TiO_2 Powders from Alcohol Solution", Langmuir, 2, 1986, p. 251- 255.

[125] Hikov, T., Schröder, C. A., Cravillon, J., Wiebckeb, M., Huber, K., "In situ Static and Dynamic Light Scattering and Scanning Electron Microscopy Study on the Crystallization of the Dense Zinc Imidazolate Framework ZIF-8", Phys. Chem. Chem. Phys., 14, 2012, p. 511–521.

[126] Nune, S. K., Thallapally, P. K., Dohnalkova, A, Wang, C., Liuc, J. and Exarhosc, G. J., "Synthesis and properties of nano zeolitic imidazolate frameworks", Chem. Commun., 2010, 46, p. 4878–4880.

[127] Ruiz-Treviño, F.A., Paul, D.R., "Gas permselectivity properties of high free volume polymers modified by a low molecular weight additive", Journal of Applied Polymer Science, 68, 1998, p. 403-415.

[128] Moe, M., Koros, W. J., Hoehn, H. H., Husk, G.R., "Effects of film history on gas transport in a fluorinated aromatic polyimide", Journal of Applied Polymer Science, 36, 1988, p. 1833-1846.

[129] Chiou, J. S., Maeda, Y., Paul, D. R., "Gas Permeation in Polyethersulfone", Journal of Applied Polymer Science, 33,1987, p.1823-1828.

[130] Thornton, A. W., Dubbeldam, D., Liu, M.S., Ladewig, B. P., Hill, A. J., Hill, M. R., "Feasibility of zeolitic imidazolate framework membranes for clean energy applications", Energy Environ. Sci., 5, 2012, p.7637.

[131] Karkhanechi, H., Kazemian, H.,Nazockdast, H., Mozdianfard, M. R., Bidoki, S. M., "Fabrication of Homogenous Polymer-Zeolite Nanocomposites as Mixed-Matrix Membranes for Gas Separation", Chem. Eng. Technol., 35, 2012, p.885–892.

[132] Thornton, A. W., Dubbeldam, D., Liu, M. S., Ladewig, B. P., Hill A. J., Hillae, M. R., "Feasibility of zeolitic imidazolate framework membranes for clean energy applications", Energy Environ. Sci., 5, 2012, p.7637–7646.

[133] Burggraaf, A.J., "Chapter 9, Transport and separation properties of membranes with gases and vapours", Fundamentals of Inorganic Membrane Science and Technology, Elsevier Science, 1996.

[134] Chaidou, C. I. , Pantoleontos, G. , Koutsonikolas, D. E. , Kaldis, S. P., Sakellaropoulos, G. P. , "Gas Separation Properties of Polyimide-Zeolite Mixed Matrix Membranes", Separation Science and Technology, 47, 2012, p.950–962.

[135] Nik, O. G., Chen, X. Y., Kaliaguine, S., "Functionalized metal organic framework-polyimide mixed matrix membranes for CO_2/CH_4 separation", Journal of Membrane Science, Article in Press.

APPENDIX A

AMOUNTS OF MATERIALS IN MEMBRANE PREPARATION

Table A.1 Weights of polymer, filler and volume of the solvent used during pure polymer and polymer/filler membranes

Membrane Type	PES weight (gr)	ZIF-8 weight (gr)	DMF (ml)
Pure PES	2.0	0	10
PES/ZIF-8(%10)	2.0	0.2	10
PES/ZIF-8(%20)	2.0	0.4	10
PES/ZIF-8(%30)	2.0	0.6	10
PES/ZIF-8(%40)	2.0	0.8	10
PES/ZIF-8(%50)	2.0	1.0	10
PES/ZIF-8(%60)	2.0	1.2	10

Table A.2 Weights of polymer, filler, additive and volume of the solvent used during pure polymer and polymer/filler membranes

Membrane Type	PES weight (gr)	ZIF-8 weight (gr)	HMA (gr)	DMF (ml)
PES/ZIF-8(%10)/HMA(%4)	2.0	0.2	0.08	10
PES/ZIF-8(%20)/HMA(%4)	2.0	0.4	0.08	10
PES/ZIF-8(%20)/HMA(%7)	2.0	0.4	0.14	10
PES/ZIF-8(%30)/HMA(%1)	2.0	0.6	0.02	10
PES/ZIF-8(%30)/HMA(%2)	2.0	0.6	0.04	10
PES/ZIF-8(%30)/HMA(%4)	2.0	0.6	0.08	10
PES/ZIF-8(%30)/HMA(%10)	2.0	0.6	0.10	10

APPENDIX B

CALCULATION OF SINGLE PERMEABILITIES

During the gas permeation experiments, the pressure change at the permeate side were recorded to with respect to time with certain time intervals as seen in Fig.B.1. The time intervals were changing from gas to gas according to the velocity of the gases which were 5s, 10s, 30s for the gases H_2, CO_2 and CH_4, respectively.

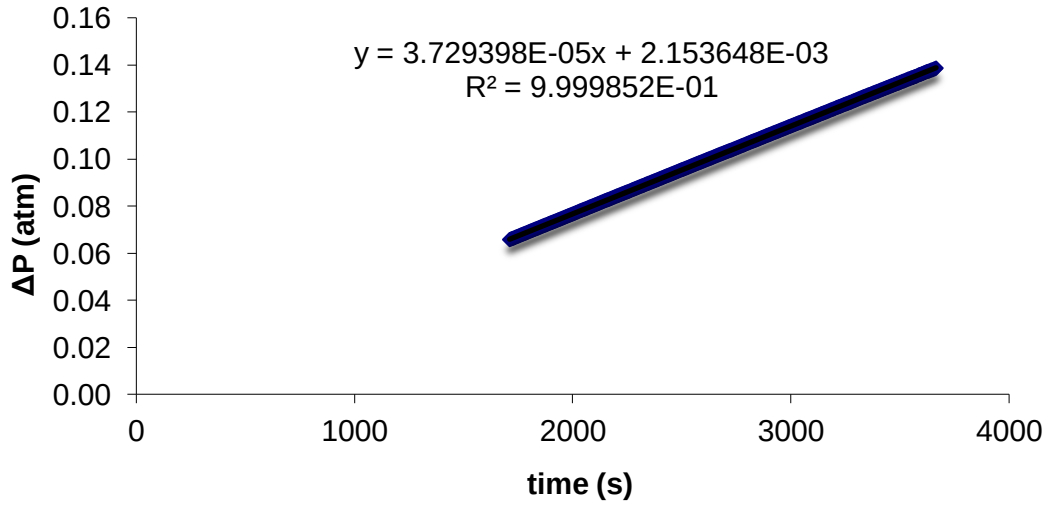

Figure B.1 Pressure change vs time graph for H_2 through PES/ZIF-8(%20) membrane

The pressure difference is calculated by substracting the initial pressure from the pressure at n^{th} time for each time.

$$\Delta P = P_n - P_0 \tag{B.1}$$

Then using the slope $(\Delta P/\Delta t)$ of the $\Delta P\ vs\ t$ graph, the change of mole of gas w.r.t time at the permeate side was calculated;

$$^{\Delta n}/_{\Delta t}\,(mol/s) = [(\Delta P/\Delta t) * V_d]/RT \tag{B.2}$$

where V_d is the dead volume of the permeate side which was measured as 22 cm^3 and T is the operation temperature which was constant in all experiment as 308.15 K.
Then, the change of volume of gas w.r.t time was calculated as follows;

$$^{\Delta V}/_{\Delta t}\,(cm^3/s) = [(\Delta n/\Delta t) * M]/\rho \tag{B.3}$$

where M is the molecular weight of the gas and ρ is the density of the gas.
Flux through the membrane, J, was calculated dividing the volume change by the effective membrane area A, which is 9.6 cm^2.

$$J(cm^3/cm^2.s) = (\Delta V/\Delta t)/A \tag{B.4}$$

The single permeabilities of the membrane were obtained by the equation in units of Barrer as follows;

$$P(Barrer) = [J * l]/\,[P_f - P_p] \tag{B.5}$$

where the P_f is feed side pressure, P_p is permeate side pressure which is the avarage of initial pressure(P_0) and the pressure at n^{th} time (P_n), both in units of cmHg and l is the membrane thickness.

APPENDIX C

CALIBRATION OF GC

For the analysis of feed and permeate gas compositions, gas chromatograph was calibrated for CO_2 and CH_4 gases. For calibration, each gas was fed to GC separately at several pressures between 0 and 100 Torr, and the areas under the peaks were recorded for all pressures. Then, the pressure versus the corresponding area were plotted as calibration curve for both gases. Pure gas calibration curves for CO_2 and CH_4 are shown in Figures C.1 and C.2, respectively. These pure gas calibration curves were used so as to calculate the partial pressures of each component in binary gas mixtures.

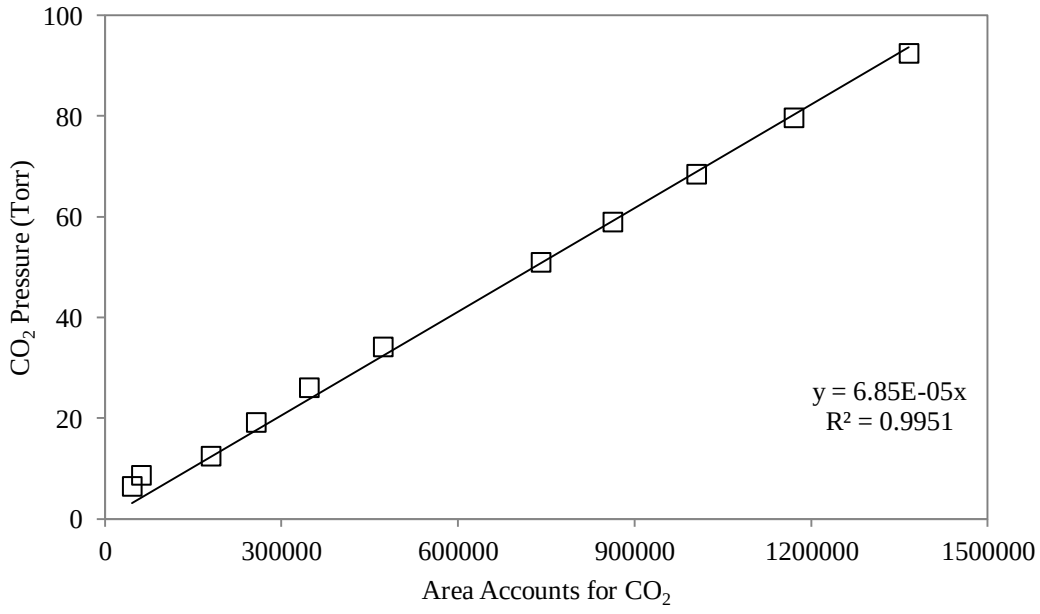

Figure C.1 The calibration curve of CO_2 for GC analysis

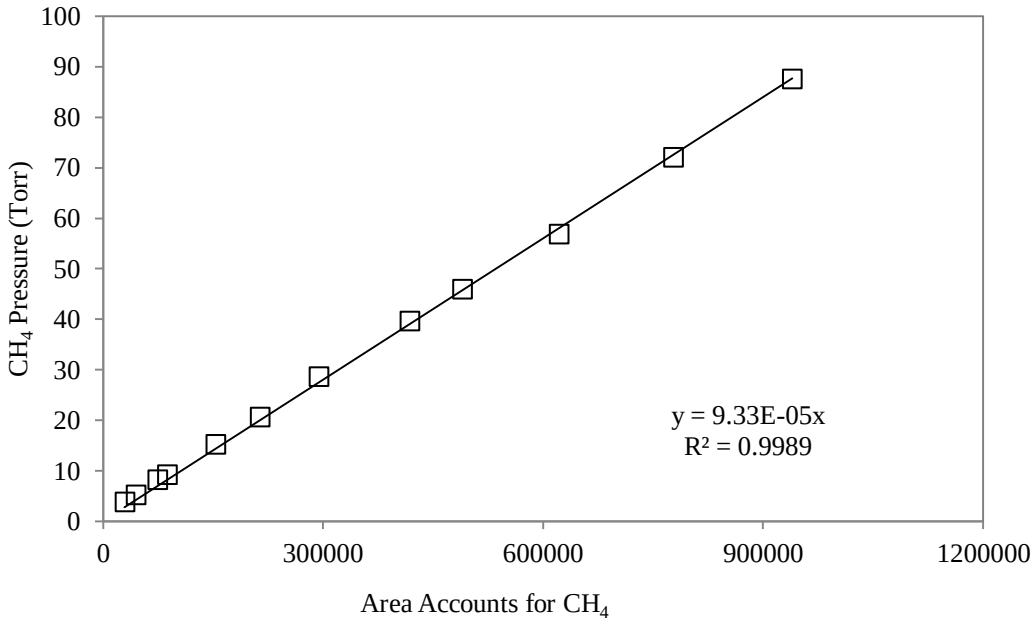

Figure C.2 The calibration curve of CH_4 for GC analysis

APPENDIX D

DETERMINATION OF PERMEABILITIES AND SELECTIVITIES OF BINARY GAS MIXTURES

Membrane Composition: Pure PES membrane
Membrane thickness: 65 μm
Gas mixture: CO_2/CH_4 with a 50/50 (volume/volume) mixture
System temperature: 35 °C

Feed Analysis

- Analysis of feed mixture at 99.8 Torr – 1st analysis

GC outputs:

Area counts for CH_4= 519936 Area counts for CO_2= 745073

Retention time for CH_4= 1.626 s Retention time for CO_2= 2.325 s

By using pure gas calibration curve equations;

Partial pressure of CO_2 = P_{CO_2feed}= 0.00006856*(area counts of CO_2)

Partial pressure of CH_4 = P_{CH_4feed} = 0.0000933*(area counts of CH_4)

P_{CO_2feed}= 0.00006856*(745073) = 51.08 Torr (D.1)

P_{CH_4feed}= 0.0000933*(519936) = 48.51Torr (D.2)

x_{CO_2feed}= (P_{CO_2feed}) / (feed pressure) (D.3)

x_{CH_4feed} = (P_{CH_4feed}) / (feed pressure) (D.4)

x_{CO_2feed}= (51.08)/ (99.8)= 0.512 (D.5)

x_{CH_4feed} = (48.51) / (99.8)=0.486 (D.6)

normalized %CO_2 in feed = (51.2/99.8) * 100 = 51.3%

normalized %CH_4 in feed = (48.6/99.8) * 100 = 48.7%

- Analysis of feed mixture at 77.6 Torr – 2nd analysis

GC outputs:

Area counts for CH_4= 392456 Area counts for CO_2= 563319

Retention time for CH_4= 1.630s Retention time for CO_2= 2.331s

P_{CO_2feed}= 0.00006856*(563319) = 38.62 Torr (D.7)

P_{CH_4feed}= 0.0000933*(392456) = 36.62 Torr (D.8)

x_{CO_2feed}= (38.62) / (77.6) =0.498 (D.9)

x_{CH_4feed} = (36.62) / (77.6)= 0.472 (D.10)

normalized %CO_2 in permeate = (49.8/97.0) * 100 = 51.3%

normalized %CH_4 in permeate = (47.2/97.0) * 100 = 48.7%

Permeate Analysis

- Analysis of permeate side gas mixture 59.9 Torr – 1st analysis

GC outputs:

Area counts for CH_4= 18963 Area counts for CO_2= 843683

Retention time for CH_4= 1.641 Retention time for CO_2= 2.325

P_{CO_2feed}= 0.00006856*(843683) = 57.84 Torr (D.11)

P_{CH_4feed}= 0.0000933*(18963) = 1.77 Torr (D.12)

x_{CO_2feed}= (57.84)/(59.9)= 0.966 (D.13)

x_{CH_4feed} = (1.77) / (59.9)= 0.029 (D.14)

normalized %CO_2 in permeate = (96.6/99.5) * 100 = 97.1%

normalized %CH_4 in permeate = (2.9/99.5) * 100 = 2.9%

- Analysis of permeate side gas mixture 48.2 Torr – 2nd analysis

GC outputs:

Area counts for CH_4= 15293 Area counts for CO_2= 681952

Retention time for CH_4= 1.638 Retention time for CO_2= 2.326

$$P_{CO_2 feed} = 0.00006856*(681952) = 46.75 \text{ Torr} \quad \text{(D.15)}$$

$$P_{CH_4 feed} = 0.0000933*(15293) = 1.43 \text{ Torr} \quad \text{(D.16)}$$

$$x_{CO_2 feed} = (46.75)/ (48.2) = 0.969 \quad \text{(D.17)}$$

$$x_{CH_4 feed} = (1.43)/ (48.2) = 0.029 \quad \text{(D.18)}$$

normalized %CO_2 in permeate = (96.9/99.8) * 100 = 97.1%

normalized %CH_4 in permeate = (2.9/99.8) * 100 = 2.9%

Calculation of Separation Selectivity

Feed Side Composition: CO_2= 0.513 , CH_4=0.487

Permeate Side Composition: CO_2= 0.971 ,CH_4=0.029

Separation selectivity is the ratio of mol fractions of gases in the permeate and feed side;

$$\alpha_{i/j} = ((x_i/x_j)_{permeate}/(x_i/x_j)_{feed}) \quad \text{(D.19)}$$

$$\alpha_{CO_2/CH_4} = [(0.971/ 0.029) /(0.513/ 0.487)] \quad \text{(D.20)}$$

$$\alpha_{CO_2/CH_4} = 31.79$$

The permeability of the gas mixture through the membrane was calculated using the slope of the pressure difference versus time graph obtained during the experiment. In order to determine the

permeabilities of each components in the gas mixture, the compositions and pressures of feed and permeate gas streams (Table D.1) were used.

Table D.1. Feed and permeate gas pressures and compositions

	Before permeation experiment	After permeation experiment
Feed pressure	2 barg (2.91 atm)	2 barg (2.91 atm)
Permeate pressure	0.5 Torr ($6.79*10^{-4}$ atm)	100 Torr (0.13 atm)
Feed composition	$x_{CO_2} = 0.512$ $x_{CH_4} = 0.488$	$x_{CO_2} = 0.512$ $x_{CH_4} = 0.488$
Permeate composition	-	$y_{CO_2} = 0.975$ $y_{CH_4} = 0.025$

The slope of the pressure difference versus time graph for CO_2/CH_4 mixture permeation experiment was obtained as $2.436*10^{-4}$ atm/min. Then the individual dp/dt data were calculated for each gases in the mixture;

$$\left(\frac{dP}{dt}\right)_{CO_2/CH_4} = 2.436 * 10^{-4} atm/min \quad \text{(D.21)}$$

$$\left(\frac{dP}{dt}\right)_{CO_2} = \left(\frac{dP}{dt}\right)_{CO_2/CH_4} * y_{CO_2} = 2.37 * 10^{-4}\ atm/min \quad \text{(D.22)}$$

$$\left(\frac{dP}{dt}\right)_{CH_4} = \left(\frac{dP}{dt}\right)_{CO_2/CH_4} * y_{CH_4} = 6.09 * 10^{-6}\ atm/min \quad \text{(D.23)}$$

The partial pressures at the feed and permeate sides were calculated as follows;

$P_{CO_{2feed}} = P_{feed} * x_{CO_2}$= 2.91atm* 0.512= 1.489 atm (D.24)

$P_{CH_{4feed}} = P_{feed} * x_{CH_4}$= 2.91atm* 0.488= 1.420 atm (D.25)

$P_{CO_{2permeate}} = P_{permeate} * y_{CO_2}$= 0.000679 atm* 0.975= 0.000662 atm (before exp.)

$P_{CO_{2permeate}} = P_{permeate} * y_{CO_2}$= 0.13 atm* 0.975= 0.127 atm (after exp.)

$$P_{CO_{2permeate-avarage}} = \frac{0.000662\ atm + 0.127\ atm}{2} = 0.0638\ atm \quad \text{(D.26)}$$

$P_{CH_4 permeate} = P_{permeate} * y_{CH_4}$= 0.000679 atm* 0.025= 0.0000169atm (before exp.)

$P_{CH_4 permeate} = P_{permeate} * y_{CH_4}$= 0.13 atm* 0.025= 0.00325 atm (after exp.)

$$P_{CH_4 permeate-avarage} = \frac{0.0000169atm + 0.00325\ atm}{2} = 0.0016\ atm \quad \text{(D.27)}$$

After that point, the same algorithm (given in Appendix B) was used for permeability calculations; the difference is only the dead volume of the system which is measured as 18 cm^3 for this set-up. The permeability was calculated with the below equations;

$$P_{CO_2(Barrer)} = \left[\frac{J_{CO_2} * l}{P_{CO_2 feed} - P_{CO_2\ permeate-avg}}\right] \quad \text{(D.28)}$$

$$P_{CH_4(Barrer)} = \left[\frac{J_{CH_4} * l}{P_{CH_4 feed} - P_{CH_4\ permeate-avg}}\right] \quad \text{(D.29)}$$

$P_{CO_2} = 4.15\ barrer$

$P_{CH_4} = 0.13\ barrer$

APPENDIX E

REPRODUCIBILITY OF THE ZIF-8 SYNTHESIS

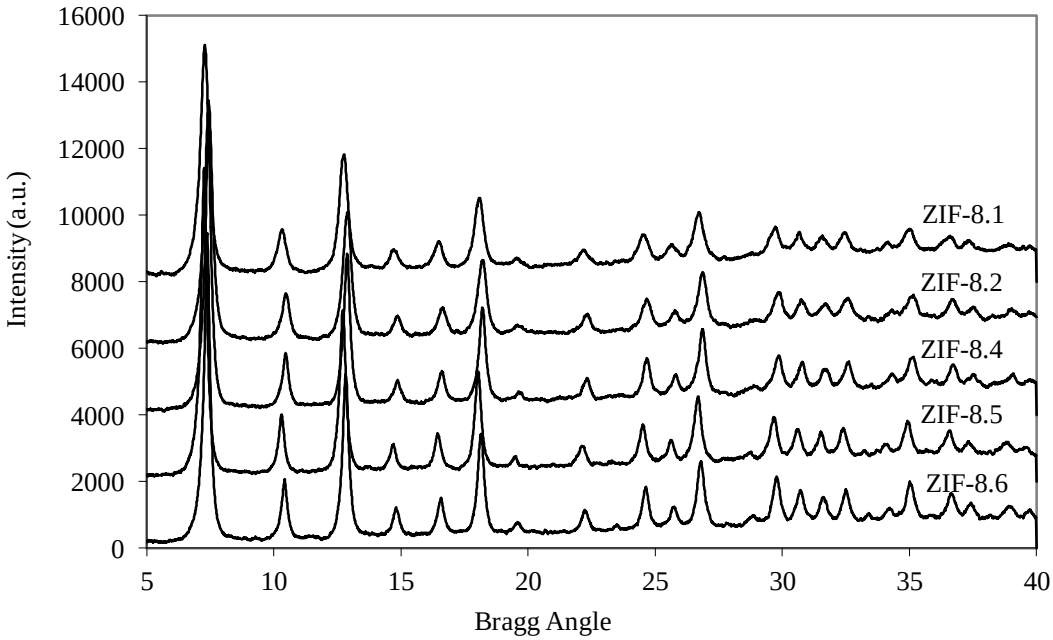

Figure E.1 XRD patterns of the second trial products synthesized with different amounts of methanol

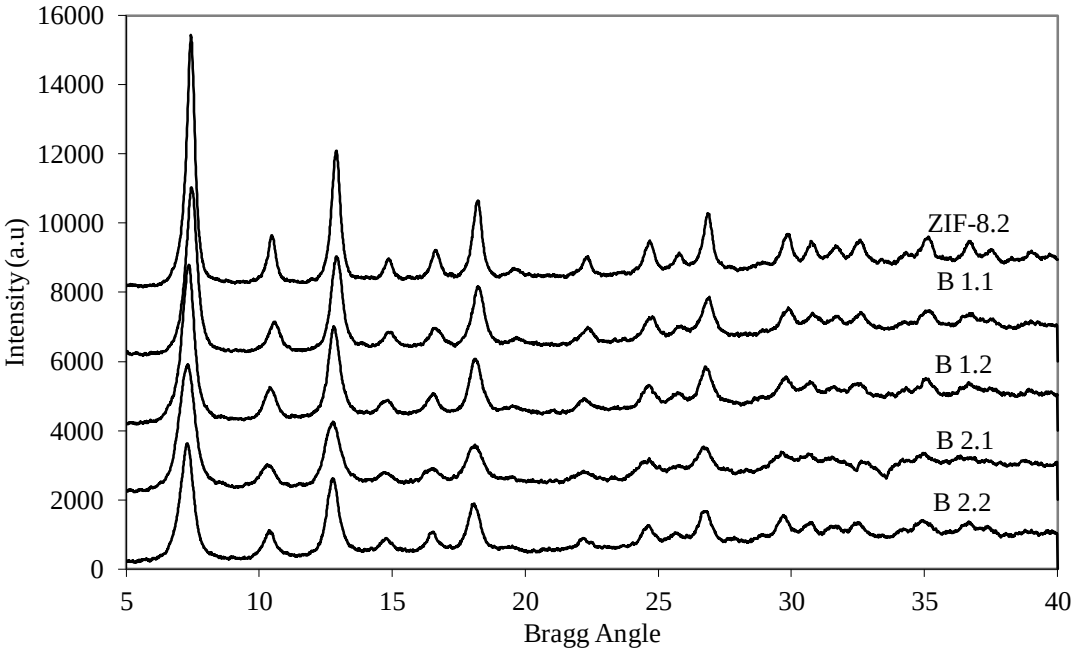

Figure E.2 XRD patterns of the ZIF-8s obtained from first trial of procedure B

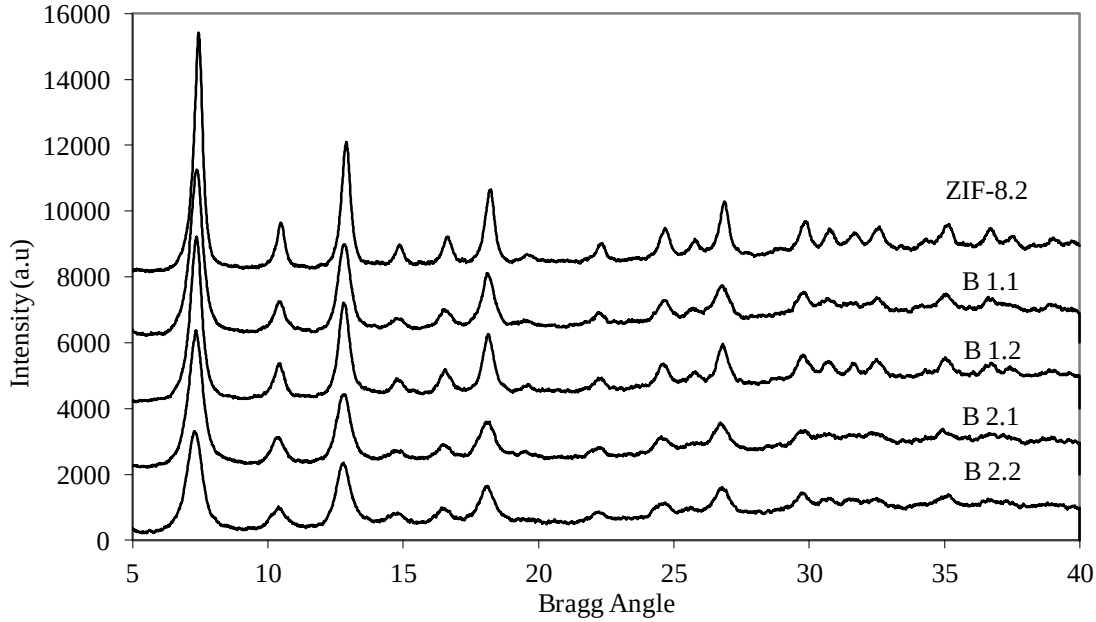

Figure E.3 XRD patterns of the ZIF-8s obtained from second trial of procedure B

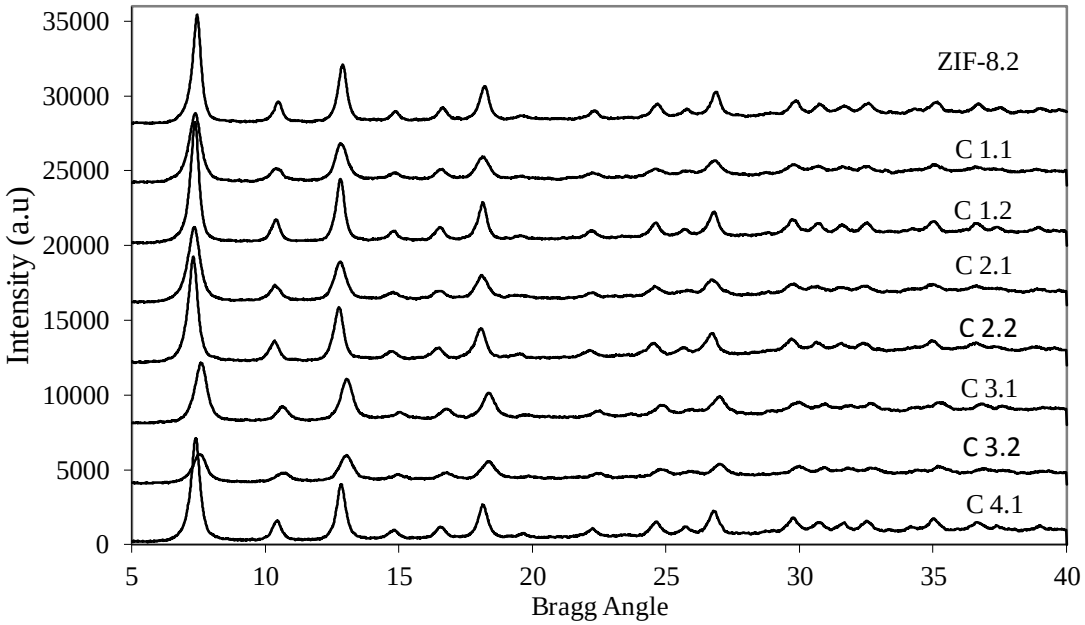

Figure E.4 XRD patterns of the ZIF-8s obtained from first trial of procedure C

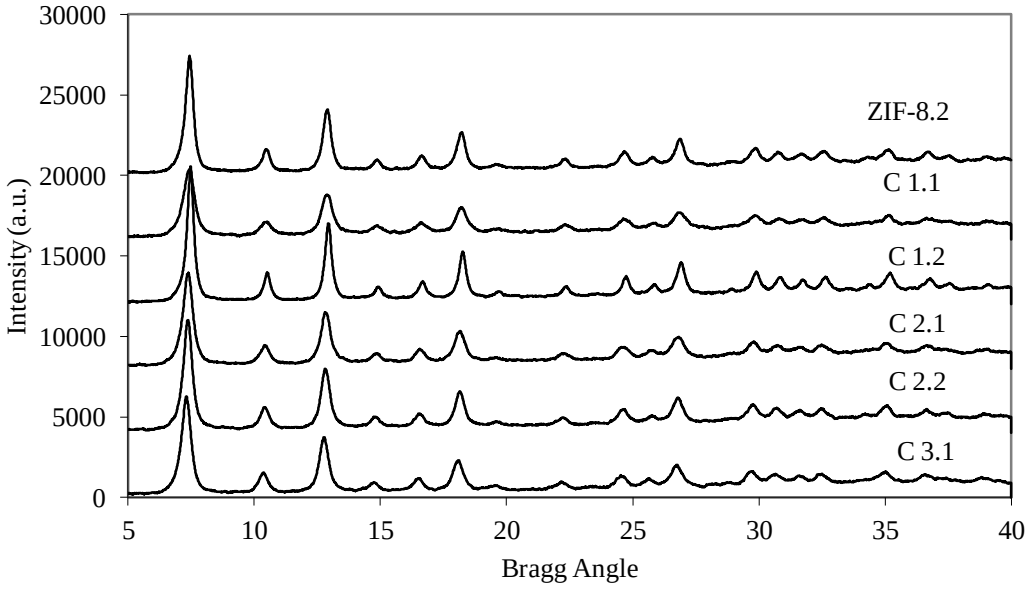

Figure E.5 XRD patterns of the ZIF-8s obtained from second trial of procedure C

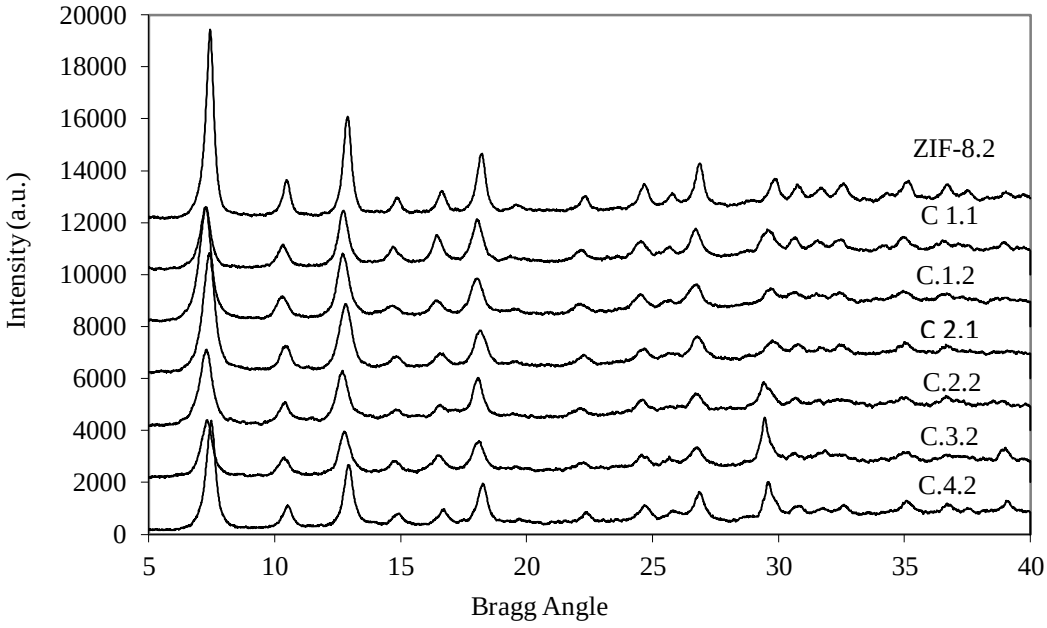

Figure E.6 XRD patterns of the ZIF-8s obtained from third trial of procedure C

APPENDIX F

SAMPLE CALCULATION OF ZIF-8 YIELD AND COMPOSITIONS OF SYHNTHESIS SOLUTIONS IN RECYCLING PROCEDURE

Considering the synthesis reaction given below, the maximum theoritical amount of ZIF-8 that can be produced at %100 yield can be calculated. Moreover, with the knowledge of initial amounts of raw materials and obtained ZIF-8 amount at the end of the reaction, the consumed and remained amounts of Zn^{+2} and Hmim sources can be calculated.

Original Synthesis

ZIF-8 Synthesis Reaction:

$$6\ Zn(NO_3)_2.6H_2O + 12C_4H_6N_2 + CH_3OH \longrightarrow Zn_6N_{24}C_{48}H_{60}\ (ZIF\text{-}8)$$

375.72 g batch solution consists of:

180.8 g MeOH	180.8 g MeOH
+	+
4.8 g $Zn(NO_3)_2.6H_2O$	10.56 g $C_4H_6N_2$

Molecular Weights of the Materials

- $Zn(NO_3)_2.6H_2O$: 297.49 g/mole
- $C_4H_6N_2$: 82.11 g/mole
- CH_3OH: 32.11 g/mole
- $Zn_6N_{24}C_{48}H_{60}$: 1365.51 g/mole

The obtained amount of ZIF-8 from given batch is known as 1.4 g experimentally. Using the stoicihometry of the ZIF-8 synthesis reaction, consumed and remaining amounts of Zn^{+2} source and Hmim was calculated easily.

Consumed Amount $Zn^{+2} = \left(\frac{Obtained\ amount\ of\ ZIF8}{1365.51 g/mole\ \ ZIF8}\right) * \left(\frac{6\ mole Zn^{+2}}{1\ mole\ ZIF8}\right) * \left(\frac{297.49\ g}{1\ mole\ Zn^{+2}}\right)$

$= \left(\frac{1.4\ g\ ZIF8}{1365.51\ g/mole}\right) * \left(\frac{6mole\ Zn^{+2}}{1\ mole\ ZIF8}\right) * \left(\frac{297.49\ g}{1\ mole\ Zn^{+2}}\right)$

$= 1.83g$

Remained Amount Zn+2= Initial Amount Zn^{+2} - Consumed Amount Zn^{+2}

=4.8 g – 1.83 g

= 2.97 g

Consumed Amount Hmim= $\left(\frac{Obtained\ amount\ of\ ZIF8}{1365.51 g/mole\ \ ZIF8}\right) * \left(\frac{12\ mole Zn^{+2}}{1\ mole\ ZIF8}\right) * \left(\frac{82.11\ g}{1\ mole\ Hmim}\right)$

$= \left(\frac{1.4\ g\ ZIF8}{1365.51\ g/mole}\right) * \left(\frac{12mole\ Zn^{+2}}{1\ mole\ ZIF8}\right) * \left(\frac{82.11\ g}{1\ mole\ Hmim}\right)$

= 1.01 g

Remained Amount Hmim= Initial Amount Hmim- Consumed Amount Hmim

=10.56 – 1.01

= 9.55 g

Remained Amount MeOH= 375.52 g – 1.4 g ZIF8 – 2.97 g Zn^{+2} – 9.55 g Hmim

= 361.6 g

In order to calculate the ZIF-8 yield of this batch, the maximum amount of ZIF-8 (that could be produced theoritically) should be calculated.

Max. ZIF-8 = $\left(\frac{4.8\ g\ Zn^{+2}}{297.49 g/mole}\right) * \left(\frac{1\ mole\ ZIF-8}{6mole\ Zn^{+2}}\right) * \left(\frac{1365.51 g/mole}{1\ mole\ ZIF-8}\right)$

= 3.67 g ZIF-8

$\%\ Yield = \frac{Obtained\ Amount\ of\ ZIF-8}{Maximum\ Amount\ of\ ZIF-8} * 100$

$= \frac{1.4\ g\ ZIF-8}{3.69\ g\ ZIF-8} * 100$

= % 37.9

<u>1st Step of the 1st Cycle (B 1.1 and C1.1)</u>

Since all the procedures and calculations are same for the first steps of the routes A and B, sample calculation is given together.

- Composition Calculation

Since only NaOH is added to the mother liquor in the first step, the composition was calculated based on the remaining amounts of Zn^{+2} and Hmim from the original synthesis solution which was calculated using the obtained ZIF-8 and the stoichiometry.

Remaining $Zn^{+2} = \frac{2.97\ g\ Zn^{+2}}{297.49\ g/mole} = 9.98 * 10^{-3}\ mole$

Remaining Hmim $= \frac{9.55\ g\ Hmim}{82.11 g/mole} = 0.116\ mole$

Remaining MeOH$= \frac{361.6\ g\ MeOH}{32.11\ g/mole} = 11.26\ mole$

Zn^{+2} / Hmim / MeOH = $9.98 * 10^{-3}$ / 0.116 / 11.26 = 1 / 11.65 / 1124

- Yield Calculation

After NaOH addition into the mother liquor and 1 hour stirring, 2.07 g ZIF-8 was recovered upon centrifugation and the remaining amount of Zn^{+2} source is known as 2.97 g from the previous calculations.

Max. ZIF-8 $= \left(\frac{2.97\ g\ Zn^{+2}}{297.49 g/mole}\right) * \left(\frac{1\ mole\ ZIF-8}{6 mole\ Zn^{+2}}\right) * \left(\frac{1365.51 g/mole}{1\ mole\ ZIF-8}\right)$

= 2.27 g ZIF-8

$\%\ Yield = \frac{2.07 g\ ZIF8}{2.27\ g\ ZIF8} * 100 = \%91.2$

- Remaining Amounts of Zn^{+2}, Hmim and MeOH

Since the synthesized ZIF-8 and the stoichiometry of the synthesis reaction is known, the consumed amount of raw materials can be calculated as it was done in the original synthesis calculations.

Consumed Amount $Zn^{+2} = \left(\frac{2.07\ g\ ZIF8}{1365.51\ g/mole}\right) * \left(\frac{6 mole\ Zn^{+2}}{1\ mole\ ZIF8}\right) * \left(\frac{297.49\ g}{1\ mole\ Zn^{+2}}\right)$

= 2.71 g

Remained Amount Zn+2 = 2.97g – 2.71g = 0.26 g

Consumed Amont Hmim $= \left(\frac{2.07\ g\ ZIF8}{1365.51\ g/mole}\right) * \left(\frac{12 mole\ Zn^{+2}}{1\ mole\ ZIF8}\right) * \left(\frac{82.11\ g}{1\ mole\ Hmim}\right)$

= 1.49 g

Remained Amount Hmim= 9.55g – 1.49g = 8.06 g

Remained Amount MeOH= 361.6g MeOH – 2.07 g ZIF8= 359.5 g MeOH

2nd Step of the 1st Cycle of B (B 1.2)

The aim in this step is to remain constant the Zn^{+2}/Hmim ratio as 1/7.9 as in original synthesis solution. Therefore, the amount of Zn^{+2}source that would be added to the second mother liquor was calculated using the ZIF-8 yield of the previous step. The remained amount of reactants were calculated above.

- Composition Calculation

The moles of the remaining reactants were calculated;

Remaining $Zn^{+2} = \frac{0.26\ g\ Zn^{+2}}{297.49\ g/mole} = 8.74 * 10^{-4}\ mole$

Remaining Hmim $= \frac{8.06\ g\ Hmim}{82.11 g/mole} = 0.098\ mole$

Remaining MeOH$= \frac{359.5\ g\ MeOH}{32.11\ g/mole} = 11.19\ mole$

In order to obtain a Zn^{+2}/Hmim ratio as 1/7.9, total Zn^{+2} mole was calculated as 0.0124 moles.

Added amount of Zn+2 = $0.0124 - 8.74 * 10^{-4} = 0.0115\ moles$

$= 0.0115\ mole * \left({}^{297.49\ g\ Zn^{+2}}/_{1\ mole\ Zn^{+2}}\right)$

= 3.43 g

Zn^{+2} / Hmim / MeOH = 0.0124/ 0.098 / 11.19 = 1 / 7.9 / 902

- Yield Calculation

After adding 3.43 g Zn^{+2} and stirring for 1 hour, 0.91 g ZIF-8 crystals were handled.

Max. ZIF-8$= \left(\frac{3.43+0.26\ g\ Zn^{+2}}{297.49 g/mole}\right) * \left(\frac{1\ mole\ ZIF-8}{6 mole\ Zn^{+2}}\right) * \left(\frac{1365.51 g/mole}{1\ mole\ ZIF-8}\right)$

= 2.92 g ZIF-8

$$\%\, Yield = \frac{0.91 g\ ZIF8}{2.92\ g\ ZIF8} * 100 = \%31.2$$

- Remaining Amounts of Zn^{+2}, Hmim and MeOH

Consumed Amount $Zn^{+2} = \left(\frac{0.91\ g\ ZIF8}{1365.51\ g/mole}\right) * \left(\frac{6 mole\ Zn^{+2}}{1\ mole\ ZIF8}\right) * \left(\frac{297.49\ g}{1\ mole\ Zn^{+2}}\right)$

= 1.19 g

Remained Amount Zn+2= 3.69g – 1.19g = 2.5 g

Consumed Amont Hmim $= \left(\frac{0.91\ g\ ZIF8}{1365.51\ g/mole}\right) * \left(\frac{12 mole\ Zn^{+2}}{1\ mole\ ZIF8}\right) * \left(\frac{82.11\ g}{1\ mole\ Hmim}\right)$

= 0.66 g

Remained Amount Hmim= 8.06 g – 0.66 g = 7.4 g

Remained Amount MeOH= 359.5g MeOH – 0.91 g ZIF8= 358.6 g MeOH

2nd Step of the 1st Cycle of C (C 1.2)

Since, initial amount of Zn^{+2} source is added to the mother liquor in route C, the composition is changing in every step.

- Composition Calculation

Since the 1.1 cycle was common for two routes, the moles of the remaining reactants were same for C 1.2;

Remaining $Zn^{+2} = \frac{0.26\ g\ Zn^{+2}}{297.49\ g/mole} = 8.74 * 10^{-4}\ mole$

Remaining Hmim $= \frac{8.06\ g\ Hmim}{82.11 g/mole} = 0.098\ mole$

Remaining MeOH$= \frac{359.5\ g\ MeOH}{32.11\ g/mole} = 11.19\ mole$

Added $Zn^{+2} = 4.8 * \left(\frac{359.5 g\ MeOH + 8.06\ g\ Hmim + 0.26\ g\ Zn^{+2}}{375.52\ g\ Batch\ Solution}\right) = 4.7\ g$

Total Amount of Zn+2 = 4.7g + 0.26 = 4.96 g

$$= 4.96\ g * \left(1\ mole\ Zn^{+2} / 297.49\ g\ Zn^{+2}\right)$$

= 0.0167 moles

Zn^{+2} / Hmim / MeOH = 0.0167/ 0.098 / 11.19 = 1 / 5.9 / 670

- Yield Calculation

After adding 4.7 g Zn^{+2} and stirring for 1 hour, 1.13 g ZIF-8 crystals were handled.

Max. ZIF-8= $\left(\frac{4.7+0.26\ g\ Zn^{+2}}{297.49 g/mole}\right) * \left(\frac{1\ mole\ ZIF-8}{6 mole\ Zn^{+2}}\right) * \left(\frac{1365.51 g/mole}{1\ mole\ ZIF-8}\right)$

= 3.79 g ZIF-8

$$\%\ Yield = \frac{1.13 g\ ZIF8}{3.79\ g\ ZIF8} * 100 = \%29.8$$

- Remaining Amounts of Zn^{+2}, Hmim and MeOH

Consumed Amount Zn^{+2} = $\left(\frac{1.13\ g\ ZIF8}{1365.51\ g/mole}\right) * \left(\frac{6 mole\ Zn^{+2}}{1\ mole\ ZIF8}\right) * \left(\frac{297.49\ g}{1\ mole\ Zn^{+2}}\right)$

= 1.48 g

Remained Amount Zn+2= 4.96g – 1.48g = 3.5 g

Consumed Amont Hmim = $\left(\frac{1.13\ g\ ZIF8}{1365.51\ g/mole}\right) * \left(\frac{12 mole\ Zn^{+2}}{1\ mole\ ZIF8}\right) * \left(\frac{82.11\ g}{1\ mole\ Hmim}\right)$

= 0.82 g

Remained Amount Hmim= 8.06 g – 0.82 g = 7.24 g

Remained Amount MeOH= 359.5g MeOH – 1.13 g ZIF8= 358.4 g MeOH

APPENDIX G

SAMPLE TGA THERMOGRAMS OF PREPARED MEMBRANES

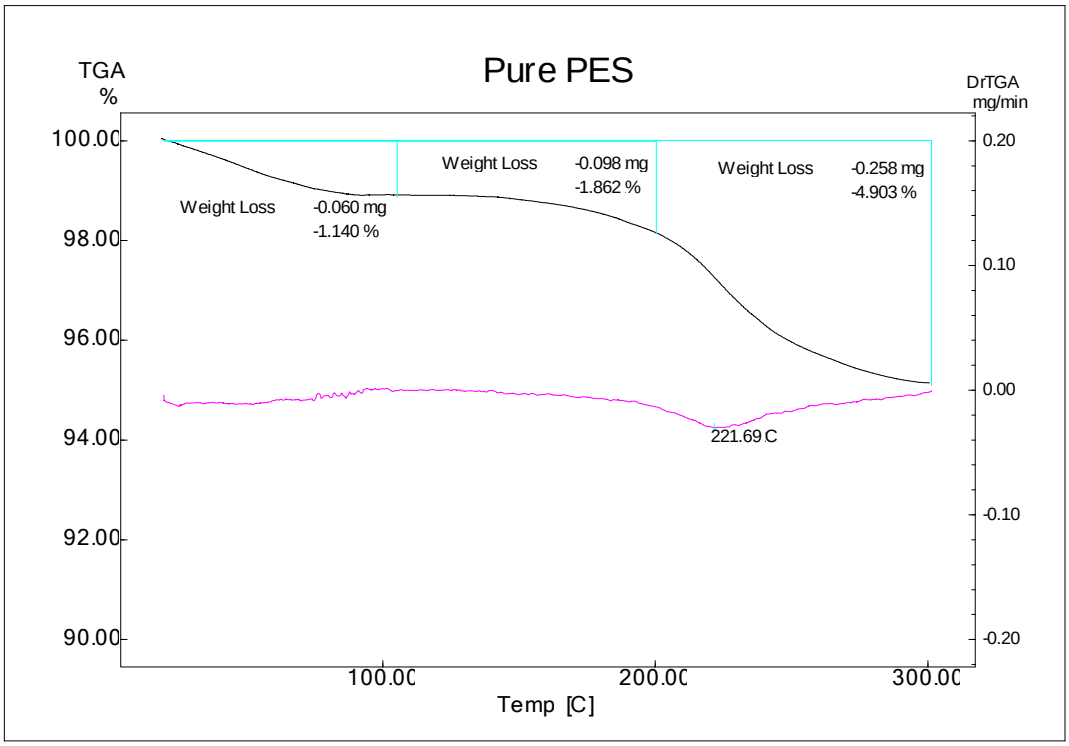

Figure G.1 TGA thermogram of pure PES membrane

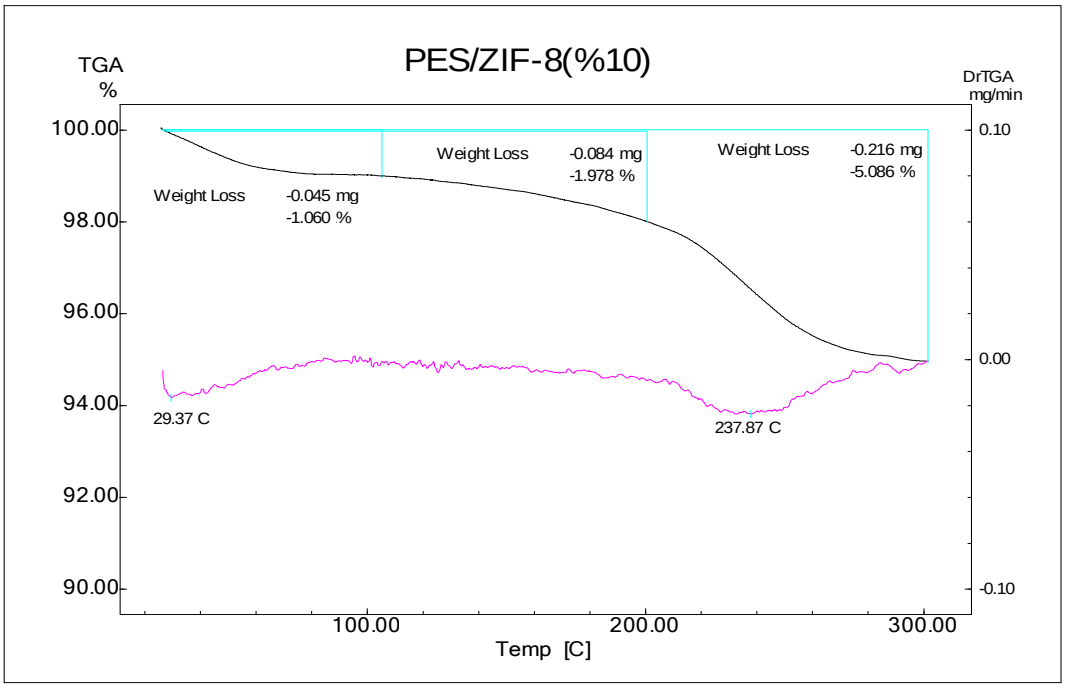

Figure G.2 TGA thermogram of PES/ZIF-8(%10) membrane

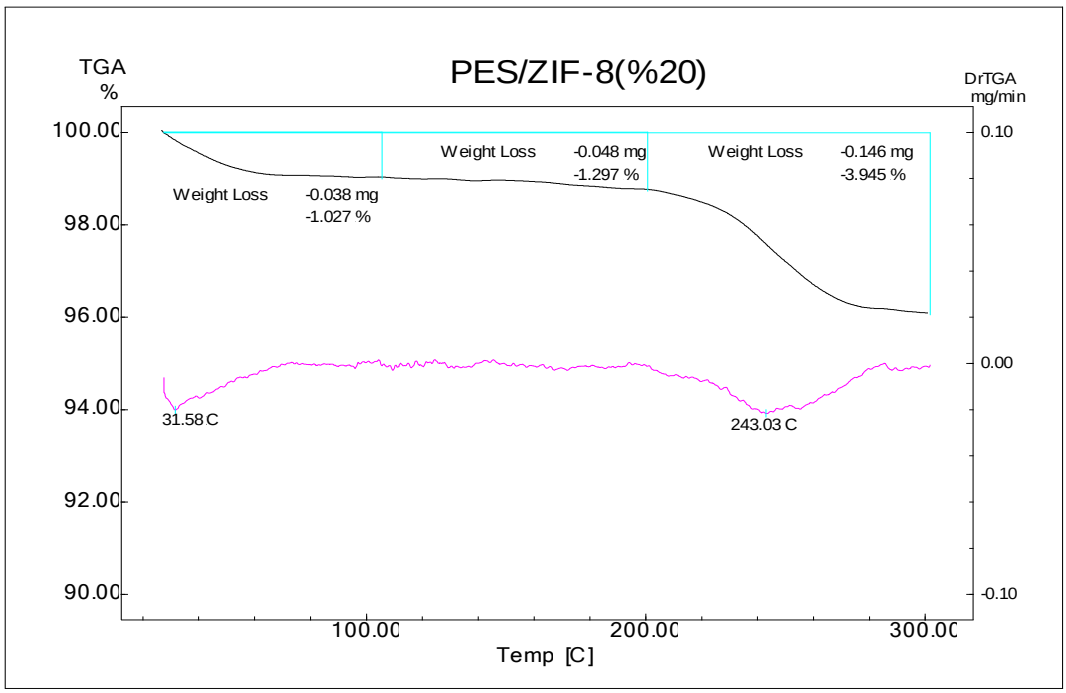

Figure G.3 TGA thermogram of PES/ZIF-8(%20) membrane

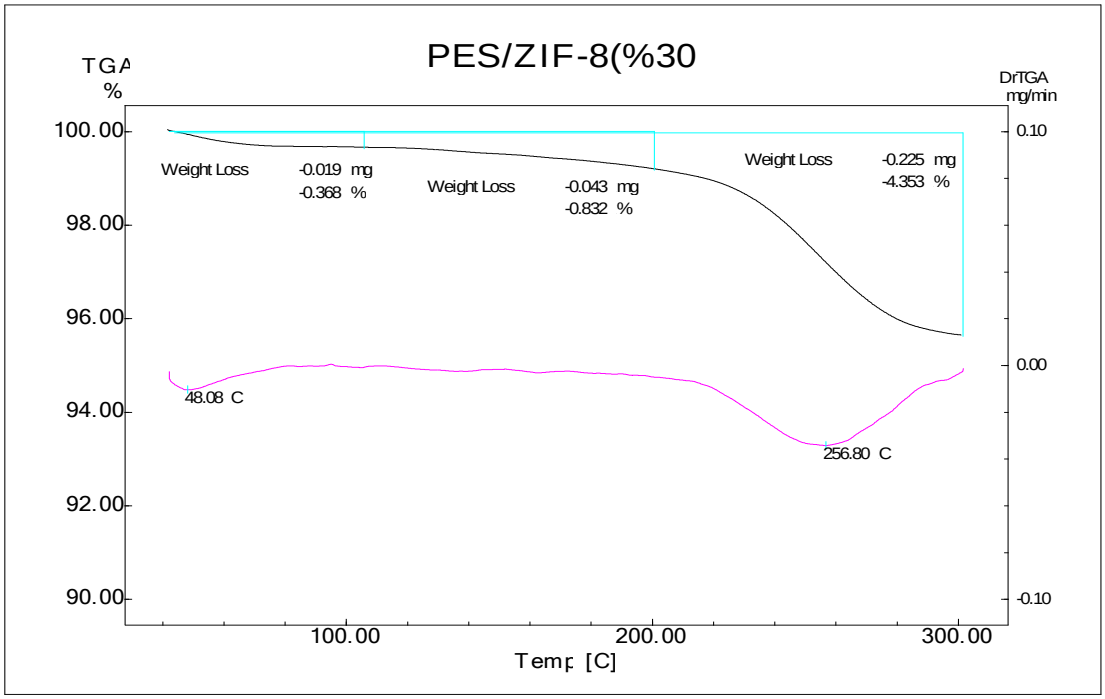

Figure G.4 TGA thermogram of PES/ZIF-8(%30) membrane

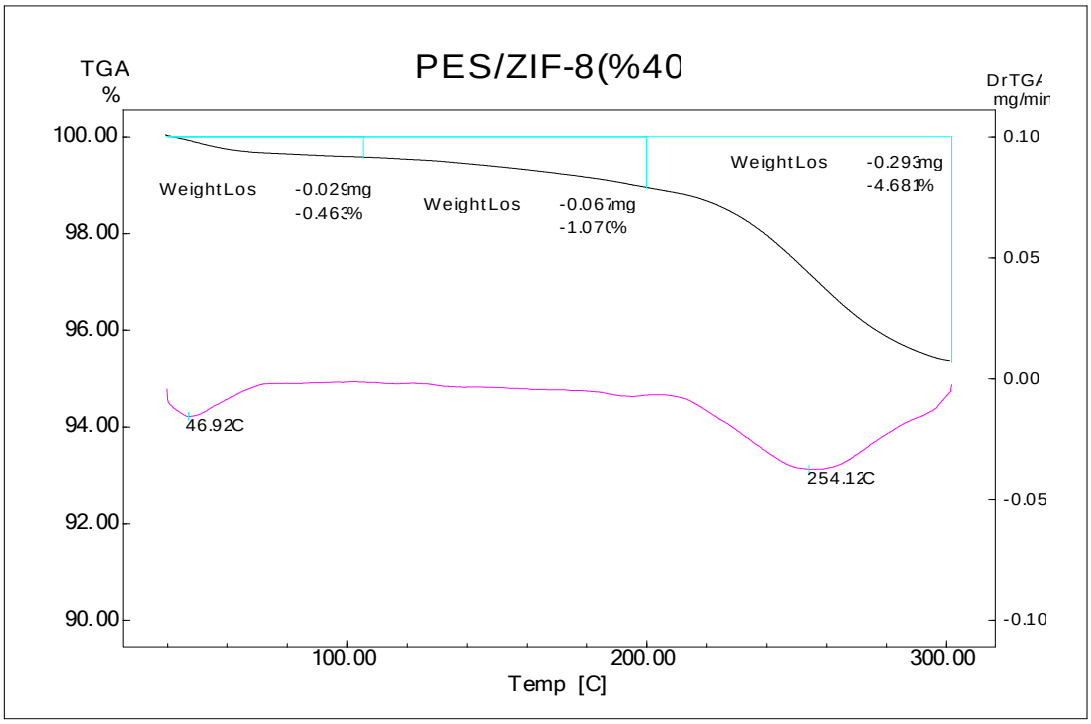

Figure G.5 TGA thermogram of PES/ZIF-8(%40) membrane

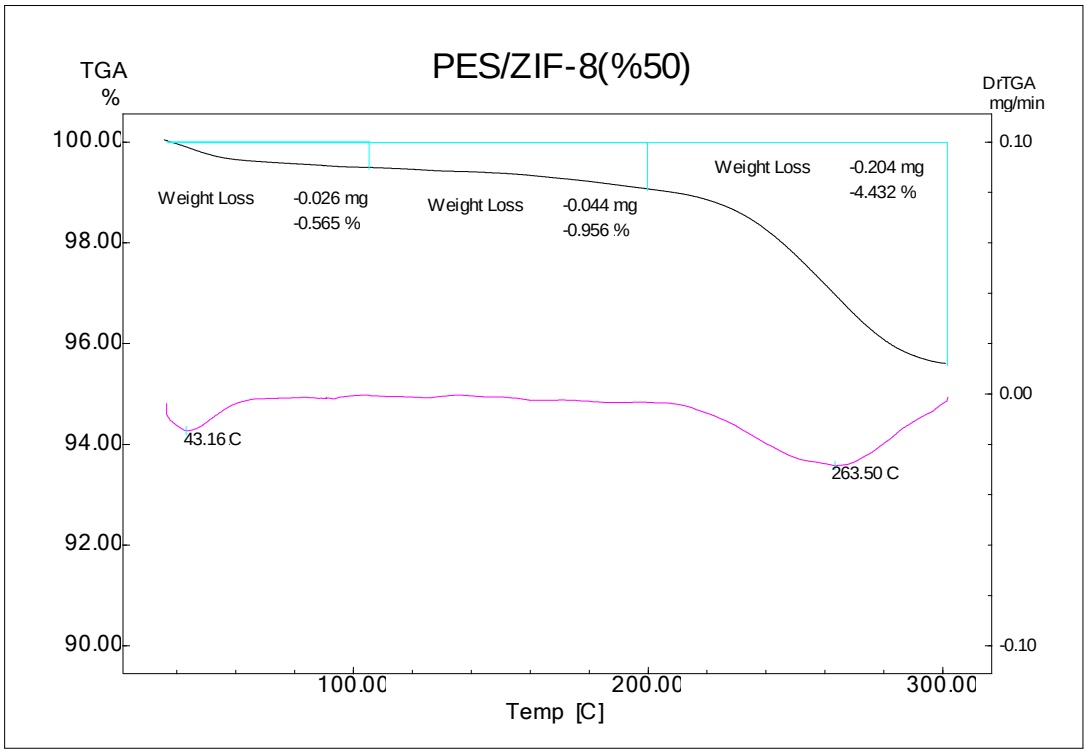

Figure G.6 TGA thermogram of PES/ZIF-8(%50) membrane

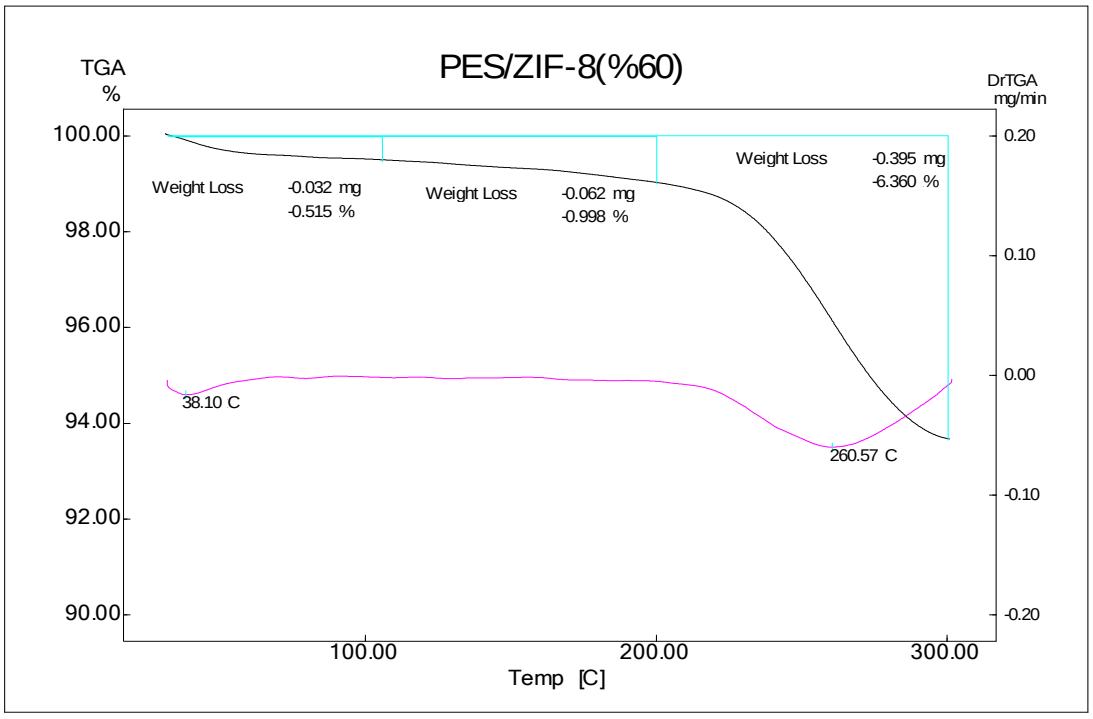

Figure G.7 TGA thermogram of PES/ZIF-8(%60) membrane

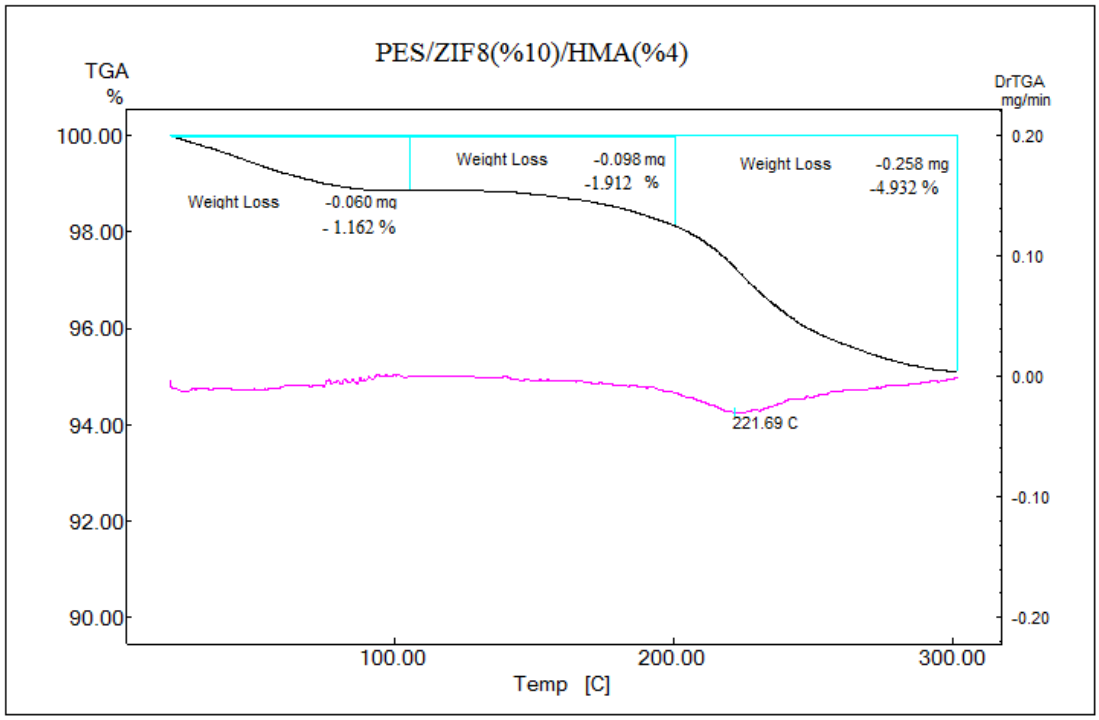

Figure G.8 TGA thermogram of PES/ZIF-8(%10)/HMA(%4) membrane

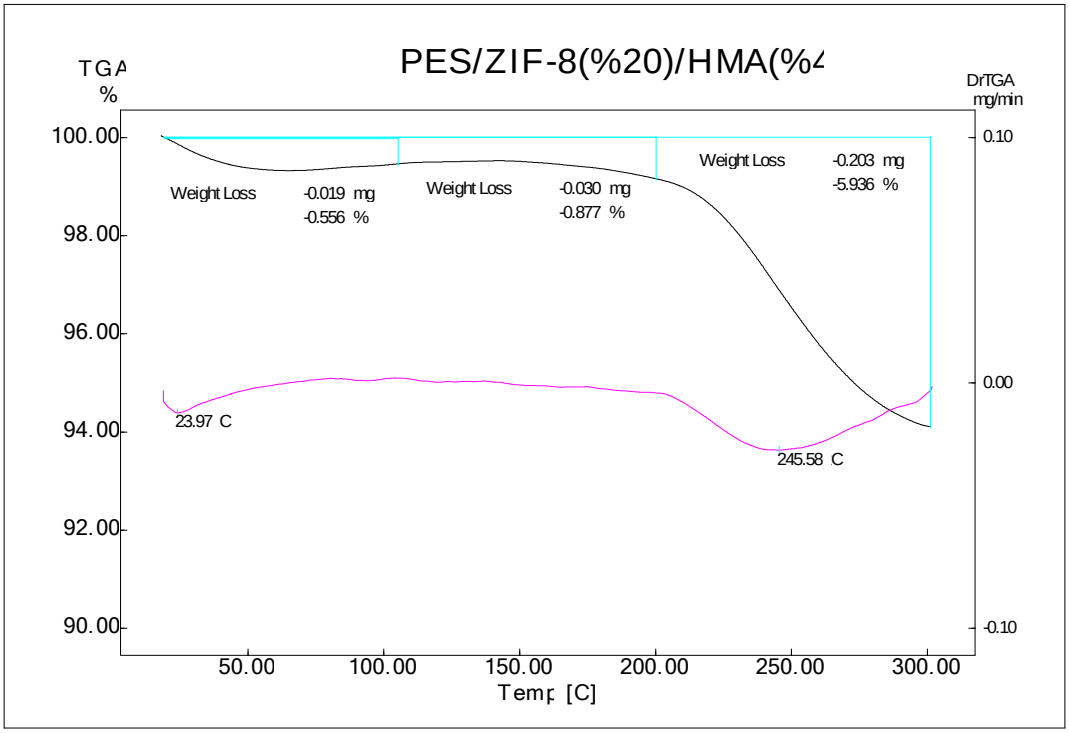

Figure G.9 TGA thermogram of PES/ZIF-8(%20)/HMA(%4) membrane

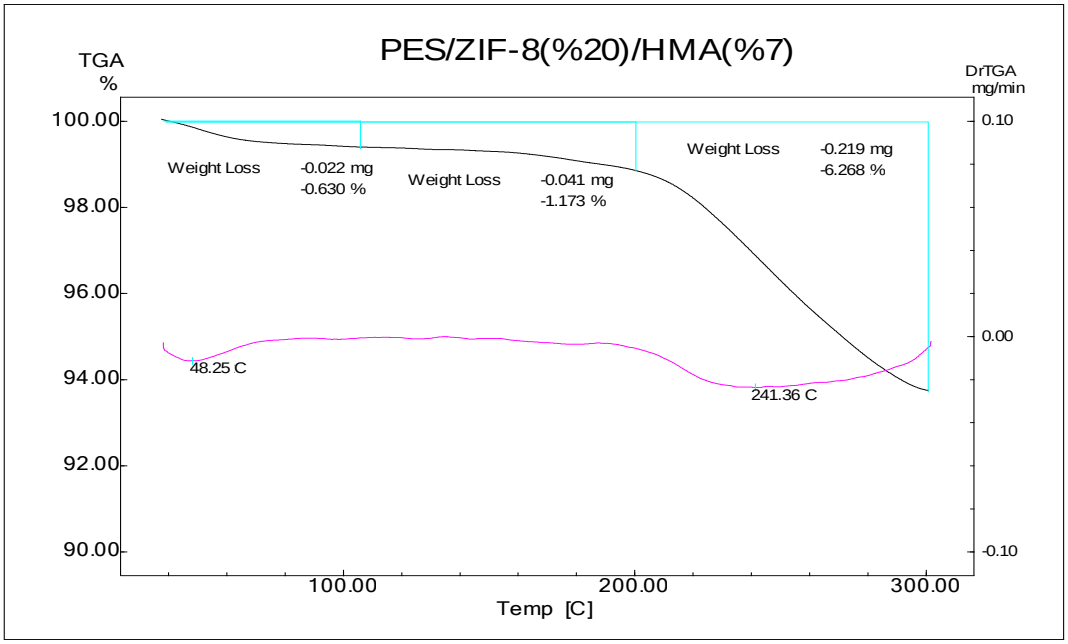

Figure G.10 TGA thermogram of PES/ZIF-8(%20)/HMA(%7) membrane

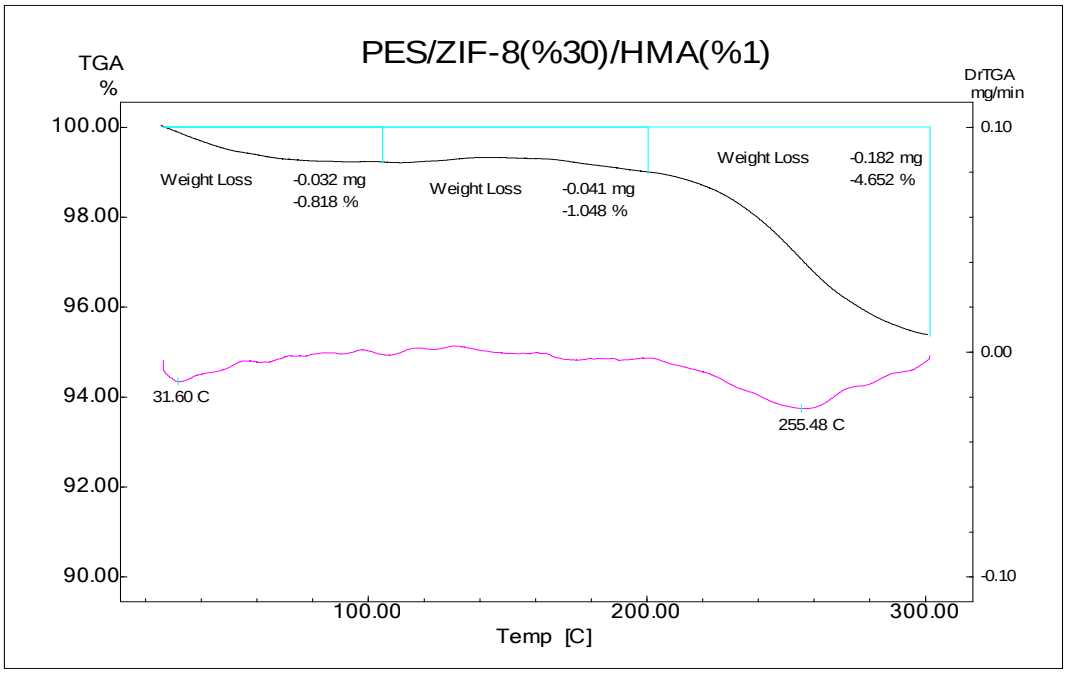

Figure G.11 TGA thermogram of PES/ZIF-8(%30)/HMA(%1) membrane

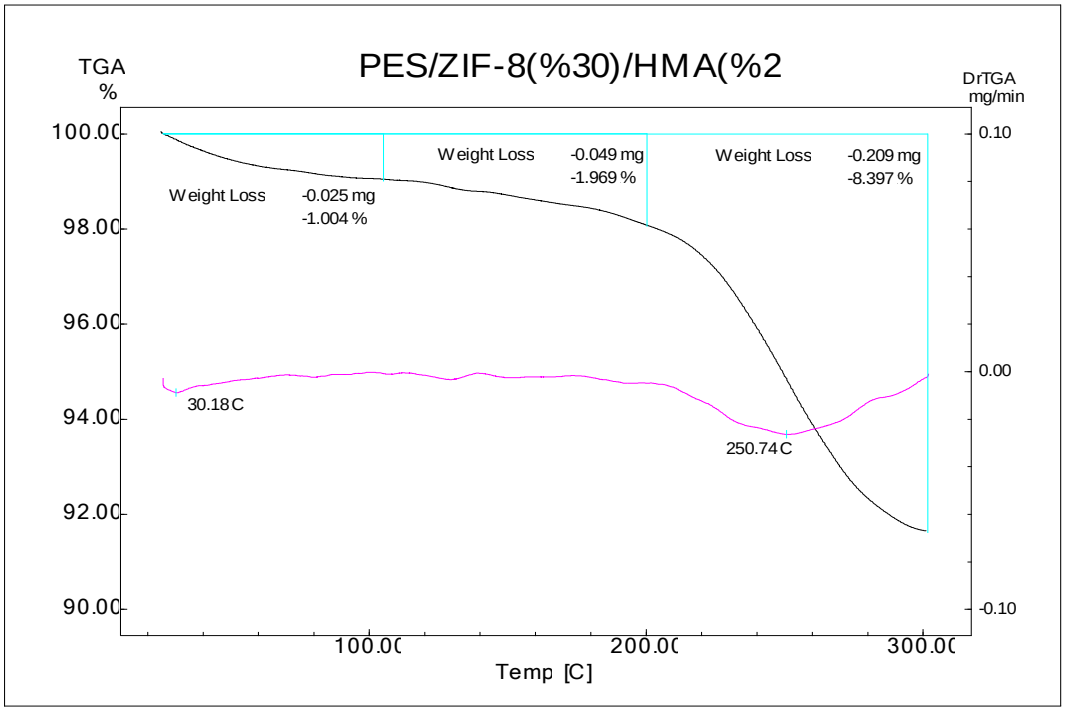

Figure G.12 TGA thermogram of PES/ZIF-8(%30)/HMA(%2) membrane

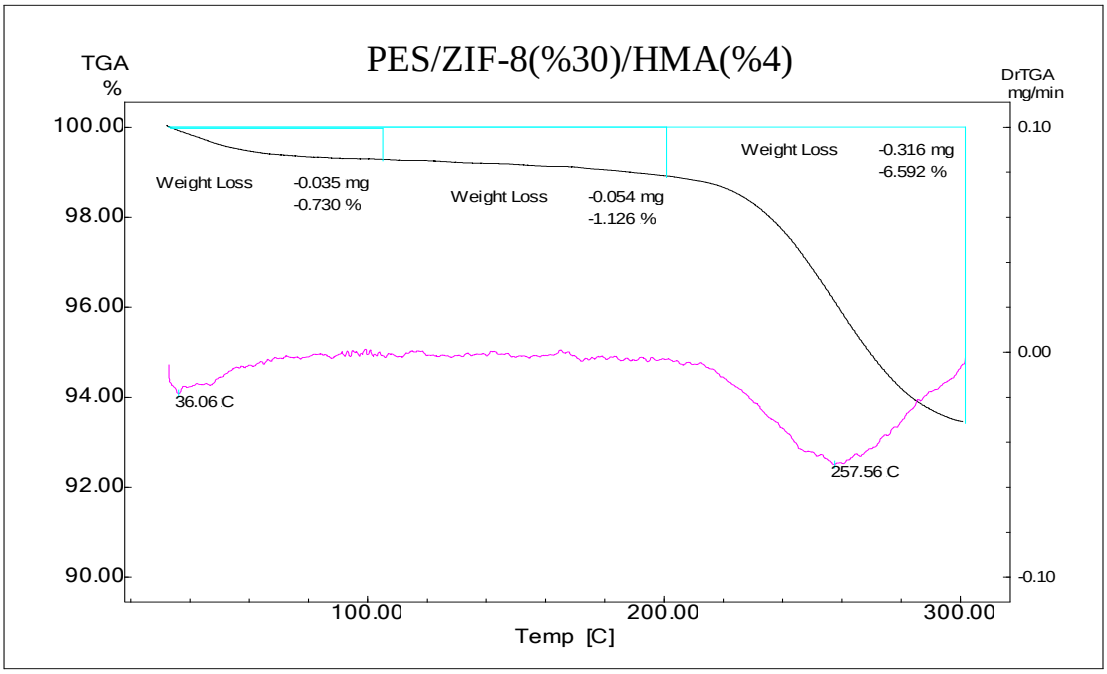

Figure G.13 TGA thermogram of PES/ZIF-8(%30)/HMA(%4) membrane

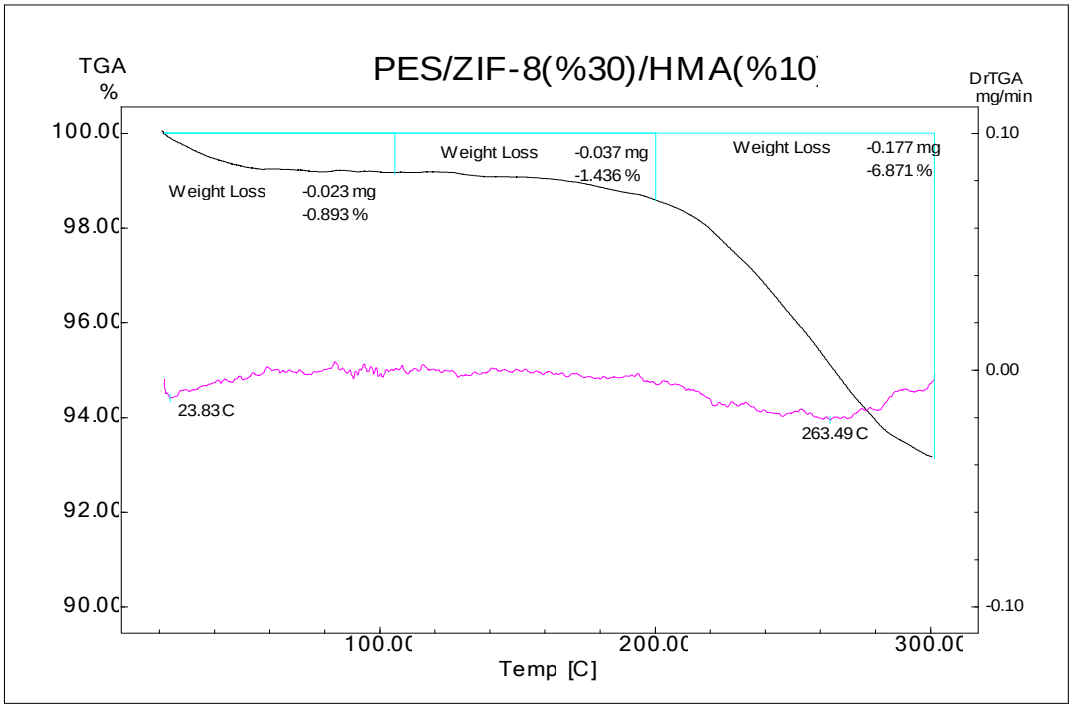

Figure G.14 TGA thermogram of PES/ZIF-8(%30)/HMA(%10) membrane

APPENDIX H

SAMPLE THERMOGRAMS AND WEIGHT LOSSES OF THE MEMBRANES UP TO 650 ^{O}C

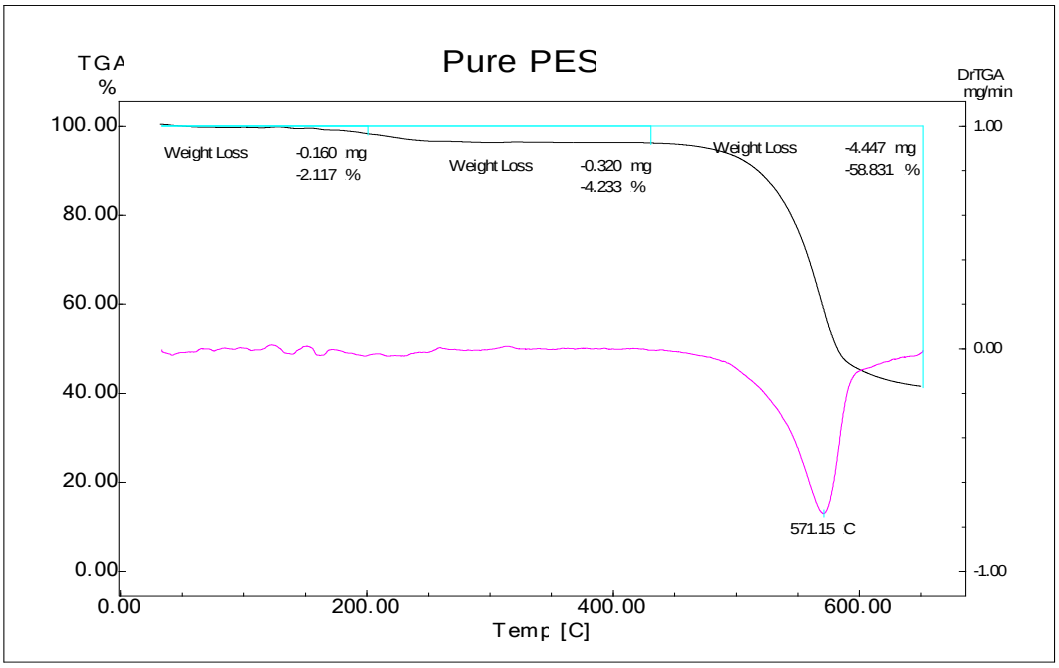

Figure H.1 The TGA thermogram of Pure PES membrane up to 650 ^{o}C

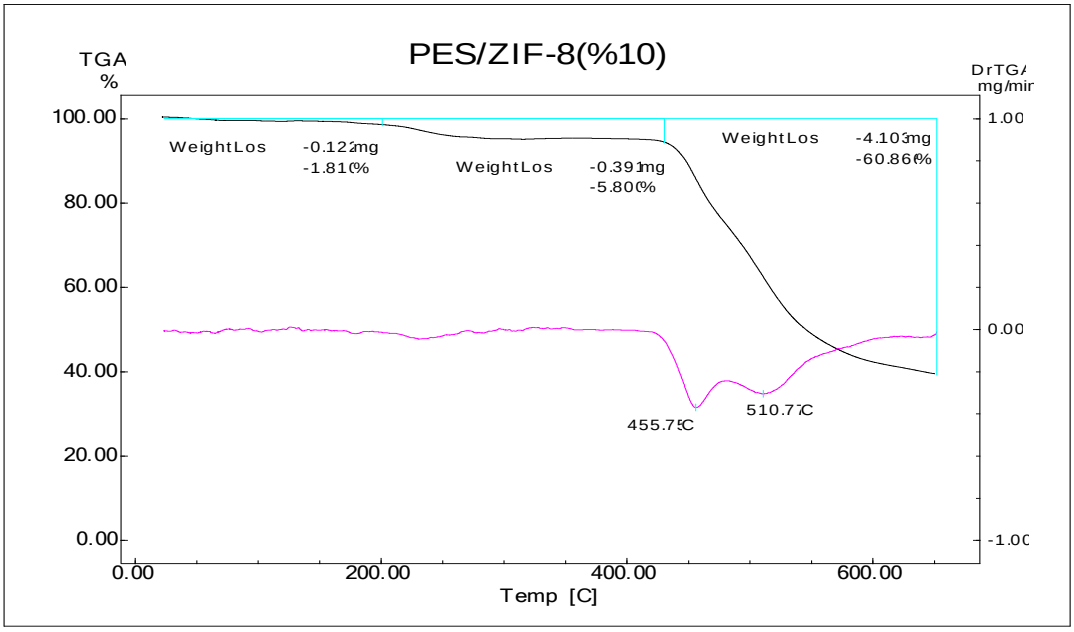

Figure H.2 The TGA thermogram of PES/ZIF-8(%10) membrane up to 650 °C

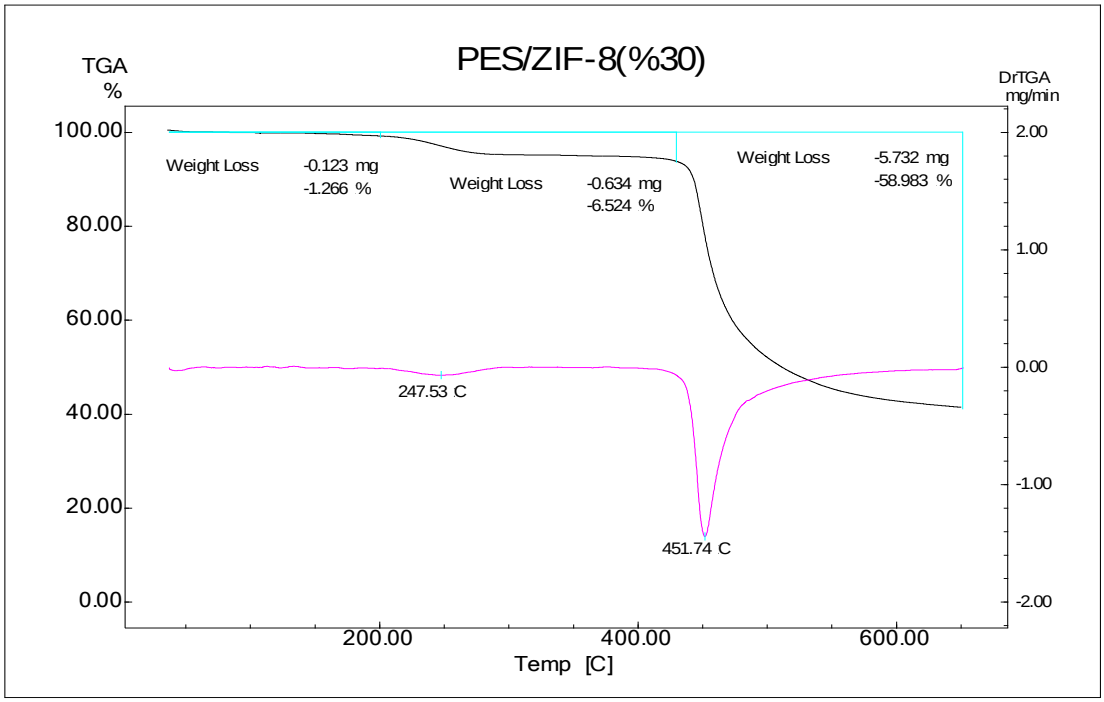

Figure H.3 The TGA thermogram of PES/ZIF-8(%30) membrane up to 650 °C

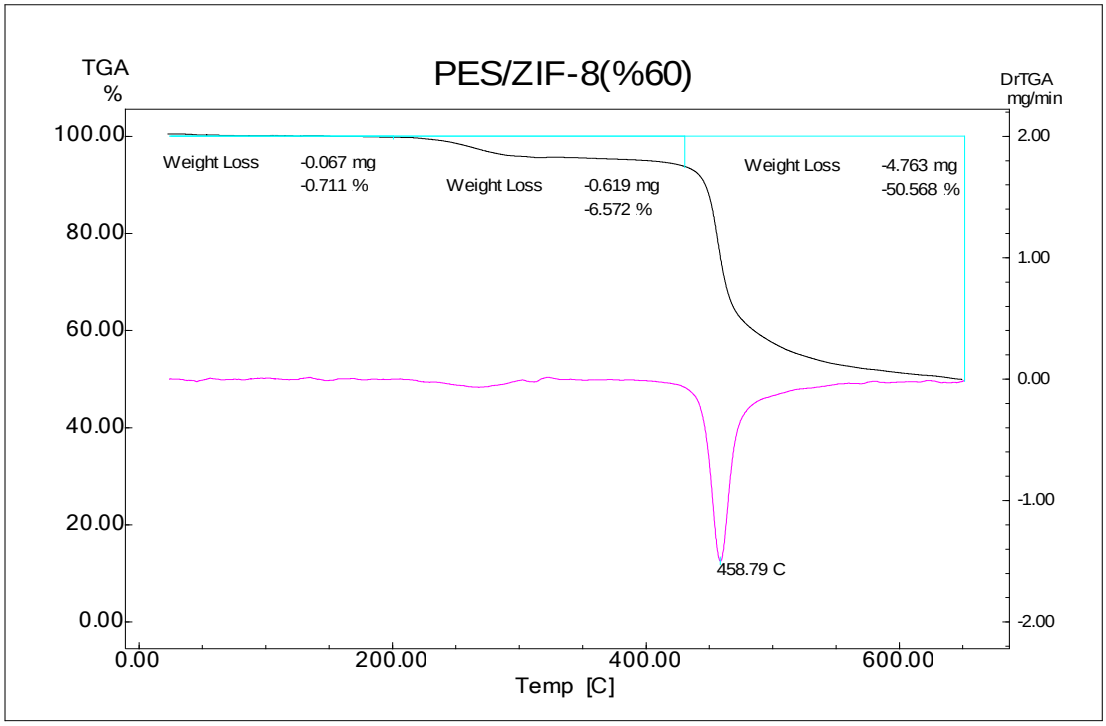

Figure H.4 The TGA thermogram of PES/ZIF-8(%60) membrane up to 650 °C

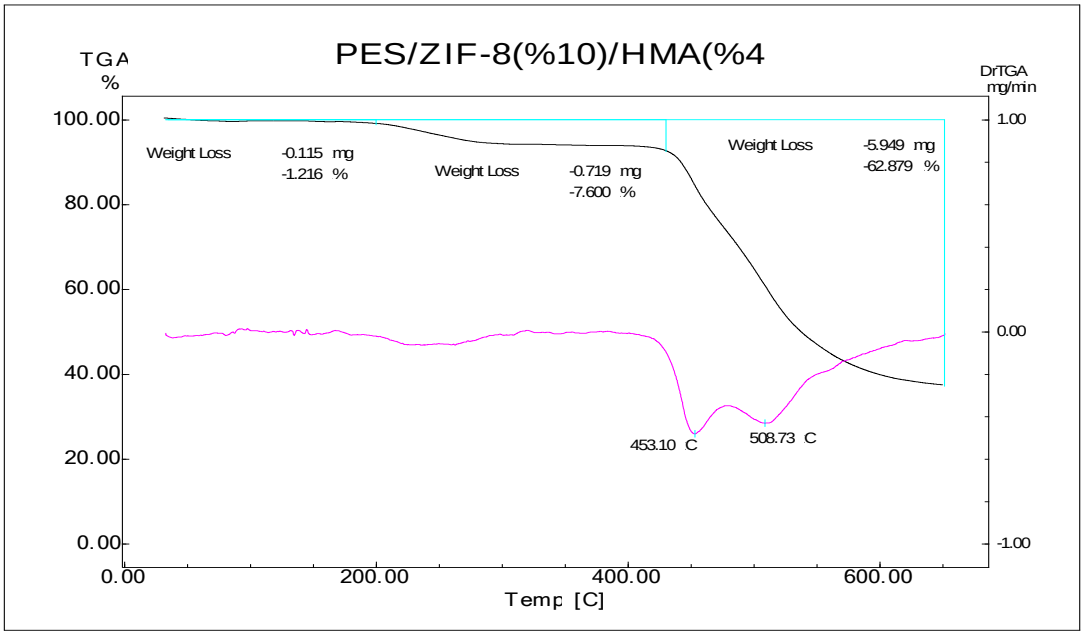

Figure H.5 The TGA thermogram of PES/ZIF-8(%10)/HMA(%4) membrane up to 650 °C

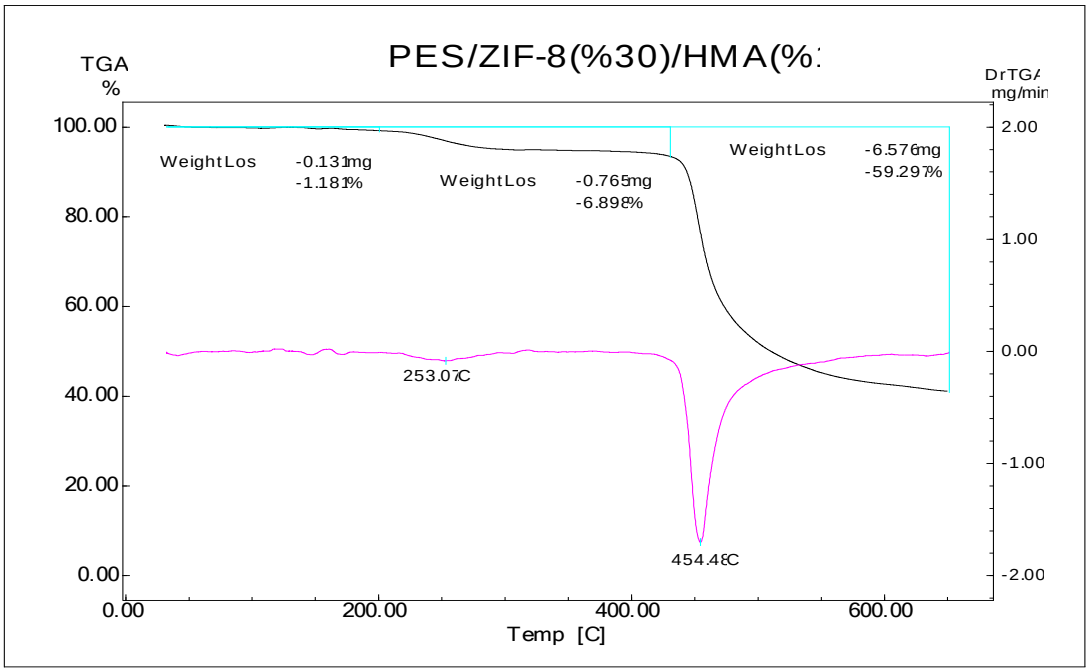

Figure H.6 The TGA thermogram of PES/ZIF-8(%30)/HMA(%1) membrane up to 650 ^{o}C

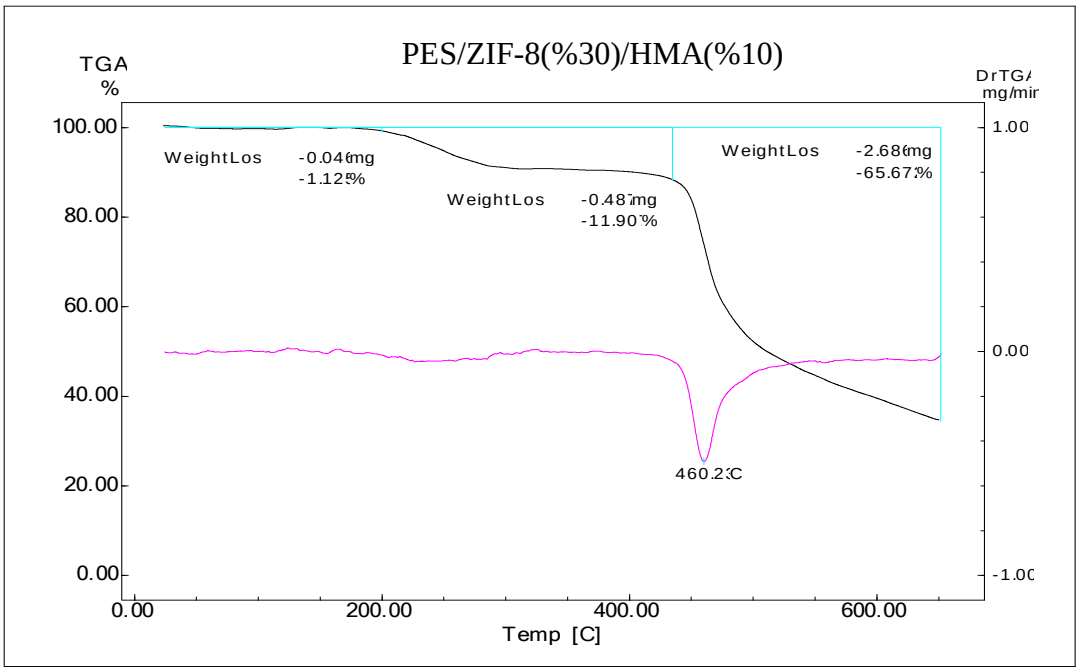

Figure H.7 The TGA thermogram of PES/ZIF-8(%30)/HMA(%10) membrane up to 650 ^{o}C

APPENDIX I

BACK CALCULATION OF ZIF-8 AMOUNT IN THE MEMBRANES

TGA analysis was performed in air atmosphere up to 800^{O}C so as to decompose the polymer and ZIF-8 crystals completely. Since the solid residue obtained after burning experiment is known to be only zinc oxide[REF-6FDA-DAM], the amount of ZIF-8 crystals in the membrane could be back calculated. Figure I.1 indicates the TGA thermogram of the pure ZIF-8 crystals performed in air atmosphere up to 800^{O}C of which result implies that the ZnO mass percentage of pure ZIF-8 crystals was about 34.7 %.

$$x_{ZnO} = 0.347$$

Considering the PES/ZIF-8(%20) membrane, the total initial amount used in analysis and the amount of ZnO handled after burning are given below;

$$m_{total} = 5.59\, mg$$

$$m_{ZnO} = 0.24\, mg$$

Then the amount of ZIF-8 crystals in the membrane was calculated as;

$$m_{ZIF-8} = \frac{m_{ZnO}}{x_{ZnO}} = \frac{0.24\, mg}{0.347} = 0.69\, mg$$

The ZIF-8 percent in the membrane formulation is calculated as follows;

$$\%ZIF-8 = \frac{m_{ZIF-8}}{m_{total} - m_{ZIF-8}} * 100 = \frac{0.69\, mg}{5.59mg - 0.69\, mg} * 100$$

= 14.1 %

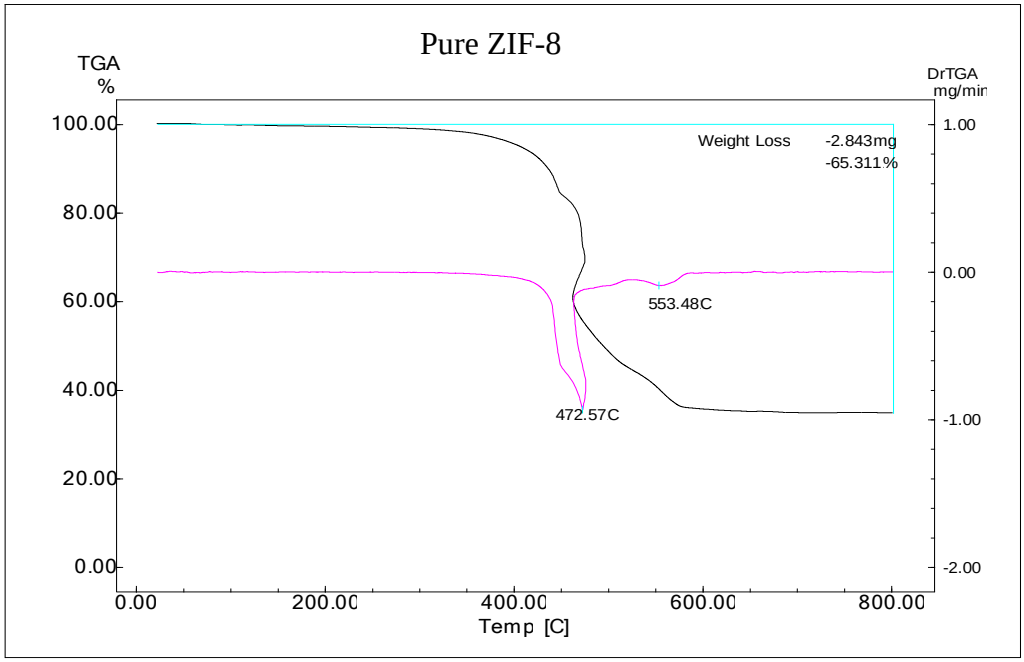

Figure I.1 TGA thermogram of pure ZIF-8 crystals

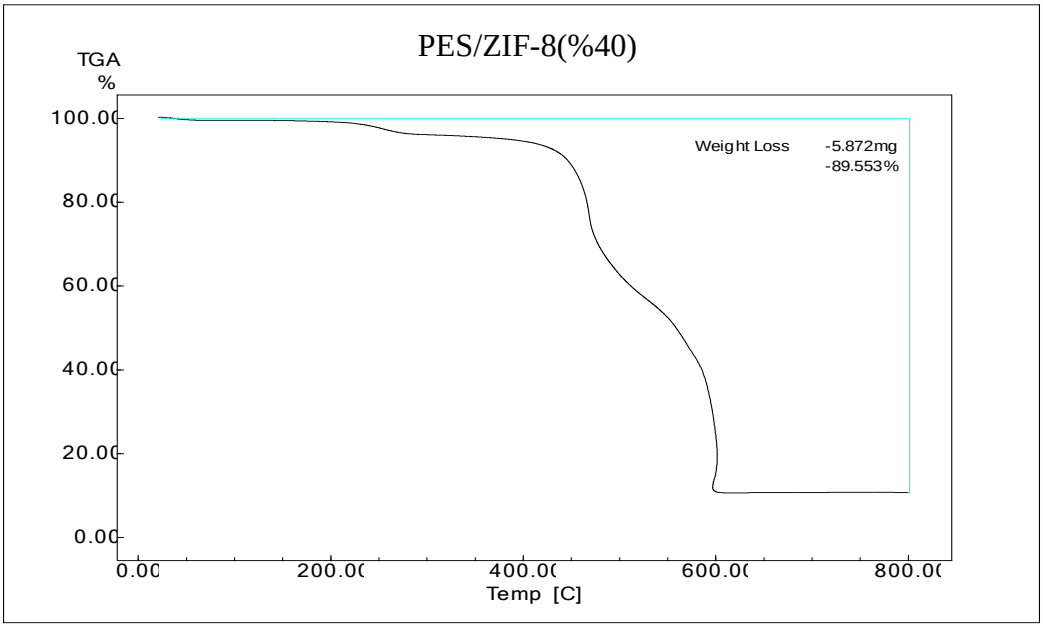

Figure I.2 TGA thermogram of PES/ZIF-8(%40) membrane

Table I.1 Analysis results of TGA residues and calculated ZIF-8 loadings

Membrane Code	MembraneComposition	ZnO(mg)	ZIF-8(mg)	ZIF-8 (w/w %)
NK-77	PES/ZIF-8(%10)	0.06	0.17	3.9
NK-72	PES/ZIF-8(%10)/HMA(%4)	0.08	0.23	4.4
NK-102	PES/ZIF-8(%20)	0.43	1.24	17.0
NK-49	PES/ZIF-8(%20)/HMA(%7)	0.24	0.69	14.0
NK-87	PES/ZIF-8(%30)	0.58	1.67	27.0
NK-74-1st part	PES/ZIF-8(%30)/HMA(%1)	0.54	1.56	27.4
NK-74-2nd part	PES/ZIF-8(%30)/HMA(%1)	0.34	0.98	23.5
NK-54	PES/ZIF-8(%40)	0.68	1.96	42.7
NK-84	PES/ZIF-8(%40)	0.50	1.44	32.9
NK-47	PES/ZIF-8(%50)	0.82	2.36	41.2
NK-91	PES/ZIF-8(%50)	1.47	4.24	44.2
NK-41	PES/ZIF-8(%60)	0.82	2.36	42.1
NK-93	PES/ZIF-8(%60)	1.76	5.07	55.8

APPENDIX J

SAMPLE DSC THERMOGRAMS OF PREPARED MEMBRANES

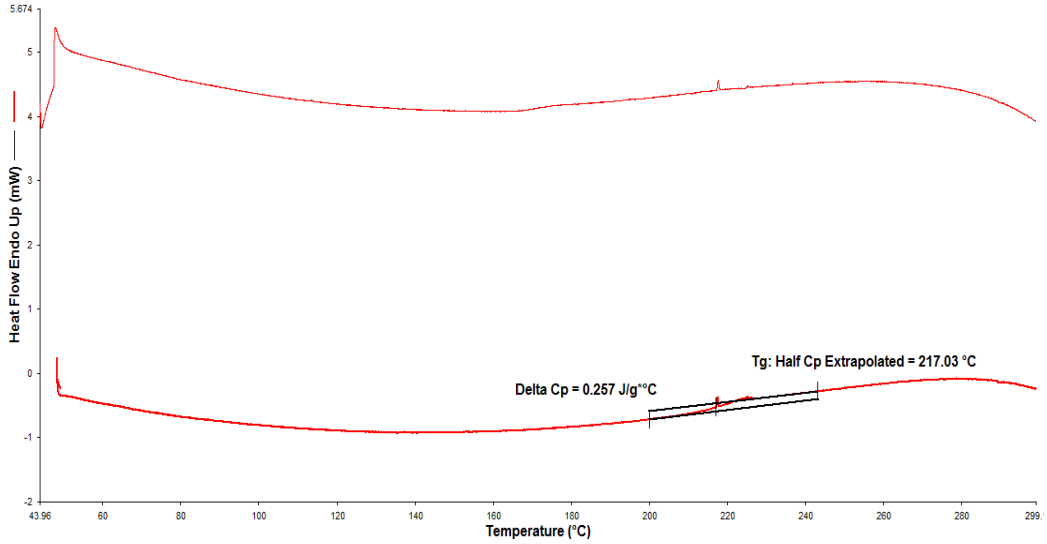

Figure J.1 DSC thermogram of Pure PES membrane

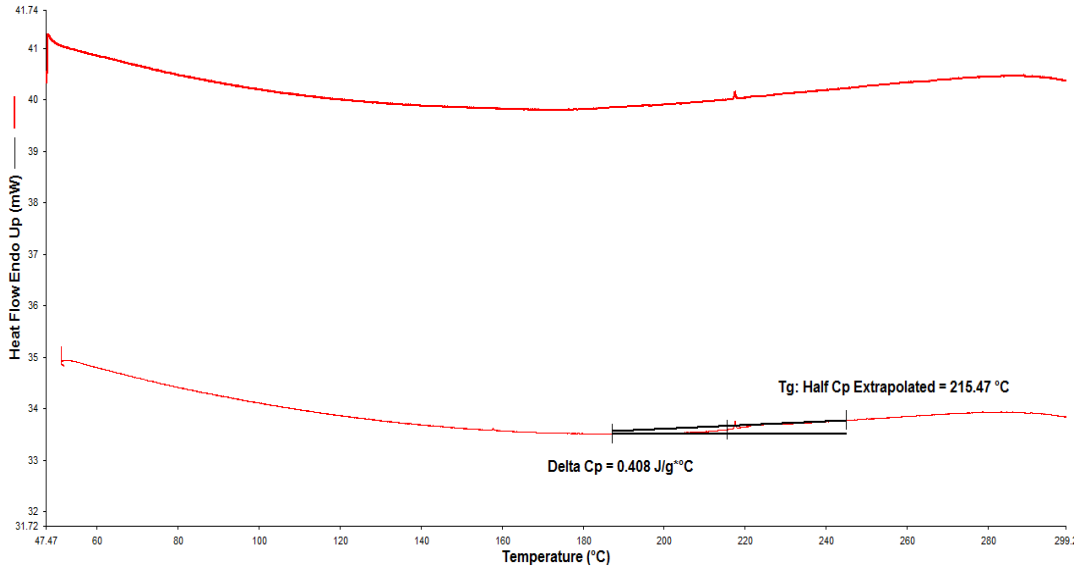

Figure J.2 DSC thermogram of PES/ZIF-8(%10) membrane

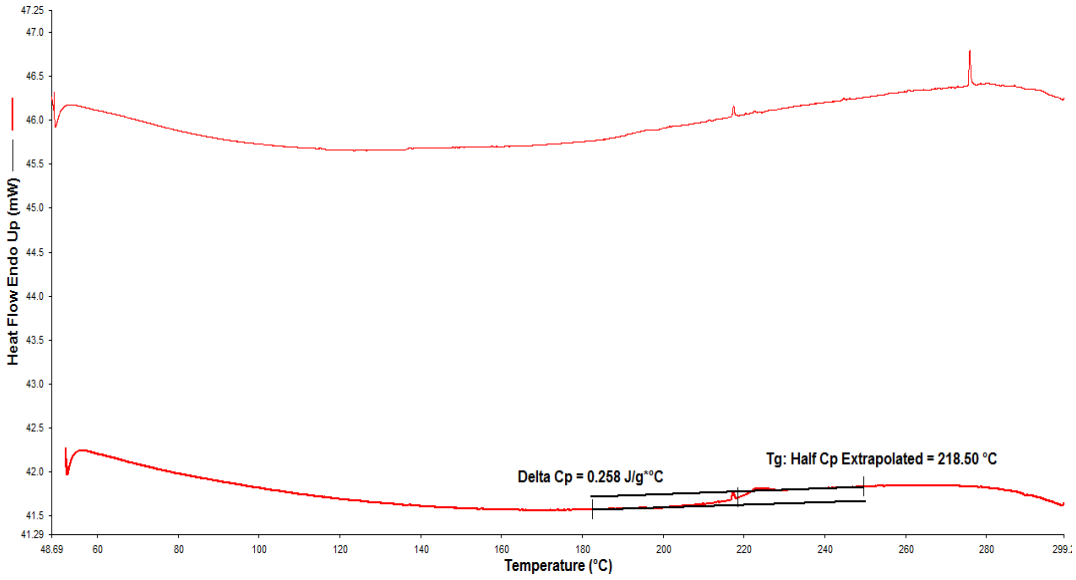

Figure J.3 DSC thermogram of PES/ZIF-8(%20) membrane

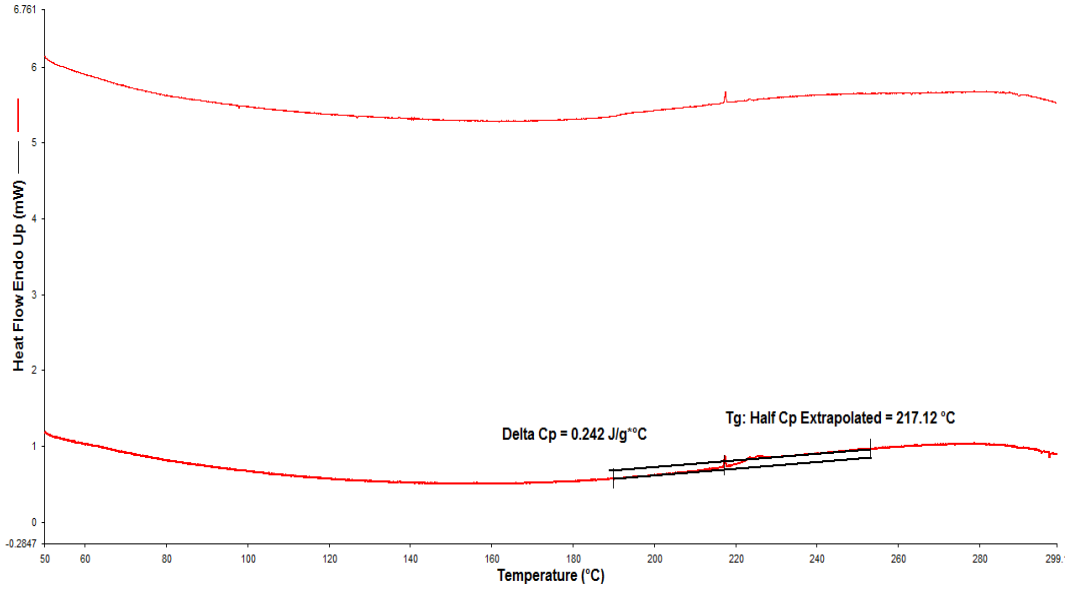

Figure J.4 DSC thermogram of PES/ZIF-8(%30) membrane

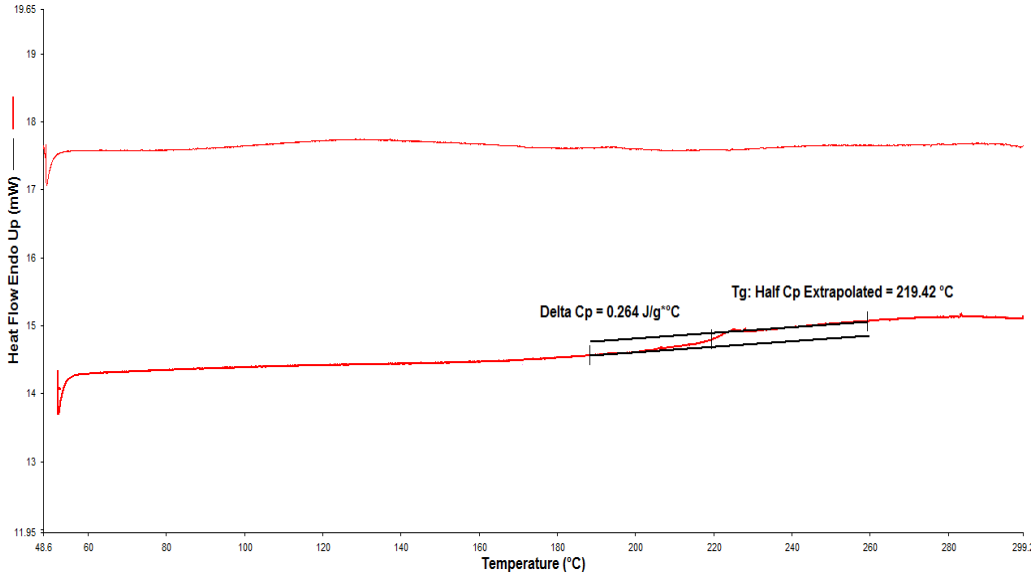

Figure J.5 DSC thermogram of PES/ZIF-8(%40) membrane

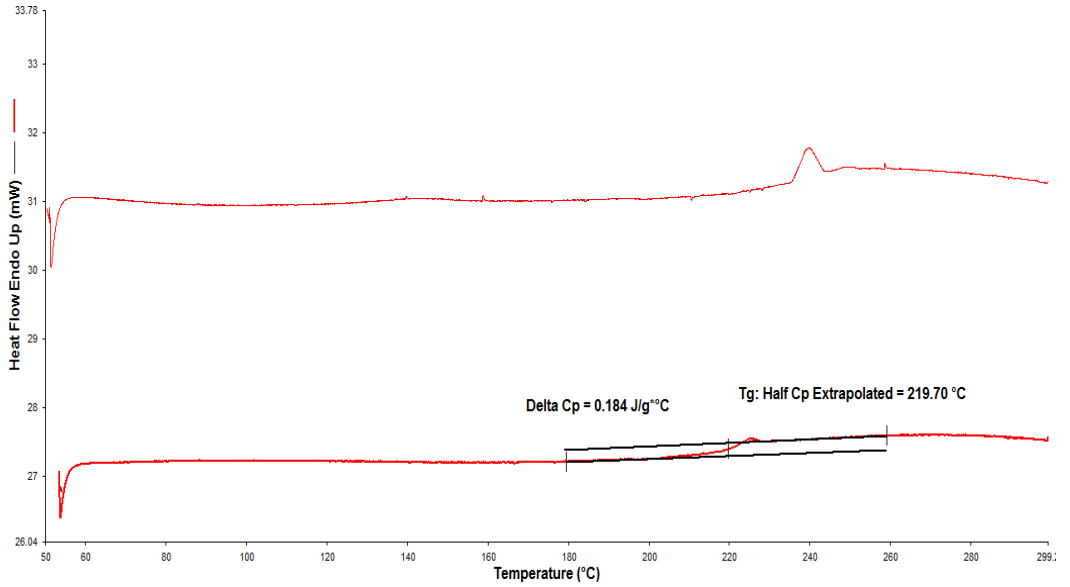

Figure J.6 DSC thermogram of PES/ZIF-8(%50) membrane

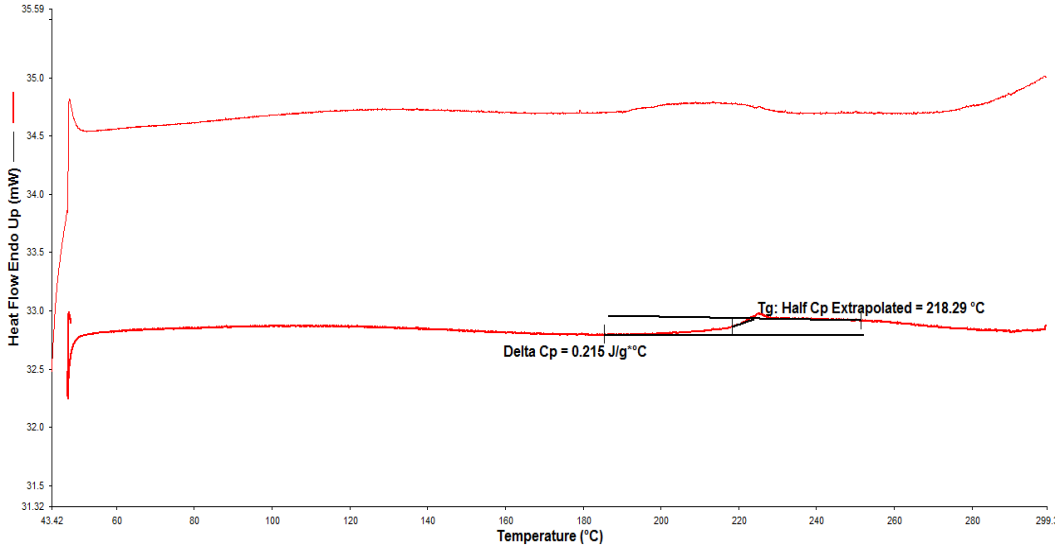

Figure J.7 DSC thermogram of PES/ZIF-8(%60) membrane

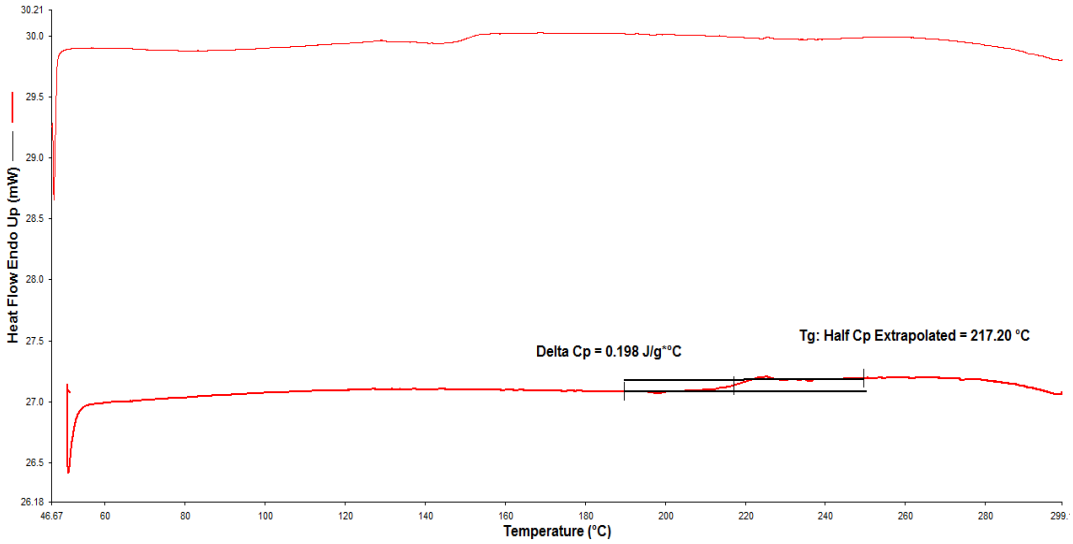

Figure J.8 DSC thermogram of PES/ZIF-8(%10)/HMA(%4) membrane

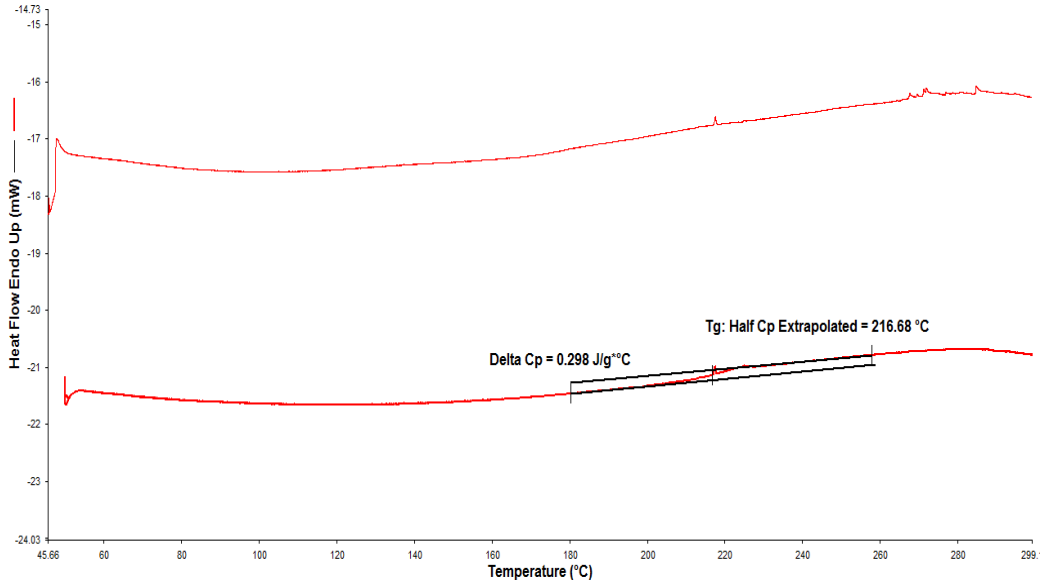

Figure J.9 DSC thermogram of PES/ZIF-8(%20)/HMA(%4) membrane

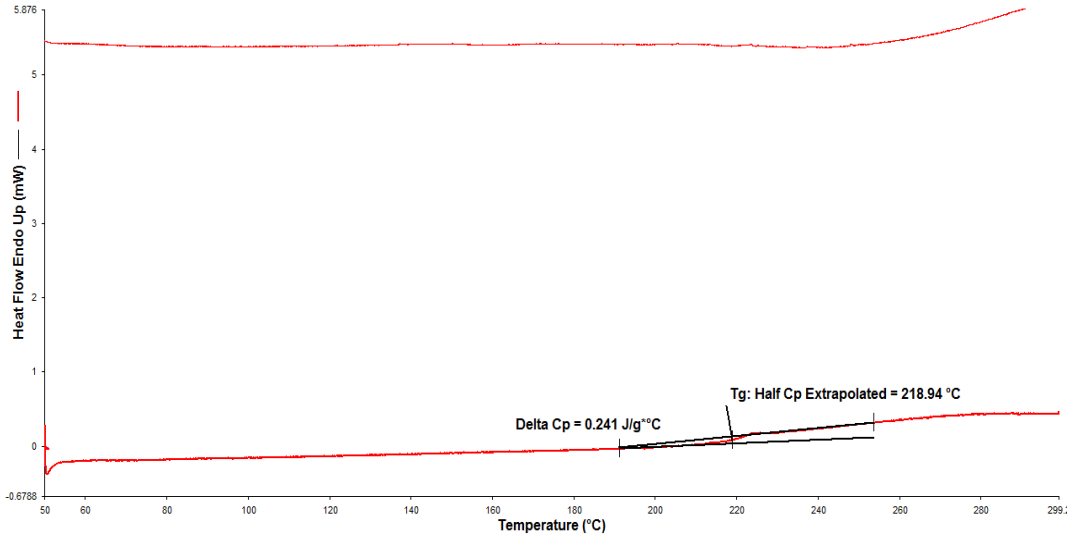

Figure J.10 DSC thermogram of PES/ZIF-8(%20)/HMA(%7) membrane

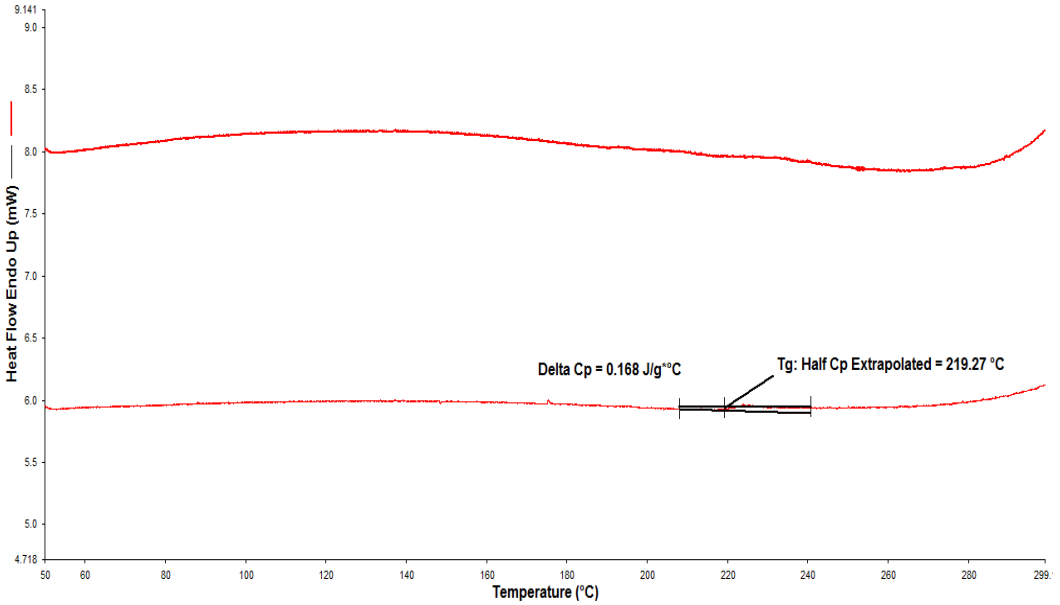

Figure J.11 DSC thermogram of PES/ZIF-8(%30)/HMA(%1) membrane

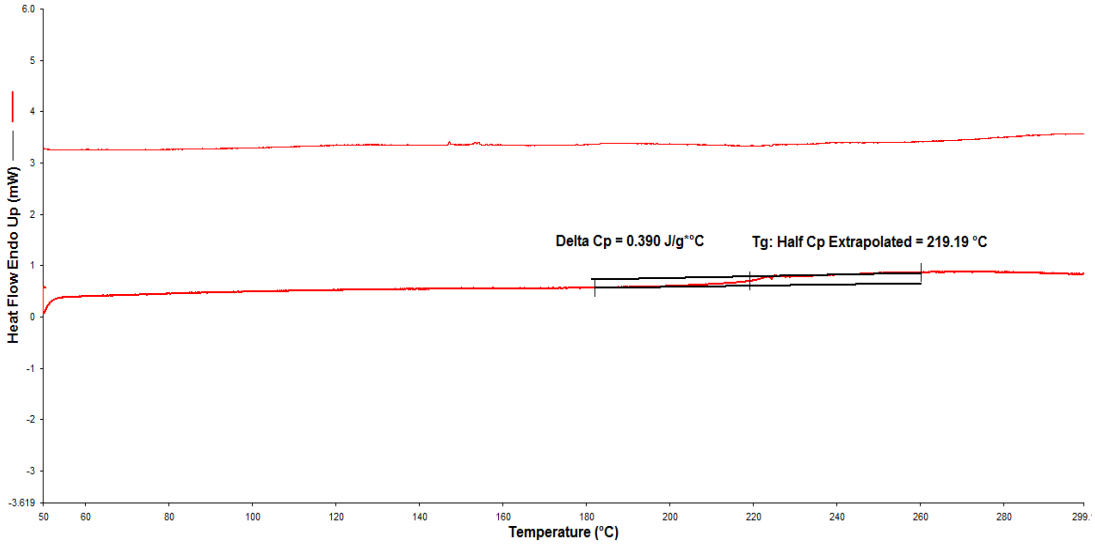

Figure J.12 DSC thermogram of PES/ZIF-8(%30)/HMA(%2) membrane

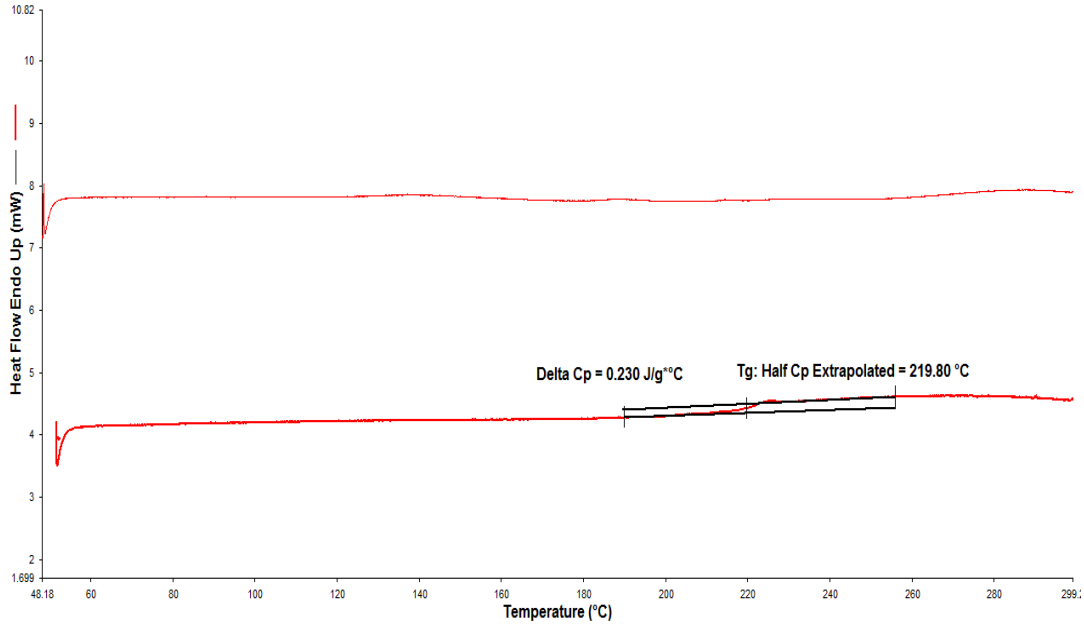

Figure J.13 DSC thermogram of PES/ZIF-8(%30)/HMA(%4) membrane

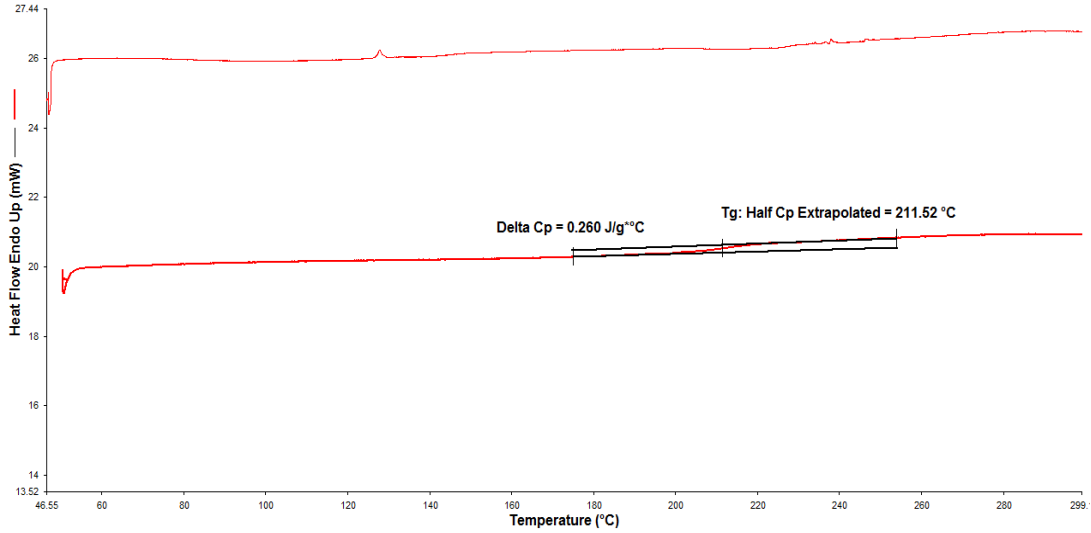

Figure J.14 DSC thermogram of PES/ZIF-8(%30)/HMA(%10) membrane

APPENDIX K

REPRODUCIBILTY OF SINGLE GAS PERMEABILITY EXPERIMENTS

Table K.1 Reproducibility data for Pure PES membranes

Membrane Number	Thickness (μm)	Run Number	Permeability(Barrer)			Ideal Selectivity		
			H_2	CO_2	CH_4	H_2/CO_2	CO_2/CH_4	H_2/CH_4
NK14	60	1	9.37	4.46	0.13			
		2	9.72	4.51	-			
		Avg.	9.55	4.49	0.13	2.13	34.54	73.46
NK30	60	1	9.63	4.42	0.13			
		2	9.22	4.48	-			
		Avg.	9.43	4.45	0.13	2.12	34.23	72.54
NK110	60	1	9.40	4.55	0.13			
		2	9.52	4.49	-			
		Avg.	9.46	4.52	0.13	2.09	34.77	72.77

Table K.2 Reproducibility data for PES/ZIF-8(%10) membranes

Membrane Number	Thickness (μm)	Run Number	Permeability(Barrer)			Ideal Selectivity		
			H_2	CO_2	CH_4	H_2/CO_2	CO_2/CH_4	H_2/CH_4
NK65	75	1	15.20	7.13	0.25	2.12	28.44	60.28
		2	14.94	7.08	-			
		Avg.	15.07	7.11	0.25			
NK80-1st Part	60	1	16.16	6.84	0.23	2.40	29.48	70.83
		2	16.42	6.72	-			
		Avg.	16.29	6.78	0.23			
NK80-2nd Part	50	1	17.02	6.82	0.24	2.44	28.92	70.63
		2	16.88	7.06	-			
		Avg.	16.95	6.94	0.24			
NK-88-1st Part	70	1	15.19	7.86	0.24	2.03	31.83	64.54
		2	15.78	7.42	-			
		Avg.	15.49	7.64	0.24			
NK-88-2nd Part	65	1	15.86	7.82	0.25	2.03	30.88	62.60
		2	15.44	7.62	-			
		Avg.	15.65	7.72	0.25			
NK104-1st Part	65	1	15.42	7.18	0.25	2.13	28.84	61.36
		2	15.25	7.24	-			
		Avg.	15.34	7.21	0.25			
NK104-2nd Part	60	1	15.38	7.12	0.24	2.13	29.83	63.67
		2	15.17	7.19	-			
		Avg.	15.28	7.16	0.24			
NK105-1st Part	65	1	14.64	7.27	0.24	2.02	30.16	60.83
		2	14.55	7.20	-			
		Avg.	14.60	7.24	0.24			
NK105-2nd Part	70	1	13.94	7.01	0.23	2.00	30.39	60.87
		2	14.05	6.97	-			
		Avg.	14.00	6.99	0.23			

Table K.3 Reproducibility data for PES/ZIF-8(%20) membranes

Membrane Number	Thickness (μm)	Run Number	Permeability(Barrer)			Ideal Selectivity		
			H_2	CO_2	CH_4	H_2/CO_2	CO_2/CH_4	H_2/CH_4
NK28-1st Part	75	1	26.25	12.79	0.43			
		2	26.52	12.98	-			
		Avg.	26.39	12.89	0.43	2.05	29.98	61.37
NK28-2nd Part	85	1	26.29	13.06	0.42			
		2	26.89	12.23	-			
		Avg.	26.59	12.65	0.42	2.10	30.12	63.31
NK40-1st Part	80	1	26.42	12.10	0.41			
		2	25.92	12.45	-			
		Avg.	26.17	12.28	0.41	2.13	29.95	63.83
NK40-2nd Part	90	1	25.88	11.21	0.43			
		2	26.16	11.80	-			
		Avg.	26.02	11.51	0.43	2.26	26.76	60.51
NK86-1st Part	70	1	26.12	12.23	0.42			
		2	25.70	12.41	-			
		Avg.	25.91	12.32	0.42	2.10	29.33	61.69
NK86-2nd Part	75	1	26.35	13.11	0.43			
		2	26.19	11.87	-			
		Avg.	26.27	12.49	0.43	2.10	29.05	61.09
NK97-1st Part	90	1	26.14	12.71	0.42			
		2	27.03	12.84	-			
		Avg.	26.59	12.78	0.42	2.08	30.43	63.31
NK97-2nd Part	75	1	26.42	12.94	0.43			
		2	26.24	13.05	-			
		Avg.	26.33	12.99	0.43	2.03	30.21	61.23
NK102-1st Part	85	1	26.40	11.88	0.43			
		2	25.79	12.21	-			
		Avg.	26.09	12.05	0.43	2.17	28.02	60.67
NK102-2nd Part	90	1	26.55	12.19	0.44			
		2	27.38	12.05	-			
		Avg.	26.97	12.12	0.44	2.23	27.55	61.29

Table K.4 Reproducibility data for PES/ZIF-8(%30) membranes

Membrane Number	Thickness (μm)	Run Number	Permeability(Barrer)			Ideal Selectivity		
			H_2	CO_2	CH_4	H_2/CO_2	CO_2/CH_4	H_2/CH_4
NK46-1st Part	75	1	60.97	28.59	1.17			
		2	60.94	29.92	-			
		Avg.	60.96	29.26	1.17	2.08	25.01	52.10
NK46-2nd Part	75	1	60.41	26.46	1.12			
		2	58.84	26.87	-			
		Avg.	59.63	26.67	1.12	2.25	23.80	53.23
NK50-1st Part	85	1	52.04	25.45	0.97			
		2	51.02	25.08	-			
		Avg.	51.53	25.27	0.97	2.04	26.05	53.12
NK50-2nd Part	75	1	51.82	26.43	0.98			
		2	52.96	25.81	-			
		Avg.	52.39	26.12	0.98	2.01	26.65	53.46
NK58 1st part	70	1	48.80	22.43	0.95			
		2	47.65	23.21	-			
		Avg.	48.23	22.82	0.95	2.11	24.02	50.77
NK87 1st Part	90	1	42.12	21.75	0.81			
		2	41.51	21.53	-	1.93	26.72	51.63
		Avg.	41.82	21.64	0.81			
NK87 2nd Part	90	1	40.29	21.35	0.79			
		2	40.62	20.86	-	1.92	26.72	51.22
		Avg.	40.46	21.11	0.79			
NK106 1st Part	85	1	53.01	32.04	1.90			
		2	52.76	31.99	-			
		Avg.	52.89	32.02	1.90	1.65	16.85	27.84
NK106 2nd Part	80	1	54.56	34.90	1.75			
		2	56.21	35.03	-			
		Avg.	55.39	34.97	1.75	1.58	19.98	31.65
NK107 1st Part	85	1	43.88	27.51	2.75			
		2	42.26	27.47	-			
		Avg.	43.07	27.49	2.75	1.56	9.99	15.66
NK107 1st Part	80	1	48.65	30.13	1.56			
		2	47.82	29.56	-			
		Avg.	48.24	29.85	1.56	1.62	19.13	30.92

Table K.5 Reproducibility data for PES/ZIF-8(%40) membranes

Membrane Number	Thickness (μm)	Run Number	Permeability(Barrer)			Ideal Selectivity		
			H_2	CO_2	CH_4	H_2/CO_2	CO_2/CH_4	H_2/CH_4
NK48-1st Part	75	1	70.51	34.04	1.43			
		2	69.28	32.88	-			
		Avg.	69.89	33.46	1.43	2.08	23.39	48.87
NK48-2nd Part	75	1	68.47	32.91	1.42			
		2	67.93	34.97	-			
		Avg.	68.20	33.94	1.42	2.01	23.90	48.03
NK54	90	1	70.38	41.95	2.37			
		2	69.38	42.80	-			
		Avg.	69.88	42.38	2.37	1.65	17.88	29.48
NK56	70	1	74.63	38.37	2.26			
		2	73.16	37.68	-			
		Avg.	73.89	38.03	2.26	1.94	16.83	32.69
NK84	80	1	40.46	27.41	1.18			
		2	39.35	27.25	-			
		Avg.	39.91	27.33	1.18	1.46	23.16	33.82
NK85-1st Part	90	1	36.04	21.92	0.89			
		2	35.54	21.75	-			
		Avg.	35.79	21.84	0.89	1.64	24.54	40.21
NK85-2nd Part	90	1	35.05	23.55	2.08			
		2	35.48	23.10	-			
		Avg.	35.27	23.33	2.08	1.51	11.22	16.96
NK93-1st Part	95	1	43.91	30.58	1.40			
		2	44.04	30.01	-			
		Avg.	43.98	30.29	1.40	1.45	21.64	31.41
NK93-2nd Part	100	1	42.83	28.81	2.32			
		2	43.12	27.89	-			
		Avg.	42.98	28.35	2.32	1.52	12.22	18.53
NK-94	100	1	38.66	25.19	1.08			
		2	39.08	24.72	-			
		Avg.	38.87	24.96	1.08	1.56	23.11	35.99
NK95	100	1	35.38	26.74	1.26			
		2	37.21	26.30	-			
		Avg.	36.29	26.52	1.26	1.37	21.05	28.80

Table K.6 Reproducibility data for PES/ZIF-8(%50) membranes

Membrane Number	Thickness (μm)	Run Number	Permeability(Barrer)			Ideal Selectivity		
			H_2	CO_2	CH_4	H_2/CO_2	CO_2/CH_4	H_2/CH_4
NK47-1st Part	90	1	118.55	62.45	3.85			
		2	115.16	61.92	-			
		3	118.82	62.74	-			
		Avg.	117.51	62.37	3.85	1.88	16.20	30.52
NK47-2nd Part	100	1	116.81	61.11	3.78			
		2	113.92	60.11	-			
		3	115.01	-	-			
		Avg.	115.25	60.61	3.78	1.90	16.03	30.49
NK91-1st Part	100	1	48.13	31.14	1.31			
		2	46.49	31.34	-			
		Avg.	47.31	31.24	1.31	1.51	23.92	36.11
NK91-2nd Part	100	1	38.74	28.08	1.09			
		2	41.15	27.95	-			
		Avg.	39.95	28.02	1.09	1.43	25.71	36.65
NK92-1st Part	100	1	41.49	28.88	1.12			
		2	41.11	28.76	-			
		Avg.	41.30	28.82	1.12	1.43	25.73	36.88
NK92-2nd Part	100	1	44.52	28.59	2.02			
		2	44.20	27.92	-			
		Avg.	44.36	28.26	2.02	1.57	13.99	21.96

Table K.7 Reproducibility data for PES/ZIF-8(%60) membranes

Membrane Number	Thickness (μm)	Run Number	Permeability(Barrer)			Ideal Selectivity		
			H_2	CO_2	CH_4	H_2/CO_2	CO_2/CH_4	H_2/CH_4
NK32	100	1	167.52	114.76	9.43			
		2	168.05	118.43	-			
		Avg.	167.79	116.59	9.43	1.44	12.36	17.79
NK41	100	1	105.92	81.80	5.06			
		2	103.31	80.80	-			
		3	101.40	-	-			
		Avg.	103.54	81.30	5.06	1.27	16.07	20.46
NK96	110	1	50.44	40.12	1.79			
		2	49.49	39.32	-			
		Avg.	49.97	39.72	1.79	1.26	22.19	27.92

Table K.8 Reproducibility data for PES/ZIF-8(%10)/HMA(%4) membranes

Membrane Number	Thickness (μm)	Run Number	Permeability(Barrer)			Ideal Selectivity		
			H_2	CO_2	CH_4	H_2/CO_2	CO_2/CH_4	H_2/CH_4
NK66-1st Part	70	1	8.65	2.90	0.088			
		2	8.48	2.84	-			
		Avg.	8.57	2.87	0.088	2.99	32.61	97.38
NK66-2nd Part	60	1	8.75	3.14	0.10			
		2	8.81	3.25	-			
		Avg.	8.78	3.19	0.10	2.75	31.90	87.80
NK72	70	1	8.42	3.37	0.11			
		2	8.73	3.25	-			
		Avg.	8.58	3.31	0.11	2.59	30.09	78.00
NK100-1st Part	60	1	9.06	3.24	0.10			
		2	8.91	3.12	-			
		Avg.	8.99	3.18	0.10	2.83	31.80	89.90
NK100-2nd Part	50	1	9.12	3.15	0.11			
		2	8.93	3.08	-			
		Avg.	9.03	3.12	0.11	2.89	28.36	82.09
NK101-1st Part	50	1	8.84	3.41	0.12			
		2	8.99	3.37	-			
		Avg.	8.92	3.39	0.12	2.63	28.25	74.33

Table K.9 Reproducibility data for PES/ZIF-8(%20)/HMA(%4) membranes

Membrane Number	Thickness (μm)	Run Number	Permeability(Barrer)			Ideal Selectivity		
			H_2	CO_2	CH_4	H_2/CO_2	CO_2/CH_4	H_2/CH_4
NK52-1st Part	55	1	15.61	5.97	0.20			
		2	15.33	6.13	-			
		Avg.	15.47	6.05	0.20	2.56	30.09	76.97
NK52-2nd Part	50	1	15.16	5.66	0.21			
		2	15.67	5.72	-			
		Avg.	15.42	5.69	0.21	2.71	27.09	73.43
NK55	70	1	15.20	6.22	0.19			
		2	15.38	5.85	-			
		Avg	15.29	6.04	0.19	2.53	32.65	82.65
NK98 1st Part	60	1	15.10	5.63	0.22			
		2	15.34	5.71	-			
		Avg.	15.22	5.67	0.22	2.68	25.77	69.18
NK98 2nd Part	60	1	16.15	6.49	0.24			
		2	16.48	6.32	-			
		Avg.	16.32	6.41	0.24	2.55	26.71	68.00
NK99 1st Part	60	1	15.54	5.49	0.25			
		2	16.02	5.46	-			
		Avg.	15.78	5.48	0.25	2.88	21.92	63.12
NK99 2nd Part	60	1	15.12	5.74	0.23			
		2	15.21	5.56	-			
		Avg.	15.17	5.65	0.23	2.68	23.54	63.21

Table K.10 Reproducibility data for PES/ZIF-8(%20)/HMA(%7) membranes

Membrane Number	Thickness (μm)	Run Number	Permeability(Barrer)			Ideal Selectivity		
			H_2	CO_2	CH_4	H_2/CO_2	CO_2/CH_4	H_2/CH_4
NK49-1st Part	70	1	14.69	5.12	0.148			
		2	14.27	4.73	-			
		Avg.	14.48	4.93	0.148	2.94	33.31	97.84
NK49-2nd Part	70	1	14.21	4.91	0.150			
		2	14.59	5.07	-			
		Avg.	14.40	4.99	0.150	2.89	33.27	96.00
NK81-1st Part	80	1	13.07	4.27	0.116			
		2	12.39	4.43	-			
		Avg.	12.73	4.35	0.116	2.93	37.50	109.74
NK81-2nd Part	80	1	13.32	4.32	0.119			
		2	13.10	4.51	-			
		Avg.	13.21	4.42	0.119	2.99	37.14	111.01

Table K.11 Reproducibility data for PES/ZIF-8(%30)/HMA(%1) membranes

Membrane Number	Thickness (μm)	Run Number	Permeability(Barrer)			Ideal Selectivity		
			H_2	CO_2	CH_4	H_2/CO_2	CO_2/CH_4	H_2/CH_4
NK69-1st Part	70	1	25.96	11.22	0.281			
		2	25.68	11.02	-			
		Avg.	25.82	11.12	0.281	2.32	39.57	91.88
NK69-2nd Part	70	1	28.75	11.39	0.36			
		2	27.51	11.82	-			
		Avg.	28.13	11.61	0.36	2.42	32.25	78.14
NK-73	70	1	20.75	9.57	0.40			
		2	21.56	9.65	-			
		Avg.	21.16	9.61	0.40	2.20	24.03	52.90
NK-76-1st Part	70	1	25.34	11.37	0.39			
		2	24.66	11.27	-			
		Avg.	25.00	11.32	0.39	2.21	29.03	64.10
NK-76-2nd Part	70	1	26.49	12.53	0.57			
		2	26.04	11.23	-			
		Avg.	26.27	11.88	0.57	2.21	20.84	46.08
NK-79-1st Part	80	1	20.01	11.23	0.39			
		2	20.35	10.45	-			
		Avg.	20.18	10.85	0.39	1.86	27.82	51.74
NK-79-2nd Part	80	1	19.28	10.25	0.37			
		2	19.72	11.05	-			
		Avg.	19.50	10.65	0.37	1.83	28.78	52.70

Table K.12 Reproducibility data for PES/ZIF-8(%30)/HMA(%2) membranes

Membrane Number	Thickness (μm)	Run Number	Permeability(Barrer)			Ideal Selectivity		
			H_2	CO_2	CH_4	H_2/CO_2	CO_2/CH_4	H_2/CH_4
NK64	90	1	23.97	11.90	0.41			
		2	25.21	11.72	-			
		Avg.	24.59	11.81	0.41	2.08	28.81	59.98
NK83-1st Part	70	1	28.74	11.32	0.44			
		2	28.16	10.32	-			
		Avg.	28.45	10.82	0.44	2.63	24.59	64.66
NK83-2nd Part	70	1	27.87	10.23	0.45			
		2	27.39	10.89	-			
		Avg.	27.63	10.56	0.45	2.62	23.46	61.40

Table K.13 Reproducibility data for PES/ZIF-8(%30)/HMA(%4) membranes

Membrane Number	Thickness (μm)	Run Number	Permeability(Barrer)			Ideal Selectivity		
			H_2	CO_2	CH_4	H_2/CO_2	CO_2/CH_4	H_2/CH_4
NK60-1st Part	80	1	20.80	10.57	0.51			
		2	21.68	11.51	-			
		Avg.	21.24	11.04	0.51	1.92	21.65	41.65
NK-60-2nd Part	70	1	21.48	10.13	0.45			
		2	21.76	11.01	-			
		Avg.	21.62	10.57	0.45	2.05	23.48	48.04
NK-61	100	1	24.61	13.88	0.56			
		2	24.59	13.28	-			
		Avg.	24.50	13.58	0.56	1.80	24.25	43.75
NK-82-1st Part	60	1	16.28	6.16	0.18			
		2	15.55	5.86	-			
		Avg.	15.92	6.01	0.18	2.65	33.38	88.44
NK-82-2nd Part	60	1	19.62	7.25	0.21			
		2	19.31	6.87	-			
		Avg.	19.47	7.06	0.21	2.76	33.62	92.71

Table K.14 Reproducibility data for PES/ZIF-8(%30)/HMA(%10) membranes

Membrane Number	Thickness (μm)	Run Number	Permeability(Barrer)			Ideal Selectivity		
			H_2	CO_2	CH_4	H_2/CO_2	CO_2/CH_4	H_2/CH_4
NK70-1st Part	70	1	13.23	4.29	0.135			
		2	13.29	4.87	-			
		Avg.	13.26	4.58	0.135	2.89	33.93	98.22
NK70-2nd Part	70	1	14.02	5.10	0.14			
		2	13.82	4.98	-			
		Avg.	13.92	4.88	0.14	2.78	34.86	99.43
NK78-1st Part	80	1	13.68	4.93	0.21			
		2	13.44	4.87	-			
		Avg.	13.56	4.90	0.21	2.75	23.47	64.57
NK78-2nd Part	80	1	14.12	4.98	0.20			
		2	14.01	5.02	-			
		Avg.	14.07	5.00	0.20	2.81	25.00	70.35

APPENDIX L

REPRODUCIBILTY OF HIGH PRESSURE GAS PERMEABILITY EXPERIMENTS

Table L.1 The results of high pressure permeation experiments for Pure PES membranes

Membr. Code	Membr. Type	Feed Pressure	Run #	Permeability(Barrer)			Ideal Selectivity		
				H_2	CO_2	CH_4	H_2/CO_2	CO_2/CH_4	H_2/CH_4
NK-30	Pure PES	3 bar	1st	9.54	4.28	0.131			
			2nd	9.48	4.25	-			
			Avg.	9.52	4.27	0.131	2.23	32.59	72.67
		6 bar	1st	9.47	3.82	0.107			
			2nd	9.91	3.81	-			
			Avg.	9.69	3.82	0.107	2.54	35.70	90.56
		8 bar	1st	9.77	3.77	0.091			
			2nd	9.88	3.77	-			
			Avg.	9.83	3.77	0.091	2.61	41.43	108.02
		10 bar	1st	9.84	3.60	0.083			
			2nd	9.72	3.59	-			
			Avg.	9.78	3.60	0.083	2.72	43.37	117.83
		12 bar	1st	9.77	3.49	0.079			
			2nd	9.63	3.51	-			
			Avg.	9.70	3.50	0.079	2.77	44.30	122.78
NK-110	Pure PES	3 bar	1st	9.40	4.55	0.139			
			2nd	9.43	4.48	-			
			3rd	9.39	4.51	-			
			Avg.	9.41	4.51	0.139	2.09	32.45	67.70
		6 bar	1st	9.35	4.24	0.115			
			2nd	9.37	4.20	-			
			3rd	9.40	4.18	-			
			Avg.	9.37	4.21	0.115	2.23	36.61	81.48
		8 bar	1st	9.39	4.09	0.100			
			2nd	9.38	4.11	-			
			3rd	9.41	3.87	-			

Table L.1 The results of high pressure permeation experiments for Pure PES membranes (cont'd)

			Avg.	9.39	4.02	0.100	2.34	40.20	93.90
		10 bar	1st	9.49	3.87	0.092			
			2nd	9.47	3.85	-			
			3rd	9.45	3.89	-			
			Avg.	9.47	3.87	0.092	2.45	42.07	102.93
		12 bar	1st	9.41	3.69	0.087			
			2nd	9.43	3.73	-			
			3rd	9.39	3.71	-			
			Avg.	9.41	3.71	0.087	2.54	42.64	108.16

Table L.2 The results of high pressure permeation experiments for PES/HMA(%4) membranes

Membrane Code	Membrane Type	Pressure	Run #	Permeability(Barrer)			Ideal Selectivity		
				H_2	CO_2	CH_4	H_2/CO_2	CO_2/CH_4	H_2/CH_4
NK-111 1st Part	PES/HMA(%4)	3 bar	1st	5.79	1.87	0.060			
			2nd	5.89	1.88	-			
			3rd	5.93	1.89	-			
			Avg.	5.87	1.88	0.060	3.12	31.33	97.83
		6 bar	1st	5.95	1.78	0.053			
			2nd	6.05	1.79	-			
			3rd	5.96	1.78	-			
			Avg.	5.99	1.78	0.053	3.37	33.59	113.02
		8 bar	1st	6.08	1.71	0.047			
			2nd	5.99	1.70	-			
			3rd	6.01	1.68	-			
			Avg.	6.03	1.70	0.047	3.55	36.17	128.30
		10 bar	1st	6.04	1.66	0.040			
			2nd	5.98	1.65	-			
			3rd	6.01	1.67	-			
			Avg.	6.01	1.66	0.040	3.62	41.50	150.25
		12 bar	1st	6.05	1.61	0.032			
			2nd	6.01	1.60	-			
			3rd	5.98	1.59	-			
			Avg.	6.01	1.60	0.032	3.76	50.00	187.81
NK-111 2nd Part	PES/HMA(%4)	3 bar	1st	5.92	1.92	0.061			
			2nd	5.89	1.89	-			
			3rd	5.94	1.93	-			
			Avg.	5.92	1.91	0.061	3.10	31.31	97.05
		6 bar	1st	5.97	1.83	0.052			
			2nd	5.99	1.79	-			
			3rd	5.95	1.81	-			
			Avg.	5.97	1.81	0.052	3.30	34.81	114.81
		8 bar	1st	5.99	1.80	0.046			
			2nd	6.02	1.79	-			
			3rd	5.98	1.75	-			
			Avg.	6.00	1.78	0.046	3.37	38.70	130.43
		10 bar	1st	6.03	1.70	0.039			
			2nd	6.01	1.67	-			
			3rd	6.04	1.70	-			
			Avg.	6.03	1.69	0.039	3.57	43.33	154.62
		12 bar	1st	5.99	1.63	0.033			
			2nd	6.02	1.59	-			
			3rd	5.98	1.62	-			
			Avg.	6.00	1.62	0.033	3.70	49.09	181.82

Table L.3 The results of high pressure permeation experiments for PES/ZIF-8(%10) membranes

Membr. Code	Membr. Type	Feed Pressure	Run #	Permeability(Barrer)			Ideal Selectivity		
				H_2	CO_2	CH_4	H_2/CO_2	CO_2/CH_4	H_2/CH_4
NK-65 1st Part 75μm	PES/ZIF-8(%10)	3 bar	1st	14.92	7.04	0.24			
			2nd	14.90	7.21	0.23			
			3rd	14.97	6.84	-			
			Avg.	14.93	7.03	0.24	2.12	29.29	62.21
		6 bar	1st	14.61	6.33	0.21			
			2nd	14.73	6.27	0.20			
			3rd	14.69	6.30	-			
			Avg.	14.68	6.30	0.21	2.33	30.00	69.91
		8 bar	1st	14.93	5.58	0.18			
			2nd	14.89	5.54	0.18			
			3rd	14.95	5.61	-			
			Avg.	14.92	5.58	0.18	2.67	31.00	82.89
		10 bar	1st	14.89	4.78	0.15			
			2nd	14.81	4.82	0.14			
			3rd	14.93	4.83	-			
			Avg.	14.88	4.81	0.14	3.09	34.36	106.29
		12 bar	1st	14.94	4.63	0.11			
			2nd	14.98	4.72	0.11			
			3rd	14.96	4.66	-			
			Avg.	14.96	4.67	0.11	3.20	42.45	136.00
NK-65 2nd Part	PES/ZIF-8(%10)	3 bar	1st	15.21	7.33	0.25			
			2nd	15.22	7.21	-			
			3rd	15.17	-	-			
			Avg.	15.20	7.27	0.25	2.09	29.08	60.80
		6 bar	1st	15.01	6.52	0.21			
			2nd	14.98	6.56	-			
			3rd	15.12	-	-			
			Avg.	15.04	6.54	0.21	2.30	31.14	71.62
		8 bar	1st	15.38	5.91	0.19			
			2nd	15.42	5.96	-			
			3rd	15.25	5.95	-			
			Avg.	15.35	5.95	0.19	2.58	31.32	80.79
		10 bar	1st	14.92	5.28	0.15			

Table L.3 The results of high pressure permeation experiments for PES/ZIF-8(%10) membranes (cont'd)

			2nd	15.03	5.12	0.14			
			3rd	15.11	5.26	-			
			Avg.	15.02	5.01	0.15	2.99	33.40	100.13
		12 bar	1st	15.26	4.91	0.10			
			2nd	15.32	4.81	0.10			
			3rd	15.36	4.86	-			
			Avg.	15.31	4.86	0.10	3.15	48.60	153.10
NK-80 1st Part 70μm	PES/ZIF-8(%10)	3 bar	1st	16.17	7.09	0.25			
			2nd	16.31	7.02	-			
			3rd	16.04	6.89	-			
			Avg.	16.17	6.98	0.25	2.32	27.92	64.68
		6 bar	1st	15.94	5.79	0.21			
			2nd	16.04	6.01	-			
			3rd	16.07	6.03	-			
			Avg.	16.02	5.94	0.21	2.70	28.29	76.29
		8 bar	1st	16.01	5.43	0.18			
			2nd	16.12	5.37	-			
			3rd	15.98	5.46	-			
			Avg.	16.04	5.42	0.18	2.96	30.11	89.11
		10 bar	1st	15.97	5.20	0.15			
			2nd	16.02	5.22	-			
			3rd	15.88	5.21	-			
			Avg.	15.96	5.21	0.15	3.06	34.73	106.40
		12 bar	1st	16.04	5.04	0.12			
			2nd	15.98	5.01	-			
			3rd	16.18	4.98	-			
			Avg.	16.07	5.01	0.12	3.21	41.75	133.92

Table L.4 The results of high pressure permeation experiments for PES/ZIF-8(%20) membranes

Membr. Code	Membr. Type	Feed Pressure	Run #	Permeability(Barrer)			Ideal Selectivity		
				H_2	CO_2	CH_4	H_2/CO_2	CO_2/CH_4	H_2/CH_4
NK-28 1st Part 80μm	PES/ZIF-8(%20)	3 bar	1st	26.71	13.26	0.43			
			2nd	26.65	13.20	-			
			Avg.	26.68	13.23	0.43	2.02	30.77	62.05
		6 bar	1st	26.31	11.53	0.30			
			2nd	26.37	11.48	-			
			Avg.	26.34	11.51	0.30	2.29	38.36	87.8
		8 bar	1st	26.42	10.57	0.27			
			2nd	26.53	10.61	-			
			3rd	26.48	-	-			
			Avg.	26.48	10.59	0.27	2.50	39.22	98.07
		10 bar	1st	26.82	9.74	0.25			
			2nd	26.74	9.84	-			
			3rd	26.79	-	-			
			Avg.	26.78	9.79	0.25	2.74	39.16	107.12
		12 bar	1st	26.47	9.48	0.18			
			2nd	26.52	9.52	-			
			3rd	26.56	-	-			
			Avg.	26.52	9.50	0.18	2.79	52.78	147.33
NK-28 2nd Part 90 μm	PES/ZIF-8(%20)	3 bar	1st	26.32	13.46	0.43			
			2nd	26.42	12.78	-			
			Avg.	26.37	13.12	0.43	2.01	30.51	61.33
		6 bar	1st	26.78	12.14	0.32			
			2nd	26.72	12.35	-			
			Avg.	26.76	12.25	0.32	2.18	38.28	83.63
		8 bar	1st	26.81	11.33	0.28			
			2nd	26.84	11.31	-			
			3rd	26.78	-	-			
			Avg.	26.81	11.32	0.28	2.37	40.43	95.75
		10 bar	1st	27.02	10.43	0.24			
			2nd	26.92	10.24	-			
			3rd	27.01	10.11	-			
			Avg.	26.98	10.26	0.24	2.63	42.75	112.42
		12 bar	1st	26.81	9.81	-			
			2nd	26.79	9.79	-			

Table L.4 The results of high pressure permeation experiments for PES/ZIF-8(%20) membranes (cont'd)

			3rd	26.84	9.74	-			
			Avg.	26.81	9.78	-	2.74	-	-

NK-40 1st Part 80 μm	PES/ZIF-8(%20)	3 bar	1st	25.28	11.78	0.45			
			2nd	25.48	11.67	-			
			Avg.	25.38	11.73	0.45	2.16	26.06	56.40
		6 bar	1st	24.81	10.28	0.34			
			2nd	25.21	10.43	-			
			Avg.	25.01	10.36	0.34	2.41	30.47	73.56
		8 bar	1st	25.33	9.58	0.29			
			2nd	25.51	9.52	-			
			3rd	25.23	-	-			
			Avg.	25.36	9.55	0.29	2.66	32.93	87.45
		10 bar	1st	25.16	8.96	0.26			
			2nd	25.61	9.02	-			
			3rd	25.26	-	-			
			Avg.	25.34	8.99	0.26	2.82	34.58	97.46
		12 bar	1st	25.18	8.11	0.21			
			2nd	25.28	8.32	-			
			3rd	25.32	-	-			
			Avg.	25.26	8.22	0.21	3.07	39.14	120.29
NK-102 1st Part 85 μm	PES/ZIF-8(%20)	3 bar	1st	26.06	11.53	0.43			
			2nd	26.02	11.67	-			
			Avg.	26.04	11.60	0.43	2.25	26.98	60.56
		6 bar	1st	26.03	10.74	0.29			
			2nd	25.82	10.68	-			
			Avg.	25.93	10.71	0.29	2.42	36.93	89.41
		8 bar	1st	25.39	10.46	0.26			
			2nd	25.89	10.28	-			
			Avg.	25.64	10.37	0.26	2.47	39.88	98.62
		10 bar	1st	25.21	10.19	0.23			
			2nd	25.35	9.88	-			
			Avg.	25.28	10.04	0.23	2.52	43.65	109.91
		12 bar	1st	25.73	9.13	0.20			
			2nd	26.27	8.92	-			
			Avg.	26.00	9.03	0.20	2.88	45.15	130.00

Table L.5 The results of high pressure permeation experiments for PES/ZIF-8(%10)/HMA(%4) membranes

Membr. Code	Membr. Type	Feed Pressure	Run #	Permeability(Barrer)			Ideal Selectivity		
				H_2	CO_2	CH_4	H_2/CO_2	CO_2/CH_4	H_2/CH_4
NK-100 2nd Part	PES/ZIF-8(%10)/HMA(%4)	3 bar	1st	9.01	2.98	0.11			
			2nd	9.04	3.02	-			
			3rd	8.99	3.01	-			
			Avg.	9.01	3.00	0.11	3.00	27.27	81.91
		6 bar	1st	8.86	2.78	0.088			
			2nd	8.92	2.73	-			
			3rd	8.89	2.81	-			
			Avg.	8.89	2.77	0.088	3.21	31.48	101.02
		8 bar	1st	8.96	2.54	0.075			
			2nd	9.02	2.61	-			
			3rd	8.89	2.55				
			Avg.	8.96	2.57	0.075	3.49	34.27	119.47
		10 bar	1st	8.88	2.33	0.062			
			2nd	8.81	2.37	-			
			3rd	8.93	2.35	-			
			Avg.	8.87	2.35	0.062	3.77	37.90	143.06
		12 bar	1st	8.88	2.27	0.05			
			2nd	8.92	2.25	-			
			3rd	8.96	2.24	-			
			Avg.	8.92	2.25	0.05	3.96	45.00	178.40
NK-72 1st Part	PES/ZIF-8(%10)/HMA(%4)	3 bar	1st	8.93	3.21	0.112			
			2nd	8.98	3.26	-			
			3rd	9.01	3.29	-			
			Avg.	8.97	3.25	0.112	2.76	29.02	80.09
		6 bar	1st	8.79	3.05	0.09			
			2nd	8.82	3.02	-			
			3rd	8.81	3.04	-			
			Avg.	8.81	3.04	0.090	2.90	33.78	97.89
		8 bar	1st	8.91	2.99	0.074			
			2nd	8.97	2.95	-			
			3rd	8.94	2.98	-			
			Avg.	8.94	2.97	0.074	3.01	40.14	120.81

		10 bar	1 st	8.87	2.84	0.065	3.12	43.69	136.15
			2nd	8.82	2.82	-			
			3rd	8.85	2.85	-			
			Avg.	8.85	2.84	0.065			
		12 bar	1st	8.78	2.75	0.053	3.19	52.08	166.23
			2nd	8.85	2.79	-			
			3rd	8.81	2.73	-			
			Avg.	8.81	2.76	0.053			

Table L.5 The results of high pressure permeation experiments for PES/ZIF-8(%10)/HMA(%4) membranes(cont'd)

NK-100 1st Part 60mm	PES/ZIF-8(%10)/HMA(%4)	3 bar	1st	9.07	3.09	0.10	2.89	28.64	82.73
			2nd	9.12	3.15	0.12			
			3rd	9.11	3.21	-			
			Avg.	9.10	3.15	0.11			
		6 bar	1st	9.33	2.93	0.089	3.17	33.41	105.79
			2nd	9.32	2.96	0.087			
			3rd	9.29	2.94	-			
			Avg.	9.31	2.94	0.088			
		8 bar	1st	9.32	2.75	0.079	3.39	34.81	118.10
			2nd	9.34	2.78	0.079			
			3rd	9.33	2.71	-			
			Avg.	9.33	2.75	0.079			
		10 bar	1st	9.31	2.59	0.067	3.56	38.53	137.35
			2nd	9.37	2.62	0.068			
			3rd	9.35	2.64	-			
			Avg.	9.34	2.62	0.068			
		12 bar	1st	9.24	2.49	0.052	3.77	46.79	176.23
			2nd	9.38	2.43	0.054			
			3rd	9.41	2.51	-			
			Avg.	9.34	2.48	0.053			

Table L.6 The results of high pressure permeation experiments for PES/ZIF-8(%20)/HMA(%4) membranes

Membr. Code	Membr. Type	Feed Pressure	Run #	Permeability(Barrer)			Ideal Selectivity		
				H_2	CO_2	CH_4	H_2/CO_2	CO_2/CH_4	H_2/CH_4
NK-52 1st Part	PES/ZIF-8(%20)/HMA(%4)	3 bar	1st	15.75	5.81	0.24			
			2nd	15.76	5.85	-			
			3rd	15.72	5.82	-			
			Avg.	15.74	5.83	0.24	2.70	24.29	65.58
		6 bar	1st	15.87	5.15				
			2nd	15.67	5.18	-			
			3rd	15.81	5.12	-			
			Avg.	15.78	5.15	0.19	3.06	27.11	83.05
		8 bar	1st	15.82	5.02				
			2nd	15.84	4.98	-			
			3rd	15.79	5.01	-			
			Avg.	15.82	5.00	0.16	3.16	31.25	98.88
		10 bar	1st	15.74	4.48	0.13			
			2nd	15.78	4.55	-			
			3rd	15.82	4.51	-			
			Avg.	15.78	4.51	0.13	3.50	34.69	121.38
		12 bar	1st	15.85	4.25	0.12			
			2nd	15.89	4.22	-			
			3rd	15.79	4.28	-			
			Avg.	15.84	4.25	0.12	3.73	35.42	132.00
NK-52 2nd Part	PES/ZIF-8(%20)/HMA(%4)	3 bar	1st	16.02	5.92	0.25			
			2nd	16.05	5.86	-			
			3rd	15.97	-	-			
			Avg.	16.01	5.89	0.25	2.72	23.56	64.04
		6 bar	1st	16.12	5.35	0.20			
			2nd	16.06	5.29	-			
			3rd	16.05	-	-			
			Avg.	16.08	5.32	0.20	3.02	26.60	80.40
		8 bar	1st	15.92	5.14	0.17			
			2nd	15.98	5.08	-			
			3rd	16.01	-	-			
			Avg.	15.97	5.11	0.17	3.13	30.06	106.47

		10 bar	1st	16.03	4.71	0.15	3.46	30.93	106.87
			2nd	16.06	4.57	-			
			3rd	15.99	-	-			
			Avg.	16.03	4.64	0.15			
		12 bar	1st	15.97	4.44	0.13	3.67	33.62	123.46
			2nd	16.05	4.30	-			
			3rd	16.12	-	-			
			Avg.	16.05	4.37	0.13			

Table L.6 The results of high pressure permeation experiments for PES/ZIF-8(%20)/HMA(%4) membranes (cont'd)

NK-55 1st Part	PES/ZIF-8(%20)/HMA(%4)	3 bar	1st	15.77	5.99	0.24	2.64	24.88	65.67
			2nd	15.72	6.03	-			
			3rd	15.78	5.89	-			
			Avg.	15.76	5.97	0.24			
		6 bar	1st	15.69	5.30	0.20	2.96	26.50	78.45
			2nd	15.71	5.34	-			
			3rd	15.66	5.27	-			
			Avg.	15.69	5.30	0.20			
		8 bar	1st	15.47	5.25	0.17	2.98	30.76	91.47
			2nd	15.58	5.21	-			
			3rd	15.61	5.22	-			
			Avg.	15.55	5.23	0.17			
		10 bar	1st	15.61	5.05	0.15	3.11	33.47	104.13
			2nd	15.66	5.02	-			
			3rd	15.59	4.99	-			
			Avg.	15.62	5.02	0.15			
		12 bar	1st	15.68	4.73	0.13	3.34	36.23	120.85
			2nd	15.73	4.71	-			
			3rd	15.71	4.69	-			
			Avg.	15.71	4.71	0.13			